THEORETICAL AND EXPERIMENTAL STUDY OF A DEHUMIDIFICATION SYSTEM BASED ON LIQUID DESICCANTS FOR AIR CONDITIONING APPLICATIONS

Juan Prieto González

Juan Prieto González

THEORETICAL AND EXPERIMENTAL STUDY OF A DEHUMIDIFICATION SYSTEM BASED ON LIQUID DESICCANTS FOR AIR CONDITIONING APPLICATIONS

DOCTORAL THESIS

Supervised by

Prof. Alberto Coronas

Dr. Jordi Ortiga Guillén

Department of Mechanical Engineering

UNIVERSITAT ROVIRA I VIRGILI

Tarragona, June 2016

UNIVERSITAT
ROVIRA I VIRGILI
DEPARTAMENT D'ENGINYERIA MECÀNICA
Escola Tècnica Superior d'Enginyeria Química (ETSEQ).
Av. Països Catalans 26. 43007 Tarragona (Spain)

WE STATE that the present study, entitled "Theoretical and experimental study of a dehumidification system based on liquid desiccants for air conditioning applications", presented by Mr. Juan Prieto González for the Award of the degree of Doctor, has been carried out under our supervision at the CREVER research group in Department of Mechanical Engineering of this university, and that it fulfills all the requirements to be eligible for the International Doctorate Award.

Tarragona, May 16, 2016

Doctoral Thesis Supervisors:

Dr. Alberto Coronas

Dr. Jordi Ortiga

Acknowledgments

I want to express my sincere acknowledge to Prof. Dr. Alberto Coronas, who gave the opportunity to join the CREVER research group and to develop this thesis. I also appreciate much his guidance. Of course, I would like to add to my appreciation to my co-supervisor Dr. Jordi Ortiga, who helped me so much throughout the development of the thesis.

I gratefully acknowledge the financial support received from the Nanocool Project, an European Project co-founded by the European Commission within the Seventh Framework Programme (FP7), Grant agreement no: 314701. All the partners of the Nanocool Project are acknowledged for all the information and effort provided. The financial support of the Universitat Rovira i Virgili for my research visit at the Technion – Israel Institute of Technology for three months is also appreciated.

Many thanks to Prof. Dr. Gershon Grossman and Dr. Khaled Gommed for their help and valuable teachings during my research stay at the Technion – Israel Institute of Technology for three months.

I would also like to thank to the current and previous members of CREVER group for their support and friendship, especially to Dr. Arturo Ordóñez, Dr. Daniel Salavera, Dr. Joaquín Rodríguez, Dr. Andry Cera, Dr. Dereje Ayou, Antonio Atienza, Rubén Sánchez and Adriana Coca.

Special thanks to Marina Rodríguez who supported me whenever I needed. Of course, I cannot forget my parents and sister, who, despite the distance, gave me the suggestions and the support I needed.

Abstract

Abstract

The energy demand for air conditioning is rising in the last years because the global warming is making that cooling loads are becoming larger during longer periods. Moreover, the standard of living and the demand of comfort are increasing, what make air conditioning more and more present not only in industrial countries, but also in developing countries, where dehumidification has often a greater impact than sensible load.

Comparing with other desiccant systems, hybrid desiccant systems are more efficient when humidity and temperature are required to be separately controlled. Furthermore, liquid desiccant systems offer attractive benefits in terms of energy efficiency, energy storage and working temperatures in comparison with solid desiccant systems. However, liquid desiccant systems have not been deeply used yet, due principally to the corrosiveness of the conventional liquid desiccant materials with most of the metallic materials, with exception of titanium and tantalum, which are very expensive materials.

The main objective of this thesis is to make a theoretical and an experimental study of a hybrid liquid desiccant system using rustproof and cost-effective materials, keeping a good performance of the system and achieving high energy efficiency. The thesis is mainly focused on the principal components of the liquid desiccant system: the absorber and the regenerator.

This thesis has been carried out under an European Project of the Seventh Framework Programme (FP7), whose acronym is nanoCOOL. The main objective of the Project was to develop, manufacture and operate an innovative hybrid liquid desiccant system. Therefore, some of the results taken from the studies carried out in this thesis have been used for the developing of the system. Moreover, the experimental performance data of the nanoCOOL demonstrative hybrid liquid desiccant system when it operates in a real application in Taiwan has been used for its evaluation.

In a first stage of the thesis, a state-of-the-art, that assesses the main liquid desiccant materials, the available air-solution contactors and different system configurations, is presented. From this study, it was selected the LiCl-H_2O as liquid desiccant due to its low vapour pressure. In addition, air-solution contactors of the falling-film with horizontal tubes were chosen due to its good heat and mass transfer and its low pressure drops in the air side. Furthermore, liquid desiccant system has been decided to be coupled with a vapour compression heat pump because it provides cooling to the absorber and heating to the regenerator with the same energy source.

Since LiCl-H_2O is a very corrosive material, tubes made of polypropylene, high density polyethylene, low density polyethylene, polyamide and graphite were tested. Moreover, LiCl-H_2O has a high surface tension and, therefore, wettability of tubes has a high effect on the heat and mass transfer of the air-solution contactors. For this reason, wettability of tubes was evaluated and was taken into consideration in the selection of the tube material. Some of the tested tubes contained a surface plasma treatment that improves the wetting of the plastic material when LiCl-H_2O is around the tubes. As result, polypropylene with surface treatment was chosen as the best material among the tested materials to be used in the hybrid system. Furthermore, correlations that determine the minimum liquid desiccant flow rate required to fully wet the tubes were obtained.

Then, two small-scale air-solution contactors were compared in order to verify that polypropylene with surface treatment has a better performance than standard polypropylene, when it is used as an absorber of a liquid desiccant system. Higher performance in all, air cooling (about 29 %), heat duty (about 17 %), global heat transfer coefficient between the water and the liquid desiccant (up to 54 %), and dehumidification (about 20 %) was achieved with the air-solution contactor with treated polypropylene tubes.

Following to the material selection, the design and sizing of the whole hybrid liquid desiccant system was done. The system was designed to operate in two locker rooms of a swimming-pool in Taipei (Taiwan). Once it was made and before was sent to Taiwan, the system was completely assembled and set-up at the Universitat Rovira i Virgil, Tarragona (Spain).

The performance of the hybrid liquid desiccant system has been evaluated during its operation in both locations, Spain and Taiwan. In this sense, two absorbers with different tube arrangements (in-line and staggered) and a regenerator with staggered arrangement have been experimentally evaluated. Inlet liquid desiccant temperature has been found as the variable that has the highest effect on the dehumidification of air in the absorber, and on the regeneration of the liquid desiccant in the regenerator. This demonstrates that the global heat transfer coefficient in the air-solution contactors is very important on their performance. Although better performance was expected in the absorber with staggered arrangement, the absorber with in-line arrangement achieved higher dehumidification and air cooling provided to the air. The mass transfer coefficient in the in-line arrangement is 20 % higher and the global heat transfer coefficient is 9 % higher. Furthermore, correlations for the tube-solution heat transfer coefficient and for the mass transfer coefficient in the air side of the air-solution contactors were obtained as function of the air velocity.

On the other hand, the performance of the whole system has been also evaluated. The maximum cooling production measured in real operation conditions of the hybrid liquid desiccant system is 34 kW and the maximum dehumidification is almost 0.012 kg_w/kg_a. In terms of global COP of the system, it is mainly affected by the cooling load and the hot water temperature: the lower the hot water temperature and the higher the cooling load, the higher the global COP. Furthermore, the system presents an adequate control of temperature and humidity of the locker rooms at different ambient and operational conditions.

The system has been modelled for being dynamically simulated. The correlations of the tube-solution heat transfer coefficient and of the mass transfer coefficient in the air side obtained for the air-solution contactors were used. Results taken from simulations have been compared with the experimental data of the prototype, showing only small deviations.

In order to optimize the annual performance of the real hybrid liquid desiccant system, a multi-objective optimization, in which the conditions of three operational variables (inlet water temperature in the absorber and regenerator, and minimum LiCl mass concentration at the entrance of the absorber) and two control strategies were evaluated, by using the dynamic model. Two objectives have been chosen to be minimized: the number of hours out of comfort conditions and the energy consumption of the heat pump. According to this, the best control strategy is the one that actuates the regenerator as function of the LiCl mass concentration at the entrance of the absorber. Moreover, for the annual operation of the system, the inlet water temperature in the absorber should be 12 °C, the inlet water temperature in the regenerator should be 51 °C and the minimum lithium chloride mass concentration should be 32.5 %. In addition to this, a monthly optimization of the system, in the same way than the annual optimization, was performed. In comparison with the annual optimization, the monthly optimization reduces the number of hours out of comfort in more than 19 % and the energy consumption of the heat pump in 1.5 %.

Finally, a sensitivity analysis of the system by varying the inlet water temperature in the absorber, the inlet water temperature in the regenerator, and minimum LiCl mass concentration at the entrance of the absorber was done. According to the results obtained, inlet water temperatures affect more to the system performance than LiCl mass concentration. In this sense, when the inlet water temperature in the regenerator is higher and the inlet water temperature in the absorber is lower; the number of hours out of comfort is lower, the air cooling in the absorber is higher, the chilled water energy provided to the absorber and the cooling coil is higher, the hot water energy required by the regenerator and the coil is higher, and the energy consumption of the heat pump is higher too.

Resumen

La demanda energética de climatización se ha incrementado en los últimos años debido a que el calentamiento global ha aumentado las cargas de refrigeración durante un mayor periodo de tiempo. Además, el nivel de vida y los estándares de confort han aumentado, lo que hace que los sistemas de climatización estén cada vez más presentes no sólo en los países desarrollados, sino también en los países en desarrollo, donde la deshumectación del aire tiene, a menudo, un mayor impacto que la carga sensible.

Comparados con otros sistemas desecantes, los sistemas desecantes híbridos son más eficientes cuando la humedad y la temperatura son controladas de manera separada. Además, los sistemas de desecantes líquidos ofrecen atractivos beneficios cuando se comparan con los sistemas desecantes sólidos en términos de eficiencia energética, acumulación energética y temperaturas de funcionamiento. Sin embargo, los sistemas desecantes líquidos no se han utilizado demasiado, debido principalmente, a la corrosión que producen los materiales desecantes líquidos convencionales en la mayoría de metales, con la excepción del titanio y del tántalo, que son materiales muy caros.

El principal objetivo de esta tesis es realizar un estudio teórico y experimental de un sistema híbrido basado en desecantes líquidos que utiliza materiales no corrosibles y económicamente viables, manteniendo unas buenas prestaciones del sistema y consiguiendo una alta eficiencia energética. La tesis se centra en los principales elementos de un sistema de desecantes líquidos: el absorbedor y el regenerador.

Esta tesis se ha desarrollado bajo un Proyecto Europeo del Seventh Framework Programme (FP7) cuyo acrónimo es nanoCOOL. El principal objetivo del proyecto era desarrollar, fabricar y operar un sistema híbrido de desecantes líquidos innovador. Por tanto, algunos de los resultados que se han conseguido en los estudios llevados a cabo en esta tesis se han utilizado para la el desarrollo de este sistema. Además, se han utilizado los resultados experimentales del equipo demostrativo desarrollado en el Proyecto nanoCOOL, cuando éste operaba en una aplicación real en Taiwán, para la evaluación de sus prestaciones.

Como primera etapa en esta tesis se presenta el estado del arte de la tecnología de desecantes líquidos, que evalúa los principales materiales desecantes líquidos, los distintos contactores de aire-solución disponibles y distintas configuraciones de estos sistemas. De este estudio se concluye que el LiCl-H_2O es el material desecante líquido más propicio, debido, principalmente, a su baja presión de vapor. Además, se han elegido contactores de aire-solución de película descendente con tubos horizontales porque presentan una buena transferencia de calor y de masa sin ir en perjuicio de las pérdidas de presión en el lado del aire. Asimismo, se ha decidido que el sistema de desecantes líquidos vaya acoplado una bomba de calor de compresión de vapor, porque ésta puede suministrar el frío y el calor al absorbedor y al regenerador, respectivamente, empleando para ello la misma fuente de energía.

Debido a que el LiCl-H_2O es un material muy corrosivo, se han ensayado tubos de polipropileno, de polietileno de alta densidad, de polipropileno de baja densidad, de poliamida y de grafito. Además, como el LiCl-H_2O tiene una alta tensión superficial, la mojabilidad de los tubos es un factor determinante en la transferencia de calor y de masa en los contactores de aire-solución. Por esta razón, la mojabilidad de estos tubos se ha evaluado para que sea una de las variables a tener en cuenta para la selección del material de los tubos a emplear en el sistema híbrido completo. Algunos de los tubos ensayados contienen un tratamiento superficial de plasma que mejora su mojabilidad cuando el LiCl-H_2O fluye alrededor de ellos. Como resultado de este estudio, se ha seleccionado al polipropileno que contiene tratamiento superficial de plasma como el mejor material de los probados para su uso en el sistema híbrido. Además, para cada material ensayado, se han obtenido correlaciones que determinan el caudal mínimo de desecante líquido necesario para mojar los tubos completamente.

Posteriormente, dos contactores de aire-solución de pequeño tamaño se han comparado para verificar que el polipropileno con tratamiento de plasma superficial tiene mejores prestaciones que el polipropileno

estándar, cuando se utiliza como absorbedor de un sistema de desecantes líquidos. Se han conseguido mejores prestaciones en el enfriamiento del aire (el 29 %), en el calor extraído (el 17 %), en el coeficiente global de transferencia de calor entre el agua y la película de desecante (hasta el 54 %) y en la deshumectación del aire (el 20 %) en el contactor de aire-solución que contiene tubos de polipropileno con tratamiento superficial.

Después de la selección del material, el sistema híbrido basado en desecantes líquidos se ha diseñado y dimensionado. El sistema ha sido diseñado para operar en dos vestuarios de una piscina de Taipei (Taiwan). Una vez diseñado y construido, y antes de ser enviado a Taiwan, el sistema fue montado de manera completa por primera vez, y puesto a punto en la Universitat Rovira i Virgili en Tarragona (España).

Las prestaciones del sistema se han evaluado durante su operación en Tarragona y en Taipei. De este modo, dos absorbedores con distintas disposiciones de tubo (cuadrada y triangular) y un regenerador con disposición de tubo triangular, se han podido analizar experimentalmente. Las temperaturas del desecante líquido a la entrada del absorbedor y el regenerador son las variables que más afectan en la deshumectación del aire y en la regeneración de desecante, respectivamente. Esto corrobora que el valor del coeficiente de transferencia de calor en el absorbedor y en el regenerador es de una gran importancia en las prestaciones de ambos. Por otro lado, aunque se esperaba conseguir mejores prestaciones en el absorbedor con disposición triangular, es el de disposición cuadrada el que ha conseguido una mayor deshumectación y un mayor enfriamiento del aire. De esta manera, el coeficiente global de transferencia de calor en el absorbedor con disposición cuadrada es un 20 % mayor, y el coeficiente global de transferencia de calor es un 9 % mayor que el de disposición triangular. Asimismo, se han obtenido correlaciones para el coeficiente de transferencia de calor tubo-solución y para el coeficiente de transferencia de masa en el lado del aire en función de la velocidad del aire a su paso por el absorbedor y el regenerador.

Por otro lado, las prestaciones del sistema híbrido al completo también han sido evaluadas. La capacidad de enfriamiento máxima del sistema medida en condiciones de operación reales es de 34 kW y la máxima dehumectación obtenida es de casi 0.012 kg_w/kg_a. En términos de COP del sistema, éste se ve afectado principalmente por la demanda de frío y la temperatura del agua caliente: menores temperaturas de agua caliente y mayores demandas de frío aumentan el COP del sistema. Más aún, el sistema presenta un control adecuado de la temperatura y la humedad del aire de los vestuarios a diferentes condiciones de operación.

También, el sistema ha sido modelado para ser simulado de manera dinámica. Para ello, se han empleado las correlaciones para los coeficientes de transferencia de calor y de masa obtenidos a partir de los datos medidos del sistema. Los resultados obtenidos de la simulación dinámica se han comparado con los datos experimentales del prototipo, arrojando sólo pequeñas desviaciones entre ambos.

Para optimizar las prestaciones anuales del sistema híbrido, se ha llevado a cabo una optimización multi-objetivo, utilizando el modelo de simulación dinámica desarrollado, sobre tres variables operaciones del sistema: la temperatura del agua a la entrada del absorbedor y el regenerador, y la concentración másica mínima de LiCl a la entrada del absorbedor; y dos estrategias de control. Se han escogido dos objetivos a minimizar: el número de horas fuera de condiciones de confort en el local y la energía consumida por la bomba de calor. Según los resultados obtenidos, la mejor estrategia de control es la que hace actuar al regenerador en función de la concentración de desecante a la entrada del absorbedor. Además, la temperatura a la entrada del absorbedor debe ser 12 °C, la temperatura de entrada al regenerador de 51 °C y la concentración másica mínima de LiCl de 32.5 % para conseguir la operación óptima del sistema durante todo el año. Asimismo, se ha realizado una optimización mensual del sistema de la misma manera que la optimización anual. Comparada con la optimización anual, la optimización mensual reduce el número de horas fuera de condiciones de confort en más del 19 % y la energía consumida por la bomba de calor es un 1.5 % menor.

Por último, se ha realizado un análisis de sensibilidad del sistema híbrido en el que se varían las temperaturas del agua a la entrada del absorbedor y a la entrada del regenerador, y la concentración

másica de LiCl mínima a la entrada del absorbedor. Según los resultados obtenidos de las simulaciones dinámicas, las temperaturas del agua a la entrada del absorbedor y el regenerador afectan en mayor medida a las prestaciones totales del sistema que la concentración másica mínima de LiCl. En este sentido, cuando la temperatura del agua en el regenerador es más alta y la temperatura del agua a la entrada del absorbedor es más baja, se disminuye el número de horas fuera de condiciones de confort y se aumenta: el frío aportado por el absorbedor al aire, el frío aportado por la bomba de calor al absorbedor y a la batería de frío, el calor aportado al regenerador y a la batería de calor y la energía consumida por la bomba de calor.

Resumen

Resum

La demanda energètica de climatització s'ha incrementat en els últims anys a causa que l'escalfament global ha augmentat les càrregues de refrigeració durant un major període de temps. A més, el nivell de vida i els estàndards de confort han augmentat, la qual cosa fa que els sistemes de climatització estiguin cada vegada més presents, no només als països desenvolupats, sinó també als països en desenvolupament, on la deshumidificació de l'aire té sovint, un major impacte que la càrrega sensible.

Comparats amb altres sistemes dessecants, els sistemes dessecants híbrids són més eficients quan la humitat i la temperatura són controlades de manera separada. A més, els sistemes de dessecants líquids ofereixen atractius beneficis en termes d'eficiència energètica, acumulació energètica i temperatures de funcionament en comparació amb els sistemes dessecants sòlids. No obstant això, els sistemes dessecants líquids no s'han utilitzat massa, principalment a causa de la corrosió que produeixen els materials líquids convencionals en la majoria de metalls, amb l'excepció del titani i del tàntal que són materials molt cars.

El principal objectiu d'aquesta tesi és realitzar un estudi teòric i experimental d'un sistema híbrid basat en dessecants líquids que utilitza materials no corrosibles i econòmicament viables, mantenint unes bones prestacions del sistema i aconseguint una alta eficiència energètica. La tesi se centra en els principals elements d'un sistema de dessecants líquids: l'absorbidor i el regenerador.

Aquesta tesi s'ha desenvolupat dins el marc del Projecte Europeu del Seventh Framework Programme (FP7) l'acrònim del qual és nanoCOOL. El principal objectiu del projecte era desenvolupar, fabricar i operar un innovador sistema híbrid de dessecants líquids. Per tant, alguns dels resultats que s'han aconseguit en els estudis duts a terme en aquesta tesi, s'han utilitzat per al desenvolupament d'aquest sistema. També s'han utilitzat els resultats experimentals de l'equip demostratiu desenvolupat en el Projecte nanoCOOL, quan aquest operava en una aplicació real a Taiwan, per a l'avaluació de les seves prestacions.

Com a primera etapa en aquesta tesi es presenta l'estat de l'art de la tecnologia de dessecants líquids, que avalua els principals materials dessecants líquids, els diferents contactors d'aire-solució disponibles i diferents configuracions d'aquests sistemes. D'aquest estudi es conclou que el LiCl-H_2O és el material dessecant líquid més propici, gràcies a la seva baixa pressió de vapor. A més, s'han triat contactors d'aire-solució de pel·lícula descendent amb tubs horitzontals perquè presenten una bona transferència de calor i de massa sense perjudici de les pèrdues de pressió en el costat de l'aire. Així mateix, s'ha decidit que el sistema de dessecants líquids vagi acoblat a una bomba de calor de compressió de vapor, perquè pot subministrar el fred i la calor a l'absorbidor i al regenerador, respectivament, emprant per a això la mateixa font d'energia.

A causa que el LiCl-H_2O és un material molt corrosiu, s'han assajat tubs de polipropilè, de polietilè d'alta densitat, de polipropilè de baixa densitat, de poliamida i de grafit. A més, com el LiCl-H_2O té una alta tensió superficial, la mullabilitat dels tubs és un factor determinant en la transferència de calor i de massa en els contactors d'aire-solució. Per aquesta raó, la mullabilitat d'aquests tubs s'ha avaluat perquè sigui una de les variables a tenir en compte per a la selecció del material dels tubs a emprar en el sistema híbrid complet. Alguns dels tubs assajats tenen un tractament superficial de plasma que millora la seva mullabilitat quan el LiCl-H_2O flueix al voltant d'ells. Com a resultat d'aquest estudi s'ha seleccionat el polipropilè que conté tractament superficial de plasma com el millor material dels provats. A més, per a cada material assajat, s'han obtingut correlacions que determinen el cabal mínim de dessecant líquid necessari per mullar els tubs completament.

Posteriorment, dos contactors d'aire-solució de petita escala s'han comparat per verificar que el polipropilè amb tractament de plasma superficial té millors prestacions que el polipropilè estàndard, quan s'utilitza com a absorbidor d'un sistema de dessecants líquids. S'han aconseguit millors prestacions en el refredament de l'aire (sobre el 29 %), en la calor extreta (sobre el 17 %), en el coeficient global de transferència de calor

entre l'aigua i la pel·lícula de dessecant (fins al 54 %) i en la deshumidificació de l'aire (sobre el 20 %) en el contactor d'aire-solució que conté tubs de polipropilè amb tractament superficial.

Després de la selecció del material, el sistema híbrid basat en dessecants líquids s'ha dissenyat i dimensionament. El sistema s'ha dissenyat per operar en dos vestuaris d'una piscina de Taipei (Taiwan). Una vegada dissenyat i construït, i abans de ser enviat a Taiwan, el sistema va ser muntat de manera completa per primera vegada, posat punt i assajat a la Universitat Rovira i Virgili a Tarragona (Espanya).

Les prestacions del sistema s'han avaluat durant la seva operació a Tarragona i en Taipei. D'aquesta manera, dos absorbidors amb diferents disposicions de tub (quadrada i triangular) i un regenerador amb disposició de tub triangular, s'han pogut analitzar experimentalment. Les temperatures del dessecant líquid a l'entrada de l'absorbidor i el regenerador són les variables que més afecten en la deshumidificació de l'aire i a la regeneració del dessecant, respectivament. Això mostra que el valor del coeficient de transferència de calor en l'absorbidor i en el regenerador és d'una gran importància en les prestacions de tots dos. D'altra banda, encara que s'esperava aconseguir millors prestacions en l'absorbidor amb disposició triangular, és el de disposició quadrada el que ha aconseguit una major deshumidificació i un major refredament de l'aire. D'aquesta manera, el coeficient global de transferència de calor en l'absorbidor amb disposició quadrada és un 20 % major, i el coeficient global de transferència de calor és un 9 % major que el de disposició triangular. També s'han obtingut correlacions per al coeficient de transferència de calor tub-solució i per al coeficient de transferència de massa en el costat de l'aire en funció de la velocitat de l'aire al seu pas per l'absorbidor i el regenerador.

D'altra banda, les prestacions del sistema híbrid al complet també han estat avaluades. La capacitat de refredament màxima del sistema mesurada en condicions d'operació reals és de 34 kW i la màxima deshumidificació obtinguda és de gairebé 0.012 kg_w/kg_a. En termes de COP del sistema, aquest es veu afectat principalment per la demanda de fred i la temperatura de l'aigua calenta: menors temperatures d'aigua calenta i majors demandes de fred augmenten el COP del sistema. A més, el sistema presenta un control adient de la temperatura i la humitat de l'aire dels vestuaris a diferents condicions d'operació.

També, el sistema ha estat modelat per ser simulat de manera dinàmica, emprat les correlacions per als coeficients de transferència de calor i de massa obtinguts a partir de les dades mesurades del sistema. Els resultats obtinguts de la simulació dinàmica s'han comparat amb les dades experimentals del prototip, obtenint només petites desviacions entre tots dos.

Per optimitzar les prestacions anuals del sistema híbrid, s'ha dut a terme una optimització multi objectiu, utilitzant el model de simulació dinàmica desenvolupat, sobre tres variables operacionals del sistema: la temperatura de l'aigua a l'entrada de l'absorbidor i el regenerador, i la concentració màssica mínima de LiCl a l'entrada de l'absorbidor; i també dues estratègies de control. S'han escollit dos objectius a minimitzar: el nombre d'hores fora de condicions de confort en el local i l'energia consumida per la bomba de calor. Segons els resultats obtinguts, la millor estratègia de control és la que fa actuar al regenerador en funció de la concentració de dessecant a l'entrada de l'absorbidor. A més, la temperatura a l'entrada de l'absorbidor ha de ser 12 °C, la temperatura d'entrada al regenerador de 51 °C i la concentració màssica mínima de LiCl de 32.5 % per aconseguir l'operació òptima del sistema durant tot l'any. Posteriorment, s'ha realitzat una optimització mensual del sistema de la mateixa manera que l'optimització anual. Comparada amb l'optimització anual, l'optimització mensual redueix el nombre d'hores fora de condicions de confort en més del 19 % i l'energia consumida per la bomba de calor és un 1.5 % menor.

Finalment, s'ha realitzat una anàlisi de sensibilitat del sistema híbrid en el qual es varien les temperatures de l'aigua a l'entrada de l'absorbidor i a l'entrada del regenerador, i la concentració màssica de LiCl mínima a l'entrada de l'absorbidor. Segons els resultats obtinguts de les simulacions dinàmiques, les temperatures de l'aigua a l'entrada de l'absorbidor i el regenerador afecten en major mesura a les prestacions totals del sistema que la concentració màssica mínima de LiCl. En aquest sentit, quan la temperatura de l'aigua en el regenerador és més alta i la temperatura de l'aigua a l'entrada de l'absorbidor és més baixa, disminueix el nombre d'hores fora de condicions de confort i augmenta: el fred aportat per l'absorbidor a l'aire, el fred

aportat per la bomba de calor a l'absorbidor i a la bateria de fred, la calor aportada al regenerador i a la bateria de calor i finalment l'energia consumida per la bomba de calor.

Contributions by the author

Contributions by the author

Articles in scientific journals

- Khaled Gommed, Gershon Grossman, **Juan Prieto**, Jordi Ortiga, Alberto Coronas (2015). Experimental comparison between internally and externally cooled air-solution contactors, *Science and Technology for the Built Environment,* 21:3, 267-274. ISSN: 2374-4731.
- Adirana Coca-Ortegón, **Juan Prieto**, Alberto Coronas (2016). Modelling and dynamic simulation of a hybrid liquid desiccant system regenerated with solar energy, *Applied Thermal Engineering*, 97, 109–117. ISSN: 1359-4311
- **Juan Prieto**, Jordi Ortiga, Alberto Coronas (2016). Hydrodynamic study of falling-film on non-metallic horizontal tubes working with LiCl-H_2O solution, *International Journal of Heat and Mass Transfer.* (in progress).
- **Juan Prieto,** Antonio Atienza, Jordi Ortiga, Alberto Coronas (2016). Modeling, validation and dynamic simulation of a hybrid liquid desiccant system, *Applied Thermal Engineering* (in progress).
- **Juan Prieto,** Jordi Ortiga, Laura Alonso, Xabier Peña, Khaled Gommed, Gershon Grossman, Yi-Jiun Peter Lin, Alberto Coronas. Experimental performance of a hybrid liquid desiccant system, *International Journal of Refrigeration* (in progress).
- **Juan Prieto,** Jordi Ortiga, Alberto Coronas. Experimental evaluation and modelling of non-adiabatic air solution contactors of a hybrid liquid desiccant system made of polypropylene with improved surface, *International Journal of Heat and Mass Transfer* (in progress).

Papers in Congresses, Conferences, Seminars, Workshops and Symposia

- **Juan Prieto**, Jordi Ortiga, Alberto Coronas. Performance analysis of a hybrid liquid desiccant system for air-conditioning applications, *43rd Congress KGH*, Belgrade, Serbia, 5-7 December, 2012 (Oral presentation).
- **Juan Prieto,** Jordi Ortiga, Alberto Coronas. Modelización de un sistema de desecantes líquidos integrado en una unidad de tratamiento de aire. *8º Congreso Nacional de Ingeniería Termodinámica*, Burgos, España, 19-21 de junio de 2013 (Oral presentation).
- **Juan Prieto,** Jordi Ortiga, Alberto Coronas, Khaled Gommed, Gershon Grossman. State-of-the-art of air-liquid contactors for liquid desiccant systems in air-conditioning applications. *EUROTHERM Seminar nº 100. International Workshop on New Working Fluids for Absorption Heat Pumps and Refrigeration Systems,* Tarragona, Spain, July, 2013 (Oral presentation).
- Khaled Gommed, Gershon Grossman, **Juan Prieto**, Jordi Ortiga, Alberto Coronas. Experimental Comparison between Internally and Externally Cooled Air-Solution Contactors. *International Sorption Heat Pump Conference (ISHPC 2014),* Maryland, USA, March 31 – April 2, 2014 (Oral presentation). ISBN: 9781632665966.
- **Juan Prieto**, Jordi Ortiga, Alberto Coronas. Efecto de la mejora de la mojabilidad en un absorbedor de película descendente para un sistema con desecantes líquidos. *VII Congreso Ibérico de Ciencias y Técnicas del Frío (CYTEF),* Tarragona, España, 18-20 de junio de 2014 (Oral presentation). ISBN: 978-84-617-1304-2.
- **Juan Prieto**, Jordi Ortiga, Alberto Coronas. Sensitivity analysis of the operational variables of a liquid desiccant system. *VII Congreso Ibérico de Ciencias y Técnicas del Frío (CYTEF),* Tarragona, España, 18-20 de junio de 2014 (Oral presentation). ISBN: 978-84-617-1304-2.
- Adriana Coca Ortegón, **Juan Prieto**, Alberto Coronas. Dynamic Simulation Methodology of a Hybrid Liquid Desiccant System (HLDS) Regenerated with Solar Energy to Control Humidity and Temperature Separately for Air Conditioning Applications. *International Conference on Polygeneration (ICP 2015)*, Chennai, India, 18-20 February, 2015 (Poster presentation).

- **Juan Prieto**, Jordi Ortiga, Alberto Coronas. Theoretical and experimental study of a dehumidification system based on liquid desiccants for air conditioning applications. *Jornadas Hispano-Brasileñas de sostenibilidad energética en edificios y procesos.* Tarragona, España, Julio, 2015 (Oral presentation).
- Laura Alonso, Xabier Peña, Carol Pascual, **Juan Prieto**, Jordi Ortiga, Khaled Gommed. Design, simulation and testing of a hybrid liquid desiccant for the independent control of temperature and humidity. *CISBAT 2015,* Lausanne, Switzerland, 9-11 September, 2015. ISBN: 978-2-9701052-0-6.
- **Juan Prieto**, Jordi Ortiga, Alberto Coronas. "New Developments on Liquid Desiccant Systems for Air Conditioning Applications". 4th National Conference on Refrigeration and Air Conditioning (NCRAC-2015), Chennai, India, Octubre 2015 (Oral presentation).
- **Juan Prieto**, Jordi Ortiga, Alberto Coronas. A new hybrid liquid desiccant system with improved plastic tubes. *VIII Congreso Ibérico de Ciencias y Técnicas del Frío (CYTEF),* Coimbra, Portugal, 3-6 de mayo de 2016 (Oral presentation). ISBN: 978-989-99080-4-8.
- **Juan Prieto,** Jordi Ortiga, Xabier Peña, Laura Alonso, Khaled Gommed, Gershon Grossman, Alberto Coronas. Experimental Analysis of a Hybrid Liquid Desiccant System with Non-Adiabatic Air-Solution Contactors at Different Working Conditions. *12th REHVA World Congress CLIMA2016*, Aalborg, Denmark, 22-25 May, 2016 (Oral presentation).
- **Juan Prieto,** Jordi Ortiga, Alberto Coronas. Experimental comparison of two small-scale air-solution contactors for liquid desiccant systems made of polypropylene. *IVth International Sumposium on Innovative Materials for Processes in Energy Systems IMPRES 2016*, Taormina, Sicily, Italy, 23-26 October, 2016 (Accepted).

Other contributions

- Khaled Mohamed Ramadan, **Juan Prieto,** Alberto Coronas. Modeling and Dynamic Simulation of an Off-Grid PV Cooling System for an Office Building in Different Climate Locations. *VIII Congreso Ibérico de Ciencias y Técnicas del Frío (CYTEF),* Coimbra, Portugal, 3-6 de mayo de 2016 (Poster presentation). ISBN: 978-989-99080-4-8.
- Adriana Coca-Ortegón, **Juan Prieto**, Xavier Felipe, Alberto Coronas. Evaluación de estrategias para minimizar las emisiones de co2 de un sistema solar de refrigeración y producción de calor aplicado a una industria láctea de pequeño tamaño *VIII Congreso Ibérico de Ciencias y Técnicas del Frío (CYTEF),* Coimbra, Portugal, 3-6 de mayo de 2016 (Oral presentation). ISBN: 978-989-99080-4-8.
- K. Gommed, G. Grossman, **J. Prieto**, J. Ortiga, A. Coronas. Performance analysis of different absorber configurations for liquid dessicant systems. *VII Congreso Ibérico de Ciencias y Técnicas del Frío (CYTEF),* Tarragona, España, 18-20 de junio de 2014 (Oral presentation). ISBN: 978-84-617-1304-2.
- L. Alonso, X. Peña, **J. Prieto**, K. Gommed, G. Grossman. Design and simulation of a hybrid liquid desiccant system for a case study in Taiwan. *VII Congreso Ibérico de Ciencias y Técnicas del Frío (CYTEF),* Tarragona, España, 18-20 de junio de 2014 (Oral presentation). ISBN: 978-84-617-1304-2.

Participation in projects

- Nanocool: An Energy Efficient Air Conditioning system with Temperature and Humidity independent control based on the combination of a Liquid Desiccant Cycle with adapted conventional air cooling system. Seventh Framework Programme. THEME [EeB.NMP.2012-4] [Nanotechnology based approaches to increase the performance of HVAC systems]. Grant agreement no: 314701. Principal investigator at Universitat Rovira i Virgili: Alberto Coronas (September 2012- February 2016).

Internships

- Technion, Israel Institute of Technology, Faculty of Mechanical Engineering (Israel).
  Advisor: Prof. Gershon Grossman.
  Period: June 2013 – September 2013.
  Topic: Experimental study on air-solution contactors for liquid desiccant systems.
  Scolarship: URV – Grants for short stays in foreign countries (AEE2013).

Contributions by the author

LIST OF CONTENTS

LIST OF FIGURES

LIST OF TABLES

List of contents

Nomenclature

A	Contact surface (m^2)
Ar	Archimedes number (-)
C	Heat capacity rate (kW/°C)
Ca	Capillarity constant, (m)
c_p	Specific heat (kJ/kg·K)
COP	Coefficient of performance (-)
d	Diameter (m)
D	Mass diffusivity (m^2/s)
F	Correction factor for ΔT_{LM} method (-)
g	Gravity acceleration (9.81 m/s^2)
Ga	Galileo number (-)
Gz	Graetz number (-)
h	Enthalpy (kJ/kg)
H	Relative humidity (%)
HC	Heat capacity ratio (-)
Hg	height (m)
k	Thermal conductivity (kW/m·K)
L	Length (m)
Le	Lewis number (-)
m	Mass flow rate (kg/s)
M	Mass (kg)
n	Constant (-)
N	Constant used for correlations (-)
NTU	Number of heat transfer units (-)
Nu	Nusselt number (-)
Oh	Ohnesorge number (-)
p	Pressure (kPa)
pitch	Tube pitch (-)
P	Constant used for correlations (-)
Pr	Prandtl number (-)
Q	Heat transfer (kW)
r	Roughness factor (-)
R	Thermal resistance (m^2°C/kW)
R^2	Coefficient of determination (-)
Re	Reynolds number (-)
s	Tube distance (m)
Sc	Schmidt number (-)
Sh	Sherwood number (-)
split	Split solution ratio (-)
t	Time (s)
T	Temperature (°C)
UA	Global heat transfer coefficient (kW/°C)
v	Volumetric flow rate (l/h)
V	Velocity (m/s)
W	Humidity ratio (kg_w/kg_a)
Wd	Width (m)
We	Webber number
X	Lithium Chloride mass fraction (%)

Greeks

α	Convective heat transfer coefficient (kW/m^2·K)
β	Surface tension (N/m)
δ_s	Film thickness (m)
ε	Friction coefficient of tube (-)
γ	Interfacial tension energy
θ	Contact angle (rad)
λ	Wavelength (m)
ρ	Density (kg/m^3)
μ	Dynamic viscosity (N-s/m^2)
v	Cinematic viscosity (m^2/s)
σ	Mass transfer coefficient (kg/m^2·s)
Γ	Liquid mass flow rate per unit of length of tube (kg/s-m)
Λ	Diameter parameter (-)
ΔΩ	Dehumidified water ratio (kg/m^2·s)
ΔT_{LM}	Logarithmic mean temperature difference (°C)

Subscripts

a	Air
abs	Absorber
ad	Air duct
amb	Ambient conditions
b	Bottom
cp	Change phase
c	Critical
cc	Cooling coil
ccf	Counter-current flow
co	Cold fluid
cond	Condenser of the heat pump
comp	Compressors of the heat pump
eq	Air-solution equilibrium conditions
evap	Evaporator of the heat pump
Gl	Global
h	Hot fluid
hc	Heating coil
HX	Heat exchanger
HP	Heat pump
i	Internal
in	Inlet
I	Interface
IS	Solution-interface
lat	Latent
LDS	Liquid desiccant subsystem
LV	Liquid to vapour
max	Maximum
min	Minimum

o	External
out	Outlet
p	Passes
r	Roughness
real	Real values from measurements
rec	Recirculated
reg	Regenerator
room	Room conditions
s	Solution film
sen	Sensible
set	Set point conditions
sup	Supply conditions
SL	Solid to liquid
SV	Solid to vapour
t	Tube
T	Dangerous
Tank	Tank
top	Top
vent	Ventilation

Chapter 1. Introduction, objectives and methodological approach

1.1. Introduction

Recently, the energy demand for air conditioning is rising around the world because of two main reasons: the global warming issue, which is already a fact, is making that cooling loads are becoming larger during longer periods; and the standard of living and the demand of comfort are increasing. In this sense, left graph of Figure 1.1 shows that increasing of cooled-floor area is happening not only in the Southern countries of Europe, but also in the Northern countries. Moreover, according to the right graph of Figure 1.1, air-conditioning market on the Northern countries of the European Union is having a higher impact with respect to the total market.

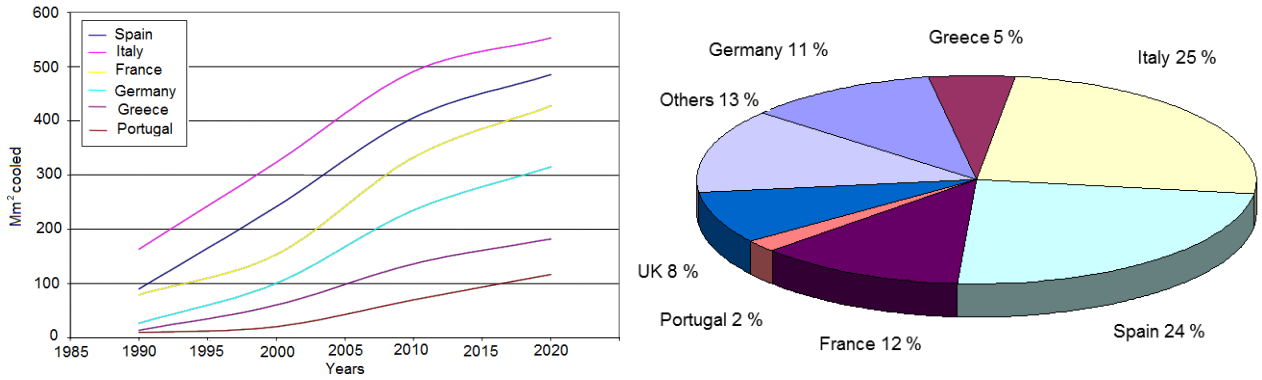

Figure 1.1. Evolution of cooled-floor area from 1990 to 2020 at the national level of the EU (left), and air-conditioning market on the EU in 2005 (right, adapted from [1]).

On the other hand, most of the developing countries are located in tropical zones. In these countries, both, sales (left graph of Figure 1.2) and electrical consumption are becoming the highest in the world, and expectations of electrical consumption do not tend to stop in the following 15 years (see right graph of Figure 1.2). In these regions, humidity has often a higher importance than temperature and, therefore, dehumidification is very important in order to maintain comfort requirements inside buildings.

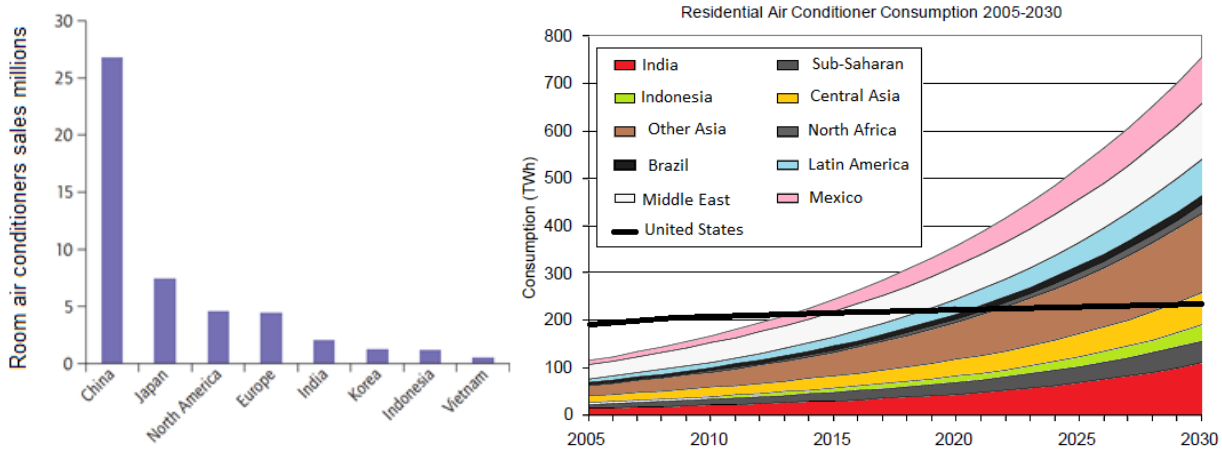

Figure 1.2. Sales of residential air conditioners in 2008-2009 by country (left) (adapted from [2]). Projection of Base Case Residential Air Conditioner Consumption by Region 2000-2030 (right) (adapted from [3]).

Regarding the European standards, they are claiming for different air conditioning practices than American standards in order to increase the air quality [1]. According to these standards, central air conditioners should operate with minimum air circulation, providing the maximum dryness and achieving a good

independent control of humidity and temperature. In order to implement these new practices, the required method tends to use radiant cooling to handle sensible load, and high dehumidification with low-velocity distribution to handle the latent load.

In applications where dehumidification is important, desiccant systems are a good alternative to conventional air conditioners, because they open new possibilities in air conditioning technologies due to the following aspects:

- Use of low temperature heat sources, such as solar or waste thermal energy, in order to regenerate the system, instead of electrical power.
- Control of the humidity of the air independently of the temperature control.
- Achieve very low levels of humidity.
- Can be employed in combination with vapor compression systems offering a more efficient way to control separately humidity and temperature.
- Can operate without using greenhouse gases because conventional refrigerants are not required.

1.1.1. Desiccant systems

Depending on how the moist air is processed from ambient conditions to supply air conditions, the desiccant systems can be classified as:

- Conventional air conditioners.
- Desiccant systems combined with evaporation cooling.
- Hybrid desiccant systems.

1.1.1.1. Conventional air conditioners

Figure 1.3 illustrates the required components when a conventional air conditioner has to control temperature and humidity of moist air. In this case, air, which is at mixing conditions between room and ambient conditions, is cooled down through a cooling coil. A heating coil is after required in order to achieve the supply air temperature.

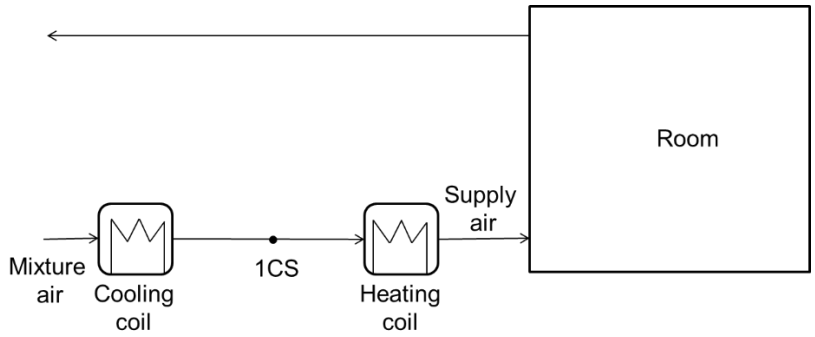

Figure 1.3. Required components when a conventional air conditioner has to control temperature and humidity of moist air.

In conventional air conditioners, moist air must be cooled down below its dew point in order to dehumidify the air up to the required supply humidity ratio (point 1CS in Figure 1.4). The supply humidity ratio depends on the average water temperature: the lower average water temperature, the lower humidity ratio. Moreover, water temperature must be below the dew point temperature. Therefore, if very low humidity ratios are required, the chiller has to provide very cold water, affecting to the COP of it. Typically, the moist air must be post heated in order to achieve the supply air temperature. Both, cooling and heating can be provided by the evaporator and the condenser of the same heat pump.

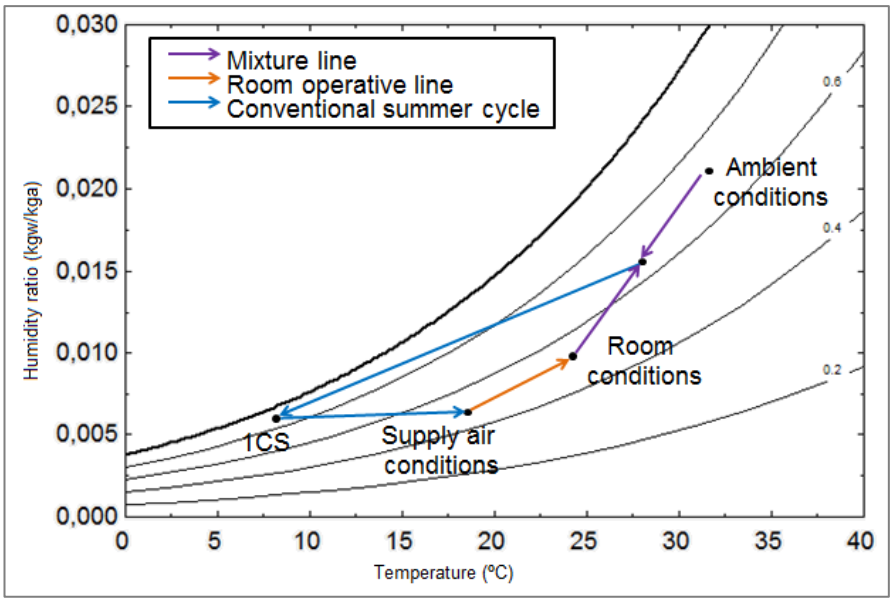

Figure 1.4. Moist air process in conventional air conditioners.

1.1.1.2. Desiccant systems combined with evaporative cooling

Figure 1.5 illustrates the required components when a desiccant system combined with evaporative cooling has to control temperature and humidity of moist air. In this case, air, which is at ambient conditions, is dehumidified firstly through a dehumidifier of the desiccant system. Then, a heat recuperator cools the air down. Finally, an evaporative cooler permits achieving the supply air humidity ratio and temperature. If the evaporative cooling is not enough to reach supply air temperature, an additional cooling coil can be added either before or after the evaporative cooler. At the same time, an additional evaporative cooler and a heating coil are required to regenerate the desiccant with the return air.

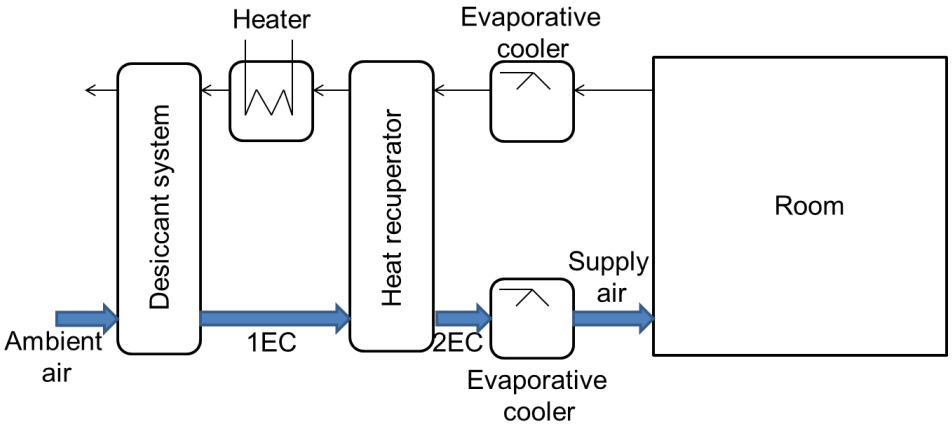

Figure 1.5. Control of humidity and temperature with desiccant system and evaporative cooling.

In desiccant systems combined with evaporative cooling, moist air is dehumidified by direct contact with the desiccant material (liquid or solid). The moist air conditions after the dehumidifier mostly depend on the desiccant temperature and water content. In these systems, the moist air typically follows the isenthalpic line up to point 1EC (see Figure 1.6). The outlet air humidity in this point must be low enough in order to provide the air the capability of being cooled with the evaporative cooler. After the dehumidifier, a heat recuperator pre-cools the air up to point 2EC. Finally, a humidifier cools the air down by an evaporative cooling process. Only heating, to regenerate the desiccant, and water, for the evaporative coolers, are required in this system.

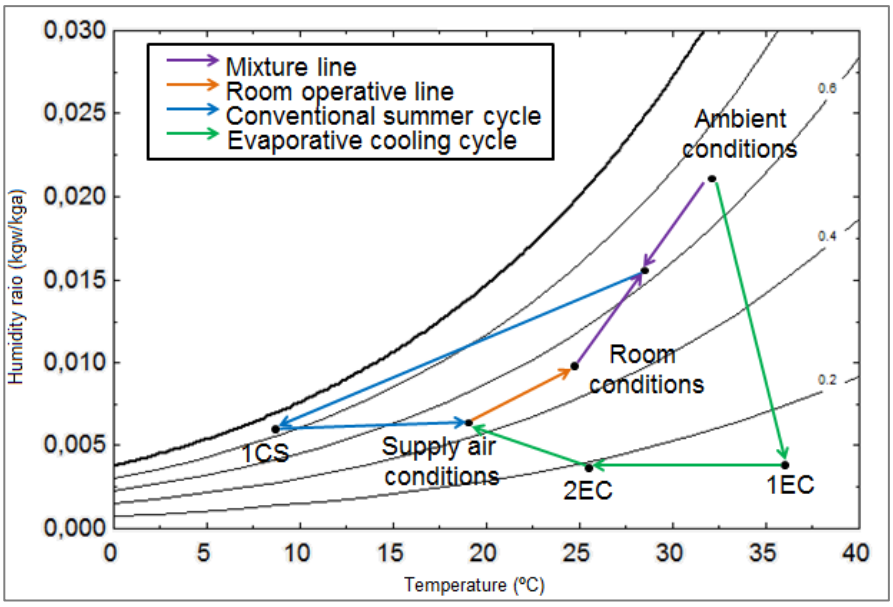

Figure 1.6. Supply moist air process in desiccant systems combined with evaporative cooling.

1.1.1.3. Hybrid desiccant systems

In the combination of desiccant systems with vapour compression systems, which is called hybrid desiccant systems, the desiccant system handles the latent cooling load, and a vapour compression or absorption refrigeration system handles the sensible cooling load. Figure 1.7 illustrates the required components of a hybrid desiccant system. In this case, air, which is at mixing conditions between room and ambient conditions, is firstly dehumidified through a dehumidifier of the desiccant system. After the dehumidification, the moist air is cooled down through a cooling coil. The desiccant material is regenerated by either using air at room conditions or at ambient conditions.

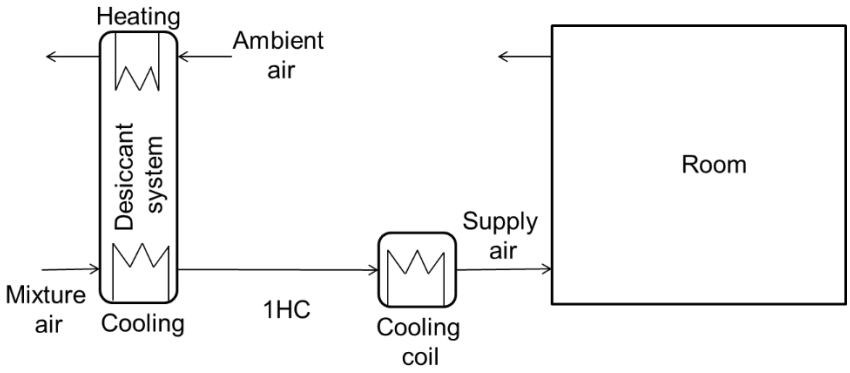

Figure 1.7. Control of humidity and temperature with a hybrid desiccant system.

Moist air at mixing conditions between room and ambient conditions is dehumidified, without achieving the dew point of the air, by direct contact with the desiccant material that can be cooled. The air temperature and the humidity ratio at the outlet of the dehumidifier (point 1HC in Figure 1.8) mostly depend on the temperature and water content of the desiccant material. Therefore, supply air humidity ratio may be controlled by the desiccant conditions. After being dehumidified, moist air is typically cooled in order to achieve the supply air temperature. Heating, to regenerate the desiccant, and cooling, to dehumidified and cool the moist air is required in these systems.

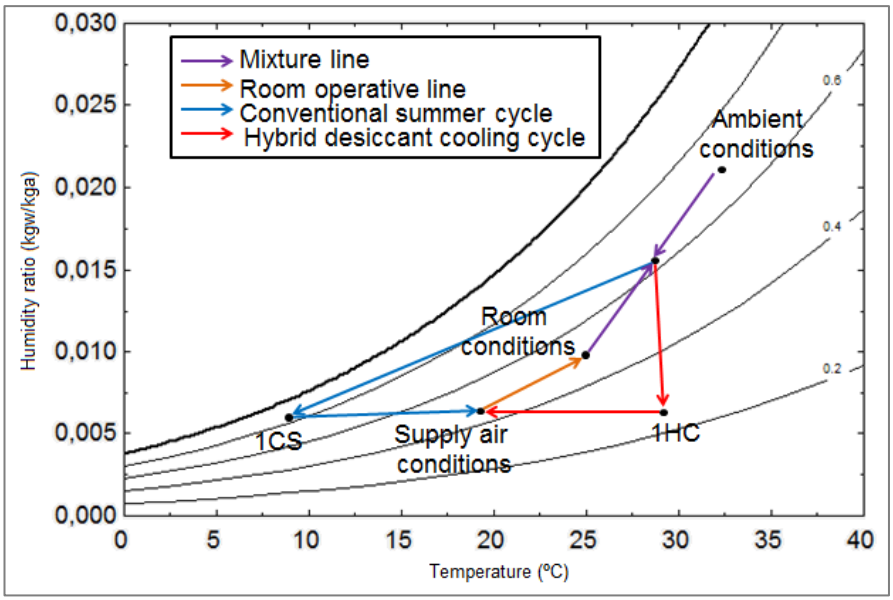

Figure 1.8. Control of humidity and temperature with a hybrid desiccant system.

1.1.1.4. Summary of the desiccant systems

Figure 1.9 shows the process that moist air follows in order to achieve the supply air conditions for the three described desiccant systems. As it can be observed, conventional air conditioners must over-cool the air in order to dehumidify the air. On the other hand, in the combination of desiccant system with evaporative cooling, moist air must be over-dehumidified in order to cool the air. However, the cycle in hybrid liquid desiccant system is more efficient because moist air is dehumidified until the required supply air humidity ratio without achieving the dew point and without over-dehumidifying the air.

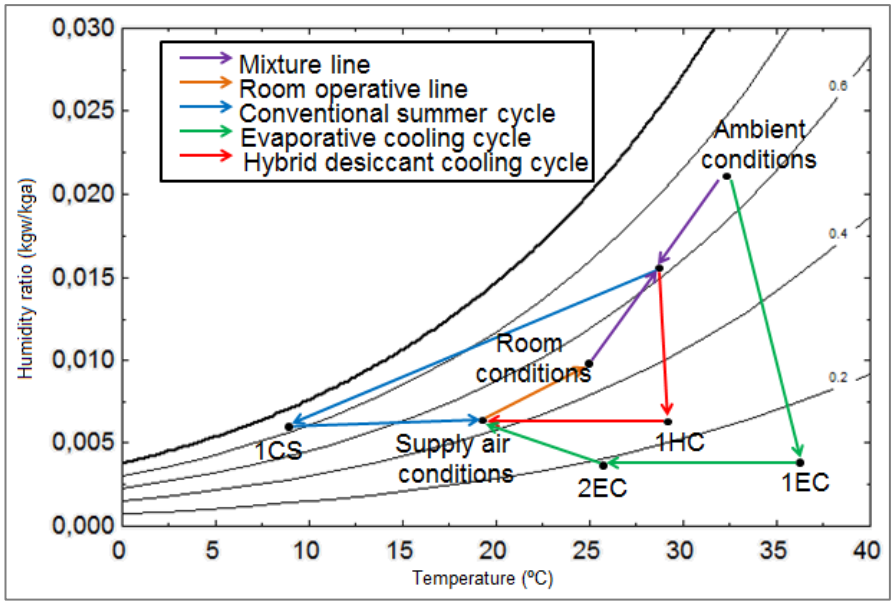

Figure 1.9. Control of humidity and temperature with the desiccant systems.

Compared with desiccant systems coupled with evaporative cooling, hybrid desiccant systems are less affected by the weather conditions when handling sensible load. However, hybrid desiccant systems are less advantageous than evaporative coolers considering the investment costs.

Sometimes, in hybrid desiccant systems, waste heat from the condenser of a vapour compression heat pump, and from the absorber and condenser in an absorption system, may be used as part of the heat needed for the desiccant regeneration.

Due to the fact that it is not required to reach the dew point in order to dehumidify the air, hybrid desiccant systems have three advantages with respect the conventional systems:

- Lower cooling demand to achieve the supply air conditions.
- Higher evaporator temperatures in the chiller, which enhances the global COP of the system.
- Post heating is not required.

1.1.2. Liquid desiccant systems

A liquid desiccant is a solution of water and a material that has a strong affinity for water. The absorption of moisture is driven by a difference between water vapour pressure of the desiccant at its surface and of the surrounding air. When the vapour pressure at the desiccant surface is lower than that of the moist air, the desiccant attracts moisture until equilibrium is reached. Conversely, when vapour pressure at the surface is higher than that of the surrounding air, the desiccant releases moisture. The liquid desiccant material most used is a solution of LiCl-H_2O, because its low vapour pressure permits to obtain high dehumidification at low concentrations of lithium chloride.

The main parts of a liquid desiccant system (Figure 1.10) are the two air-solution contactors: the absorber and the regenerator. In the absorber, moist air is dehumidified by direct contact with the liquid desiccant in an exothermic process, and therefore, cooling is required to remove the heat produced during the dehumidification process. In the regenerator, the water absorbed is released by direct contact with moist air in endothermic process, and therefore, heating is required to regenerate the solution through this component.

A solution-solution heat exchanger is often added in order to improve the performance of the system. Sometimes, it is also recommended to include a liquid desiccant storage as buffer.

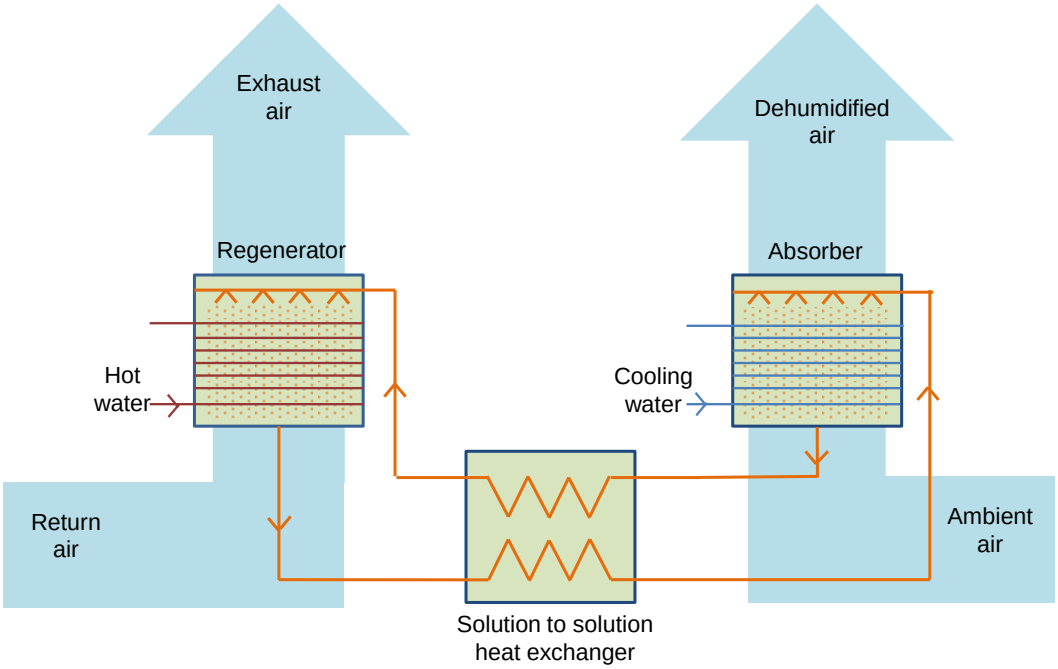

Figure 1.10. Schematic figure of a liquid desiccant system.

1.1.3. Liquid desiccant systems vs. Solid desiccant systems

Solid desiccant systems have been much more used than liquid desiccant systems in air conditioning applications. However, compared with solids, liquid desiccant systems have several advantages [4]:

- Lower pressure drops of air in the air-solution contactors.
- Chemical energy storage can be used.
- Lower regeneration temperature.
- Potential to remove a number of pollutants from the process air.
- Adaptability and flexibility in terms of allowing pumping the diluted solution from the absorber to the regenerator.
- Possibility of internal heat recuperation, which increases the COP of the system and decreases the size of the system.

On the other hand, there are some disadvantages which have made these systems less attractive:

- Liquid desiccants are usually very corrosive.
- Carryover of desiccant.

1.1.4. Air-solution contactors for liquid desiccant systems

Absorbers and regenerators used by commercial liquid desiccant systems are usually of the adiabatic packed-bed type. This is the case of Kathabar (USA) [5], Advantix (USA-Israel) [6], Ficom (Australia) [7] or Dyna-air (Japan) [8] systems. This type provides a high contact surface and is made of cellulose which is a very cheap material.

However, Lowenstein [9] listed the most important disadvantages associated with adiabatic packed-beds compared to internally-cooled air contactors:

- Higher air pressure drop.
- The liquid desiccant flow rate must be higher in order to prevent a high difference temperature of the desiccant in the air-solution contactor.
- The change in concentration of the desiccant is slight, making the desiccant storage not viable and less effective than in non-adiabatic air-solution contactors.
- Because the desiccant flow is high, the heat coming back on the absorber by the concentrated desiccant that returns from the regenerator can be a significant fraction of the total cooling provided by the absorber. This reduces the COP of the system.
- Air velocities are low to avoid high pressure drops and entrainment of droplets in the air stream.

1.1.5. New developments on liquid desiccant systems

In the last years, new developments on liquid desiccant cooling systems have been focused on different areas such as the use of new materials, the use of non-adiabatic air-solution contactors, the elimination of carry over or the operation of the system with different working conditions when it is operating in combination of vapour compression chillers.

As it is explained above, non-adiabatic air-solution contactors can be used in order to improve the performance of the system. However, most of the liquid desiccants are very corrosive with most of the metallic materials excluding titanium and tantalum, which are very expensive. For this reason, plastic materials, such as polypropylene or polyethylene, could be a good alternative for these applications despite their poorer thermal conductivity and wettability.

Other developments are related with the reduction of the carry over, which can be very problematic for the maintenance of the installation. Moreover, this problem may lead to the corrosion of devices placed inside the conditioned room. In this case, there are three possibilities in order to avoid this problem:

- Reduction of the desiccant flow rate through the absorber and regenerator. However this reduction is restricted by the wettability of the liquid around the tubes.
- Reduction of the air velocity through the absorber and the regenerator. This reduction is also restricted by the size of the system and the minimum air flow rate. Moreover, low velocities of air may affect the mass transfer through the air-solution contactors.
- Implementation of new demisters.

Lately, operation conditions of liquid desiccant system have been changed by some researchers in order to be used in combination with vapour compression heat pumps. This is what Chen et al. [10] proposed with a hybrid liquid desiccant system that can operates at lower temperatures in the absorber, allowing also lower concentrations in the liquid desiccant system and, therefore, permitting regeneration at suitable temperatures to be provided by the condenser of a heat pump.

1.1.6. Potentials of liquid desiccant systems

From the economical point of view, the decision of using a desiccant system for air conditioning depends on how much dehumidification is required to be provided by the system along the year. The higher dehumidification, the more viable the desiccant system is. In this sense, dehumidification mainly depends on how big the internal latent loads and the ambient humidity are.

Notwithstanding that the internal loads determine the air supply conditions, weather with high ambient humidity is more suitable for desiccant systems. Figure 1.11 illustrates the latent cooling required for a room with the same internal loads for two different locations: Tarragona, with a Mediterranean climate, and Taipei, with a subtropical climate. In this comparison, internal loads are constant along the year; therefore, air supply conditions are the same in every moment: 0.007 kg_w/kg_a, 19 °C and 2000 m^3/h.

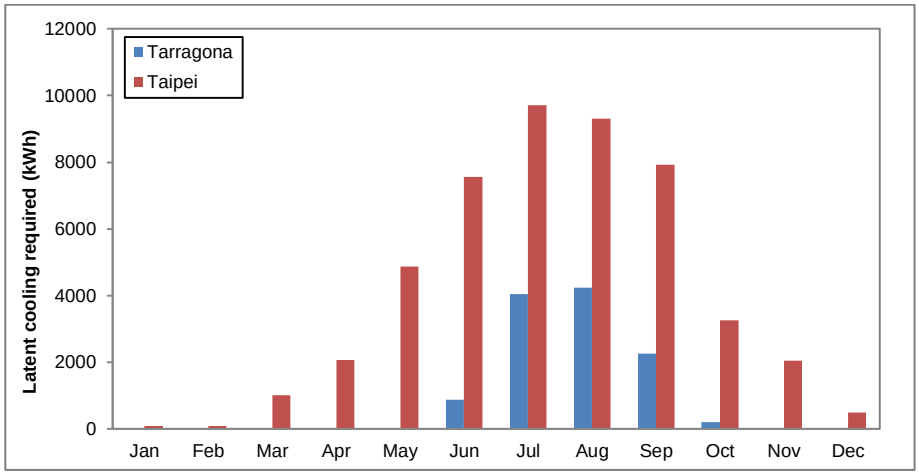

Figure 1.11. Latent cooling required for a room with the same internal loads in Taipei (Taiwan) and Tarragona (Spain).

Moreover, the desiccant system has to operate under these conditions during 4086 hours in Taipei, and during 1165 hours in Tarragona. Therefore, it can be deduced that desiccant systems are much more appropriate in a subtropical or tropical climate than in a Mediterranean climate.

In any case, in applications where high latent internal loads have to be handled, or where low internal humidity is required, desiccant systems start to be more competitive from the economical point of view.

1.2. Thesis structure and methodological approach

Table 1.1 contains the structure of this thesis, which is divided in 9 chapters. In addition, as summary, the main results expected to be obtained in every chapter are included. Moreover, Figure 1.12 illustrates and

schematic description of the methodology used in this thesis. This figure includes how the results of the chapters are used as inputs of following chapters.

Chapter 2 contains the basics of liquid desiccant systems and materials. In addition, this chapter includes a state-of-the-art of the air-solution contactors being mainly focused on the falling-film typology. Then, a review with different configurations of liquid desiccant system is presented. Finally, some of the liquid desiccant systems available on the market are described. The main results of this chapter are: the selection of the LiCl-H_2O as liquid desiccant material, the selection of air-solution contactors of the falling-film with horizontal tubes type, and the selection of liquid desiccant system coupled with a vapour compression heat pump because as configuration of the system.

Chapter 3 presents an experimental hydrodynamic study of falling-film with horizontal tubes made of polypropylene, high density polyethylene, low density polyethylene, polyamide and graphite. Wettability of tubes was evaluated and was taken into consideration in the selection of the tube material. In order to improve its wettability when LiCl-H_2O is around the tubes, some of the tested tubes contained a surface plasma treatment that improves the wetting of the plastic material. As result, polypropylene with surface plasma continuous treatment was chosen as the best material among the tested materials. Furthermore, correlations for the minimum flow rate required to fully wet the tubes were obtained.

Chapter 4 includes an experimental study of two air-solution contactors, when they operate as absorber of a liquid desiccant system, with the same dimensions and geometry made of polypropylene. The only difference between them is that one of the air-solution contactors contains a surface plasma continuous treatment on tubes, in order to improve the wettability when LiCl-H_2O is flowing around the horizontal tubes. Dehumidification, air cooling, heat duty and global heat transfer coefficient between the water and liquid desiccant are compared in order to assess the effect of the wettability on their performance.

Chapter 5 describes the methodology used for the sizing and design of the hybrid liquid desiccant system, which is based on the results of previous chapters and on the results obtained from the experimental tests done during the stay at the Technion, and on some assumptions. A sensitivity analysis that verifies the assumptions taken during the sizing and design process are included in the end of this chapter. As a result, the hybrid liquid desiccant system is sized and designed to be operated in two locker rooms of a swimming-pool in Taipei (Taiwan)

Chapter 6 describes the final hybrid liquid desiccant system as well as the control strategy (in a simple way) used for the demonstration period. The tests bench where the hybrid liquid desiccant system was set-up in Tarragona is also described. Finally, this chapter describes the set-up performed on the system before being sent to Taiwan. As main result, the hybrid liquid desiccant system was ready to be operated in an automatic way in the demonstration site.

Chapter 7 contains the experimental results of the hybrid liquid desiccant system. Absorber and regenerator performance, as well as the whole system performance when it works at full and partial load are presented in this chapter. In addition, correlations of the heat and mass transfer coefficients of the absorber and regenerator are obtained. Finally, the operation of the system during three different days is analysed in order to verify that the separate control of humidity and temperature is reached by the system.

Chapter 8 describes the model to be dynamically simulated. The simulated results with this model are compared with the experimental results, showing small deviations between them. Moreover, several simulations have been carried out in order to choose the control strategy and working conditions of the system that minimize the heating transferred in the condenser of the heat pump and the hours of discomfort of the room.

Finally, **Chapter 9** gives the general conclusions and future outlooks regarding the study reported in this thesis. The future outlooks are detailed focusing on what could be improved from this thesis and providing suggestion for future research directions.

Table 1.1. Thesis structure.

Chapters		Results
1.	**Introduction, objectives and methodological approach**	-
2.	**State-of-the-art of liquid desiccant systems for air-conditioning applications**	Use of falling-film with horizontal tubes
		Use of hybrid liquid desiccant system combined with vapour compression chiller
		Use of LiCl-H_2O as liquid desiccant material
3.	**Hydrodynamic study of falling-film with horizontal tubes for air-solution contactors in liquid desiccant systems**	Selection of Polypropylene
		Correlations for minimum liquid desiccant flow rate
4.	**Experimental study of a small-scale internally-cooled air-solution contactor for liquid desiccant systems made of polypropylene. Comparison with a surface treated polypropylene air-solution contactor**	Better performance with polypropylene with plasma treatment
5.	**Sizing and design of a hybrid liquid desiccant system**	Sizing and design of a hybrid liquid desiccant system
6.	**Description and set-up of a hybrid liquid desiccant system with treated polypropylene air-solution contactors**	Definition of the control strategies
		Set-up of the system
7.	**Experimental performance of a hybrid liquid desiccant system**	Real performance of the system
		New heat and mass transfer coefficients
8.	**Modelling, validation and dynamic simulation of a hybrid liquid desiccant system**	Model for the dynamic simulation of the system
		Annual performance
		Selection of the best control strategy
9.	**Conclusions and Future Work**	-

Figure 1.12 illustrates the methodological approach followed for the development of the thesis. In this figure, the chapters (inside boxed with black borders) are linked by the results (inside boxes with discontinuous blue boxes). In this way, it is shown how results from previous chapters are used as inputs of following chapters.

At the beginning of the thesis, the state-of-the-art of the liquid desiccant technology helped to set the air-solution contactor typology (falling-film with horizontal tubes), the liquid desiccant material (LiCl-H_2O) and the liquid desiccant system configuration for the hybrid liquid desiccant system (liquid desiccant coupled with a vapour compression heat pump).

During the first year an experimental study was carried out (Gommed et al. [11]) in order to compare three different air-solution contactors: an adiabatic packed-bed, and two falling-film with horizontal tubes: one made of titanium and a second made of high density polyethylene. In this study, wettability was found as the key factor in the poorer performance of a high density polyethylene air-solution contactor in comparison with a titanium air-solution contactor. Moreover, heat and mass transfer coefficients taken from these tests were used for the design of the hybrid liquid desiccant system (Chapter 5).

Since wettability was found as a key factor, a hydrodynamic study among 10 different tubes was then performed in order to choose the best rust-proof material. Correlations to calculate the minimum liquid desiccant flow rate to fully wet the tube surface were also obtained from this study. As a result, polypropylene with continuous surface treatment II was selected as the material for the air-solution contactors.

In order to verify that the surface treatment enhances the performance of the air-solution contactors, two air-solution contactors made of polypropylene, one standard and other with the surface treatment chosen in previous chapter, were compared. The air-solution contactor with surface treatment confirmed a better performance than the standard, with higher dehumidification and heat duty.

With the results obtained from chapters 2 to 4 as well as from the results of the experimental comparison made during the stay at the Technion, the hybrid liquid desiccant system could be sized and designed. Some

assumptions and construction constrictions, such as the air-solution contactor tube arrangement or tower dimensions, were also considered for this purpose.

In the meantime the hybrid liquid desiccant system was being manufactured, several control strategies were developed. After being manufactured, and before being sent to Taiwan, the hybrid liquid desiccant system was set-up at URV facilities. The test bench was modified in order to simulate tropical conditions. Some previous results of the air-solution contactors and the whole system could be measured in Tarragona during the summer of 2015.

From November 2015, the hybrid liquid desiccant system has been operating in Taiwan Building Technology Center in Taipei (Taiwan). The performance of the system at real working conditions has been obtained since that moment. Different control strategies and control parameters have been tried in order to get the performance of the system at different conditions. Results of the air-solution contactors as well as the whole system and the control strategies have been analysed.

From measured results, models developed along the designed phase of the hybrid liquid desiccant system could be completed with heat and mass transfer correlations. Models for the dynamic simulation of the liquid desiccant system were then elaborated. These models have been compared with the experimental data of the demonstrative system. Once the models were validated, annual simulations at different working conditions, and with different control strategies were done in order to optimize the system performance in terms of minimizing the heating transferred in the condenser of the heat pump and the hours of discomfort of the room.

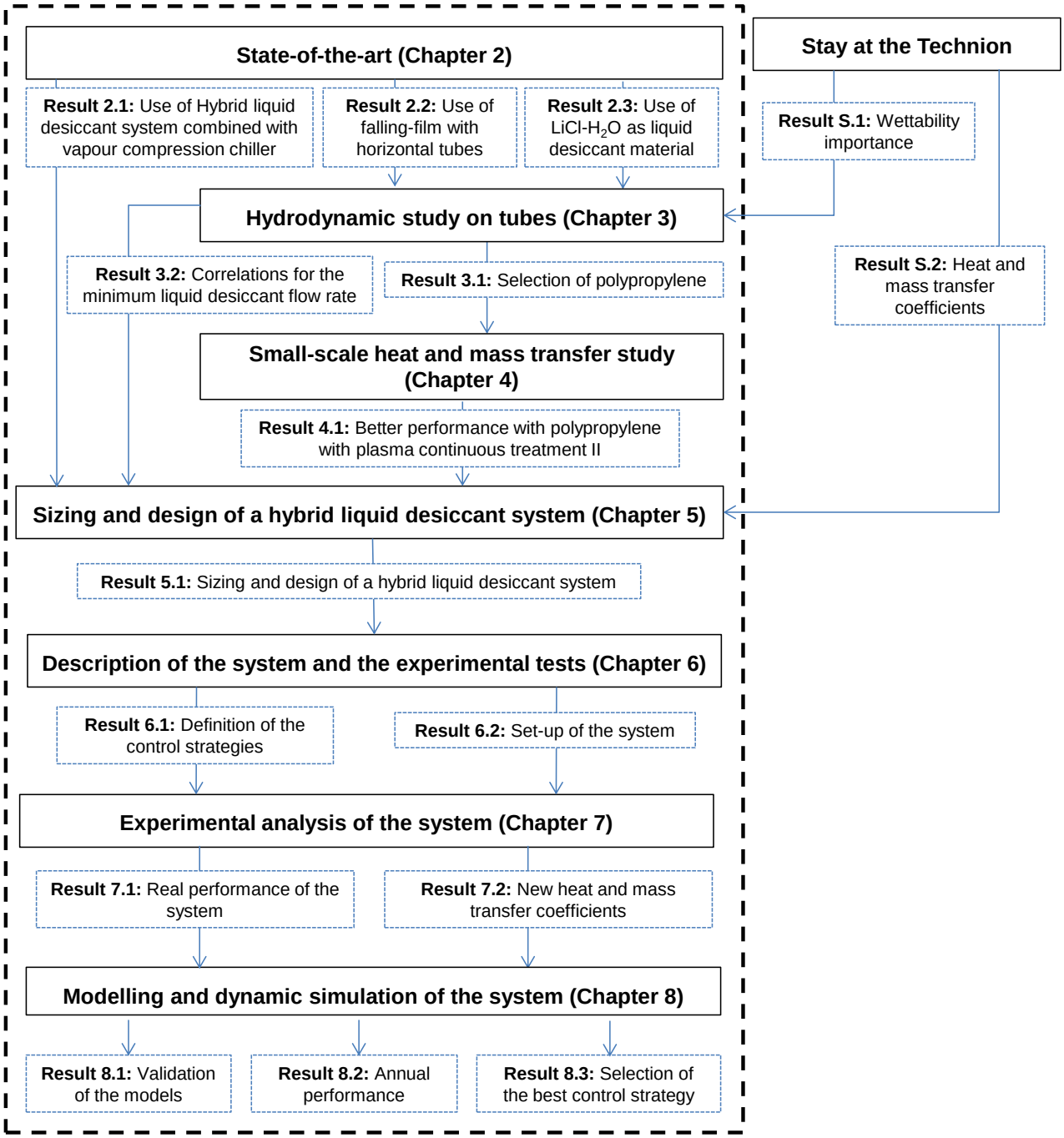

Figure 1.12. Methodological approach.

Chapter 2. State-of-the-art of liquid desiccant technology for air conditioning applications

2.1. Historical overview

Desiccant air conditioning technology was developed before the arrival of vapour compression cooling. The Kathabar liquid desiccant system, introduced in 1910, was the first air conditioning used of a technology that had been largely used in chemical process and petroleum refining operations. During the 1930s, the Niagara Blower Company began using a desiccant solution (Triethylene Glycol) as a mean of removing frost from evaporator coils in refrigeration systems [12].

Probably, the very first system of this type proposed and discussed in the open literature is the shown in Figure 2.1, designed by Bichowsky and Kelley in 1935 [13]. This system already includes all the principal elements of a modern open absorption air conditioning system using LiCl-H_2O as desiccant. Forrest (1935) designed a similar system introducing an evaporative cooler.

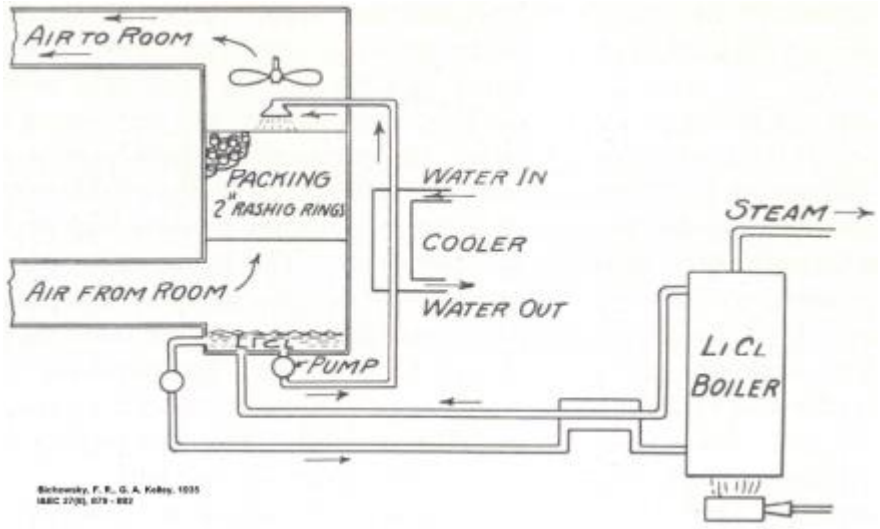

Figure 2.1. Schematic of the liquid desiccant system proposed in 1935 by Bichowsky & Kelley for the dehydration of air [14].

Solar energy started to be used as heating source of liquid desiccant systems in the middle 50s. In 1955, Löf [15] proposed a solar energy system, which preheated air for regeneration to save gas consumption from the boiler. Later, in 1969, Kakabaev and Golaev [16] were the first to investigate the use of solar energy for regeneration of a liquid desiccant flowing over a slanted blackened surface. Robinson [17], in 1982, tested a desiccant cooling system with water from a well for removing sensible heat, and a calcium chloride-water mixture regenerated in a solar collector, for removing latent heat. In the middle of the 80s, Mecler [18] designed and installed several air conditioning systems for air conditioning of commercial and institutional buildings.

New developments on liquid desiccant systems have been concentrated in different areas such as the use of new materials, the use of non-adiabatic air-solution contactors of the falling-film, the elimination of carry over, the integration of the system with other HVAC technologies and the operation of the system at different working conditions. Figure 2.2 shows an evolution of the journal papers per year since 1980 to 2014 (adapted from [19]). It can be observed how the amount of studies has increased during the last 35 years, especially in the last decade.

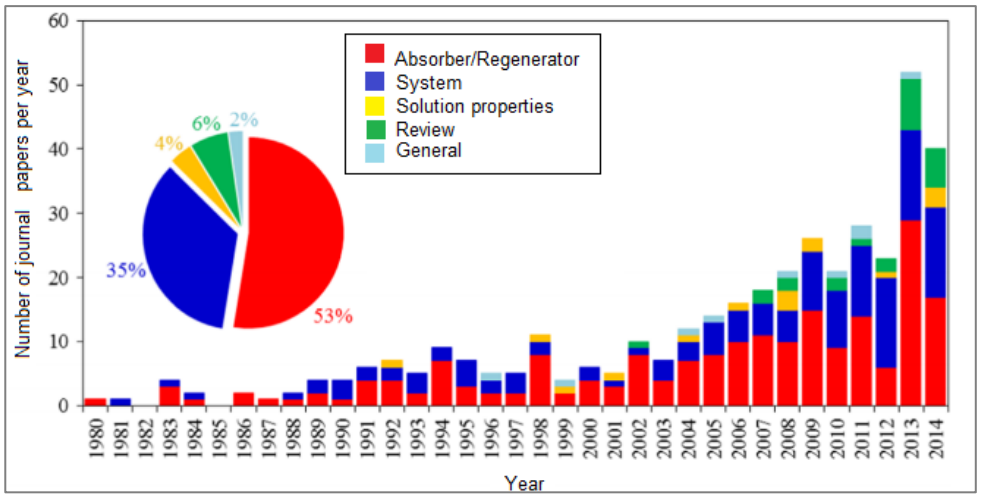

Figure 2.2. Classification of the journal papers based on liquid desiccant systems from 1980 to 2014 (adapted from [19]).

2.2. The basics of liquid-desiccant air conditioners

As it is mentioned in Section 1.1.2, a liquid desiccant is a solution of water and a material that has a strong affinity for water. Sorption is driven by a difference between the vapour pressure of the desiccant material at its surface and of the surrounding air. When the vapour pressure at the desiccant surface is lower than that of the moist air, the desiccant attracts moisture until equilibrium is reached.

The simplest liquid desiccant cycle is comprised by two air-solution contactors, two water-solution heat exchangers and one solution-solution heat exchanger. Figure 2.3 shows a scheme of this system and Figure 2.4 shows the cycle of it.

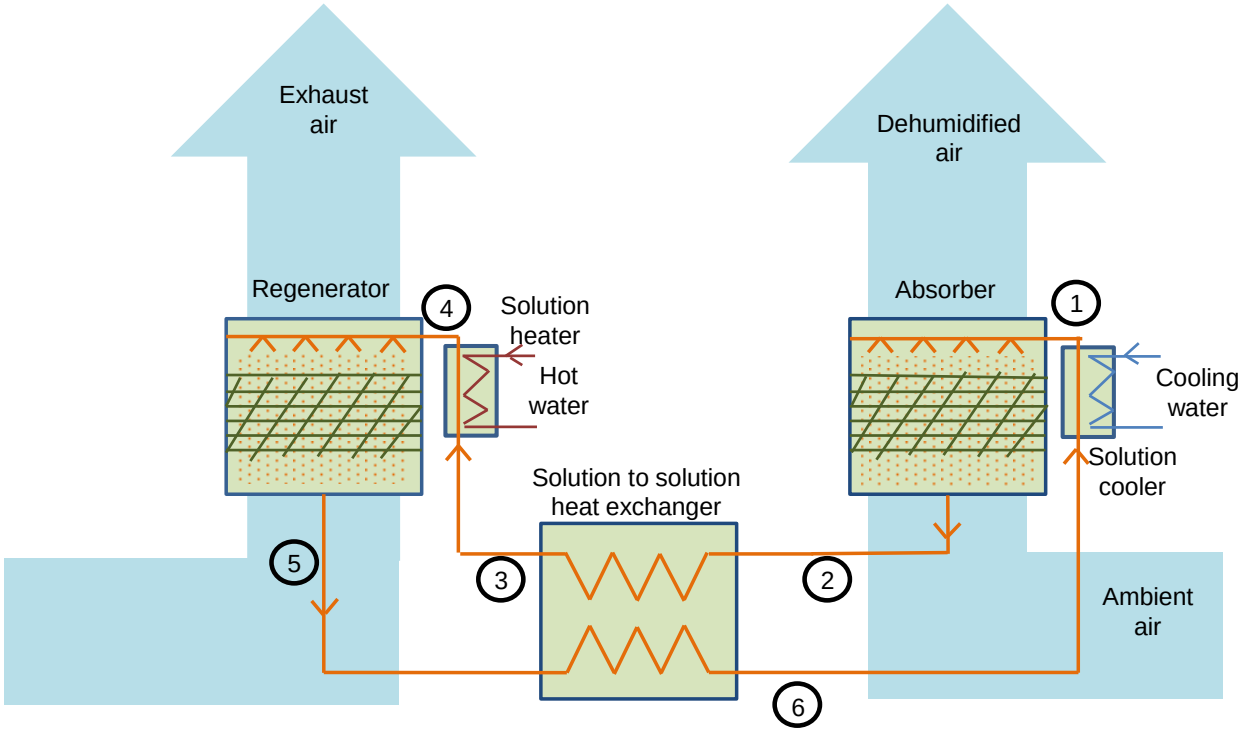

Figure 2.3. Schematic figure of a liquid desiccant system.

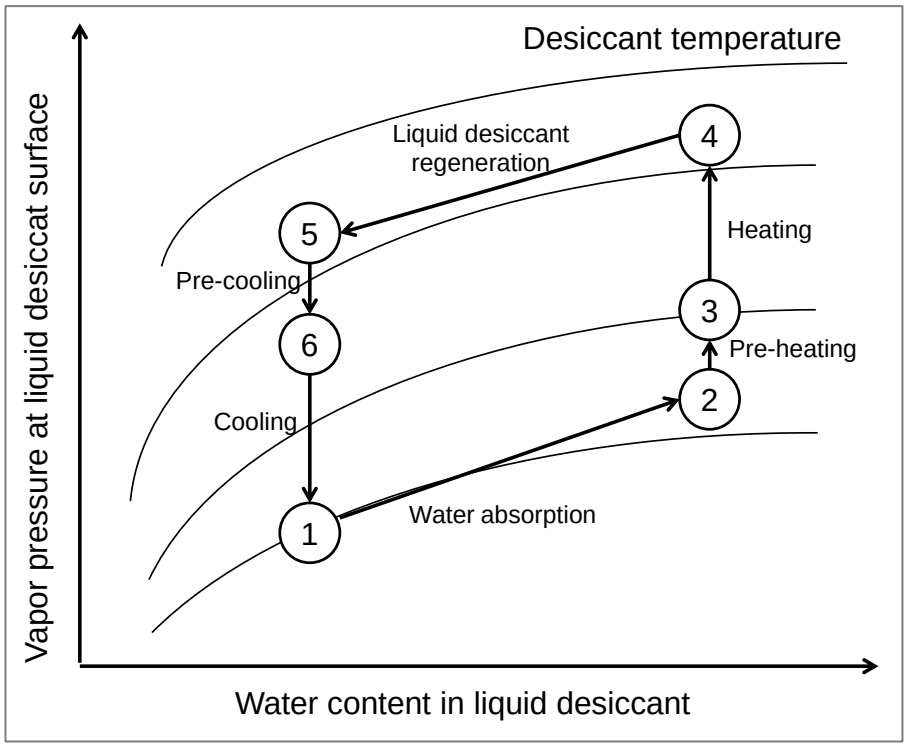

Figure 2.4. Liquid desiccant cycle.

Vapour pressure of water depends on both, the water content in the liquid desiccant and the liquid desiccant temperature. The higher the water content and the desiccant temperature, the higher the vapour pressure of water. Therefore, at the entrance of the absorber (point 1), the liquid desiccant should be cold and the water content must be low in order to reduce its vapour pressure. Dehumidification of moist air occurs in the absorber, where the water content and temperature (if the absorber is of the adiabatic type) of the liquid desiccant rise. Therefore, the water vapour pressure increases at its surface (point 2). The liquid desiccant is then pre-heated in a solution heat exchanger (point 3) and heated after in a water-solution heat exchanger (point 4). At the entrance of the regenerator (point 4), the liquid desiccant should be hot and the water content must be high in order to increase its vapour pressure. Regeneration of the liquid desiccant occurs in the regenerator where water content and temperature (if the regenerator is of the adiabatic type) of the liquid desiccant decreases. The liquid desiccant is pre-cooled in a solution heat exchanger (point 5) and cooled after in a water-solution heat exchanger (point 6).

For a given liquid desiccant mass concentration, if liquid desiccant temperature is changed, the line that vapour pressure of water closely follows a line of constant relative humidity in a psychrometric chart [20]. This line represents the minimum humidity ratio that moist air could achieve when it is put in contact with the liquid desiccant. Figure 2.5 shows this behaviour for different mass concentrations of LiCl.

If the dehumidification is done in an adiabatic way, the line that the moist air follows in the psychrometric chart is near the constant enthalpy line, in the same way that the evaporative cooling, but in the opposite direction (see Figure 2.5). Therefore, the so called brine-bulb temperature is a function of the liquid desiccant concentration and the air temperature and humidity. Brine-bulb temperature will always be slightly higher than the temperature at which a line of constant enthalpy from the air state point intersects the equilibrium relative humidity curve for the desiccant. This is due to the heat, which is released when the desiccant absorbs the water vapour, includes the chemical heat of mixing between the desiccant and the water.

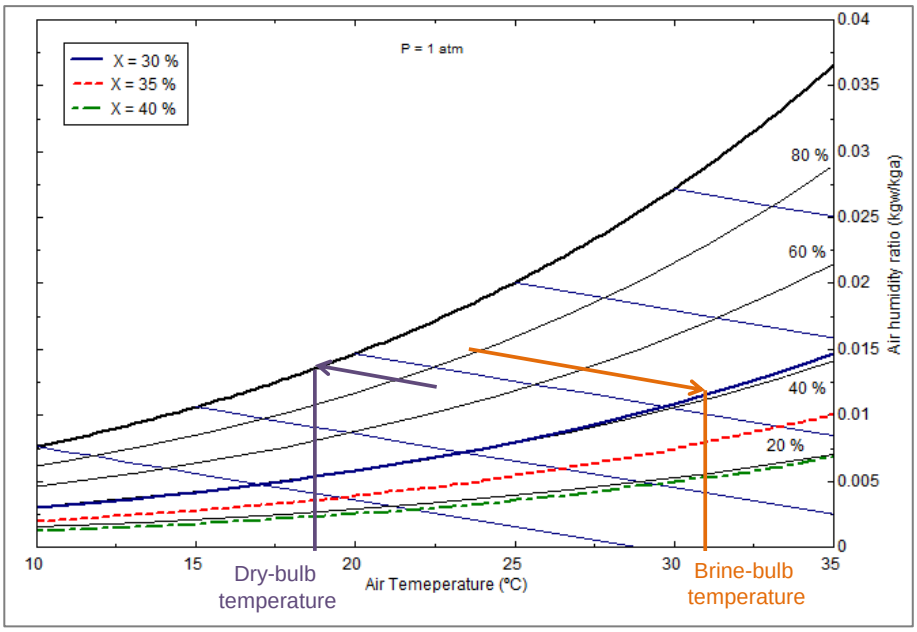

Figure 2.5. Psychrometric performance of lithium chloride at different concentrations.

2.3. Liquid desiccants materials

The desiccant system behaviour is highly influenced by the characteristics of the desiccant materials [21]. In this sense, research institutions and manufactures have focused on material science. Al-Farayedhi et al. [22] listed several considerations in choosing the optimal liquid desiccant solution:

- Low vapour pressure.
- Low vapour pressure of solute.
- Non-corrosive and chemically stable.
- Performance of solution steady over large concentration range.
- High solubility.
- Low viscosity.
- Non-toxic, harmless.
- Low cost.

Other properties are also important:

- Low surface tension.
- High boiling point.
- High energy storage density.
- High durability
- Low crystallization point.

The desiccant solutions commonly used are essentially five [14]: aqueous solutions of Triethylene Glycol (TEG), and of the alkali halides, chlorides of lithium, calcium and magnesium and lithium bromide.

Formulations for the thermal properties for alkali halides can be obtained from the researches made by Conde [23] (LiCl and $CaCl_2$), Patek and Klomfar [24] (LiCl) and McNeely [25] (LiBr).

Figure 2.6 shows the equilibrium humidity ratio on a psychrometric chart of solutions with several concentrations. From this figure, it could be derived that the absorber efficiency of the desiccants enhances with lower temperatures and higher concentrations. In addition, LiCl has better absorption performance that LiBr and $CaCl_2$ [26]. However, LiCl is the most expensive. The price and vapour pressure of lithium bromide

are intermediate. Triethylene glycol is the earliest used desiccant, but the liquid residence caused by its high viscosity makes the system operation unstable [4]. However, triethylene glycol has a very low vapour pressure. Other physical properties of desiccants that are important for evaluating the heat and mass transfer processes and the pumping requirements are listed in Table 2.1 [27].

The corrosion effect on the operating components of the system should also be taken into account. Either adding additives to the liquid desiccant or choosing parts in contact with the solution made of synthetic plastic or non-corrosive metals, such as titanium, are the most used methods to avoid corrosion.

In addition to dehumidification, desiccant liquids are capable of absorbing inorganic (Chung et al. [28]) and organic (Kathabar Systems [5]) contaminants in the air, which improves the indoor air quality.

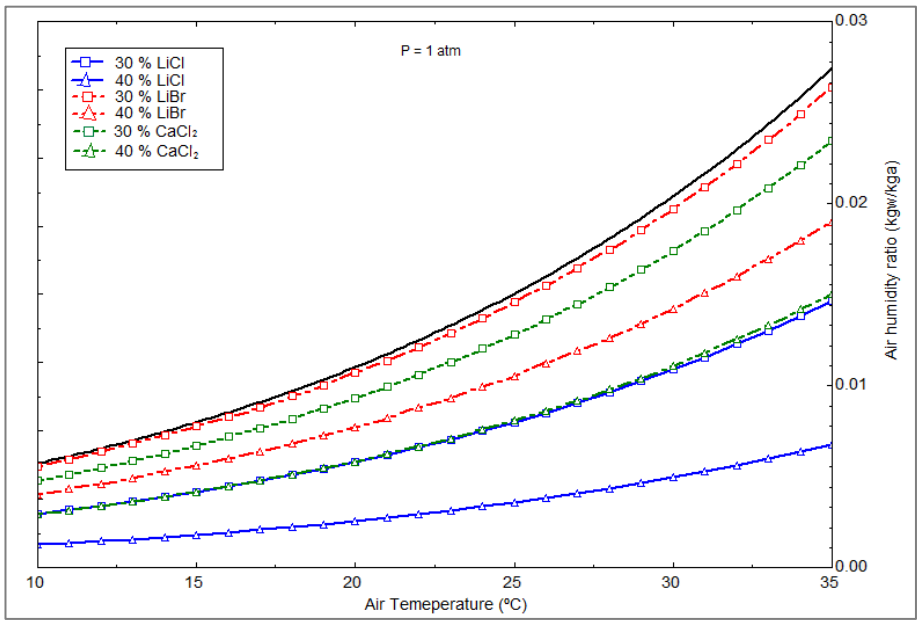

Figure 2.6. Psychrometic chart with the equilibrium humidity ratio of LiCl, LiBr and $CaCl_2$ at different conenctrations.

Table 2.1. Physical properties of Liquid Desiccants at 25 °C [27].

Desiccant	Density 10^3 (kg/m^3)	Viscosity 10^3 (Ns/m^2)	Surface tension 10^3 (N/m)	Specific heat (kJ/kg°C)
95 % by weight triethylene glycol	1.1	28	46	2.3
55 % by weight lithium bromide	1.6	6	89	2.1
40 % by weight calcium chloride	1.4	7	93	2.5
40 % by weight lithium chloride	1.2	9	96	2.5

2.4. Absorbers/Regenerators

The performance, cost, size and reliability of an absorber/regenerator depend on two independent parameters: desiccant material and matrix geometry. The air dehumidification is generally effected by sprinkling the liquid desiccant from the top and bringing it into contact with the inlet process air. The desirable characteristics for high-performance liquid desiccant absorber and regenerators are (Pesaran et al. [4]):

- Lacking corrosion and carryover.
- High heat and mass transfer rates or high NTUs.
- Low pressure drops.
- Small liquid-side resistance to moisture diffusion.
- Large contact transfer surface area per unit volume.
- Compatible desiccant/contact materials.

- Use of common materials of construction and inexpensive manufacturing techniques.
- Low heat input for regeneration.

Under laminar flow conditions, a parallel passage configuration is compact and provides heat and mass transfer rate with low pressure drop. Figure 2.7 shows the theoretical heat transfer and pressure drop characteristics of various flows geometries.

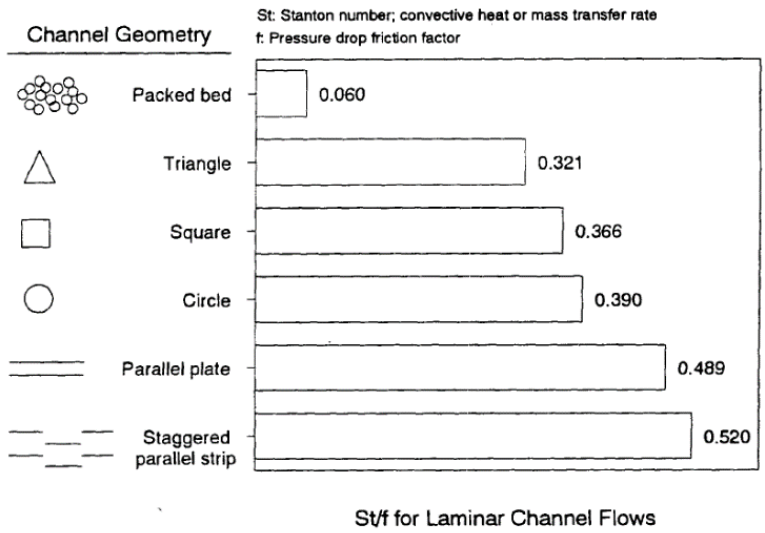

Figure 2.7. Ratio of heat-transfer rate to pressure drop for various dehumidifier passage geometries [4].

Absorber/regenerators are typically called air-solution contactors because mass and heat transfer between the air and the solution takes place through direct contact between them. Air-solution contactors can be classified in the following typologies:

- Packed-bed that can be also classified as:
  - Adiabatic.
  - Internally-cooled/heated.
- Falling-film that can be also sub-classified as:
  - Flat plates.
  - Extruded plates
  - Horizontal tubes.
  - Horizontal tubes with fins.
- Solar collector regenerator that can be also sub-classified as:
  - Open-type.
  - Close-type.
  - Natural convection.
  - Forced convection.
- Pressurized absorber.

2.4.1. Packed-bed air-solution contactors

2.4.1.1. Adiabatic packed-bed

Adiabatic packed-bed is the most used typology of air-solution contactor. Left graph of Figure 2.8 shows a scheme of the adiabatic packed bed air-solution contactor. A packed tower sprays liquid desiccant into the process air stream through a packing material. This type of equipment is relatively inexpensive and easy to build and provides large contact surface area per unit volume.

Packed-bed reactor can be characterized either by random packing, which does not have a regular geometric form, or by structured packing, which has a fixed geometric form [29]. Figure 2.9 and Figure 2.10 show the two different kinds of packing materials.

Longo and Gasparella [30] experimentally compared the performance of structured and random packing. Results obtained show better dehumidification rates and transfer efficiency for random packing (over 25 %) but lower air pressure drops for structured packing (over 70 %).

Lowenstein et al. [9] listed the most important disadvantages associated with packed beds:

- Higher air pressure drops.
- Air velocities are low to avoid high pressure drops and entrainment of droplets in the air stream (carry over).
- Size must be larger in the adiabatic air-solution contactors.

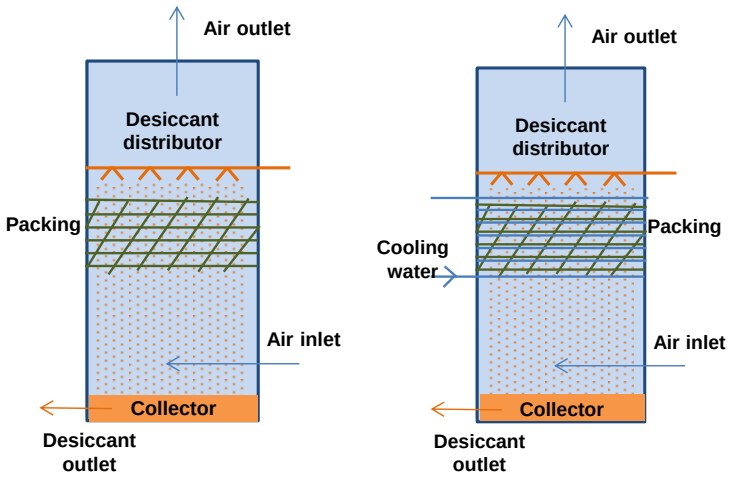

Figure 2.8. Adiabatic (left) and internally-cooled (right) packed bed air-solution contactors.

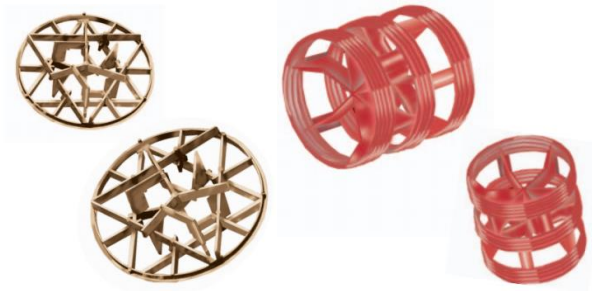

Figure 2.9. Commercially available random packings for packed beds [31].

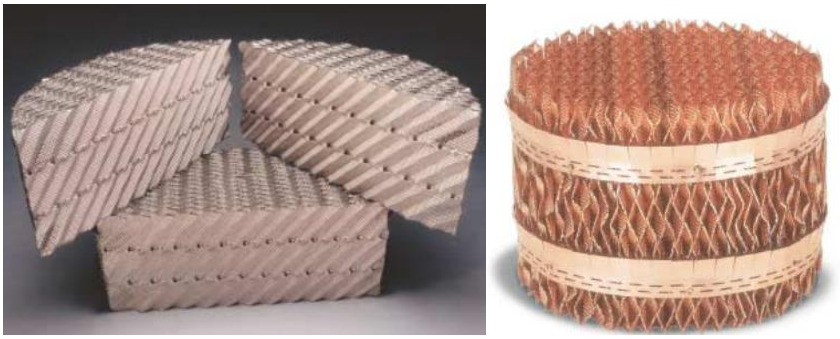

Figure 2.10. Commercially available structured packings for packed beds [32].

Moreover, this air-solution contactor typology requires higher flow rates of desiccant than falling-film air-solution contactors (Öberg and Goswami [27]) in order to avoid big temperature changes throughout it, this leads to other disadvantages:

- The desiccant storage is less effective than in non-adiabatic air-solution contactors.
- The COP of the system is lower in the adiabatic air-solution contactors.

2.4.1.2. Non-adiabatic packed-bed air-solution contactors

Despite the limitations of packed-bed air-solution contactors, this has been the focus of many R&D projects on liquid desiccant systems for air conditioning applications. Right graph of Figure 2.8 shows a scheme of the non-adiabatic packed bed air-solution contactor. Gommed, Grossman, and Ziegler [33] implemented their dehumidifier and regenerator as internally cooled units by using both copper tubes and polypropylene tubes as the contact surface. However, the copper tubes were too easily corroded by the desiccant, and the polypropylene tubes were too difficult to wet. Adiabatic packed beds with volumetric surface area of 285 m^2/m^3 were finally used. The researchers reported that LiCl solution should not be sprayed, but rather dripped over the packing, with the drops large enough not to be carried away by the air stream. Bansal et al. [34] conducted a performance analysis for an adiabatic and an internally cooled absorber, which improves the dehumidification by about the 30 % relative to adiabatic packed-bed. Table 2.2 shows the dimensions, inlet conditions and dehumidification achieved with this internally-cooled absorber.

Comparing with other configurations, internally cooled packed-bed has the following characteristics:

- High flow rates in air and solution streams to ensure the complete wetting and to prevent the desiccant heating.
- Low solution concentration differences, decreasing solution regeneration and system performance.
- High pressure drop, as in packed bed, which can be deduced from Figure 2.7.

The configuration of the complete liquid desiccant system with non-adiabatic air-solution contactors can be something similar to Figure 2.11. In this representation, absorber and regenerator are in counter-current flow disposition. In this case, water-solution heat exchangers are not required in order to cool or heat the liquid desiccant before being sprayed in the absorber or regenerator, respectively.

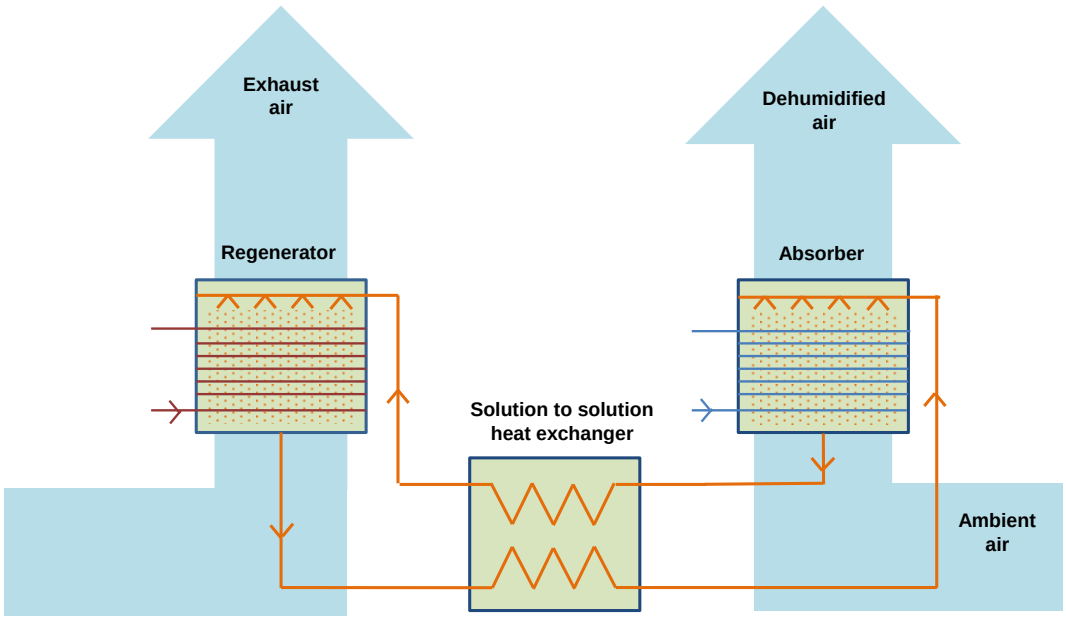

Figure 2.11. A liquid-desiccant air conditioner that uses a water-cooled conditioner and water-heated regenerator.

2.4.2. Falling-film air-solution contactors

2.4.2.1. Falling-film plates air-solution contactors

A simple alternative to packed-bed air-solution contactors is to use a twin-wall plate heat exchanger (i.e., a hollow extrusion that has two parallel walls with thin webs maintaining the space between the walls and creating a multitude of internal passages), where the outer surfaces of the reactor plates are wetted with desiccant and the process air flows in the gaps between the plates.

Läevemann et al. [35] described a water-cooled absorber that is made from twin-wall polypropylene plates, with counter-flow disposition as shown in Figure 2.12. Table 2.2 and Table 2.3 contain the number of plates, inlet conditions and dehumidification achieved in Läevemann's [35] experimental model. Other results obtained in this typology are:

- Air dehumidification is almost isothermal.
- Solution flow rate is very low compared with moist air flow rate (with a rate of 1:20), permitting high solution concentration differences (about 8 %) and increasing system performance.
- Inclusion of energy storage is possible.
- Low pressure drops.
- These absorbers require a face velocity up to 2 m/s.

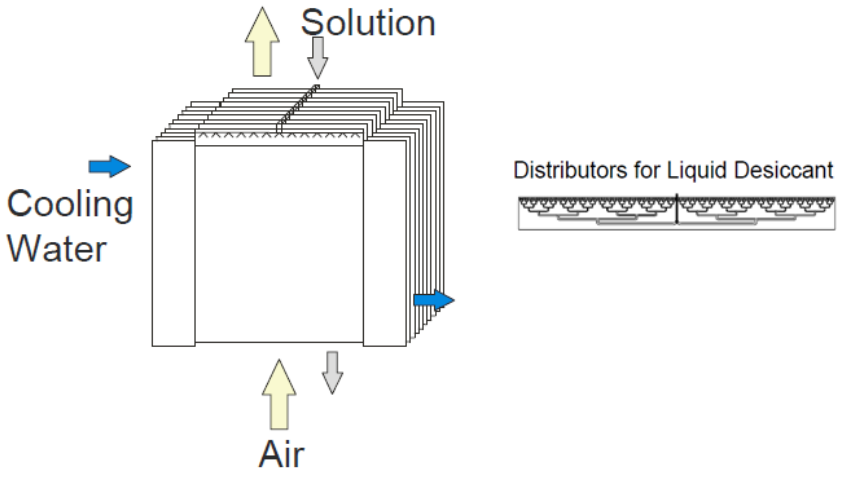

Figure 2.12. Laeveman experimental model and distributors of liquid desiccant [35].

2.4.2.2. Falling-film extruded plates air-solution contactors

A similar configuration uses extruded plates, in which cooling water flows through small tubes and outer surfaces are wetted with desiccant liquid. Four experimental models have been developed using this configuration:

- Experimental model developed by Kessling et al. [36], with a polypropylene core.
- Experimental model described by Lowenstein et al. [37], with a PVC core.
- Experimental model defined by Yonggao et al. [38], with a stainless steel core.
- Experimental model described by Liu. et al. [40], with thermally conductive polypropylene.

Performances obtained with these absorbers and regenerators are showed in Table 2.2 and Table 2.3

In order to achieve high performance, a good wetting of the surface of the material is important. In Lowenstein's patent [37], each plate is bonded to an upper and lower end-piece. The upper end-piece has a desiccant distributor that delivers very low flow of desiccant directly to the top of the plate. When the plate/end-piece assemblies are stacked, they form separate circuits for the cooling water and the liquid

desiccant. Right graph of Figure 2.13 shows a detailed picture of an extruded plate from Lowenstein's experimental model.

The plates have a total thickness of 2.5 mm and the wall thickness is 0.5 mm. The distance between two adjacent plates is also 2.5 mm. In general, the results obtained with this configuration are similar to that of Laeveman's experimental model [39].

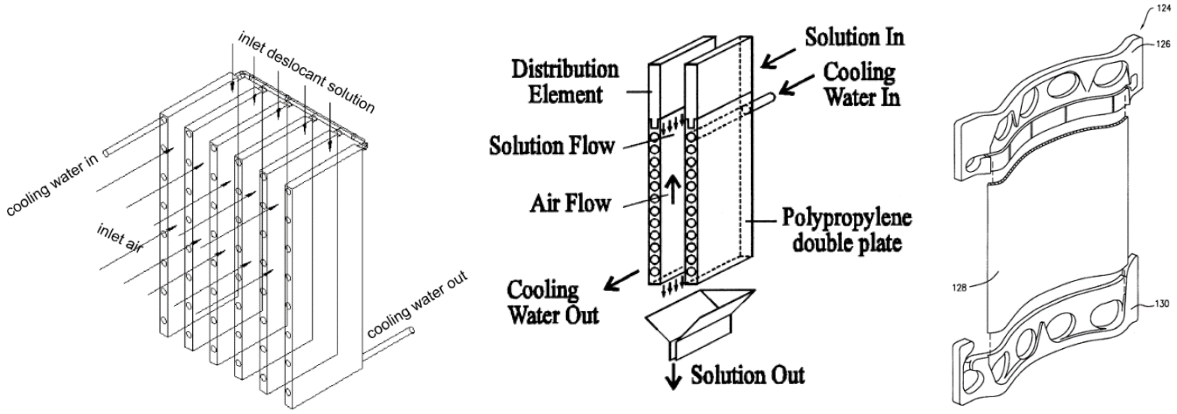

Figure 2.13. Internally-cooled absorber with extruded plates [29] left, and [36] centre, and liquid distributor [37] (right).

Liu et al. [40] experimentally studied a falling-film with extruded plates air-solution contactor with a plastic material with enhanced thermal conductivity (see Figure 2.14) , which is one of the disadvantages of plastic materials when they are compared with metallic. They tested the air-solution contactors at absorber and at regenerator conditions finding better results in terms of heat transfer and similar in terms of mass transfer than other air-solution contactors found in literature.

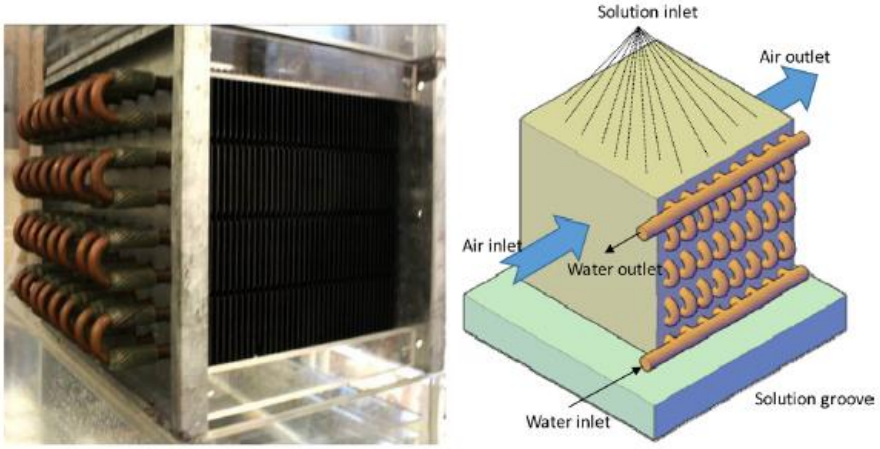

Figure 2.14. Internally-cooled absorber developed by Liu et. al [40].

2.4.2.3. Falling-film with horizontal tubes air-solution contactors

Kahn et al. [41] describe a theoretical falling-film model for absorbers. In this theoretical model the absorber is also working as a vapour compression cycle evaporator, in which the refrigerant is ammonia. Heat and mass transfer performances are evaluated as a function of inlet temperatures, flow rates, concentrations and ammonia quality for a cross-flow disposition, and assuming complete wettability of the tubes. Because of the defined assumptions and the refrigerant conditions modelled in [41] (evaporation temperature of 0 °C) it is difficult to obtain reliable results with this theoretical model.

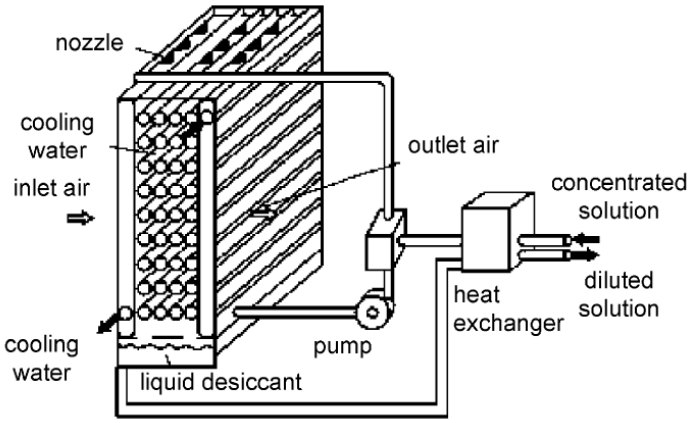

Figure 2.15. Internally water-cooled cross-flow falling film dehumidifier [29].

Gommed et al. [11] made an experimental comparison among three air-solution contactors: an adiabatic-structured packed-bed, a falling-film with horizontal tubes with staggered arrangement made of HDPE and a falling-film with horizontal tubes with staggered arrangement made of titanium (Figure 2.16). They found out that heat transfer between the solution achieved in the HDPE air-solution contactor was lower (251 W/m^2°C) than in the titanium one (676 W/m^2°C). This fact was mainly due to a worst wetting tube in the HDPE air-solution contactor.

Figure 2.16. Internally water-cooled made of HDPE (left) and titanium (right) [11].

Chung and Wu [42] experimentally compared an air-solution contactor with horizontal tubes with one with horizontal tubes and fins at absorber conditions. They could correlate the mass transfer coefficient in the air side. Moreover they found out improvements in the efficiency of the absorber with fins of 20 % with respect the one without fins.

2.4.2.4. Falling-film with tubes and fins air-solution contactors

Yamaguchi et al. [43] analysed the performance for a system with tubes and fins in the absorber and the regenerator. The absorber of the hybrid system is at the same time the absorber of the liquid desiccant system and the evaporator of the vapour compression system. The refrigerant used is R407. Some of the results obtained with this configuration are the following:

- Part of dehumidification could be obtained from moisture condensation because the refrigerant inlet temperature in the evaporator is low.
- Regenerator temperature is lower than 38 °C.
- The desiccant concentration is low, with about 28 % of LiCl.
- Desiccant flow rate is low compared with air flow rate, which permits to have a good performance system and to use energy storage.

- System COP improves from 2.71 to 3.82 due to the improvement in the compressor isentropic efficiency and the temperature effectiveness of the solution heat exchanger.

2.4.2.5. Summary of the experimental air-solution contactors of the falling-film type

Table 2.2 and Table 2.3 show the features of the internally-cooled/heated air-solution contactors found in the literature. The tables include flow disposition (parallel, cross or counter-flow), the dimensions, the desiccant material used, the inlet conditions of air and water streams and the dehumidification achieved for the different types of air-solution contactors.

Table 2.2. Experimental internally cooled absorbers.

Absorber						
Type of air-solution contactor	**Flow**	**Author**	**Material**	**Dimensions and desiccant**	**Inlet conditions**	**Dehumidification (kg_w/kg_a)**
Plates	Counter	Läevemann et al. [35]	Polypropylene	128 plates LiCl	m_a = 3200 m^3/h T_a = 25.0 ºC W_a = 0.0120 kg_w/kg_a T_w = 22.1 ºC	0.0070
Extruded plates	Counter	Yonggao et al. [38]	Stainless steal	H = 0.100 m 0.298 x 0.093 m LiCl	m_a = 220 m^3/h T_a = 30.9 ºC W_a = 0.0134 kg_w/kg_a T_w = 22.1 ºC	0.0028
		Kessling et al. [36]	Polypropylene	H = 0.460 m 0.980 x 0.011 m LiCl	m_a = 40 m^3/h T_a = 24.5 ºC W_a = 0.0144 kg_w/kg_a T_w = 24.1 ºC	0.0091
		Lowenstein et al. [37]	PVC	8 rows and 8 channels LiCl	m_a = 10200 m^3/h T_a = 29.4 ºC W_a = 0.0192 kg_w/kg_a T_w = 29.4 ºC	0.0103
	Cross	Liu et al. [40]	Thermally conductive polypropylene	H = 0.230 m 0.400 x 0.700 m A = 4.12 m^2 LiBr	m_a = 0.180 kg/s T_a = 33.5 ºC W_a = 0.0159 kg_w/kg_a T_w = 15.0 ºC	0.0018
Tubes	Counter	Gommed et al. [11]	High density polyethylene	H=0.230 m 0.400 x 0.700 m A = 6.38 m^2 LiCl	m_a = 1000 m^3/h T_a = 28.0 ºC W_a = 0.0150 kg_w/kg_a T_w = 29.0 ºC	0.0070
			Titanium	H = 0.230 m 0.400 x 0.700 m A = 4.12 m^2 LiCl	m_a = 1000 m^3/h T_a = 28.0 ºC W_a = 0.0150 kg_w/kg_a T_w = 29.0 ºC	0.0070
		Chung and Wu [42]	Stainless Steal	H = 0.150 m 0.150 x 0.150 m A = 4.12 m^2 TEG	m_a = 3.77 kg/min T_a = 20.0 ºC W_a = 0.0111 kg_w/kg_a T_w = 21.3 ºC	0.0040
Tubes and fins	Counter	Yamaguchi et al. [43]	Metallic-coated	H = 0.500 m 0.300 x 0.200 m LiCl	m_a = 300 m^3/h T_a = 30.0 ºC W_a = 0.0140 kg_w/kg_a T_{ref} = 6.1 ºC	0.0060
		Chung and Wu [42]	Stainless Steal	H = 0.150 m 0.150 x 0.150 m A = 2.53 m^2 TEG	m_a = 3.77 kg/min T_a = 25.4 ºC W_a = 0.0174 kg_w/kg_a T_w = 25.2 ºC	0.0075

Table 2.3. Experimental internally heated regenerators.

Regenerator						
Type of air-solution contactor	**Flow**	**Author**	**Material**	**Dimensions and desiccant**	**Inlet conditions**	**Regeneration (kg_w/kg_a)**
Plates	Counter	Läevemann et al. [35]	Polypropylene	128 plates, LiCl	m_a = 3200 m^3/h T_a = 25.0 ºC W_a = 0.0120 kg_w/kg_a T_w = 75.0 ºC	0.0140
Extruded plates	Counter	Yonggao et al. [38]	Stainless steal	H = 0.100 m 0.298 x 0.093 m LiCl	m_a = 220 m^3/h T_a = 26.5 ºC W_a = 0.0115 kg_w/kg_a T_w = 70.0 ºC	0.0120
	Cross	Liu et al. [40]	Thermally conductive polypropylene	8 rows and 8 channels LiBr	m_a = 0.235 kg/s T_a = 19.1 ºC W_a = 0.0050 kg_w/kg_a T_w = 36.7 ºC	0.0024
Tubes and fins	Counter	Yamaguchi et al. [43]	Metallic-coated	H = 0.500 m 0.300 x 0.200m LiCl	m_a = 600 m^3/h T_a = 30.0 ºC W_a = 0.0140 kg_w/kg_a T_{ref} = 38.3 ºC	0.0037

2.4.3. Solar collector regenerators

Despite liquid desiccant systems can be driven by any source that provides heat at low-medium temperature, most of liquid desiccant regenerator proposals have been designed to be operated by solar energy.

Kakabaev and Khandurdyev [44] presented in 1969 the first solar collector proposal to be used as source element for the regeneration process. Since then, many different configurations have been appeared. There are some cases where heat and mass transfer take place in the solar collector:

- Open-type.
- Close-type.
- Natural convection.
- Forced convection.

In some other cases, only heat transfer occurs in the solar collector.

Open-type regenerator

This is one of the simplest systems for desorbing a liquid desiccant. Figure 2.17 shows a schematic of an open solar collector with its main components. The weak solution flows on the solar collector surface and it is put in contact with the ambient air.

Several researchers, such as Kakabaev et al. [44], Collier [45] or Gandhidasan [46], used an open solar collector to regenerate the liquid desiccant. The main advantage of this configuration is that the required regeneration temperature can be low; however, the major problem of this kind of collectors is that ambient conditions, such as rain and wind, may affect to the collector performance.

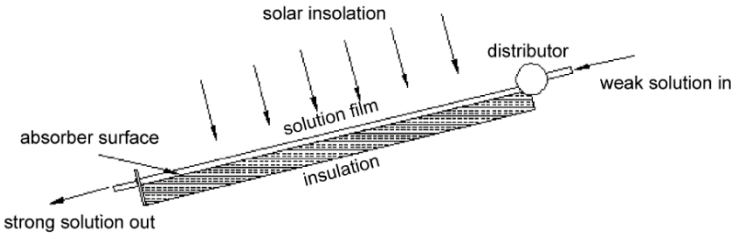

Figure 2.17. Open solar collector regenerator [29].

Close-type regenerator

With this solar configuration the regeneration process occurs throughout the solar collector but the climate problems are solved. Figure 2.18 shows a schematic of a close solar collector with its main components. In this case the desorbed water condensates in the collector glass and is driven by gravity towards a pipe to the bottom part.

Gandhidasan [47] carried out a theoretical studied for the required tilted of this solar collector. The main problem of this configuration resides on the high vapour pressure of water in the air because of the lack of ventilation which affects to the regeneration performance.

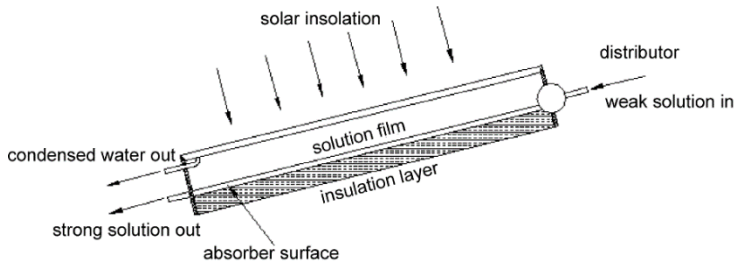

Figure 2.18. Close solar collector regenerator [29].

Natural and forced convection regenerator

The solar regenerator with convection is similar to the close-type solar collector. In this case, the top and the bottom part are opened for ventilation, either forced flow or natural flow wind. Figure 2.19 shows a schematic of a solar collector regenerator with natural or forced convection and its main components.

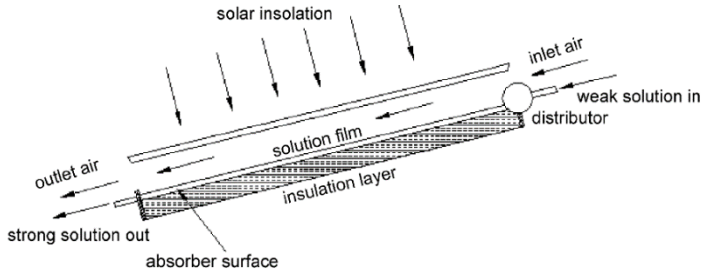

Figure 2.19. Solar collector regenerator with natural or forced convection [29].

Some researchers have been investigating this kind of regenerator solar collectors, such as Yang and Wang [48] and Alizadeh and Saman [49], carrying out experimental studies with this configuration to optimize the best kind of flow or the most appropriate glazing and insulating thickness.

This alternative permits to achieve the advantages of a good regeneration performance of the open-type solving the problems related with the ambient conditions.

Only heat transfer in solar collector

In order to increase the mass transfer surface available in a solar collector regenerator, several authors, such as Agarwal et al. [50] and Griffiths [51], combined a flat plate collector to heat the desiccant solution with a packed material for the mass transfer process with the air. This configuration achieves a better regeneration performance than the indirect regeneration. However, corrosion problems may appear when conventional solar collectors are used.

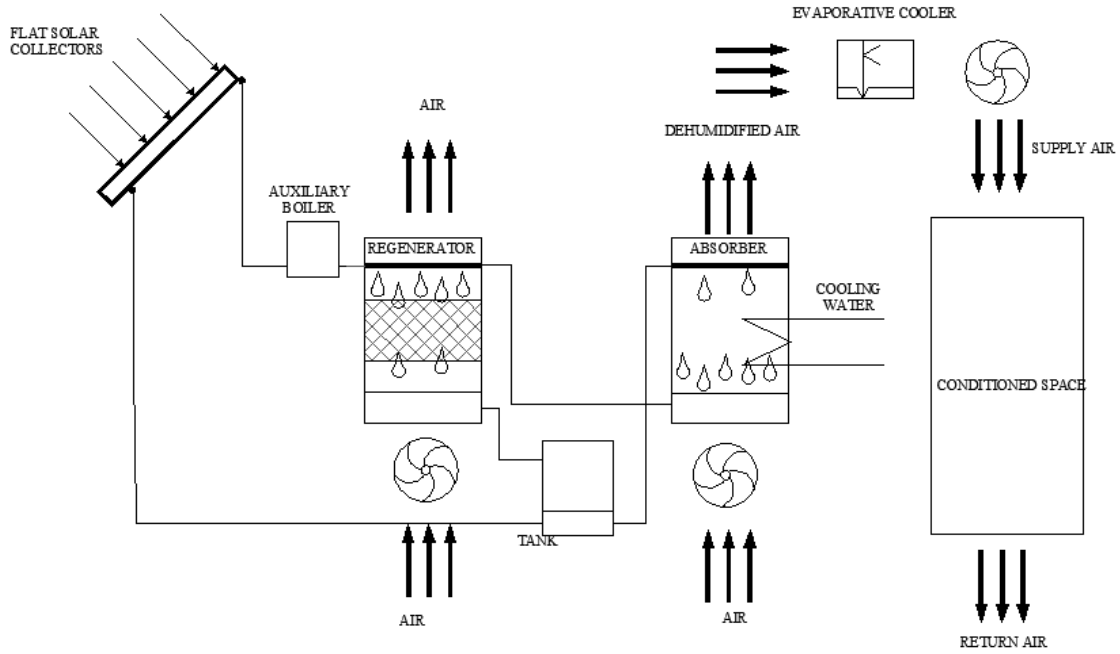

Figure 2.20. Griffiths liquid desiccant system (adapted from [51]).

9.1. General and specific thesis objectives

The main objective of this thesis is to make a theoretical and an experimental study of a hybrid liquid desiccant system using rust-proof and cost-effective materials, keeping a good performance of the system and achieving high energy efficiency. The thesis is mainly focused on the principal components of the liquid desiccant system: the absorber and the regenerator.

The specific objectives required to overcome the main objective are:

- Comprehensive review of the liquid desiccant systems that includes a study of the different liquid desiccant materials, air-solution contactors and liquid desiccant configurations. This review will help to select most appropriate liquid desiccant material, typology of air-solution contactor and system configuration.
- Selection of the rust-proof and cost-effective material that optimizes the heat and mass transfer of the air-solution contactors.
- Modelling, sizing and design of a hybrid liquid desiccant system that has to operate in two locker rooms in a swimming-pool in Taiwan Building Technology Center in Taipei (Taiwan).
- Set-up of the hybrid liquid desiccant system before the departure to the demonstration site.
- Analysis of the experimental performance of the air-solution contactors and the liquid desiccant system.
- Validation of the models for the air-solution contactors and the complete liquid desiccant system.
- Modelling of a hybrid liquid desiccant system for being dynamically simulated.
- Operational optimization of the hybrid liquid desiccant system.

Some of the results taken from the studies carried out in this thesis have been used for the developing of the system. Moreover, the experimental performance data of the demonstrative hybrid liquid desiccant system when it operates in a real application in Taiwan has been used for its evaluation.

2.4.4. Pressurized absorber

This typology of air-solution contactor has been recently proposed by Yonggao et al. [52]. The moist air is compressed before being cooled through a heat exchanger and a cooling coil, and dehumidified through an

adiabatic packed bed air-solution contactor. As it can be seen in Figure 2.21, the vapour pressure of the water increases when the moist air is compressed, what improves the dehumidification of the air. As main results, the higher air pressure, the higher dehumidification. For instance, at 0.5 MPa the supply humidity ratio achieved is 0.0009 kg_w/kg_a.

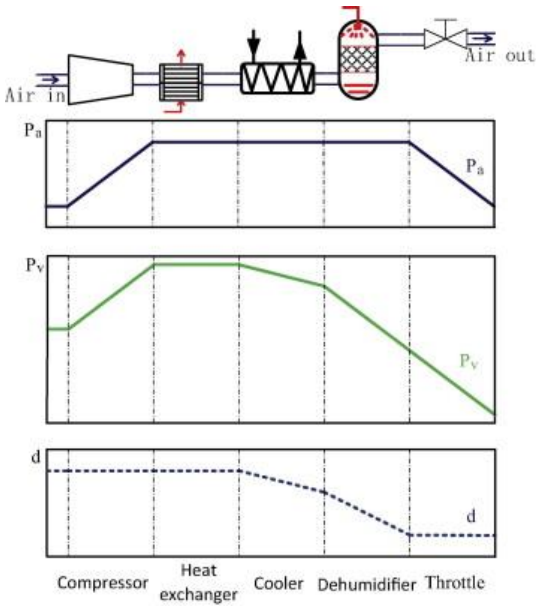

Figure 2.21. Schematic of the change of the compressed air state [52].

2.5. Energy storage

Including a tank to store the desiccant liquid may improve the performance of solar liquid desiccant systems, because the system can continue dehumidifying when there is little heat available to regenerate the solution. Moreover, energy can be stored easily and is non-dissipative due to it is in the form of latent heat in the desiccant solution. Kessling el al. [36] obtained from an experimental point of view the relationships between dehumidification enthalpy storage and different impacting factors in cooled absorber.

The energy storage capacity (*SC*) by a desiccant solution can be defined as [36]:

$$SC = \frac{m_a(W_{a,in} - W_{a,out})\rho_s \cdot h_{WS}}{m_s} = (1 - X) \cdot h_{WS} \cdot \rho_s \quad (2.1)$$

On the other hand, Gommed and Grossman [53] patented an apparatus which consists in an energy storage that is, at the same time, heat and mass transfer exchanger. This tank avoids the use of solution heat exchanger and enhances the performance and the operation control of a liquid desiccant system. Several embodiments, that can be suitable for different liquid desiccant systems, were also presented. Figure 2.22 shows one of these embodiments proposed by Gommed and Grossman.

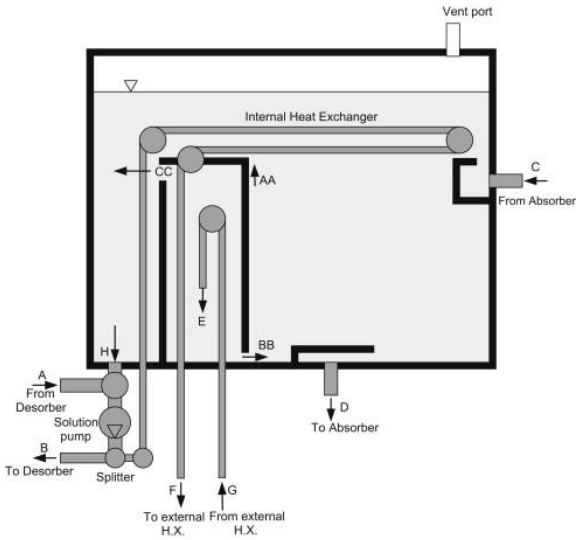

Figure 2.22. Heat and mass exchanger tank for liquid desiccant applications [54].

2.6. Liquid desiccant system configurations

A big amount of different liquid desiccant systems have been studied in the last forty five years. Despite the main concept is the same, to put in contact a liquid desiccant with moist air in order to obtain a heat and mass transfer between them, the way of providing the cooling and handling the sensible load of the air differs. In this sense liquid desiccant system can be classified as:

- Liquid desiccant system with evaporative cooling.
- Hybrid liquid desiccant systems, that can be combined with:
    - Vapour compression chillers or heat pumps.
    - Absorption chillers.

2.6.1. Combination of liquid desiccant system with evaporative cooling

In the same way than solid desiccant systems, liquid desiccant systems can be combined with evaporative coolers. In both cases, moist air must be over dehumidified in order to provide to the moist air the capability of being cooled down by the evaporative cooler. In liquid desiccant systems with evaporative coolers, heating required for the liquid desiccant regeneration is usually provided by solar energy or waste heat and cooling required for the dehumidification is usually provided by a cooling tower.

This kind of system can contain either adiabatic or non-adiabatic air-solution contactors. Gommed and Grosssman [55] designed and developed a liquid desiccant system with adiabatic packed bed air-solution contactors (see Figure 2.23). On the other hand, Chebbah [56] designed a liquid desiccant system with non-adiabatic air-solution contactors (see Figure 2.24).

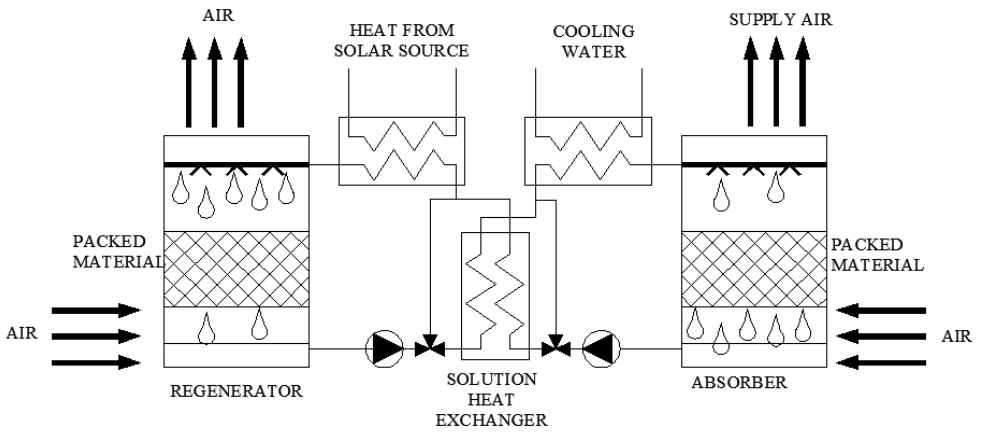

Figure 2.23. Schematic figure of the experimental set-up of Gommed and Grossman liquid desiccant system (adapted from [55]).

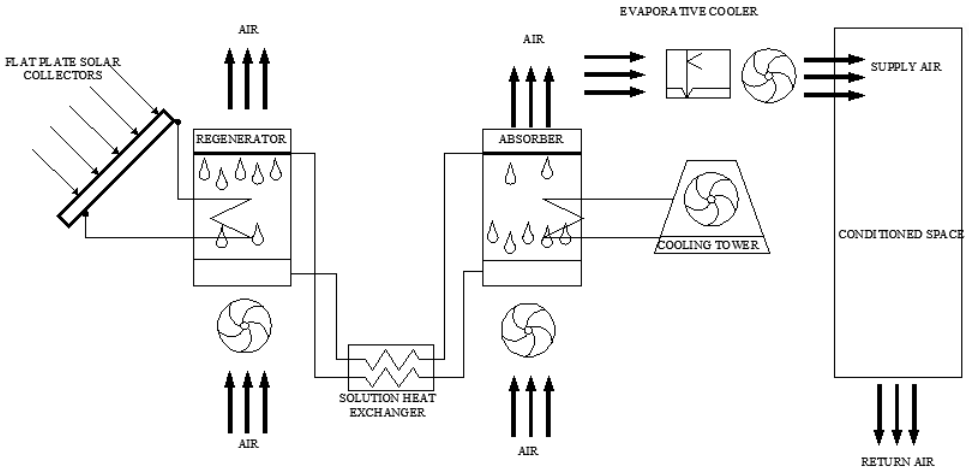

Figure 2.24. Schematic figure of the design of the liquid desiccant system proposed by Chebbah (adapted from [56]).

2.6.2. Hybrid liquid desiccant systems

Since liquid desiccant systems have a good performance when latent load has to be handled and conventional vapour compression or absorption systems are good at providing sensible cooling, a combination of both kinds of systems may decrease the required energy consumption.

In addition, waste heat from the absorption or vapour compression system can be used as part of the heat needed for the desiccant regeneration. This configuration may either decrease the required solar subsystem size or even eliminate it.

Besides the advantages achieved in the regeneration, supplying chilled water to the dehumidification process permits decreasing the liquid desiccant vapour pressure and hence increasing the absorber performance. Moreover, since the moisture is absorbed by the desiccant, the evaporator does not have to be maintained below the dew point of the supply air, which permits increasing the evaporator temperature and, therefore, reducing the absorption or vapour compression system consumption.

2.6.2.1. Combination of liquid desiccant systems with vapour compression systems

According with the review carried out by Mohammad et al. [57], COP of the hybrid liquid desiccant/vapour compression system was shown to be greater than the conventional vapour compression system by 23.1-73.8 %, and the energy savings were in the range of 26-80 %.

Peterson and Howell [58] patented, in 1990, a hybrid liquid desiccant vapour compression air-conditioning system (Figure 2.25). In this configuration the evaporator and the condenser are, at the same time, the liquid desiccant system absorber and regenerator respectively. A thermodynamic analysis of this hybrid system

was developed by Yadav [59], who compared it with a conventional vapour compression cycle, the hybrid system presented 40-80 % less electrical consumption. However, from the technical point of view this configuration may have some problems with high pressures in the condenser and absorber and the control strategy when partial load have to be handled. For these reasons, most of the hybrid liquid desiccant/vapour compression systems combine both cycles in a separated form.

Yamaguchi et al. [43] simulated and experimented a hybrid system similar than Peterson and Howell, but including a small tank in the refrigerant loop before the compressor and two liquid desiccant tanks in the liquid desiccant loop. In this case, absorber/evaporator could be operating at low temperatures and desiccant concentration could be reduced in order to operate the regenerator/condenser in a suitable temperature level to achieve a reasonable COP in the vapour compression cycle. Dehumidification achieved in this system was up to 0.0059 kg_w/kg_a.

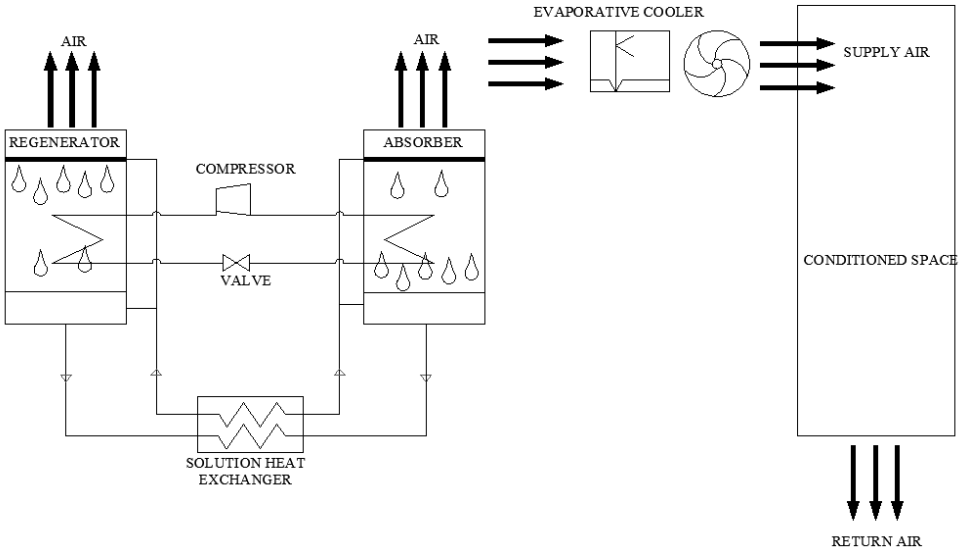

Figure 2.25. Schematic figure of the hybrid liquid desiccant/vapor compression system developed by Peterson and Howell (based on [58]).

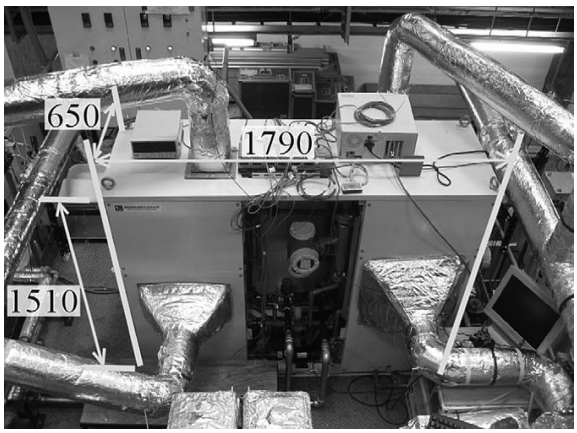

Figure 2.26. Picture of the hybrid liquid desiccant system developed by Yamaguchi et al. [43].

Several researchers have carried out comparisons between different configurations of hybrid liquid desiccant/vapour compression systems with conventional vapour compression system, such as Sick [60] and Thornbloon and Ninmo [61] (see Figure 2.27). In general, a decreasing in the electrical consumption was found when the regenerator in hybrid liquid desiccant/vapour compression systems is heated by solar energy, minimizing the operational costs.

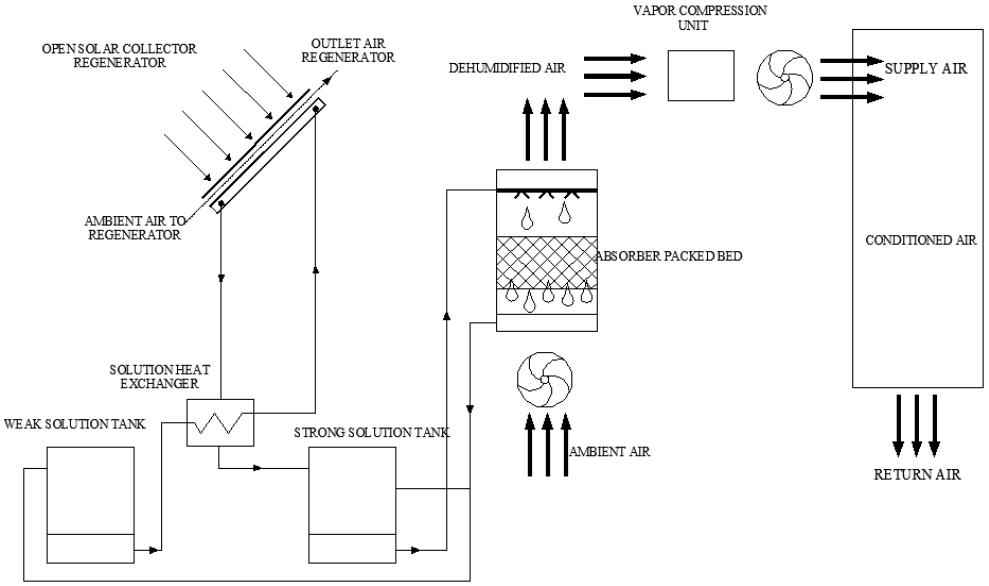

Figure 2.27. Schematic figure of the hybrid liquid desiccant/vapor compression system developed by Thornbloon and Nimmo based on [61]).

Dai et al. [62] designed and experimented a different hybrid liquid desiccant system (Figure 2.28), which consists on a vapour compression cycle, a liquid desiccant cycle and an evaporator cooler. The system COP was increased up to 23.1 % compared with the conventional vapour compression system.

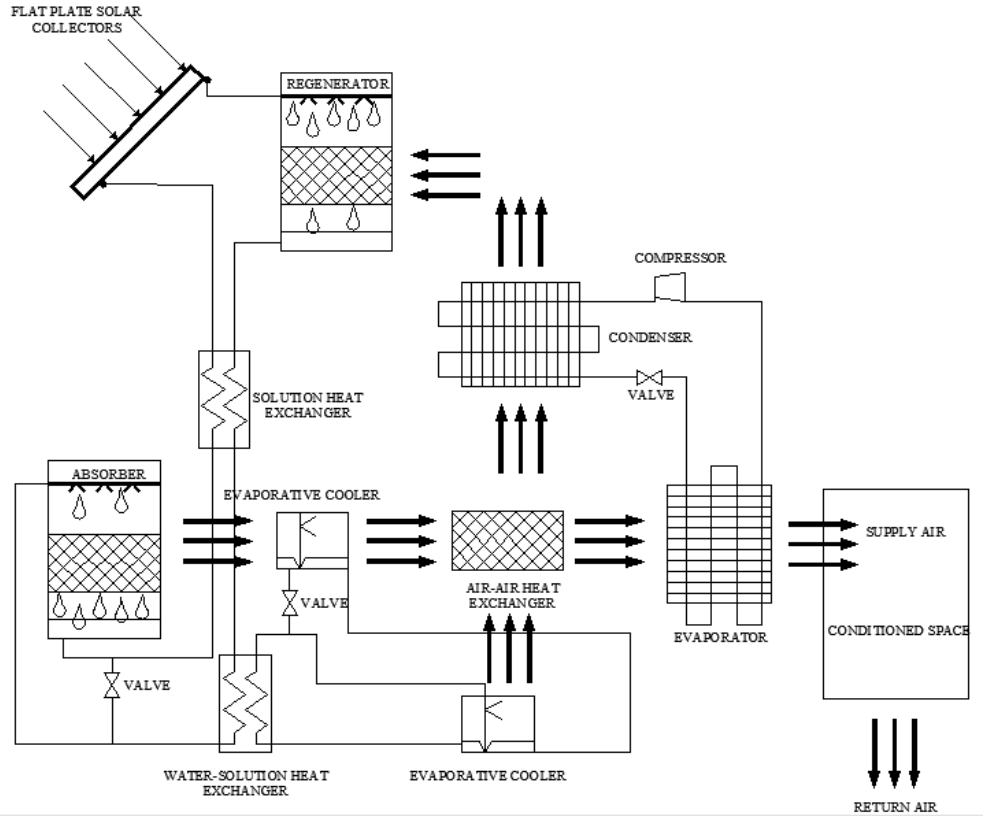

Figure 2.28. Schematic figure of the hybrid liquid desiccant/vapor compression system developed by Dai et al. (based on [62]).

Niu et al. [63] studied the control strategies of the hybrid liquid desiccant system described in Figure 2.29. The results showed that the vapour compression cycle with double compressor permits achieving the capacity matching between both cycles.

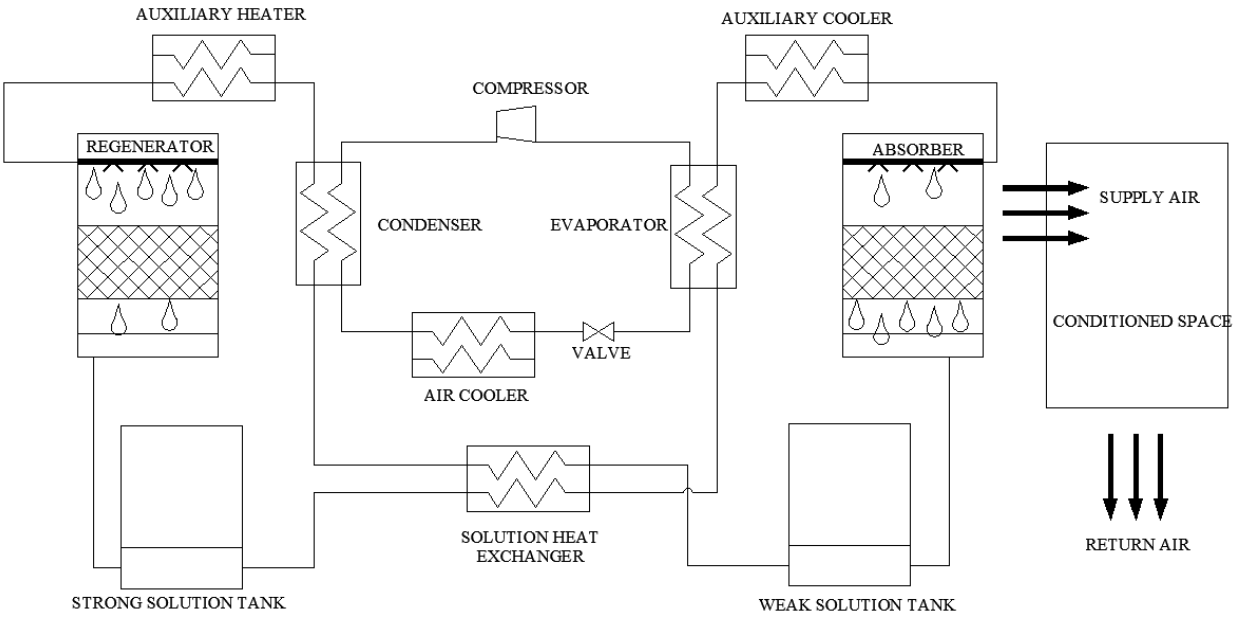

Figure 2.29. Schematic figure of the hybrid liquid desiccant/vapor compression system developed by Niu et al. (based on [63]) .

Chen et al. [10] proposed a hybrid liquid desiccant system (Figure 2.30), which can operates at low temperatures in the evaporator, allowing also low concentrations in the LDS and therefore permitting regeneration at suitable temperatures to be provided by the chiller condenser. With this proposal the overall COP of the hybrid system was up to 116 % more than that of the conventional chiller.

Figure 2.30. Chen et al. [10] hybrid liquid desiccant/vapor compression system.

2.6.2.2. Combination of LDS with absorption systems

Hybrid liquid desiccant/absorption system was firstly described by Wilkinson [64]. In this configuration, the cooling tower needed for the absorber of the absorption chiller is also used to reject heat from the absorber of the liquid desiccant. Moreover, the heat rejected from the condenser of the absorption chiller is provided to the regenerator. In this case, additional heat may be required to provide heat to the regenerator when the latent load is large compared with the sensible load. The COP of this system was predicted to be bigger than for both systems separately.

Hernández et al. [65] made a performance comparison among the solar-assisted absorption system alone, the absorption system coupled to a liquid desiccant system (Figure 2.31) and absorption system coupled to a solid desiccant system. The highest solar fraction (88.4 %) was obtained for the hybrid liquid desiccant system.

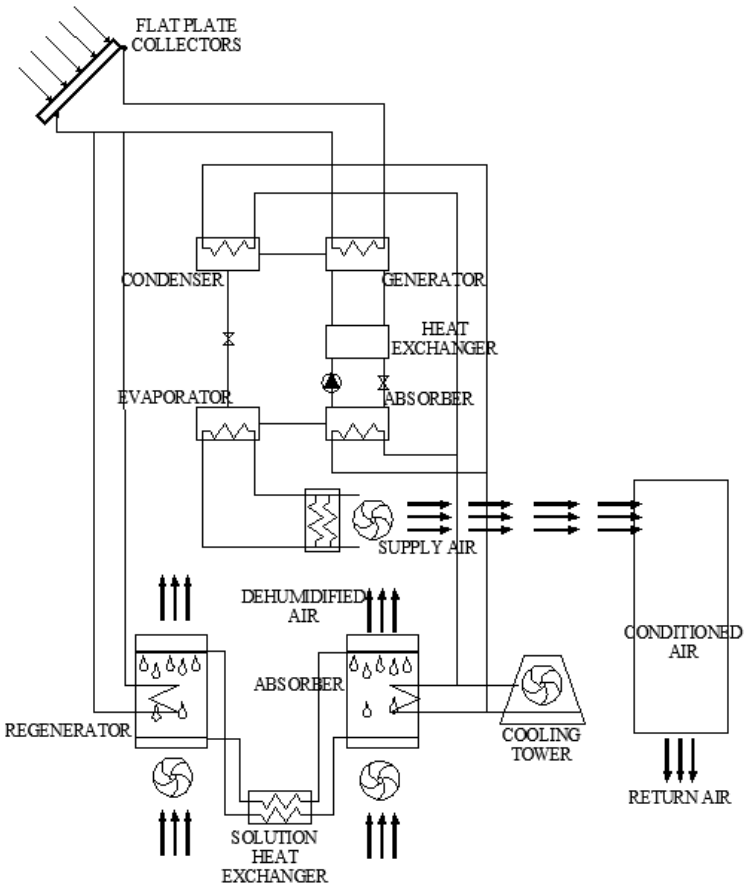

Figure 2.31. Hernández et al. hybrid liquid desiccant/absorption system (based on [65]).

Ahmed et al. [66] simulated the COP of a hybrid liquid desiccant/absorption system using LiCl solution for both cycles. According to their results, this system achieved a COP of approximately 50 % more than the obtained with the conventional absorption system.

In general, compared with the hybrid liquid desiccant/vapour compression systems, the hybrid liquid desiccant/absorption system needs more working fluid for both subsystems. However, the driving heat source could be supplied totally by solar energy or other thermal energy, without consumption of electricity [29].

2.7. Commercial liquid desiccant systems

Despite liquid desiccant systems offer a great amount of advantages in HVAC systems, especially in warm and humid climates, this technology have not achieved a great impact in this market. However, there are several liquid desiccant products for air conditioning applications on the market. Some represent the whole air-conditioning system solutions, while others have a more limited scope, such as handling the latent load alone [67].

Kathabar has manufactured desiccant dehumidification systems for almost 80 years. This company provides a wide range of packed bed dehumidifiers and regenerators. In total 14 different size conditioners are available. Vertical or horizontal air flow rate arrangement is possible to be handled. Its series are designed to handle airflows from 2550 m^3/h to 142716 m^3/h. Kathabar offers a total of eight different size regenerators, which are matched with the conditioners required for a given installation [5].

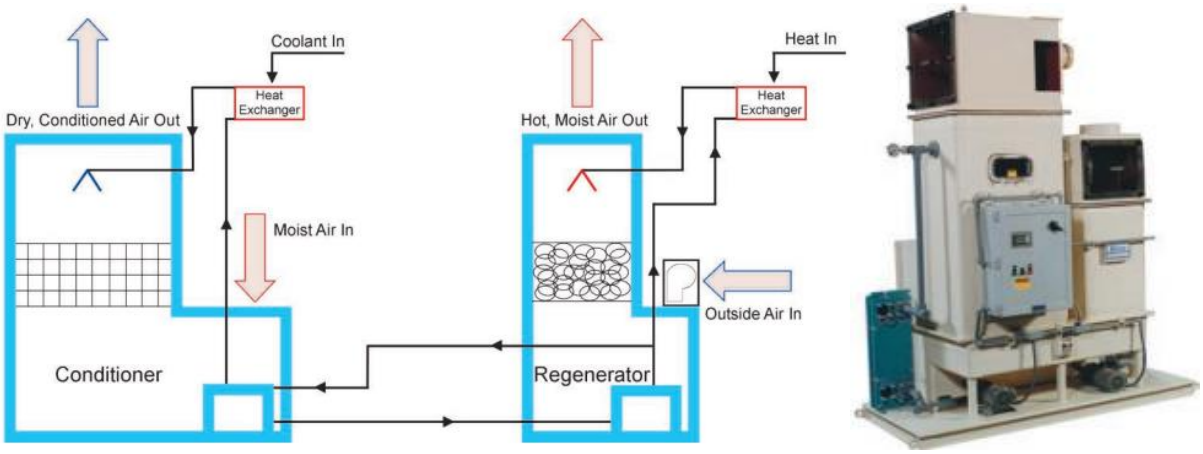

Figure 2.32. A commercially available packed bed liquid desiccant dehumidifier. Kathabar [5].

AIL Research develops two liquid desiccant systems [68]:

- LD DOAS system: This system uses water-cooled plastic-plate heat exchangers to cool and dehumidified moist air. Cooling water for the conditioner can be provided by a cooling tower or by a chiller. Temperature required for hot fluid flowing within the regenerator goes from 70 ºC to 105 ºC. Left graph of Figure 2.33 shows the LD DOAS system.

- Compressor LDDX: this system is an integrated vapour compression cycle with a desiccant cycle, where a heat exchanger works as both evaporator and dehumidifier; and condenser is also a regenerator. Figure 2.34 shows a simplified description of LDDX systems. AILR will be field operating two LDDX as part of an award under the Department of Defense's Environmental Security Certification Program (ESTCP Award).

Figure 2.33. Prototype of a 10.200 m^3/h rooftop liquid-desiccant air conditioner and liquid-desiccant conditioner. AIL Research, Inc. [68].

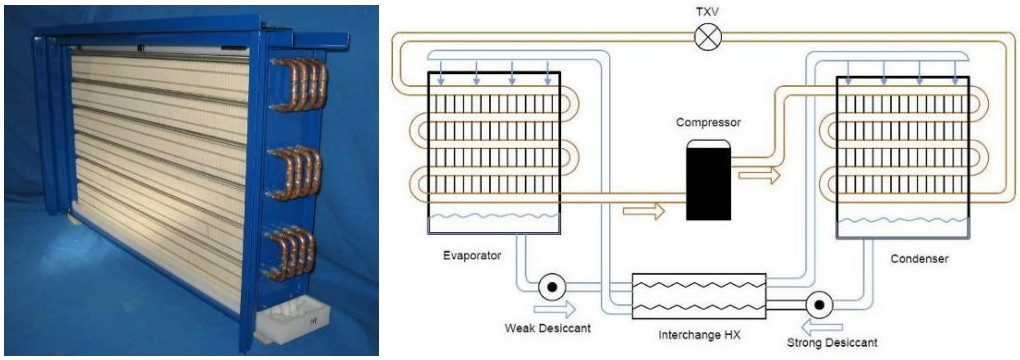

Figure 2.34. Dehumidifier-evaporator and schematic description of AIL Research LDDX system [68].

Menerga has developed an air handling unit that integrates a liquid desiccant system with adiabatic air-solution contactors combined with evaporative cooling [69]. The liquid desiccant regeneration is recommended to be supplied by solar energy. Air handling units from 2900 to 14900 m^3/h are available.

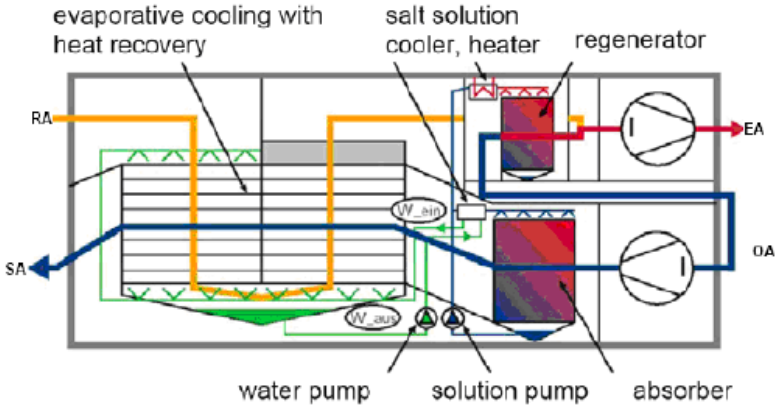

Figure 2.35. Menerga air handling unit that uses liquid desiccant technology [21].

Advantix systems - DuCool has available two different packed bed desiccant systems for small applications [6]:

- DuTreat series: It is a hybrid liquid desiccant system whose evaporator is divided in two parts: the first part cools liquid desiccant and the second part is a post cooling coil. Liquid desiccant in regenerator is heated by the condenser. These series are designed to handle airflows from 800 m^3/h to 5780 m^3/h. Top graph in Figure 2.36 shows a schematic description of DuTreat series.
- DuHandling series: It is a liquid desiccant system which solution is cooled and heated by external sources. The series are designed to handle airflows from 510 m^3/h to 5780 m^3/h. Bottom picture in Figure 2.36 shows a schematic description of DuHandling series.

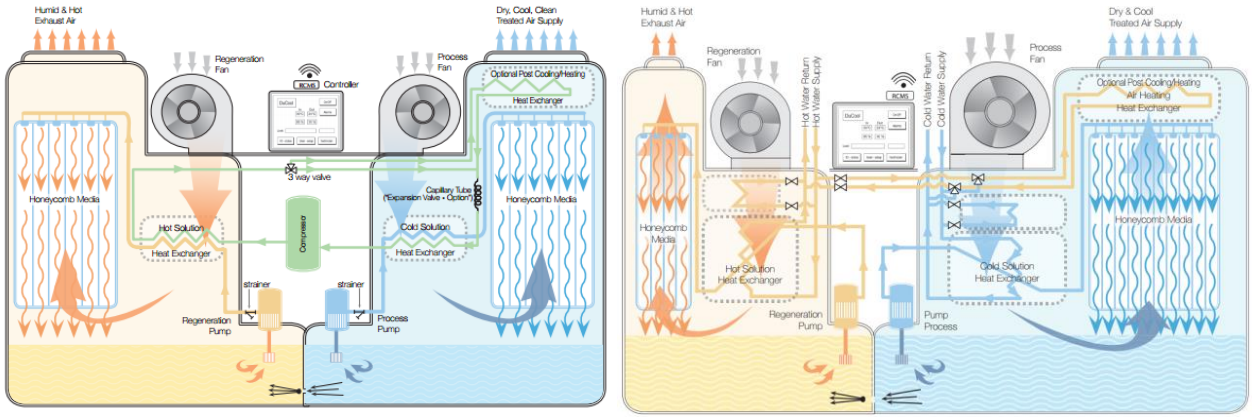

Figure 2.36. Two schematic descriptions of DuCool system [6].

Ficom manufactures what they call a *Dual Cycle Energy Recovery* (DICER-D) unit. The system is represented in Figure 2.37 and combines air dehumidification with indirect evaporative cooling in a single unit. The regeneration takes place in a separated unit [7].

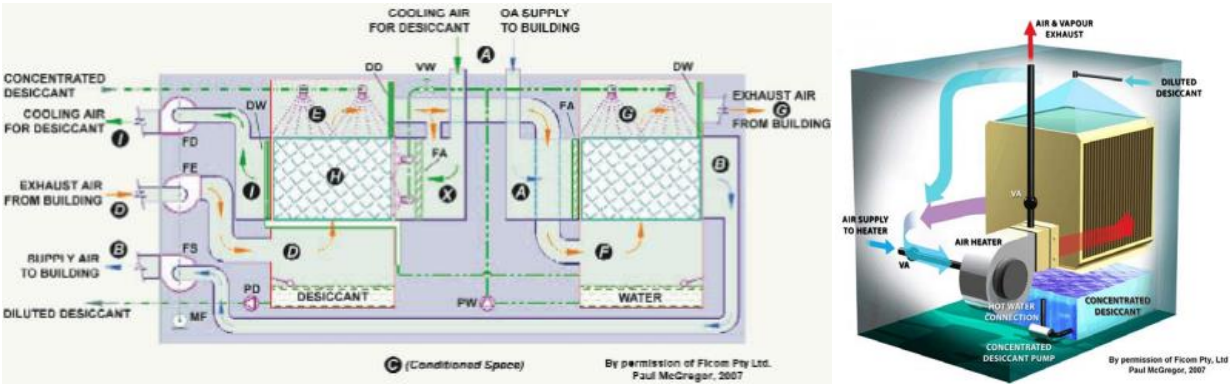

Figure 2.37. Schematic representation of Ficom's AHU and regenerator [7].

L-DCS offers a liquid desiccant system, which combines a decentralized air handling with (dehumidification and evaporative cooling) with central regeneration and desiccant storage. The absorber is internally cooled by water and the regenerator is internally heated by water at a temperature in the range of 60 – 80 ºC [70]. The absorber use a patent liquid desiccant distributor [35] to ensure a good wetting of the contacting surfaces.

DYNA-AIR is Japanese company that was founded in 2004. They sell a liquid desiccant system with adiabatic packed-bed air-solution contactors in which heating and cooling is provided by a heat pump [8] (see Figure 2.38). Nowadays, there are 5 units available from 300 to 9000 m^3/h [8].

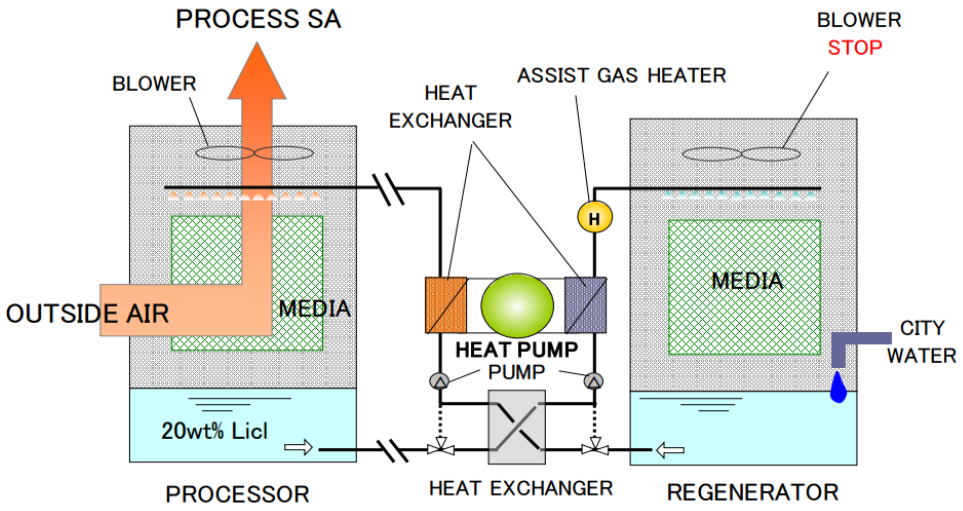

Figure 2.38. Schematic representation of DYNA-Air liquid desiccant system [71].

AEX (American Energy Exchange) has been on the market with the so-called *enthalpy pump*, which is conceived as a dehumidifier to be placed upstream of the evaporator of a conventional chiller or air conditioning unit. This component solves the carryover problem by placing a micro-porous membrane between the desiccant solution and the air [72], Figure 2.39.

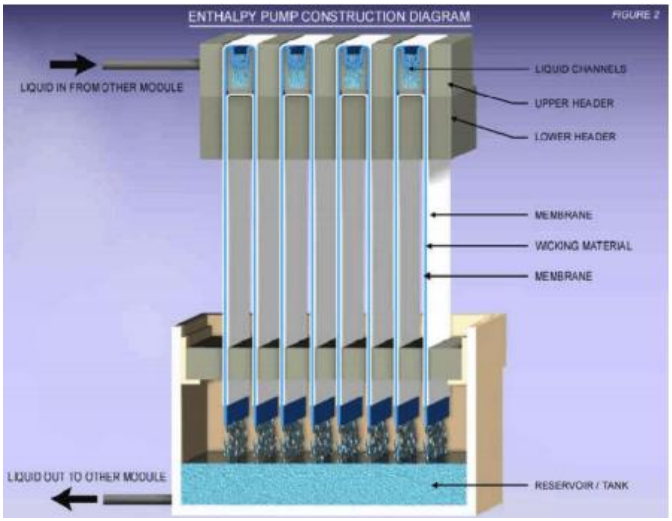

Figure 2.39. Schematic representation of the AEX Enthalpy pump [72].

2.8. Conclusions

The following conclusions are pointed out from the state-of-the-art:

- Despite liquid desiccant systems have been studied since long time ago and they have not reached a great impact on the market yet, the number of papers and studies is increasing in the last years because they offer many advantages when handling latent load.
- Among the different liquid desiccant materials, the LiCl-H_2O solution seems to be the most appropriated due to its low vapour pressure. However, this material is very corrosive and, therefore, all the elements that are in contact with it must be non-corrosive materials.
- Despite the most used air-solution contactors are the adiabatic packed bed, falling-film air solution contactors can be a good alternative to them because heat and mass transfer can be enhanced and air pressure drops can be reduced. Moreover, by using falling-film air-solution contactors the liquid desiccant flow rate can be reduced. This allows for improving the COP of the system, decreasing the carry-over of the liquid desiccant and storing more latent energy
- Lastly, liquid desiccant systems are more integrated with vapour compression systems. When liquid desiccant systems are coupled with vapour compression systems, the operational conditions of both systems change: typically evaporator and condenser temperature increase in vapour compression systems and liquid desiccant concentration and temperature decreases in liquid desiccant systems. Furthermore, cooling and heating required for a liquid desiccant system can be provided by a vapour compression heat pump, what it makes the hybrid liquid desiccant system more efficient due to it only uses the compressor of the heat pump as the only energy source.

Chapter 3. Hydrodynamic study of falling-film with horizontal tubes for air-solution contactors in liquid desiccant systems

3.1. Introduction

Two of the main conclusions taken from Chapter 2 were that LiCl-H_2O is an appropriate liquid desiccant material due to its low vapour pressure, and that falling-film can be a good alternative to adiabatic packed-beds. However, there are two problems to be solved if these liquid desiccant and air-solution contactors are chosen:

- This liquid desiccant material has a high surface tension that makes difficult the wetting of the tubes. This issue was experienced during the stay at the Technion, when three air-solution contactors were compared: and adiabatic packed-bed, a falling-film with horizontal tubes air-solution contactor made of titanium and a falling-film with horizontal tubes air-solution contactor made of high density polyethylene. From this comparison, it was concluded that the poorer dehumidification and heat transfer on the plastic air-solution contactor was mainly due to its lower wettability [11].
- This liquid desiccant is very corrosive. Therefore, non-corrosive material must be used to prevent the corrosion of the air-solution contactors.

Wettability is a key factor in the air-solution contactor performance because in one hand, liquid desiccant flow rate must be high enough in order to wet the complete surface of the tubes. In this way, higher mass transfer and heat transfer are achieved due to a grater surface contact between the air and the liquid desiccant and between the liquid desiccant and the horizontal tubes. On the other hand, a lower flow rate of liquid desiccant enhances the COP of the liquid desiccant system, reduces the electrical consumption of the pumps, reduces the carry over problem and permits higher latent energy storing because higher solution concentrations differences are achieved.

Therefore, the main objective of this chapter is to find a rust-proof material that could be completely wetted with low LiCl-H_2O flow rates. For this reason, a hydrodynamic study of different tube materials when LiCl-H_2O is flowing around them has been carried out. Due to its non-corrosion, polypropylene, high density polyethylene, low density polyethylene, polyamide and graphite have been tested. Moreover, in order to see if wettability of plastic tubes can be improved, a superficial plasma treatment has been done on polypropylene, low density polyethylene and polyamide.

In the beginning of this Chapter, a background that describes the theoretical bases of the hydrodynamic behaviour of falling-film with horizontal tubes is presented. After this, the experimental methodology is described. Finally, results and conclusions of this study are shown.

3.2. Background of the hydrodynamics of falling-film heat exchangers

Falling-film heat exchangers have been used in refrigeration, chemical, petroleum refining and desalinization industries because of its clear advantages over other technologies [73]:

- High heat transfer coefficient, allowing a better mass transfer and thus improving the cycle efficiency, minimizing the device size, resulting in reduced initial costs and space requirements.
- Low liquid flow rates, lowering the cost of the refrigeration plant and reducing risks associated with leaks or carry-over.

Despite these advantages, falling-film technology is not widely used in refrigeration and air conditioning, being almost ignored for liquid desiccant technology. On one side, this technology had not been used in these systems due to difficulties in liquid distribution and tube alignment, which affect flow uniformity and dry out, especially in deep bundles. On the other side, the high surface tension of the liquid desiccant materials makes difficult the wetting of the air-solution contactor surface, decreasing the performance of them.

However, in the last years, falling-film technology have started to be more employed in liquid desiccant systems as it is described in Chapter 2. Moreover, one of the sorts of air-solution contactors that present a greater potential to be implemented in liquid desiccant systems is falling-film with horizontal tubes.

3.2.1. Wettability, film breakdown and dry patches

Even when the film distribution is correct, break down and dry patches can appear if the flow rate of the liquid film is not sufficient. These dry patches produce a drastic reduction in the liquid-air contactor performance because the contact surface of the liquid surrounding the tubes is smaller. A schematic of falling film breakdown is shown in Figure 3.1.

In a review on a falling film evaporation on vertical surfaces, Gross [74] exposed the problem of dry patch formation. He concluded that formation of a dry patch is an instability problem related by the following forces on the film:

- Surface tension forces: the surface tension forces at the interface of the film have a tendency to enlarge the size of a dry patch.
- Marangoni effect: the surface tension gradient created by the temperature and concentration profile within the film, particularly near the boundary of a dry patch, acts to transport liquid away from the edge and hence to enlarge the dry patch.
- Liquid inertia forces: the static pressure within the liquid film at its stagnation point of a dry patch favours rewetting.
- Vapour inertia forces: the acceleration of the vapour-phase adjacent to the falling film increases or decreases the dry patch size depending on the direction of the vapour.
- Interfacial shear forces: these forces create two competing effects on a dry patch size, one trying to spread the liquid and rewet its top edge and the other trying to elongate its lower edge.

In addition, if water evaporation is high, the reduction of the film mass flow rate can produce new dry patches along the horizontal tubes. Among these forces, in liquid desiccant applications the main forces that affect the dry patch formation are the surface tension forces, the liquid inertia forces and the vapour inertia forces.

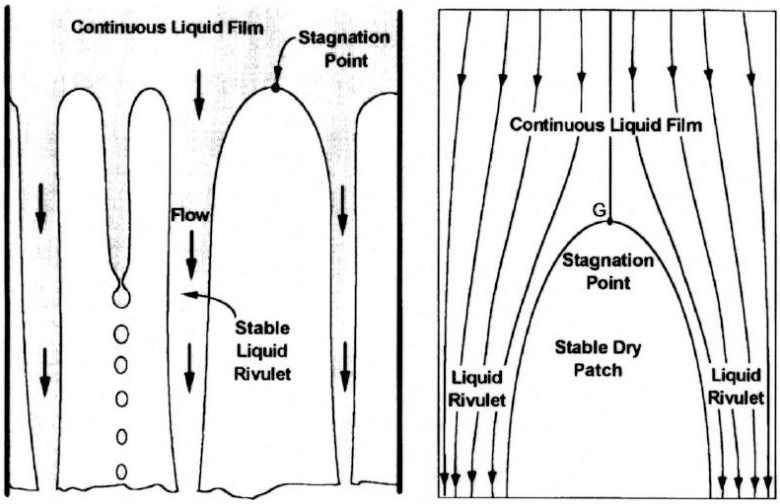

Figure 3.1. Schematic of a stable dry patch [75].

3.2.2. Surface tension and wettability

Wettability of the solution on horizontal tubes has a big effect on heat and mass transfer. If solution is able to wet the entire tube surface, a greater amount of solution will be in contact with moist air and the performance of the system will improve.

Wettability defines the preference of a solid to be in contact with one fluid rather than another. It is known that, in some cases, a liquid placed on a solid does not wet it, but it stays a drop having a contact angle between the liquid and solid phases. Wetting means that the contact angle θ between a liquid and a solid is zero or so close to zero; in this case, the liquid spreads over the solid easily. A contact angle situation is illustrated in Figure 3.2 [76]. Neglecting the effect of gravity the central relationship is the Young equation:

$$cos\theta = \frac{\gamma_{SV}-\gamma_{SL}}{\gamma_{LV}} \tag{3.1}$$

Where γ are the interfacial tensions energies between liquid, solid and vapour phases.

Figure 3.3 shows the surface tension of LiCl-H_2O solution as a function of temperature and concentration obtained from correlations given by Conde [77]. As it is shown, concentration has a higher influence in surface tension than temperature.

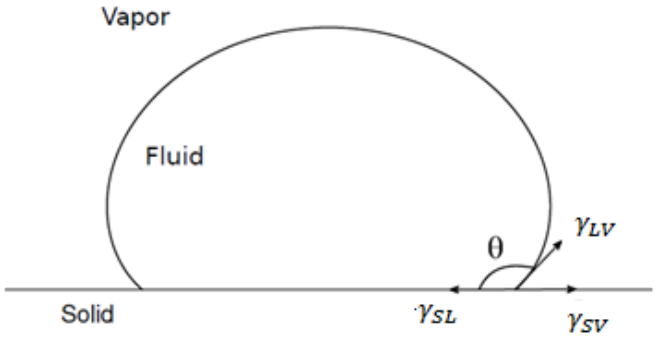

Figure 3.2. Drop and contact angle according with Young's Equation [78].

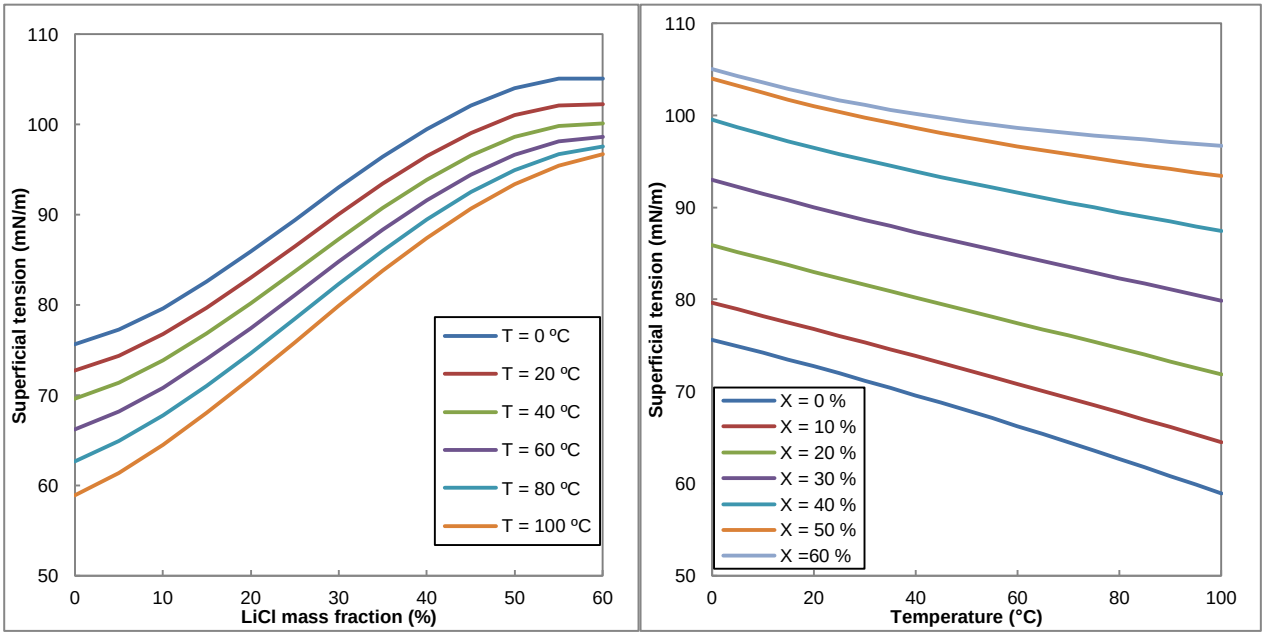

Figure 3.3. LiCl-H_2O solution surface tension as function of the LiCl mass fraction and temperature.

Qi et al. [79] experimentally investigated the contact angle of LiCl-H_2O when it is put in contact with a stainless steel plate. As expected according to the surface tension of the liquid desiccant material, the higher temperature and lower LiCl mass concentration, the lower contact angle measured.

3.2.2.1. Improvements of contact angle

Having a look on Figure 3.2, in qualitative terms, γ_{SL} and γ_{LV} should be as small as possible. From a practical point of view, one option to decrease the contact angle can be adding to the liquid phase a surfactant which is adsorbed at both the solid-liquid and the liquid-air interfaces. If the surfactant is non-volatile, it is presumed not affect γ_{SV}. In addition, γ_{LV} can be reduced with superficial treatment of the solid surface. However, these additives may reduce the dehumidification capability of the liquid desiccant material and they are not always the best solution.

On the other hand, surface roughness has an important role in wettability. When a liquid droplet wets completely a rough surface, the effect of the roughness on the contact angles is given by the following equation [80].

$$cos\theta_r = r\ cos\theta_{true} \tag{3.2}$$

Roughness factor, *r,* is the ratio of the true surface area and the projected surfaced area. For non-wetting surfaces (θ > 90°), an increment in roughness would increase the apparent contact angle, and for wetting surfaces (θ < 90°), increased roughness would reduce the apparent contact angle.

3.2.2.2. Contact angle vs. liquid inertia forces effect in film breakdown

Considering an adiabatic falling-film without vapour inertia forces, dry patch formation depends on the liquid inertia forces for a given contact angle. Under this consideration, the complete falling-film mode is the most favourable flow pattern for a good mass transfer. Total wettability is only present when liquid flow rate is kept above a certain value; this value is defined as the minimum wetting flow rate Γ_{min}.

Hartley and Murgatroyd [81] recommended two criteria for the film break-down of thin layers flowing isothermally over solid surfaces. The first model was based on a force balance at the upstream stagnation point of a dry patch. The second model was based on a stability criterion of minimum energy.

Based on these criteria, some researchers have proposed their empirical correlations (see Table 3.1). However, the validation of these correlations in falling-film reactors still remains unclear. As it is shown in Table 3.1, non-experimental studies have been done to obtain the minimum wetting flow rate in horizontal tubes yet.

Table 3.1. Minimum flow rate and film thickness correlations for falling film reactors.

Falling film type	Criteria	Minimum wetting flow rate (kg/s-m)	Authors
Vertical surface	Force balance	$1.69(\mu\rho/g)^{1/5}[\beta(1-cos\theta)]^{3/5}$	Hartley and Murgatroyd [81]
	Minimum total energy	$0.803(\mu\rho\ /\ g)^{1/5}\beta^{3/5}$	
	Empirical correlation	$(\mu\frac{\rho\beta^3}{g})^{1/5}[0.67(1-cos\theta)^{0.623}+0.26(1-cos\theta)^{2.092}]$	El-Genk et al. [75]
	Minimum total energy	$1.018(\mu\rho/g)^{1/5}[\beta(1-cos\theta)]^{3/5}$	Doniec [80]
Vertical tube	Empirical correlation	$0.13((1-cos\theta)\beta)^{0.764}\rho^{0.255}\mu^{-0.018}$	Morison et al. [82]
	Experimental data	0.222 (water as fluid)	Paramalingam et al. [83]
Single-channel	Experimental data	$k\mu[\rho(\beta(1-cos\theta))^3/\mu^4 g)]^{0.3}/\rho$ (k depends on channel dimensions)	Zhang et al. [84]

Figure 3.4 shows the minimum wetting flow rate obtained from the equations of Table 3.1 as a function of the contact angle for LiCl water solution at 30 °C and 30 % of LiCl mass fraction. In general this graph indicates a big influence of contact angle on the minimum flow rate required to achieve a complete wetting.

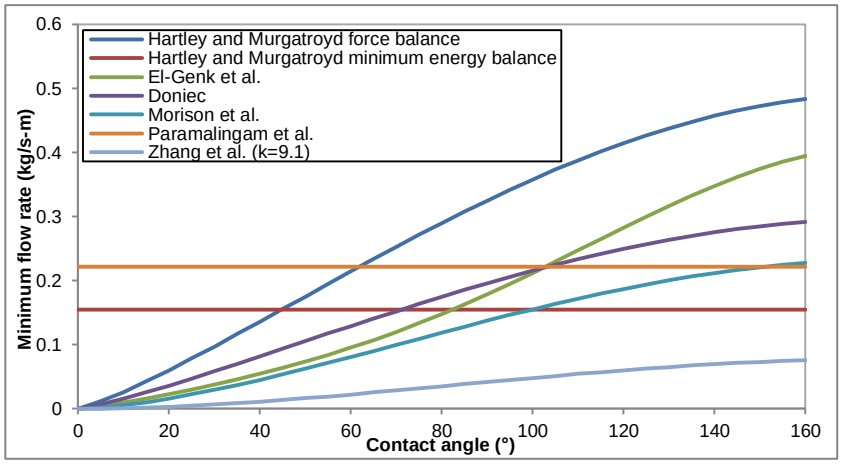

Figure 3.4. LiCl-H_2O solution minimum flow rate as a function of contact angle at 30 °C y 30 % of LiCl mass fraction.

3.2.2.3. Parameters to be considered in the wettability study

A dimensional study has been carried out in order to obtain the dimensional parameters that take part in the wetting process for falling-film with horizontal tubes considering an adiabatic falling-film without vapour inertia forces. Annex A contains the details of this dimensional study. According to the results, wettability can be fully defined as function of the film Reynolds number (Re_s), the Ohnesorge number (Oh_s) the Galileo number (Ga_s), and the tube spacing and tube diameter ratio (s/d).

$$Wettability = function(Re_s, Oh_s, \frac{s}{d}, Ga_s) \tag{3.3}$$

Where:

$$\frac{2\Gamma_s}{\mu_s} = Re_s \tag{3.4}$$

$$\frac{\rho_s \beta_s d_t}{\mu_s^2} = Oh_s \tag{3.5}$$

$$\frac{\rho_s \beta_s^3}{\mu_s^4 g} = Ga_s \tag{3.6}$$

Galileo number depends only on LiCl-H_2O properties. Figure 3.5 illustrates the modified Galileo number ($Ga^{0.25}$) as function of temperature and LiCl mass fraction. Conde correlations for LiCl-H_2O mixtures [77] have been used for this representation.

However, only one diameter has been studied for every case, thus, Ohnesorge number which would depend on LiCl-H_2O density, viscosity and surface tension, which is the same case that Galileo number, has not been taken into consideration.

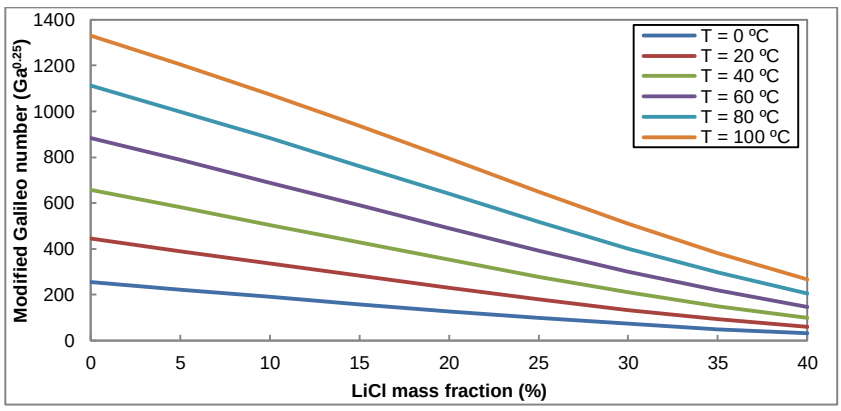

Figure 3.5. Modified Galileo number of LiCl-H_2O mixture as function of the temperature and LiCl mass fraction.

3.2.3. Hydrodynamics of a falling-film with horizontal tubes

Many factors can play a big role in the heat and mass transfer performance of an air-solution contactor, such as the physical properties of the solution, the heat flux, the liquid feeder or the air flow rate. Among all of them, one of the most important is the hydrodynamic behaviour of the falling-film, which has been studied in a deeper way by many researchers for evaporator and condenser devices. However, there are not references for desiccant liquid air-solution contactors.

3.2.3.1. Falling film inter-tube modes and transitions

From observations, falling-film inter-tube modes can be classified within 6 different modes [85]:

- Droplet mode: In this case, there is only a flow of liquid in the form of distinct droplets between tubes.
- Droplet-jet mode: This mode appears when at least one stable column exists between the tubes in addition to droplets. A column is defined as a continuous liquid link between tubes.
- Inline-jet mode: This mode occurs when there are only columns of liquid between tubes and the jet departure sites on the bottom of a tube are aligned with the jet impingement sites on the top of the same tube.
- Staggered-jet mode: In this case, there are only columns of liquid between tubes and the jet departure sites on the bottom of a tube are not aligned with the jet impingement sites on the top of the same tube.
- Jet-sheet mode: This intermediate mode contains both columns and liquid sheet flowing between tubes at different locations along the tubes.
- Sheet-mode: This mode is present when the fluid flows uniformly between the tubes as a continuous film.

Some authors join inline and staggered jet modes and call it as jet mode. Figure 3.6 shows photographs taken from every falling film mode.

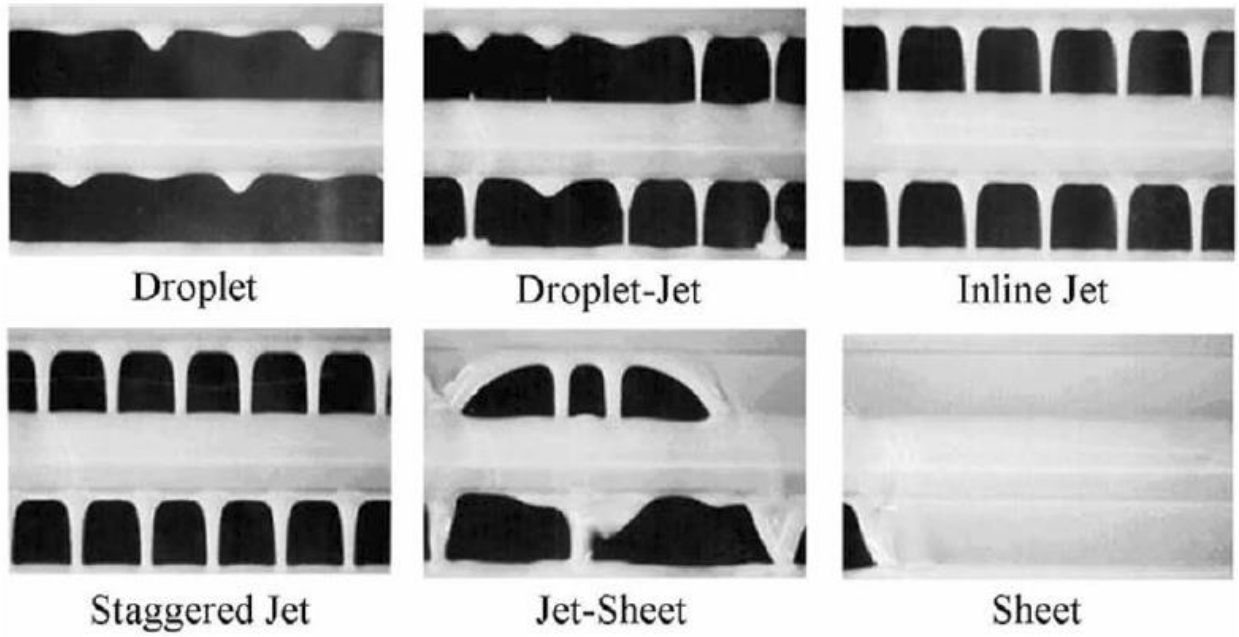

Figure 3.6. The falling film modes between horizontal tubes [86].

The flow changes from droplet to sheet mode occur when the mass flow rate is increased. Usually, there is some hysteresis in transitions when flow rate is increasing or decreasing. However, for practical desires it is probably best ignore this secondary effect on thermal design [87].

For adiabatic and smooth tubes, characterization and prediction of transition flow patterns have been studied by several researchers as Hu and Jacobi [86], Armbruster and Mitrovich [88] or Roques et al. [87] from experimental studies. All the flow mode transitions were correlated as:

$$Re_s = P \cdot Ga_s^N \tag{3.7}$$

Parameters A and B taken from Hu and Jacobi [86], Roques et al. [87] and Armbruster and Mitrovic [88] are included in the following table.

Table 3.2. Experimental parameters which predict falling film mode transitions.

Transition modes	Hu and Jacobi [86]		Roques et al. [87]		Armbruster and Mitrovic [88]	
	P	***N***	***P***	***N***	***P***	***N***
Droplet to droplet-jet	0.074	0.302	0.0417	0.3278	0.20	0.25
Droplet-jet to jet	0.096	0.301	0.0683	0.3204	0.26	0.25
Jet to jet-sheet	1.414	0.233	0.8553	0.2483	0.94	0.25
Jet-sheet to sheet	1.448	0.236	1.0680	0.2563	1.14	0.25

Figure 3.7 shows a similar effect in falling film transitions between the three models that can be due to the subjective nature of interpreting the different regimen transitions.

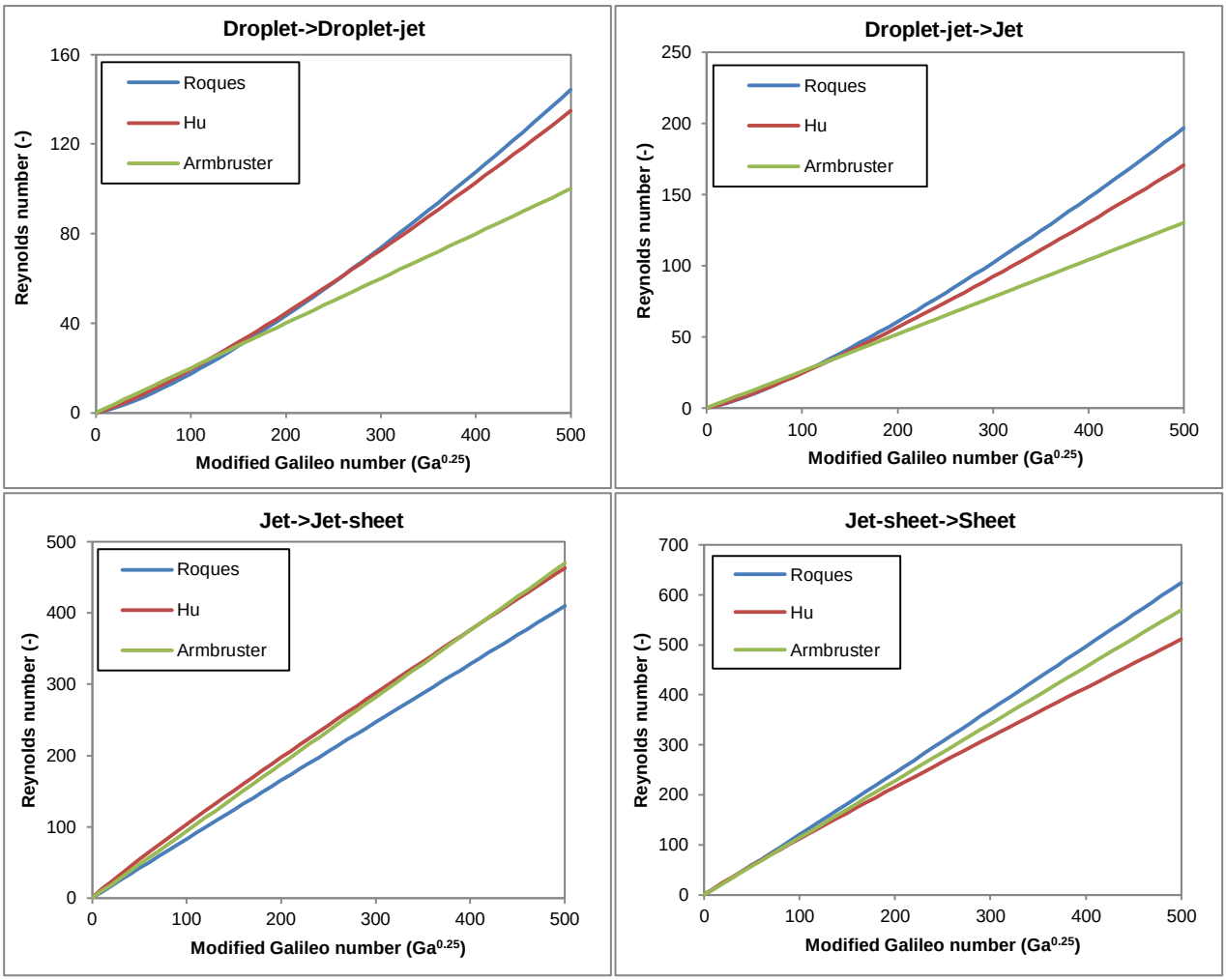

Figure 3.7. Comparison of the predictions of falling film transitions between the models given by Roques et al. [87], Armbruster and Mitrovic [88] and Hu and Jacobi [86].

3.2.4. Vapour inertia forces effect on falling-film with horizontal tubes

Tube wetting can be affected by the vapour inertia forces in the way that high air velocities may lead to the dry patch formations due to both, the dragging of the liquid desiccant and the deviation of the falling-film. The dragging of the liquid desiccant produces two undesirable effects:

- The carry-over of the liquid desiccant.
- A decreasing on the heat and mass transfer of the air-solution contactors.

Some investigations have been conducted on evaporative coolers and closed cooling towers in order to understand the effect of the air velocity on the heat transfer of falling-film with horizontal tubes. Parker and Treybal [89] observed a reduction in heat transfer by about 20 % with flowing air compared to still air. However, Mizushima et al. [90] found an increasing of about 10 %. These contradicting results were clarified by Charan and Wasekar [91] who reported that the heat transfer increases with the air velocity up to the point where the film becomes dragged off by the air flow, what reduces the tube wetting. Rana et al. [92], [93] reported similar conclusions to Charan and Wasekar, and stated that the heat transfer with flowing air can range from 0.85 to 1.7 times to the corresponding still air values. Armbruster and Mitrovic [94] also experienced remarkable improvements on the heat transfer in comparison with still air. According to these results, this improvement was mainly due to evaporation at the water surface, what means that mass transfer is also enhanced by air velocity.

Wei and Jacobi [95] investigated the effects of vapour-shear, tube diameter, tube spacing and bundle depth of the flow mode transitions on a gas counter-current flow using ethylene glycol. They observed that vapour shear tends to destabilize the sheet and jet modes. In this case spacing effects become important to mode transitions thresholds, especially for separated tubes.

Regarding the tube row effects, they observed that the flow generally became less stable farther down into the bundle from the top. In addition, the suggested a new classification of modes and developed a new regime map that takes into account the Webber number that is defined as:

$$We = \frac{\rho_s V_a^2 d_t}{\beta_s} \tag{3.8}$$

Ruan et al. [96] obtained new data on vapour-shear and feeding-length on falling film mode transitions with the following conclusions:

- A simpler mode classification scheme than Wei and Jacobi results.
- Liquid feeding length has an impact on falling-film mode transitions in quiescent surroundings. For lower *Ga* fluid, with an increasing liquid feeding length, transitions from jet to jet-sheet mode required a lower *Re*, which was opposite to other transitions.
- With an increasing *We*, the falling liquid flow became more unsteady and when the vapour velocity was larger than about 3.5m/s, stable. Steady modes were not usually present.
- Vapour shear effects on falling-film mode transitions depend on *Ga*. For higher *Ga* fluid, the unsteady effect might be more important than the shear effect. Therefore, transitions from jets to sheets occur at a higher *Re*; for a lower *Ga* fluid, the shear effect appears to be dominant with an increasing *We*. Hence, transitions between jet mode and sheet mode occur at a lower *Re*.
- A reduced hysteresis was observed when increasing *We* during experiments.
- In the limited range of these experiments, traditional Reynolds numbers showed no dependence on s/d_t.

3.3. Hydrodynamic study methodology

The experimental study is mainly focused on the hydrodynamic behaviour of a LiCl-H_2O on horizontal tubes made of different materials. In this sense, two different studies have been performed:

- Wettability study on horizontal tubes in an adiabatic falling-film without vapour inertia forces.
- Wettability study on horizontal tubes in an adiabatic falling-film with vapour inertia forces.

The main objective of the first study is to obtain the minimum liquid desiccant flow rate required to achieve full wetting around tubes. These values will be compared among the different tube materials and surface treatments in order to be used as one of the criteria for the tube material selection.

The main goal of the second study is to figure out the maximum air velocity that can be used within the air-solution contactors in order to avoid the dry patch formations. In this sense, the effect of the air velocity on the tube wetting is analysed when the minimum liquid desiccant flow rate to achieve full wetting of tube is dropped.

3.3.1. Experimental apparatus

Figure 3.8 shows the experimental apparatus used for the study carried out in this chapter. Liquid desiccant, that is stored in the reservoir 1 is pumped and heated before being dropped in a liquid distributor that feeds the horizontal tubes. Liquid desiccant is then collected and brought to a second reservoir. By using two liquid desiccant reservoirs, it is possible to supply liquid desiccant at homogeneous mass concentration and temperature conditions. Furthermore, air velocity is set by a fan of an air handling unit that contains a frequency driver.
Tubes are inside a tower made of polycarbonate. In case that liquid desiccant mass concentration decreases with time, the system is able to regenerate the solution by heating the liquid desiccant and the air. A mist eliminator is placed above the liquid distributor in order to separate the possible liquid desiccant drafted by the air.

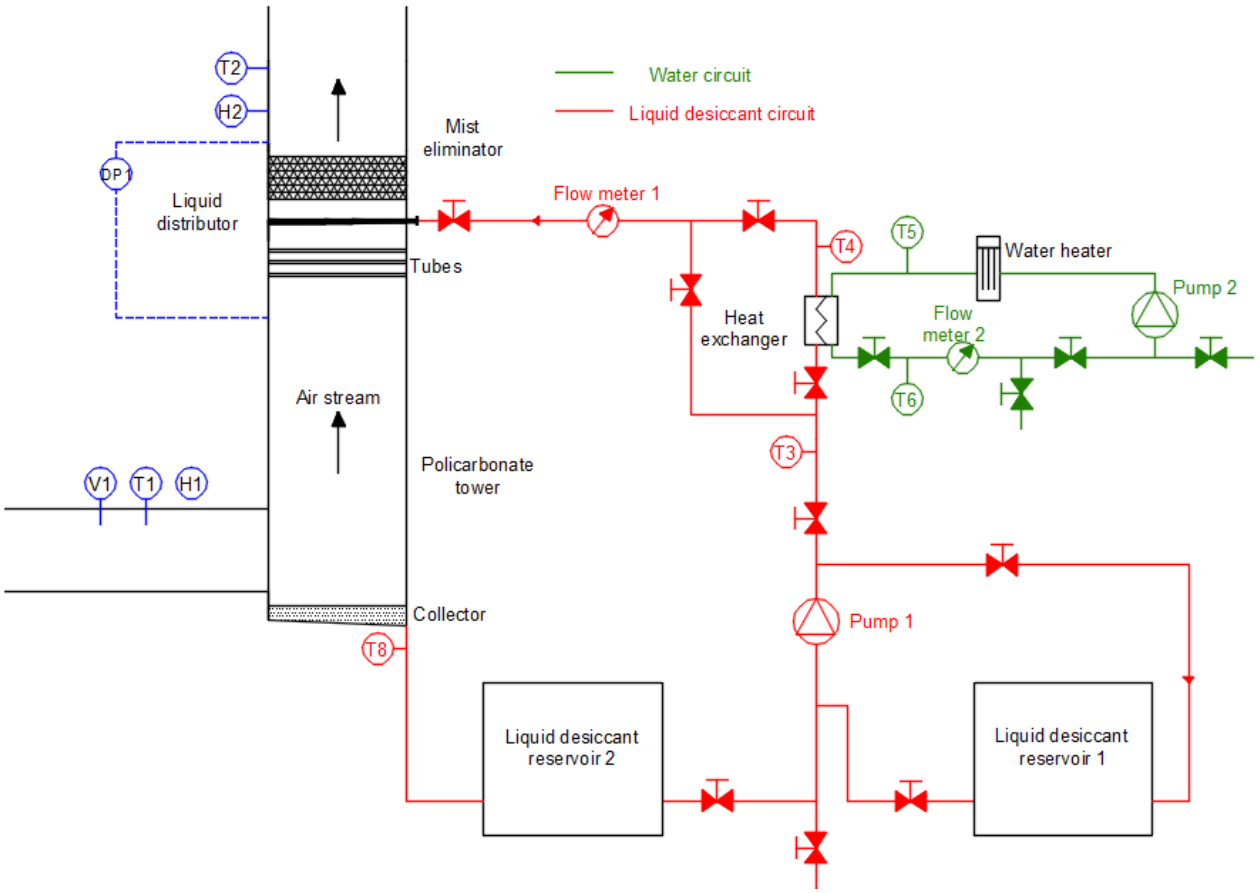

Figure 3.8. Schematic of the test bench for hydrodynamic study.

Polycarbonate tower

The tubes are tested inside a polycarbonate tower, which is a malleable material. This material is also cheap, can resist the corrosion and is transparent. Therefore, it allows seeing how it is the falling film behaviour. The tower dimensions are 1700 x 500 x 300 mm and it is supported by a metallic structure in order to improve its stability and rigidity. Figure 3.9 shows a picture of this component.

Figure 3.9. Polycarbonate tower.

Liquid distributor

Inside the polycarbonate tower is circulating the air stream and the solution, which is distributed from the top of the tower. Three liquid distributors have been tested in order to obtain an optimal liquid distribution, which is essential for a good tube wetting. All of them are made of polycarbonate and have the same dimensions, which are 10 mm of external diameter and 9 mm of internal diameter. Differences among them are related with the holes:

- Circular holes with a diameter of 1 mm separated by 2 mm between each one.
- Circular holes with a diameter of 2 mm separated by 4 mm between each one.
- Continuous linear hole with a width of 2 mm.

All of them were tested with the holes on the bottom and on the top of the distributor obtaining a better distribution when holes where located on the top. The first liquid distributor was quickly dismissed because its holes where too small to achieve a homogenous liquid distribution in all the required flow rates. However, for linear mass flow rates between 0.12 and 0.20 kg/m·s a good liquid distribution was obtained using the other distributors.

In order to improve the liquid distribution for lower mass flow rates, the surface of each distributor was sanded. This treatment was able to remove small channels which occurred when mass flow rates were low. Finally, liquid distributor with circular holes with a diameter of 2 mm was considered as the best to operate because the liquid desiccant flow was distributed more homogeneously in all the required flow rates.

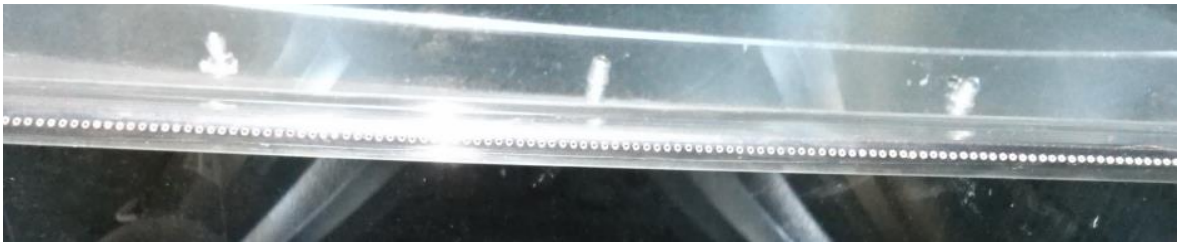

Figure 3.10. Liquid distributor with 1 mm circular holes separated by 2 mm between each one.

Mist eliminator

The mist eliminator is placed above the liquid distributor in order to separate the small solution droplets from the air, which can generate corrosion problems in the air handling unit. This mist eliminator is bought from Munters Company and consists of several curve channels (see Figure 3.11) made of polyethylene. The shade of every channel allows separating the liquid because of the inertia forces. The film generated inside the mist eliminator is driven toward the bottom using micro-channels with an inverted V shade. The dimensions recommended by the Company for our mist eliminator are 300 x 500 x 170 mm.

Figure 3.11. Mist eliminator.

Tanks

The system have two identical tanks made of polypropylene (to avoid the corrosion) of 500 l, which will contain the LiCl-H_2O solution. The size has been chosen in order to do batch tests without the need to recirculate the solution during each test.

Figure 3.12. Polypropylene tanks.

Pumps

The pump used for the water-LiCl solution circuit (Pump 1 in Figure 3.8) is a polypropylene centrifugal pump (Argal 04.08) [86] with a mechanical capacity of 0.6 kW. The mechanical energy provided by the pump is controlled by an ALTIVAR 18 variable frequency drive (Figure 3.14).

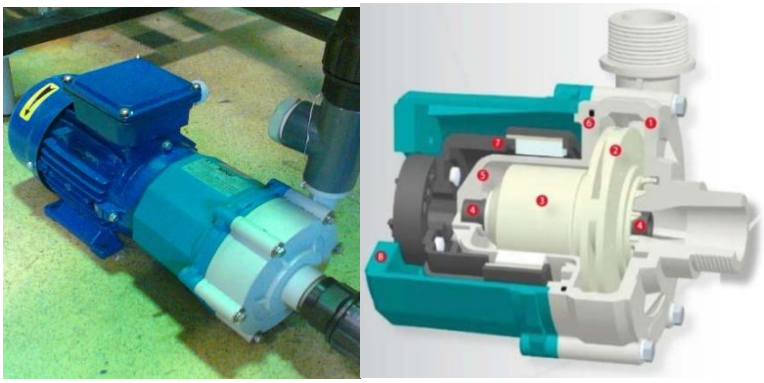

Figure 3.13. Pump for the LiCl solution [86].

Figure 3.14. Frequency driver.

Sensor elements

For the present study, it is important to measure the flow rate and the concentration of the LiCl-H_2O solution dripped over the tubes. Due to the corrosion of the LiCl-H_2O, the flow meters were carefully selected. Considering the range of flow rates to be used during the test, the flow meter selected was the following: OPTIFLUX 5100 C electromagnetic flow meter with ceramic coating (Figure 3.15). This flow meter measures the volumetric flow rate. Additional measures of density were required in order to determine the mass flow rate and LiCl mass concentration.

The LiCl mass concentration was calculated with density measurements obtained from samples from the reservoir 2. All the measurements in the air flow stream are done using standard sensors from REGIN [98]. Air temperature and humidity (T1+H1 and T2+H2 in Figure 3.8) are measured by HTDT 2200 sensors (Figure 3.16). Air velocity is measured (V1 in Figure 3.8) with AVDT25 sensor. Finally, differential pressure is measured (DP1 in Figure 3.8) with DTL150 sensor (Figure 3.16).

Temperature measures in the LiC-H_2O stream and the water circuit are made with standard PT-100 sensors. All the sensors are connected to an Agilent data logger (Figure 3.17) with the exception of the density measurements that were collected by a portable density meter (Anton Paar DMA 35).

Figure 3.15. KROHNE flow meter OPTIFLUX 5000.

Figure 3.16. REGIN temperature + humidity sensor HTDT 2200 (left) and differential pressure sensor DTL 150 (right) [87].

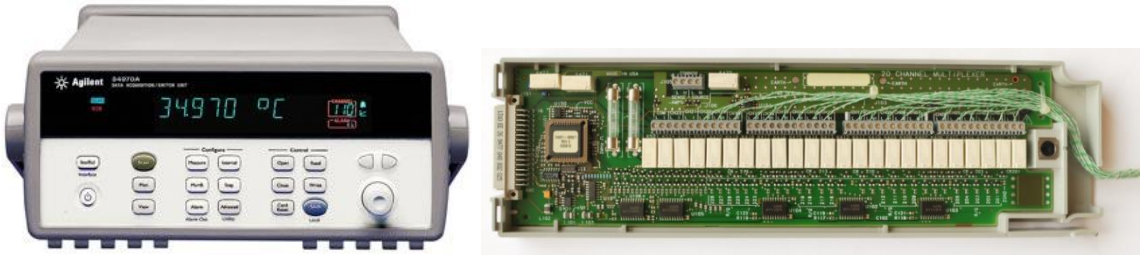

Figure 3.17. Agilent 34970A data logger [88].

The parameters, the measurement devices, their accuracies and operational ranges are listed in Table 3.3.

Table 3.3. Specifications of the different measuring devices.

Parameter	Device	Accuracy	Operational Range
Water and desiccant temperature sensors	PT-100	0.01 ºC	0-100 ºC
Water flow rate	Water flow meter	0.4 %	0-400 l/min
Desiccant flow rate	Electromagnetic flow meter	0.3 %	0-150 l/min
Air temperature	Air temperature sensor	0.2ºC	-20 - +80 ºC
Air relative humidity	Air relative humidity sensor	2 %	0-100 %
Air velocity	Air velocity sensor	0.3 m/s+ 3 %	0-10 m/s
Desiccant density	Density meter	0.001 g/cm^3	0-3 g/cm^3

3.3.2. Experimental procedure

3.3.2.1. Description of tested tubes

Hydrodynamic tests were carried out in order to determine the minimum liquid desiccant flow rate to wet completely 10 different tubes at different LiCl-H_2O conditions. The specifications of tubes are detailed in Table 3.4. Figure 3.18 to Figure 3.20 show the different tubes tested for wettability study.

Table 3.4. Specifications of tested tubes.

Material	Tube diameter (mm)	Wetted length (mm)	Tube spacing (mm)
Polypropylene	6.1	440	35 - 37
Polypropylene + batch plasma nano-layer deposition	6.1	320	38
Polypropylene + continuous deposition I	6.1	320	37
Polypropylene + continuous deposition II	6.1	320	37
Low density polyethylene	6.1	320	38 - 42
Low density polyethylene + batch plasma nano-layer deposition	6.1	320	38 - 42
Polyamide	6.1	320	40 - 47
Polyamide + batch plasma nano-layer deposition	6.1	320	44
High density polyethylene	6.1	440	34 - 38
Graphite	25.4	440	30 - 41

Figure 3.18. Standard and treated PA tubes (left) and standard and treated LDPE tubes (right).

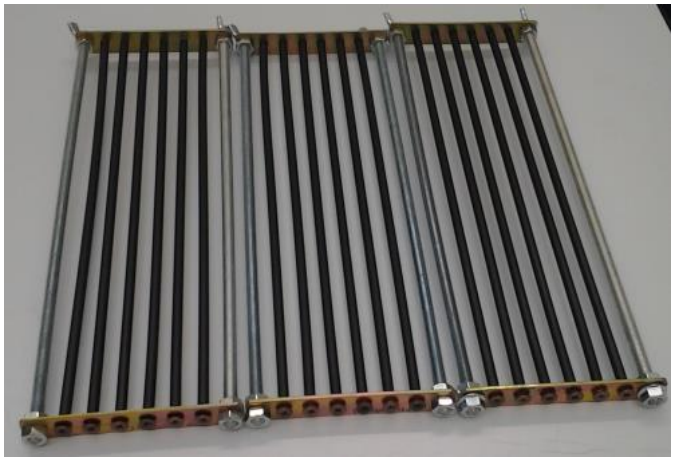

Figure 3.19. Treated PP tubes.

Figure 3.20. Standard PP, LDP and HDPE tubes (left) and graphite tubes (right).

3.3.2.2. Procedure for wettability tests

Before starting a test, the tube was adjusted to the desired tube spacing. Since the falling film flow is a gravity activated flow, a slight tube inclination could drive the liquid flow to one side and cause a non-uniform distribution of the flow. Therefore, the tubes were carefully levelled prior to a test.

The liquid pump was turned on and the test liquid circulated through the system for 30 minutes. This was done to ensure that the system was free of air and the film well distributed. The data acquisition system including devices for measuring the liquid temperature and flow rate were set up before.

To make sure that the liquid flow rates on both sides of the tube were equal, the feeding tube was rotated until the liquid fell on the top dead centre of the tube below it. For fine adjustment of the flow rate, a variable frequency driver actuating on the pump was used. The driver was first operating at full frequency and then was slowly decreasing until the dry patches on tube appeared.

In order to obtain the LiCl mass concentration density, measurements were performed with samples of the solution which were taken every time a tube was tested. Equation that correlates the temperature, density and LiCl mass concentration provided by Pàtek [24] was used.

The wettability behaviour results are presented as the minimum flow rate required to fully wetting the tube surface. In order to get these results, an observer was placed to find the film conditions at which the dry patch came out on the tube surface. Photographic equipment was used in order to give support to the visual measurements. Therefore, visual measurements were compared with pictures and recorded videos.

3.4. Experimental results

3.4.1. Surface tension vs. liquid inertia forces effect

Qualitative observations (regarding the kind of falling film mode at which full wetting is obtained) and quantitative results (relating to Reynolds number and Galileo number) have been obtained from experimental tests. Annex B contains the measurements taken at the conditions in which full wetting was obtained for all the tested tubes.

The experimental data is correlated by using the equation 3.7. In this case, this equation correlates the minimum Reynolds number required to obtain full wettability with a potential function (as it is described in Section 3.2.3.1) of the Galileo number for each kind of tube. Table 3.5 contains parameters P and N of the potential function and the coefficient of determination (R^2) of each function regarding the measurements.

Table 3.5. Parameters A and B for predictions of minimum Reynolds number to wet horizontal tubes.

Tube material	*P*	*N*	R^2
Polypropylene	0.0859	0.3485	0.9619
Polypropylene + batch plasma nano-layer deposition	0.0846	0.2622	0.9979
Polypropylene + continuous deposition I	0.0160	0.3670	0.9651
Polypropylene + continuous deposition II	0.0552	0.2768	0.9901
Low density polyethylene	0.9680	0.2385	0.9386
Low density polyethylene + batch plasma nano-layer deposition	0.1083	0.2474	0.9955
Polyamide	0.5702	0.1671	0.9576
Polyamide + batch plasma nano-layer deposition	0.2629	0.1955	0.9158
High density polyethylene	3.0553	0.1576	0.9629
Graphite	0.3851	0.1784	0.9292

3.4.1.1. Polypropylene

Four different PP tubes have been tested in order to know the minimum flow rate at which its surfaces are fully wetted with a LiCl-H_2O solution: A standard polypropylene tube and three polypropylene tubes with different plasma surface treatment.

Figure 3.21 shows two pictures of two different PP tubes. As it is clear from them, the left tube, which is a standard PP tube, is not wetted besides the film flow rate is as high as it is being dropped at jet mode. However, the right tube, which corresponds with a PP tube with the second kind of continuous treatment, is able to be full wetted with a film flow rate at droplet mode.

Figure 3.22 shows the wetting behaviour of the different tested PP tubes represented as the minimum film Reynolds number as function of the modified Galileo number, which depends on the solution properties. At the same time, Figure 3.22 contains the potential curves obtained for each tube and described Table 3.5.

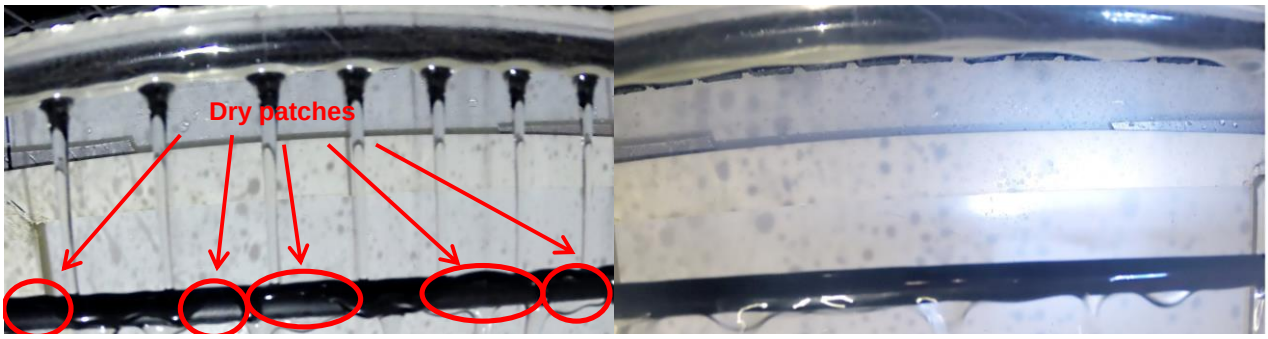

Figure 3.21. Non-wetted standard PP tube at jet mode (left) and full wetted treated PP tube at droplet mode (right).

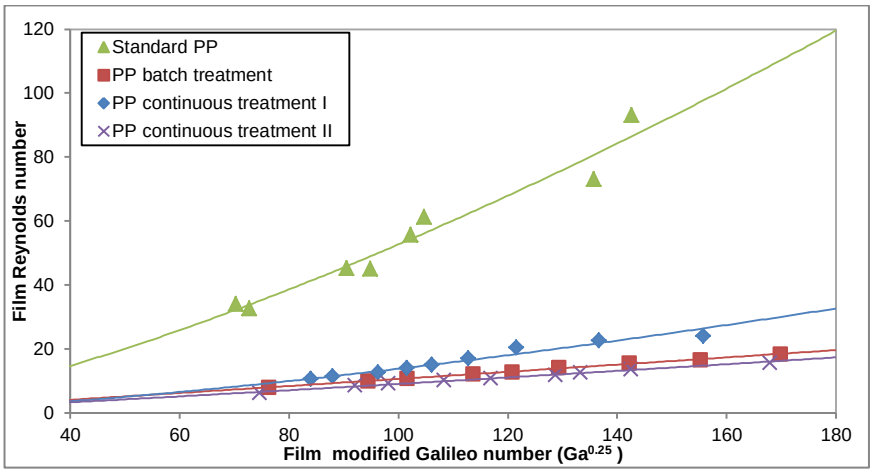

Figure 3.22. Wetting behaviour of different PP tubes. Batch treatment: batch plasma nano-layer depositions; continuous plasma deposition I; continuous treatment II: continuous plasma deposition II.

Figure 3.23 represents a comparison between measured and predicted (by the potential equations described on Table 3.5) minimum Reynolds number required to achieve full wettability in each PP tube.

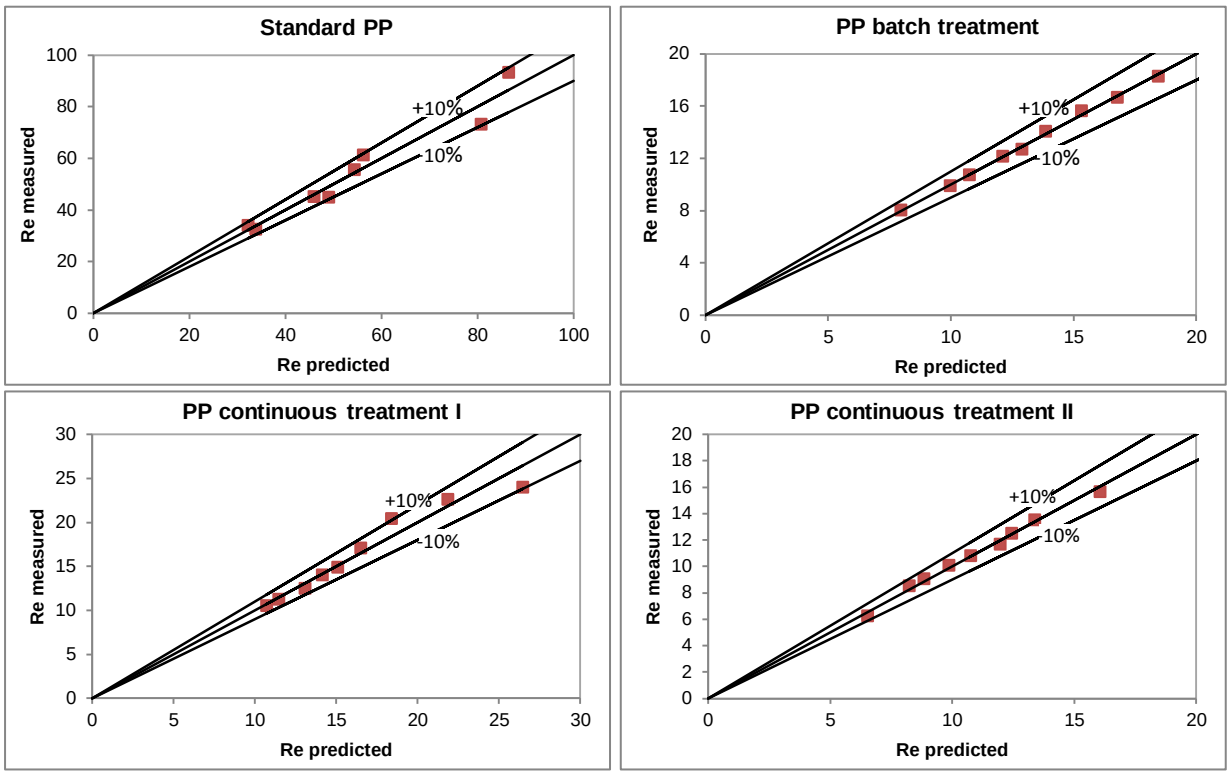

Figure 3.23. Comparison of the predictions given by for PP tubes. Batch treatment: batch plasma nano-layer depositions; continuous plasma deposition I; continuous treatment II: continuous plasma deposition II.

3.4.1.2. Low density polyethylene

Standard and treated LDPE tubes have been tested in order to know the minimum flow rate at which its surfaces are fully wetted with a LiCl-H_2O solution.

Figure 3.24 shows two pictures of both LDPE tubes. In the same way than in polypropylene, standard LDPE tube (left graph) is not wetted besides the film flow rate is as high as it is being dropped at jet mode. However, the right tube, which corresponds with a LDPE tube with the batch treatment, is fully wetted with a film flow rate at droplet mode.

Figure 3.25 shows the wetting behaviour of the different tested LDPE tubes represented as the minimum film Reynolds number as function of the modified Galileo number, which depends on the solution properties. At the same time, Figure 3.25 contains the potential curves obtained for each tube and described in Table 3.5. Figure 3.26 represents a comparison between measured and predicted by the potential equations described in Table 3.5 minimum Reynolds number required to obtain full wettability in both LDPE tubes.

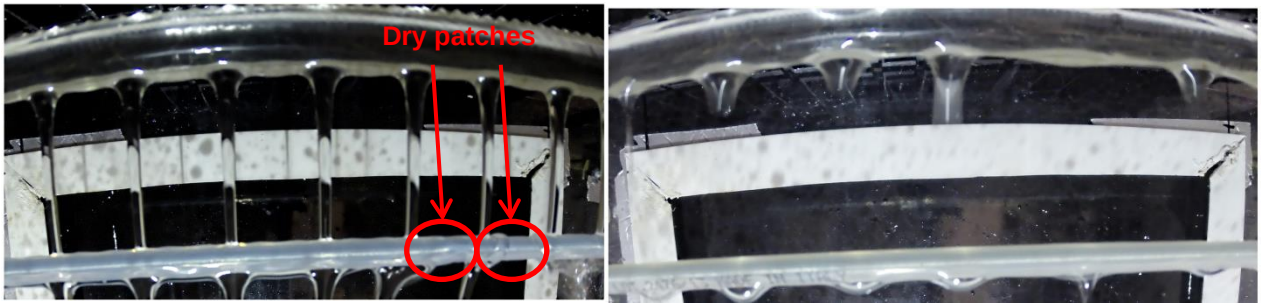

Figure 3.24. Non-wetted standard LDPE tube at jet mode (left) and full wetted treated LDPE tube at droplet mode (right).

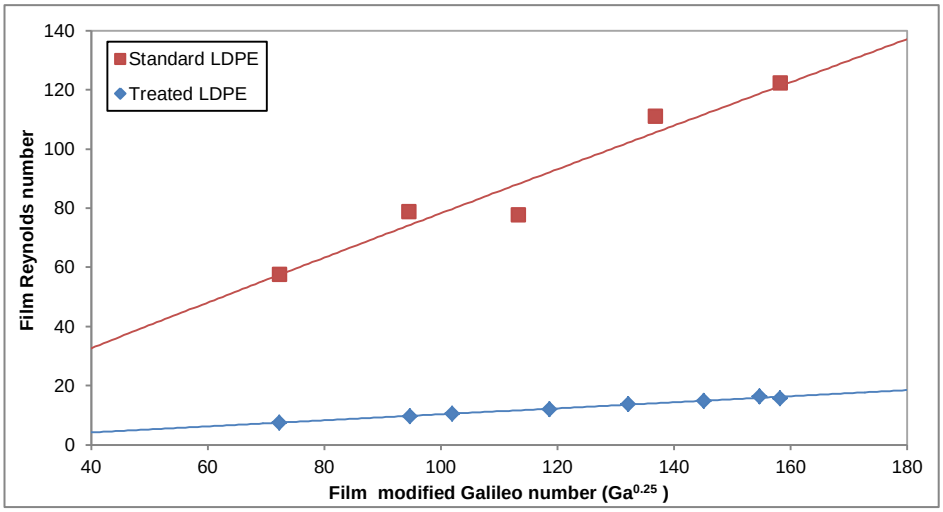

Figure 3.25. Wetting behaviour of different LDPE tubes. Treated: batch plasma nano-layer depositions.

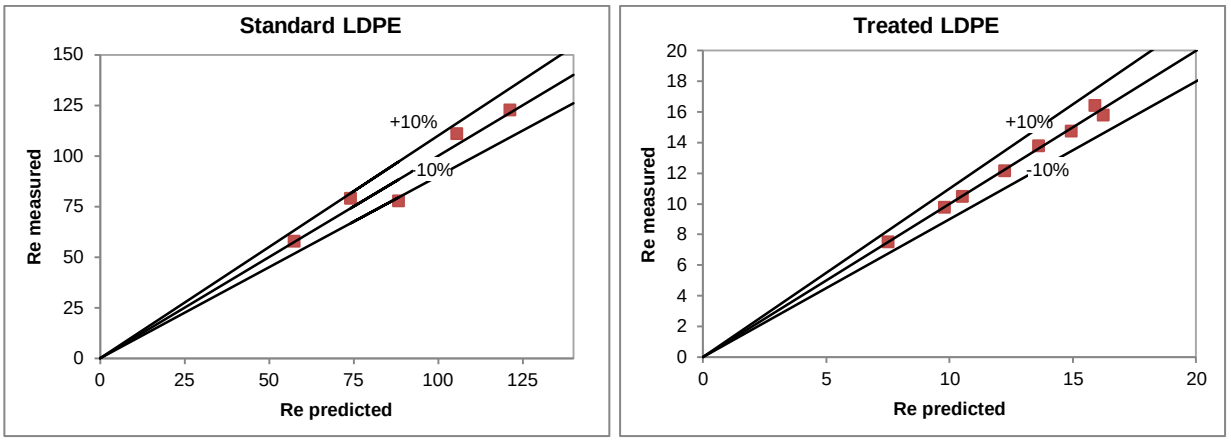

Figure 3.26. Comparison of the predictions given by Table 3.5 for LDPE tubes. Treated: batch plasma nano-layer depositions.

3.4.1.3. Polyamide

Standard and treated PA tubes have been tested in order to know the minimum flow rate at which its surfaces are fully wetted with a LiCl-H_2O solution.

Figure 3.27 shows two pictures of both PA tubes. As it is clear from them, both standard and treated PA tubes are full wetted with a film flow rate at droplet mode.

Figure 3.28 shows the wetting behaviour of the different tested PA tubes represented as the minimum film Reynolds number as function of the modified Galileo number, which depends on the solution properties. At the same time, Figure 3.28 contains the potential curves obtained for each tube and described in Table 3.5.

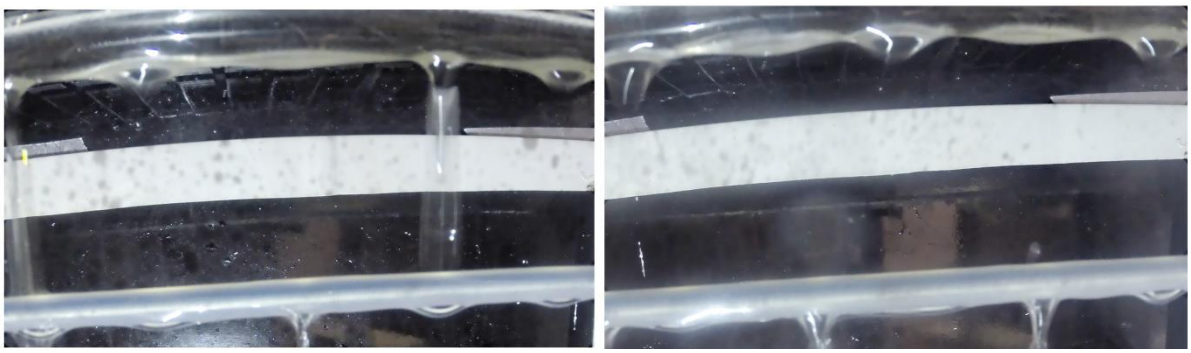

Figure 3.27. Full wetted standard (left) and treated (right) PA tubes at droplet mode.

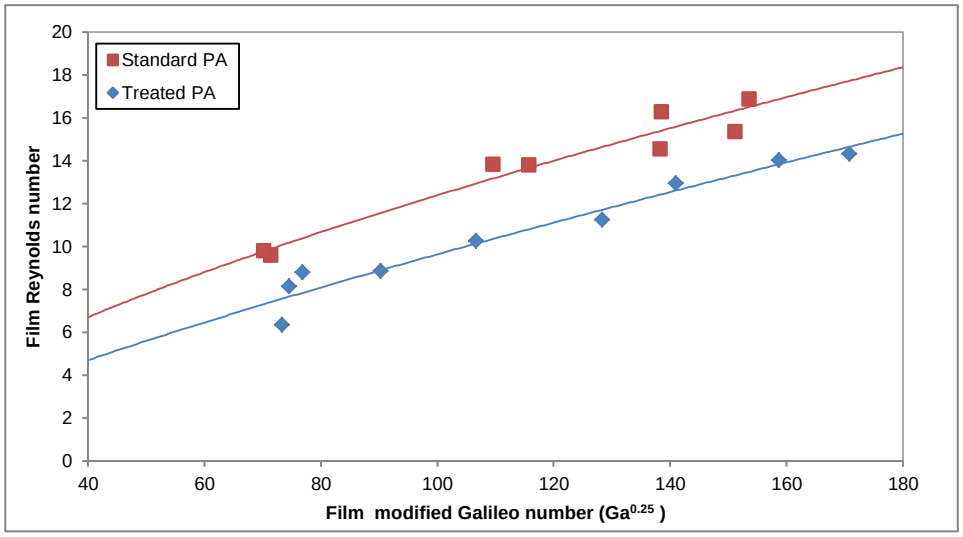

Figure 3.28. Wetting behaviour of different PA tubes. *Treated: batch plasma nano-layer depositions.*

Figure 3.29 illustrates a comparison between measured and predicted (by the potential equations described in Table 3.5) minimum Reynolds number required to obtain full wettability in both PA tubes.

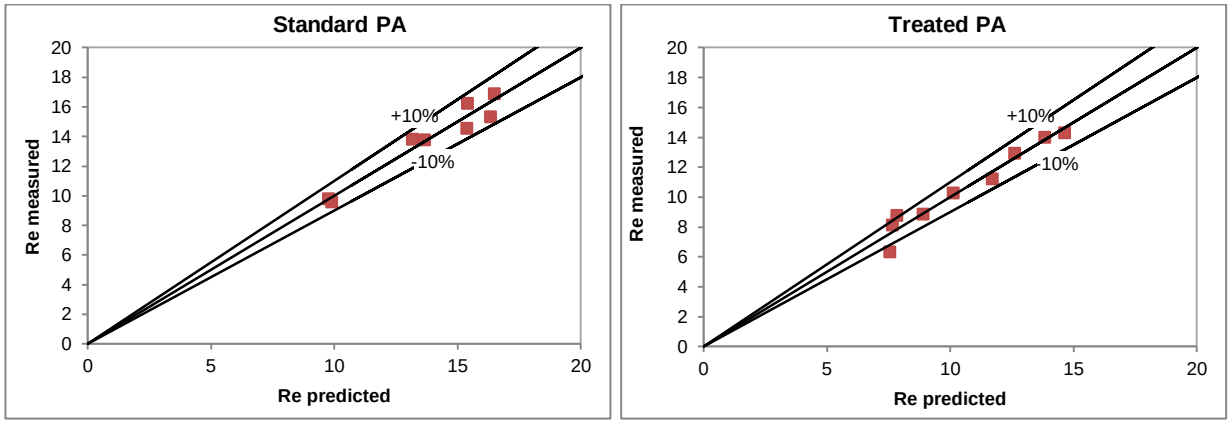

Figure 3.29. Comparison of the predictions given by Table 3.5 for PA tubes. Treated: batch plasma nano-layer depositions.

3.4.1.4. High density polyethylene

HDPE has been tested in order to know the minimum flow rate at which its surface is fully wetted with a LiCl-H_2O solution. Figure 3.32 shows a picture of a HDPE tube. As it is clear from it, HDPE tube is not fully wetted with a film flow rate at jet mode.

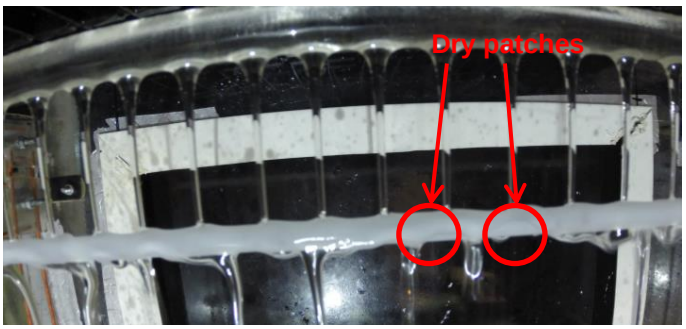

Figure 3.30. Non-wetted HDPE tube at jet mode.

Figure 3.33 illustrates a comparison between measured and predicted (by the potential equations described in Table 3.5) minimum Reynolds number required to obtain full wettability in HDPE tubes.

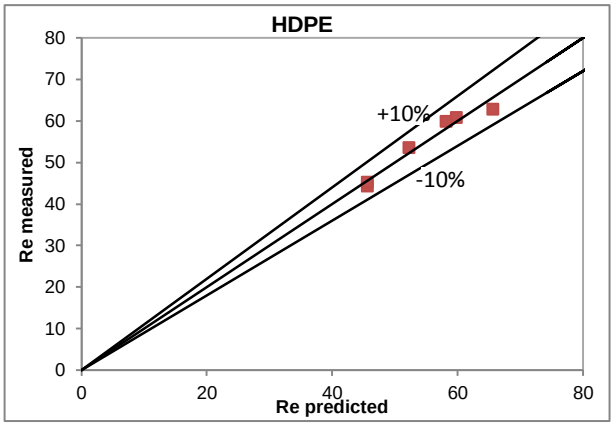

Figure 3.31. Comparison of the predictions given by Table 3.5 for HDPE tubes.

3.4.1.5. Graphite

Graphite has been tested in order to know the minimum flow rate at which its surfaces are fully wetted with a LiCl-H_2O solution. Figure 3.32 shows a picture of a graphite tube. As it is clear from it, graphite tube is full wetted with a film flow rate at droplet mode. However, this performance was not always the same. In the fists tests, the graphite tube did not have such a good wettability, and this was improving in time.

Figure 3.33 illustrates a comparison between measured and predicted (by the potential equations described in Table 3.5) minimum Reynolds number required to obtain full wettability in graphite tubes.

Figure 3.32. Full wetted graphite tube at droplet mode.

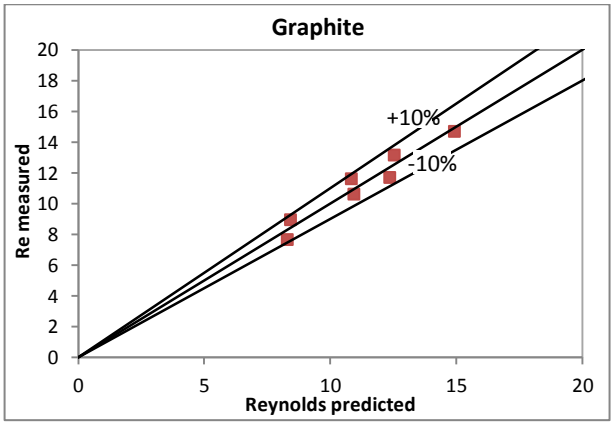

Figure 3.33. Comparison of the predictions given by Table 3.5 for graphite tubes.

3.4.2. Summary

Figure 3.34 contains the minimum film *Re* number required to achieve full wettability as function of the modified Galileo number ($Ga^{0.25}$) for all the tubes tested in the test bench designed and developed for this purpose. In addition, potential curves obtained for each tube are included in the same Figure.

In order to also have a quantitative point of view of the experimental results, a comparison with the mode film transitions curves between droplet to jet mode flow given by Hu and Jacobi [80] is presented in Figure 3.34. Apart from standard PP, standard HDPE and standard LDPE tubes, which require a flow rate above of the droplet-jet to jet transition, all the tested tubes are able to achieve full wettability in droplet mode.

Figure 3.35 contains similar information than Figure 3.34, but in this case, including only the tubes that are fully wetted with droplet mode film, in order to show more accurate information in this range where a great amount of experimental results are concentrated.

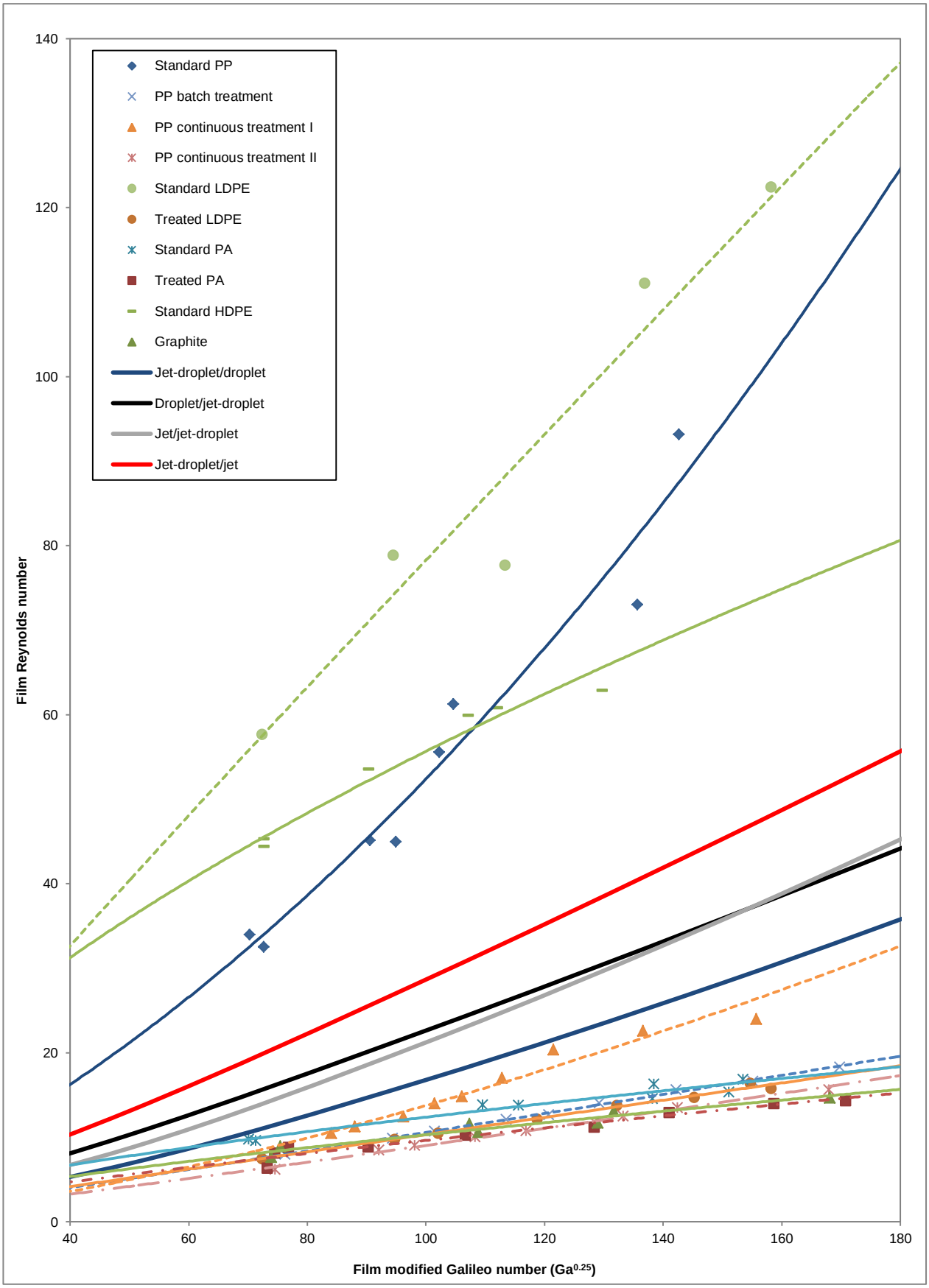

Figure 3.34. Wetting behaviour of tested tubes. Batch treatment: batch plasma nano-layer depositions; continuous plasma deposition I; continuous treatment II: continuous plasma deposition II.

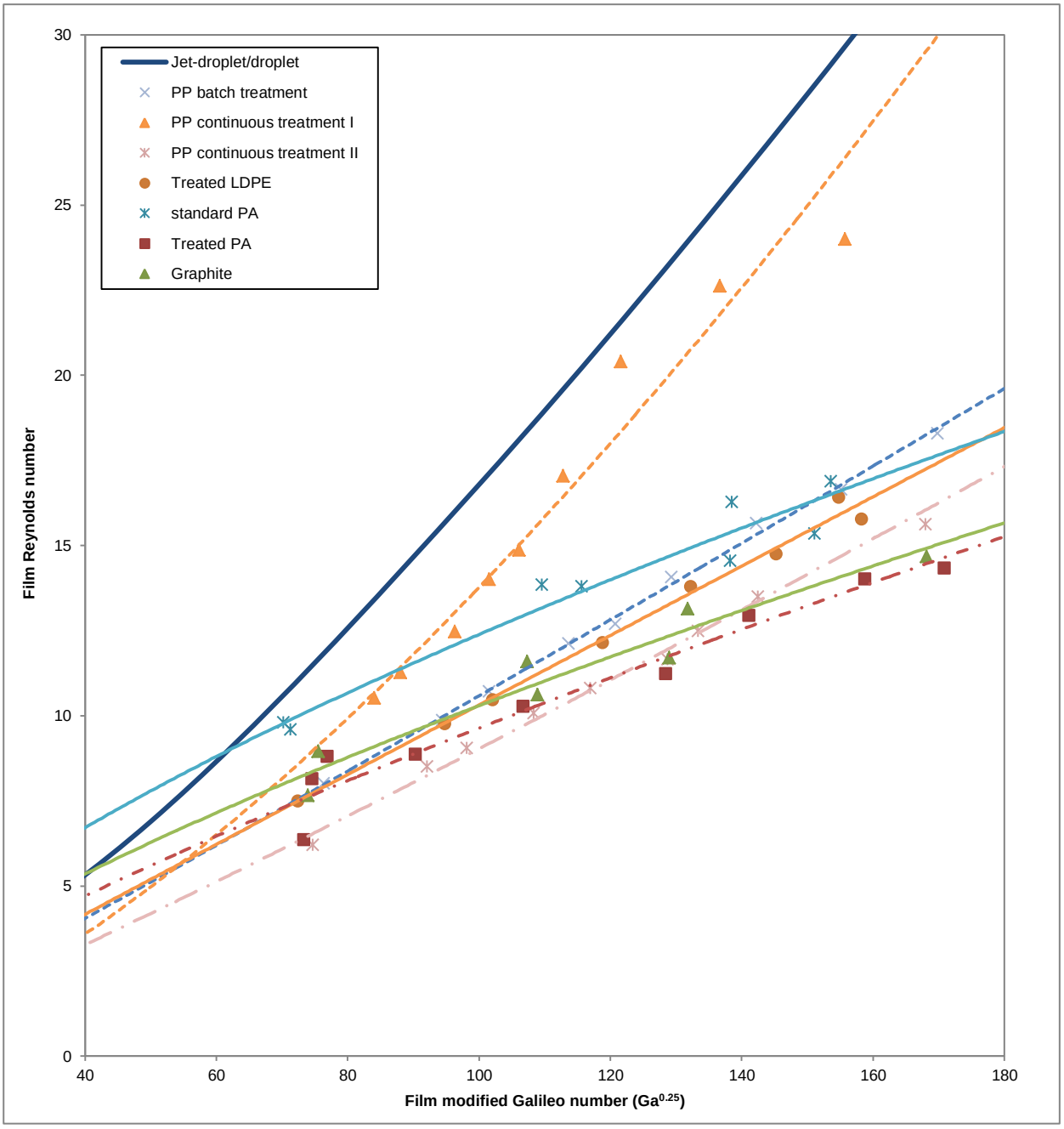

Figure 3.35. Wetting behaviour of all the tubes wetted at droplet mode. Batch treatment: batch plasma nano-layer depositions; continuous plasma deposition I; continuous treatment II: continuous plasma deposition II.

3.5. Tube spacing vs. liquid inertia forces effect

According to the dimensional analysis developed in Annex A of the present document, tube spacing and diameter ratio could have also an effect on the wettability behaviour of LiCl-H_2O solution around the horizontal tubes.

However, the experimental results gotten minimum Reynolds number required to achieve full wettability does not depend on the tube distance at it is possible to conclude observing Figure 3.36, which shows the wetting behaviour of the tubes as function of the distance-tube diameter ratio for the 10 different tubes tested.

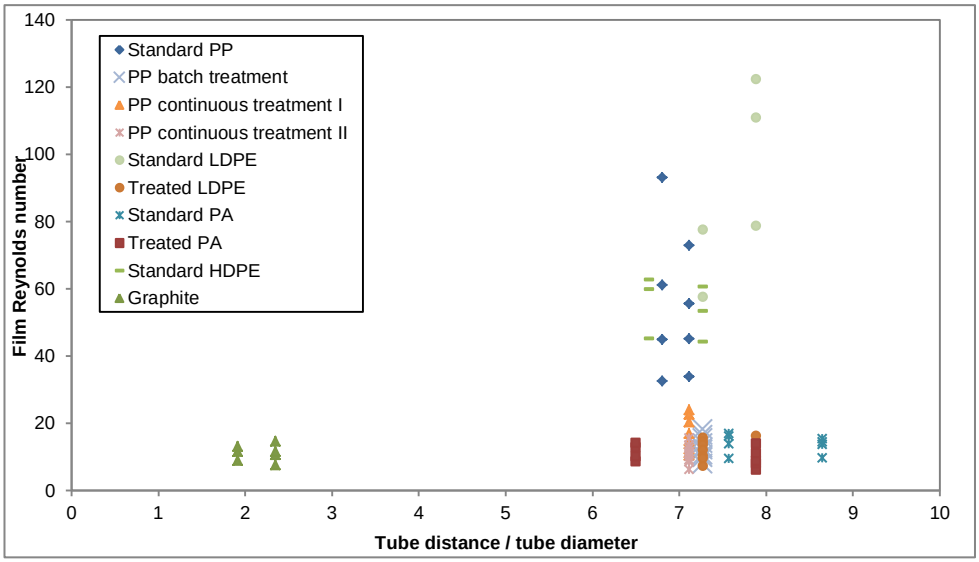

Figure 3.36. Wetting behaviour of all the tubes wetted as function of the tube distance-tube diameter ratio.

3.6. Vapour inertia forces vs. liquid inertia forces

Vapour inertia forces affect the tube wetting and, hence, the heat and mass transfer of the air-solution contactors. Therefore, an experimental study has been performed in order to know the air velocity at which dry patches on tubes, that are wetted with the minimum solution flow rate to fully wet them, start to appear. Since air velocity creates dry patches on the tubes not only due to the dragging of the liquid desiccant, but also to the deflection of the film, a column of tubes has been tested in this case in order to see if wetting is keeping in the same way along the tubes.

Figure 3.37 shows four pictures of the polypropylene tube with plasma continuous treatment II. Each picture is taken at different air velocities, from 0 m/s to 3 m/s. Similarly, liquid desiccant flow rate is the same in all the pictures. As it can be observed, tubes are fully wetted up to the air velocity of 2 m/s.

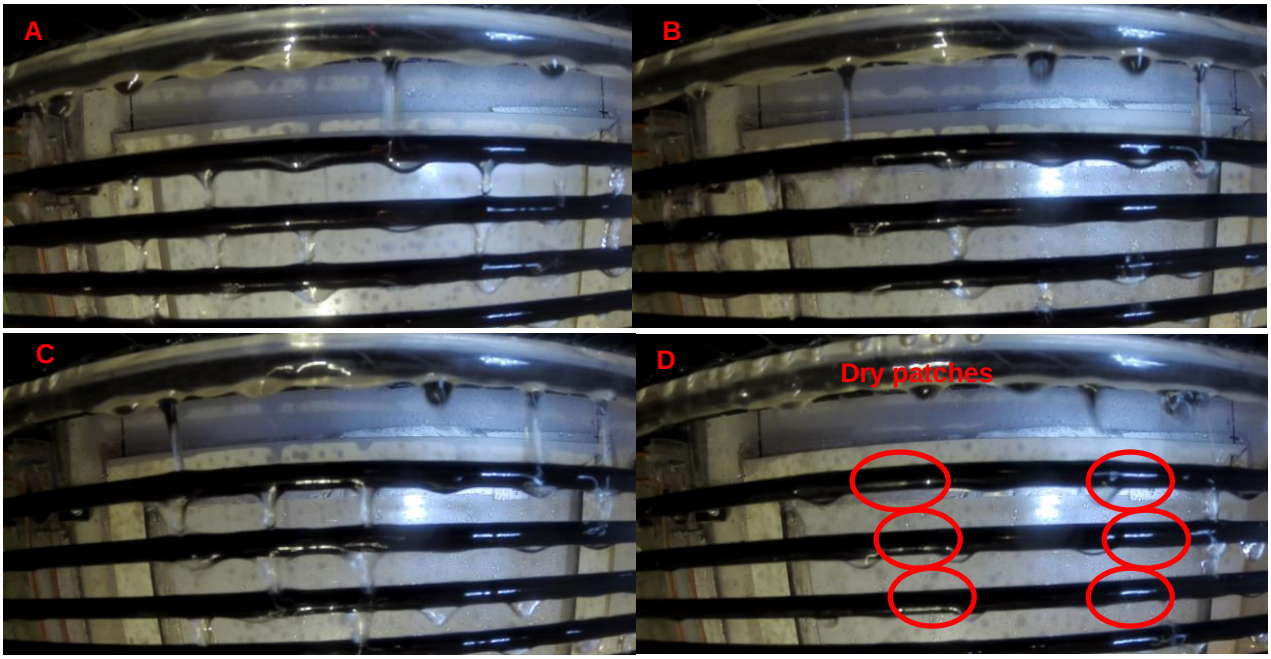

Figure 3.37. Tubes made of polypropylene with continuous plasma treatment II. A) Air velocity ≈ 0 m/s. B) Air velocity ≈ 1 m/s. C) Air velocity ≈ 2 m/s. D) Air velocity ≈ 3 m/s.

According to the observations of this test, wettability of tubes starts to be poorer for air velocities higher than 2 m/s. When air velocity is higher than 2 m/s, dry patches start to appear around the tubes placed at the bottom of the column. This effect is produced by the deflection of the film, as it is showed in Figure 3.38. For air velocities higher than 3 m/s all the tubes contain dry patches. In this case, dry patches appear for two reasons: the deflection of the film, that is becoming greater, and the dragging of the solution by the air flow.

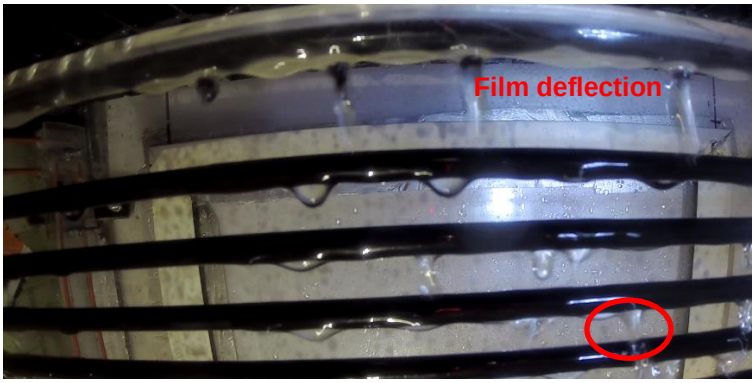

Figure 3.38. Tubes made of polypropylene with continuous plasma treatment II. Air velocity ≈ 2.5 m/s.

3.7. Conclusions

Several tests have been carried out in a small lab setup in order to compare the hydrodynamics of different types of plastic tubes (polypropylene, low density polyethylene, high density polyethylene and polyamide) and graphite with LiCl-H_2O solution. Improved surface was also tested for polypropylene, low density polyethylene and polyamide.

A dimensional analysis has been firstly carried out in order to reduce the number of variables to be correlated the test results. The Buckingham Pi theorem has been applied for this purpose and four dimensionless variables were identified: film Reynolds number (Re_s), film Ohnesorge number (Oh_s), film Galileo number (Ga_s) and spacing and tube diameter ratio (s/d_t). Film Ohnesorge number was finally dismissed because only one tube diameter was tested for each tube.

The main objective of the study was to evaluate the minimum flow rate (characterized by the film Reynolds number) in order to obtain full wettability as a function of the properties of the LiCl-H_2O solution (characterized by the film Galileo number) for each tube material when horizontal falling film is used. Quantitative (numerical correlations for film Reynolds number as function of film Galileo number) and qualitative (film mode to achieve full wettability) results have been obtained from the performed tests.

The main conclusions obtained are summarized below:

- Films Reynolds number to achieve full wettability increases with increasing film Galileo number.
- Potential equation for the film Galileo number correlates properly the film Reynolds number to obtain full wettability. These correlations have been obtained for each tube with an accuracy prediction of ±10 %.
- Not dependency on wettability behaviour for spacing a tube diameter ratio has been found.
- Standard polypropylene, low density polyethylene and high density polyethylene require jet mode to obtain full wettability. Film Reynolds number to achieve full wettability ranges from 32.8 to 122.5 as a function of the tube and film Galileo number. Standard low density polyethylene is the one that requires largest film Reynolds number.
- Standard polyamide is the only plastic that has obtained full wettability with droplet mode flow. In this case, film Reynolds number ranges from 9.6 to 16.9, which are in the same magnitude order than the treated tubes.

- Plasma surface treatment enhances the wettability of plastic tubes. In this sense, full wettability in droplet mode is achieved with all the treated plastic tubes. The best results (lower film Reynolds number) have been obtained with polyamide (batch) and polypropylene (continuous II); in both cases, wettability is very similar with film Reynolds numbers from 6.3 to 14.3.
- Full wettability of graphite tube is obtained in droplet mode. Good wetting of graphite could be related with its porosity. This was concluded because at the beginning of the study graphite wettability was poor, but after some time of operation it was observed that graphite surface contained some of the solution at the external surface improving therefore its wettability.
- Due to the plasma treatment, the wetting improvement (reduction of the film Reynolds number for complete wettability) for each tube is the following:
    - 15.8 to 33.5 % for polyamide with batch plasma nano-layer deposition.
    - 73.3 % for polypropylene with continuous plasma deposition I.
    - 83.3 % for polypropylene with continuous plasma deposition II.
    - 81.3 % for PP with batch plasma nano-layer deposition.
    - 86.7 % for LDPE with batch plasma nano-layer deposition.
- Polypropylene with continuous treatment II has been chosen as the plastic material that will be used in the air-solution contactors due to its low price, to its good wetting improvement and to its good properties to be welded, what makes easier the fabrication of the air-solution contactor.

An experimental study to set the maximum air velocity to be used with the air solution contactor has been also conducted. From this study it can be concluded that the maximum air velocity must be 2 m/s because at higher air velocities the tubes start to be not wetted due to the deflection of the film and the dragging on the liquid desiccant.

Chapter 4. Experimental performance of two small-scale internally-cooled air-solution contactors made of polypropylene

4.1. Introduction

The most common material used in liquid desiccant systems is LiCl-H_2O solution because of its low vapour pressure. However, this solution is very corrosive with most of the metallic materials excluding titanium and tantalum, which are much more expensive. For this reason, plastic materials could be a good alternative for these applications despite their poorer thermal conductivity and wettability.

A hydrodynamic study of different materials and surface treatments has been performed in Chapter 3, in order to obtain the minimum LiCl-H_2O flow rate required to wet completely the external surface of horizontal tubes. One of the main results obtained in the previous chapter has been the important reduction of the required flow rate to wet completely the tube surface for polypropylene and low density polyethylene when a surface of tubes is treated with plasma depositions.

The main objective of this chapter is to compare two air-solution contactors of the falling-film with horizontal tubes type made of polypropylene for liquid desiccant systems. The main difference between both air-solution contactors consists on their wettability when LiCl-H_2O is put in contact with them because one contains the standard polypropylene and the other the surface continuous treatment II.

This comparison evaluates how big the enhancement on the performance of the air-solution contactors is when wettability is improved. In addition, how different conditions of air, water and LiCl-H_2O affect to the performance of the exchanger is also studied in this chapter.

4.2. Description of the experimental test facilities

A test bench, which allows achieving absorber conditions in a liquid desiccant system, has been made in order to study the dehumidification process with the LiCl-H_2O solution of two heat/mass falling-film air-solution contactors with horizontal polypropylene tubes. Figure 4.1 shows a general schematic of the test bench which main purpose is to provide water, moist air and LiCl-H_2O solution to the exchangers at different conditions of flow rate, temperatures and LiCl mass concentrations.

The test bench can be divided into three different subsystems:

- The liquid desiccant subsystem which contains two solution reservoirs, that allow keeping constant the inlet liquid desiccant concentration in the air-solution contactor; a pump with a frequency driver, a heating loop which contains a pump and an electric boiler; valves and temperature and flow rate sensors.
- The air subsystem which contains a fan with a frequency driver, a humidifier, a cooling coil, a heating coil that takes the heat from a boiler and temperature, relative humidity, air velocity and pressure sensors.
- The water subsystem which is comprised by a water chiller that allows cooling the water down to 4 °C, a three way valve, valves and temperature and flow rate sensors.

All the components that are in contact with the LiCl-H_2O solution are made of non-corrosive materials. Moreover, all the sensors are connected with a data acquisition system.

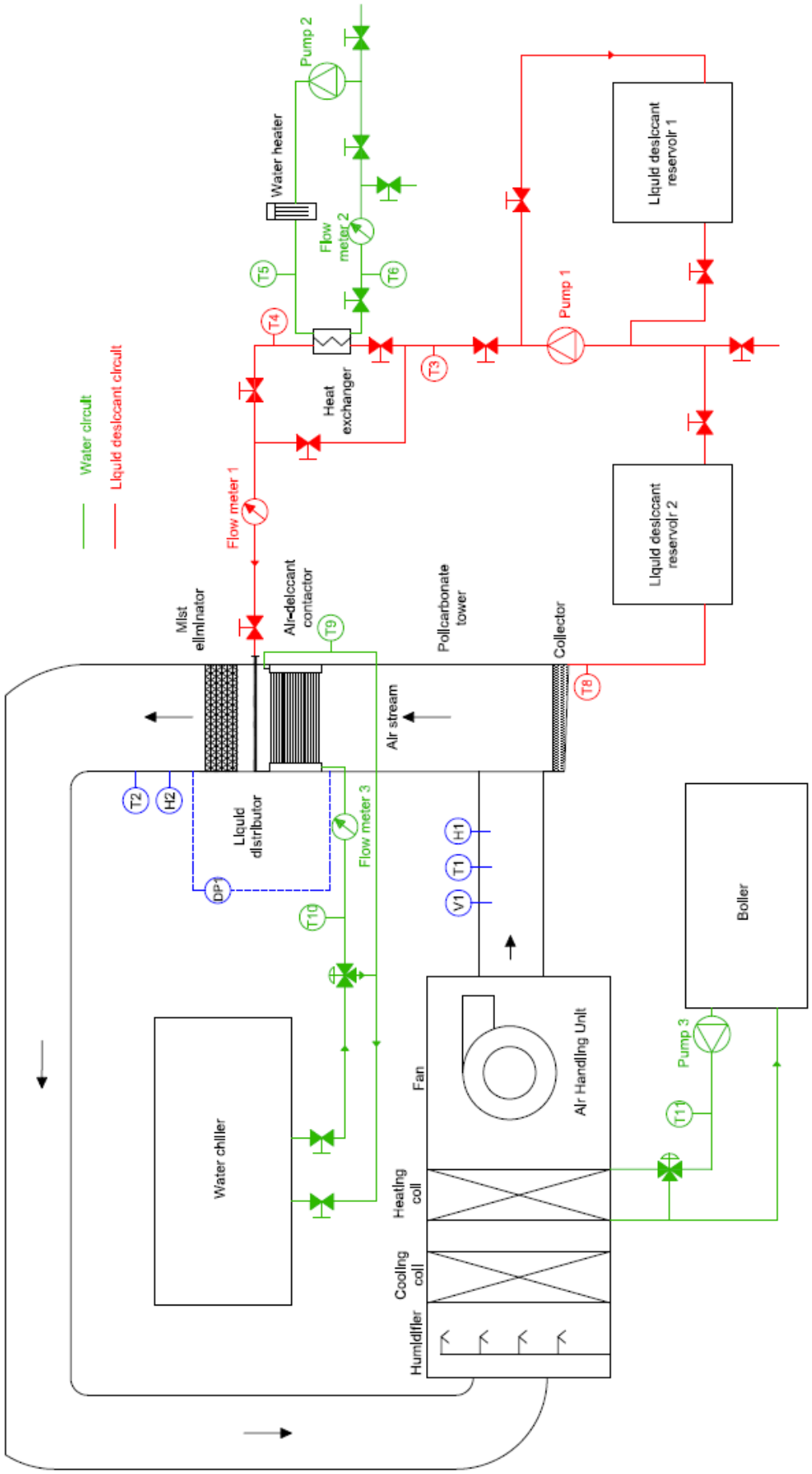

Figure 4.1. Schematic of the test bench for heat and mass transfer study.

4.2.1. Air-solution contactors description

As it is described in Chapter 2, the most common air-solution contactor is the adiabatic packed bed. However, internally-cooled absorbers and, in particular, falling-film with horizontal tubes absorbers can be an alternative to adiabatic one.

Table 4.1 contains the dimensions of tested air-solution contactors. Both air-solution contactors have the same dimensions, number of tubes and tube disposition. This permits to have a direct comparison between them. Figure 4.2 shows a drawing and a picture of one of the air-solution contactors when it was placed inside the polycarbonate tower. The exchangers only have one pass for the water stream; moreover, the inlet and outlet of the exchanger are in opposite positioning in order to have the same pressure drop through all the possible ways that water can take inside the exchangers.

Table 4.1. Heat/mass exchanger dimensions

Number of columns	4
Total number of tubes	78
Tube length (mm)	325
Outlet tube diameter (mm)	6.5
Inlet tube diameter (mm)	5.1
Tube arrangement	Staggered
Column distance (mm)	10.5
Row distance (mm)	14.4
Thermal conductivity of tubes (W/m·ºC)	0.21

Figure 4.2. Falling-film air-solution contactor.

4.2.2. Experimental apparatus

4.2.2.1. Air subsystem

Compared to the test developed for the hydrodynamic study and described in Chapter 3, the experimental study of the air-solution contactors requires a better control of temperature, humidity and flow rate of the air. For this reason, the test bench has been specially adapted to achieve the working conditions of an absorber of a liquid desiccant system.

An air handling unit (Figure 4.3) that contains a fan, a heating coil and a cooling coil provides the air at the required temperature and velocity. In this case, the cooling coil was not used because hot air is required at the entrance of the exchanger for absorber conditions.

Heat required for the heating coil has been provided by a modular gas boiler (Figure 4.4) that permits to produce a thermal capacity up to 100 kW of hot water.

On the other hand, the air ducts have been modified for two different reasons: to include a humidifier before the air handling unit, which permits to achieve the required humidity at the entrance of the exchanger; and to include a new air duct with a smaller cross section, which permits to measure with a better accuracy the air velocity. Figure 4.5 shows these two new devices. The amount of water that the humidifier can spray is 12 l/h.

Figure 4.3. Air handling unit.

Figure 4.4. Boiler.

Figure 4.5. Modifications in the air ducts. Box and loop for the humidifier (left), loop for the air velocity sensor (right).

4.2.2.2. Water subsystem

This subsystem is in charge of providing chilling water to the air-solution contactors. The main components are a water-to-water heat pump, a water loop with a three way valve and temperature and flow rate sensors.

The water-to-water heat pump has a thermal capacity of 100 kW and can produce chilling water from 4 ºC to 20 °C. The three way valve has been actuated manually in order to provide the required water flow rate to the heat exchangers. Temperature sensors are PT-100 type and flow meter is of the electromagnetic type; their specifications are shown in Table 3.3.

4.2.2.3. Sensor specifications

The parameters, the measurement devices, their accuracies and operational ranges are listed in Table 3.3. All the parameter were scanned and recorded by using an Agilent 34970A data acquisition system with the exception of the density measurements that were collected by a portable density meter.

4.3. Mathematical methodology

A mathematical model has been developed In order to obtain the performance of both heat exchangers and to establish a comparison between them. A schematic of the heat exchangers working as an absorber of a liquid desiccant system is represented in Figure 4.6. In this component, moist air, which is moved from the bottom to the top, and liquid desiccant, which is dropped from the top to the bottom, are directly in contact outside the horizontal tubes. Water is required to cool-down the solution at the same time that absorption of water is happening. In this way, the performance of the dehumidification process is more homogenous throughout the absorber than without cooling.

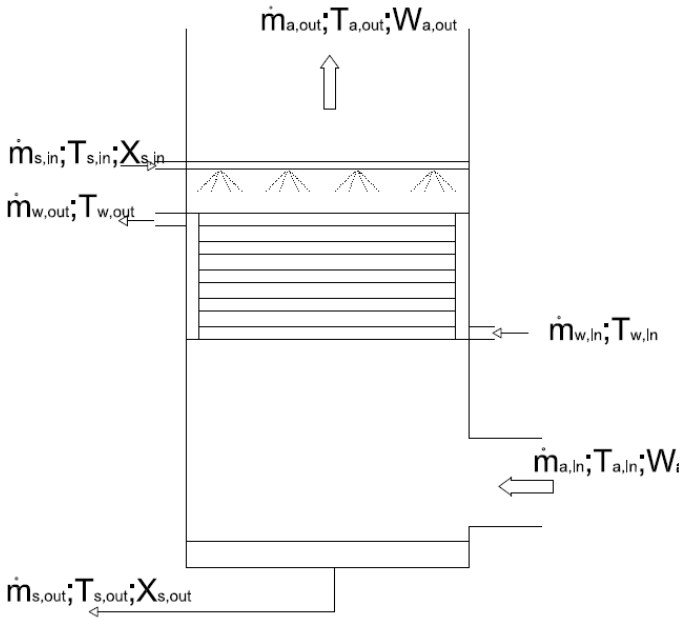

Figure 4.6. Schematic of the test bench for heat/mass exchanger.

4.3.1. Measured parameters for heat and mass transfer calculations

The following parameters have been measured in order to obtain the performance of the air-solution contactor:

- Air velocity, V_a (m/s).
- Inlet air temperature, $T_{a,in}$ (°C).
- Inlet air relative humidity, $H_{a,in}$ (%).

- Outlet air temperature, $T_{a,out}$ (°C).
- Outlet air relative humidity $H_{a,out}$ (%).
- Inlet water temperature, $T_{w,in}$(°C).
- Outlet water temperature, $T_{w,out}$ (°C).
- Volumetric water flow rate, $v_{w,in}$ (l/h).
- Inlet solution temperature, $T_{s,in}$ (°C).
- Outlet solution temperature, $T_{s,out}$ (°C).
- Volumetric solution flow rate, $v_{s,in}$ (l/h).
- Inlet solution density, $\rho_{s,in}$ (kg/m^3).

Air, water and solution inlet temperatures and flow rates are controlled parameters, as well as the air inlet humidity.

4.3.2. Calculations

The mathematical model for the evaluation of the heat exchanger performance has been carried out in Engineering Equation Solver (EES) [89]. This program contains libraries with the thermo-physical properties of the required fluids; these are water, moist air and LiCl-H_2O solution.

Thermo-physical properties included in EES for moist air are taken from Hyland and Wexler [90]. The equations are proved for a range of -100 °C to 200 °C. The thermodynamic properties for water are assumed from Haar et al. [91]. These correlations are defined up to a pressure of 815 bar. Enthalpy, specific heat, density and vapour pressure for LiCl-H_2O brine have been adopted from Pátek and Klomfar [24] formulations.

4.3.2.1. Mass transfer calculations

Dehumidified water ratio

The water absorbed in the contact surface can be obtained from air stream measurements by using the following equation:

$$\Delta\Omega\left(\frac{kg_w}{m^2 s}\right) = \frac{\dot{m}_{a,in}}{A} \cdot (W_{a,in} - W_{a,out}) \tag{4.1}$$

Where A is the contact surface between the solution film and the tubes, which is considered equal to the external surface of tubes, therefore:

$$A(m^2) = \pi \cdot d_o \cdot L_t \cdot n_t \tag{4.2}$$

Mass balance to water

The mass balance to water can be obtained from the following equation:

$$\dot{m}_{a,in} \cdot \left(W_{a,in} - W_{a,out}\right) = \dot{m}_{s,out} \cdot \left(1 - X_{s,out}\right) - \dot{m}_{s,in} \cdot \left(1 - X_{s,in}\right) \tag{4.3}$$

Mass balance lithium chloride

The mass balance to lithium chloride can be obtained from the following equation:

$$\dot{m}_{s,out} \cdot X_{s,out} = \dot{m}_{s,in} \cdot X_{s,in} \tag{4.4}$$

The two previous equations are required in order to calculate the outlet solution mass flow rate and the outlet LiCl mass concentration.

4.3.2.2. Heat transfer calculations

This section shows the calculations for the heat duty and global heat transfer coefficient.

Heat duty

The heat duty of the exchanger is produced by the water flow inside tubes. Therefore, the heat duty can be calculated by the sensible heat equation in the water stream as it is presented in the following equation:

$$\dot{Q}_w(kW) = \dot{m}_{w,in} \cdot (c_{p,w,out} \cdot T_{w,out} - c_{p,w,in} \cdot T_{w,in}) \quad (4.5)$$

Global heat transfer coefficient

The global heat transfer coefficient can be calculated as:

$$U \cdot A(\frac{kW}{°C}) = \frac{\dot{Q}_w}{\Delta T_{LM}} \quad (4.6)$$

ΔT_{LM} is the logarithmic mean temperature difference, which in this case is calculated as:

$$\Delta T_{LM}(°C) = F \cdot \Delta T_{LM,ccf} \quad (4.7)$$

Where $\Delta T_{LM,ccf}$ is the logarithmic mean temperature difference between the water stream and the solution stream at counter-current flow, this is:

$$\Delta T_{LM,ccf}(°C) = \frac{(T_{s,in} - T_{w,out}) - (T_{s,out} - T_{w,in})}{\ln \frac{(T_{s,in} - T_{w,out})}{(T_{s,out} - T_{w,in})}} \quad (4.8)$$

F is the correction-factor plot for single-pass cross-flow exchanger, one fluid mixed, other unmixed which is obtained according to the correlation presented by Bowman et al. [92].

4.3.2.3. Air cooling

Since both, temperature and humidity of moist air change through the exchanger, the air cooling is calculated as the addition of sensible cooling and latent cooling, what means:

$$\dot{Q}_a(kW) = \dot{Q}_{sen} + \dot{Q}_{lat} \quad (4.9)$$

Where sensible cooling is related to change in the moist air temperature, and therefore:

$$\dot{Q}_{sen}(kW) = \dot{m}_{a,in} \cdot (c_{p,a,in} \cdot T_{a,in} - c_{p,a,out} \cdot T_{a,out}) \quad (4.10)$$

And latent cooling is related to change in the moist air humidity ratio, and therefore:

$$\dot{Q}_{lat}(kW) = \dot{m}_{a,in} \cdot h_{cp,w} \cdot (W_{a,in} - W_{a,out}) \quad (4.11)$$

4.3.2.4. Energy balance

The energy balance of the air-solution contactor is calculated by the following equation:

$$\dot{Q}_a - \dot{Q}_w + \dot{Q}_s = 0 \quad (4.12)$$

Where $\dot{Q}_s$ is the heating of the liquid desiccant, what can be calculated as:

$$\dot{Q}_s(kW) = \dot{m}_{s,in} \cdot h_{s,in} - \dot{m}_{s,out} \cdot h_{s,out} \quad (4.13)$$

Equation 4.12 is an extra equation and is, therefore, used to verify that energy balance is happening.

4.3.3. Experimental conditions

The air-solution contactors have been tested at absorber conditions. The minimum solution flow rates for both treated and standard polypropylene exchangers are in the same range than the one obtained in the treated polypropylene tube within the wettability tests developed in Chapter 3. Table 4.2 shows the experimental conditions of both air-solution contactors.

It is important to mention that most of the conditions have been modified independently keeping constant the other variables in order to know their effect on the conditions of the air-solution contactors. However, inlet air relative humidity and LiCl mass concentration have not been changed independently because of restrictions of the test bench.

Table 4.2. Experimental conditions of treated and standard PP air-solution contactors.

Experimental conditions	Treated exchanger	Standard exchanger
Air velocity (m/s)	1.12 - 2.09	0.99 - 2.10
Solution flow rate (l/h)	122.5 - 343.8	113.3 - 314.7
Water flow rate (l/h)	321.7 - 423.5	220.7 - 325.7
Inlet water temperature (°C)	8.73 - 17.87	8.65 - 15.34
Inlet solution temperature (°C)	17.90 - 24.99	17.03 - 23.77
Inlet air temperature (°C)	29.50 - 33.60	27.03 - 32.56
Inlet air relative humidity (%)	33.2 - 46.6	35.5 - 48.5
LiCl mass concentration (%)	35.3 - 35.7	35.7 - 35.9

4.4. Air-solution contactors tests

4.4.1. Previous work

For a good falling-film behaviour, tubes have to be as straighter as possible. However, because of the way that polypropylene tubes and exchanger are made, tube supports had to be included for straightening them (see Figure 4.7).

Figure 4.7. Tube supports for exchangers.

Before starting the tests, heat exchangers were placed inside the polycarbonate tower. Because of the exchangers dimensions are smaller than the cross section of the tower, the channel showed in Figure 4.8 was made in order to make pass through the exchanger the air stream. PT-100 temperature sensors were previously calibrated. In addition, the data acquisition system was set up before starting the tests.

Figure 4.8. Polycarbonate tower with exchanger and channel.

4.4.2. Experimental procedure

In each different measurement, the experimental procedure followed up to reach steady-state conditions has been the same. The device that has been firstly operated is the boiler, which is required to achieve warm temperatures in the air. Once the desired temperature for the hot water is obtained (about 55 °C), the air handling unit fan is turned on in order to heat up the air and reach the required air velocity. The humidifier is then operated.

Once required conditions are achieved in the moist air, the water chiller including the cooling system, pumps and valves are turned on. Water temperature is set with the chiller and water flow rate with a three way valve.

After the desired conditions of the cooling water are obtained, liquid desiccant pump and electrical resistance R1 are switched on. For the fine adjustment of the liquid desiccant flow rate, a variable frequency driver actuating on its pump has been used.

In order to measure the LiCl mass concentration, density measurements were performed with samples of the solution, which were taken every time a tube was tested. Equation that correlates the temperature, density and LiCl mass concentration provided by Pàtek [24] was used. The whole system was kept working for 30 minutes after the steady-state conditions were reached.

4.5. Experimental results of the air-solution contactors

The performance of the air-solution contactors at different air velocities, inlet water temperatures and inlet solution temperatures and flow rates has been assessed. The variables that represent the exchanger performance are:

- The heat duty, which is the cooling energy provided by the cooling water inside the tubes. This parameter is defined in Equation 4.5.
- The air cooling, which is the sum of the sensible and the latent cooling provided to the air through the exchanger. This parameter is defined in Equation 4.9.
- The global heat transfer coefficient of the air-solution contactor defined in Equation 4.6.
- The dehumidified water ratio, which is the amount of water absorbed by the desiccant within the exchanger per square meter of outlet tube surface. This parameter is defined in Equation 4.1.

Annex C contains the experimental measurements obtained in these tests.

On the other hand, full wetting has not been reached in the air-solution contactor with standard polypropylene tubes, since the liquid desiccant flow rate is lower than the minimum calculated in Chapter 3.

4.5.1. Air-solution contactor with standard tubes

4.5.1.1. Heat duty

Figure 4.9 shows the heat duty of the air-solution contactor with standard tubes as function of the difference between the inlet temperature of the solution and the inlet temperature of the water and the air velocities. In general, the higher difference temperature between water and solution and the higher air velocity, the higher heat duty in the air-solution contactor. The minimum heat duty is in the range of 0.25 kW when the difference temperature is in the range of 5 °C and air velocity is about 1.2 m/s. The maximum heat duty is in the range of 0.45 kW when the difference temperature is in the range of 10 °C and air velocity is about 2 m/s. The highest uncertainty of the heat duty is 0.08 kW, moreover, the highest uncertainty of the difference temperature is 0.18 ºC, both for a confidence interval of 95 %.

On one hand, the effect of the air velocity on the heat duty can be due to two different reasons: cooling is transferred to the air flow through the dry patches of the tubes, and heat transfer to the liquid desiccant flow is enhanced by the air velocity. On the other hand, the effect of the difference temperature between the liquid desiccant and the water is expected, since heat transfer depends on temperature difference.

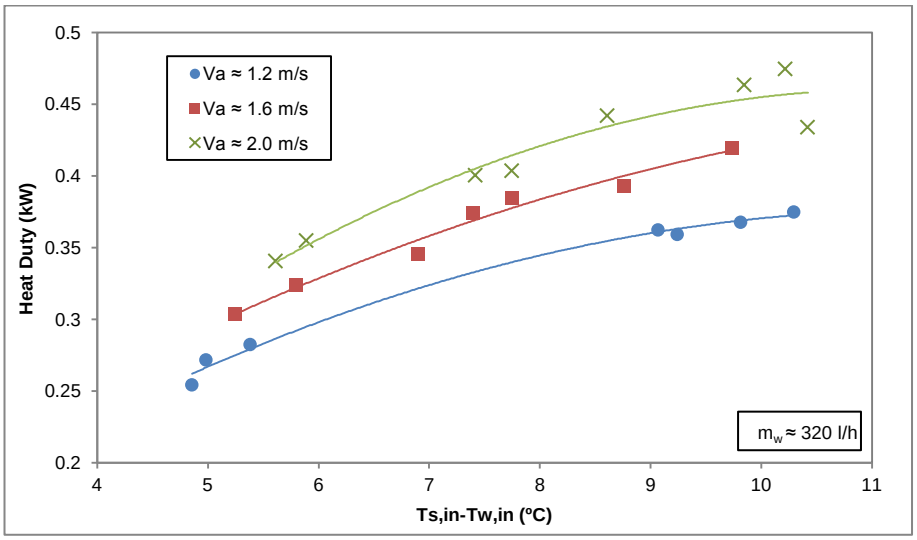

Figure 4.9. Heat duty of the air-solution contactor with standard PP tubes as function of the difference temperature between inlet solution and inlet water and air velocity.

4.5.1.2. Air cooling

Figure 4.10 shows the air cooling of the air-solution contactor with standard tubes as function of the air velocity and the Reynolds number of the solution. In general, the higher air velocity, the higher air cooling in the air-solution contactor. The Reynolds number of the solution does not seem to affect to air cooling. The minimum air cooling is in the range of 0.5 kW when the air velocity is about 1.2 m/s and the maximum air cooling is in the range of 0.8 kW when the air velocity is about 2 m/s.

On one hand, the effect of the air velocity on the air cooling can be due to two different reasons: higher heat and mass transfer between the air and the solution, and between the air and the dry patches of the tubes. On the other hand, the effect of the solution Reynolds number could be explained if wettability of tubes is not enhanced much with higher values of it.

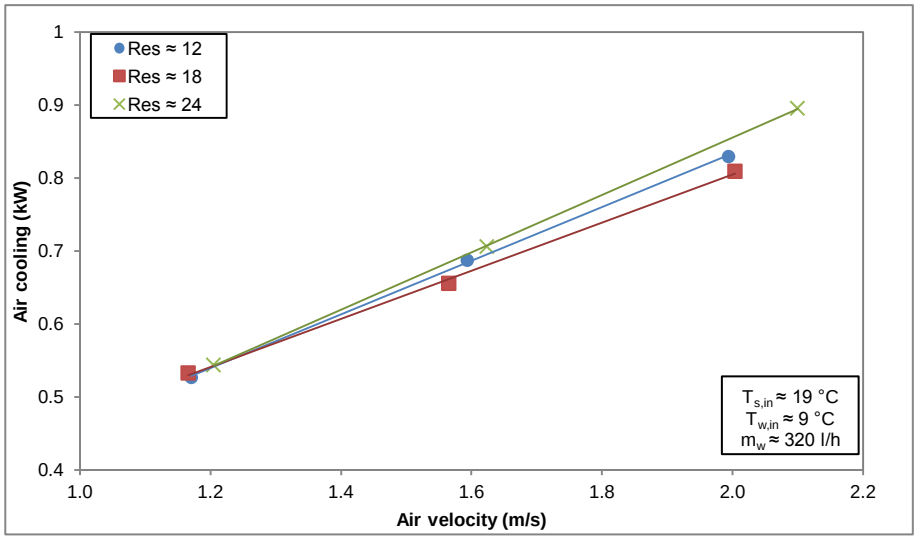

Figure 4.10. Air cooling of the air-solution contactor with standard PP tubes as function of the air velocity and the Reynolds number of the solution.

Figure 4.11 shows the air cooling of the air-solution contactor with standard tubes as function of the air velocity and the inlet water temperature. In this case, the lower inlet water temperature, the higher air cooling in the air-solution contactor. This influence is caused by two reasons:

- The solution temperature is lower along the tubes and, therefore, the dehumidification is enhanced and the heat transfer between air and the solution is higher.
- Since the tubes are not full wetted, the heat transfer between the dry patches of the tube and the air is higher because the surface temperature of tubes is lower.

The minimum heat duty is in the range of 0.5 kW when the air velocity is about 1.2 m/s and inlet water temperature is 12 °C. The maximum air cooling is in the range of 0.85 kW when the air velocity is about 2 m/s and the inlet water temperature is 9 °C. The highest uncertainty of the air cooling is 0.06 kW, moreover, the highest uncertainty of the air velocity is 0.07 m/s, both for a confidence interval of 95 %.

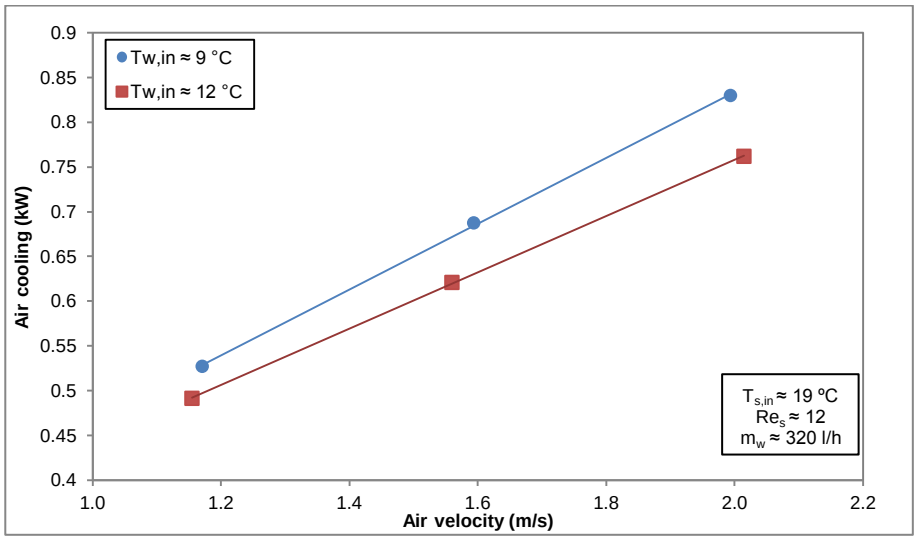

Figure 4.11. Air cooling of the air-solution contactor with standard PP tubes as function of the air velocity and the inlet water temperature.

4.5.1.3. Global heat transfer coefficient

Figure 4.12 shows the global heat transfer coefficient of the air-solution contactor with standard tubes as function of the air velocity and the solution Reynolds number. Higher air velocities and higher liquid desiccant

flow rates increase the global heat transfer coefficient of the air-solution contactor. However, the global heat transfer coefficient is almost the same when the film Reynolds number is 12 and 18, what could suggest that the tube wetting is not changing in this range. When the film Reynolds number is increased from 18 to 24 the global heat transfer coefficient rises more than 25 %, what can be justified for a better wetting of tubes in this range.

The minimum global heat transfer coefficient in about 0.039 kW/°C when the air velocity is about 1.2 m/s and the film Reynolds number is between 12 and 18. The maximum global heat transfer coefficient is in the range of 0.057 kW when the air velocity is about 2 m/s and the film Reynolds number is about 24.

The effect of the air velocity on the global heat transfer coefficient can be due to heat transfer coefficient between the liquid desiccant flow and the tube is enhanced by the air velocity.

The highest uncertainty of the global heat transfer coefficient is 0.006 kW/°C, moreover, the highest uncertainty of the air velocity is 0.07 m/s, both for a confidence interval of 95 %.

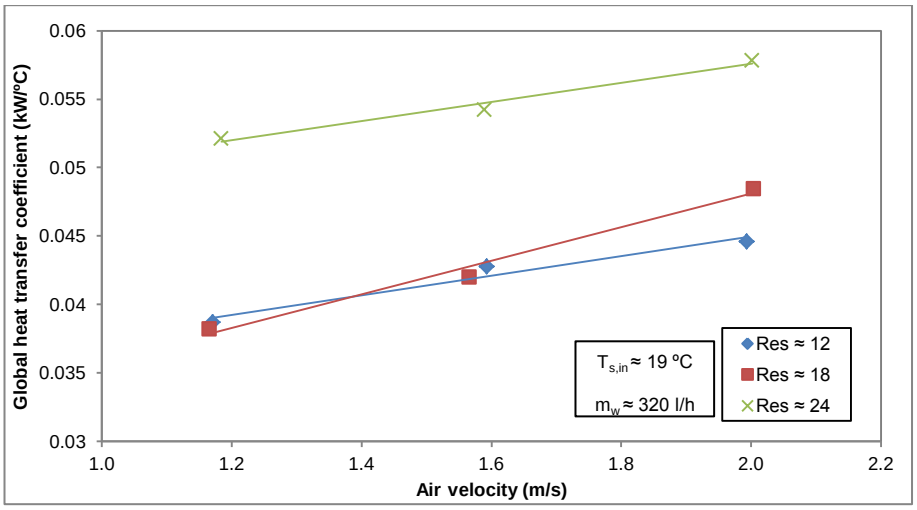

Figure 4.12. Global heat transfer coefficient of the air-solution contactor with standard PP tubes as function of the air velocity and the inlet water temperature.

4.5.1.4. Dehumidified water ratio

Figure 4.13 shows the dehumidified water ratio of the exchanger with standard tubes as function of the inlet solution temperature and the air velocity. In general, the higher air velocity the higher dehumidification in the exchanger. On the other hand, the higher inlet solution temperature, the lower dehumidification. The minimum dehumidified water ratio is in the range of $1.7 \cdot 10^{-4}$ kg/m^{2}s when the air velocity is about 1.2 m/s and the inlet solution temperature is about 24 °C. The maximum dehumidification is in the range of $3.9 \cdot 10^{-4}$ kg/m^{2}s when the air velocity is about 2 m/s and the inlet solution temperature is about 17 °C.

The air velocity enhances the water absorption because mass transfer is increased with higher Reynolds of the air. On the other hand, the higher solution temperature the higher vapour pressure of water in the desiccant.

Solution Reynolds number that, in principle, could affect to the dehumidification has a negligible influence on the air dehumidification compared to air velocity and inlet solution temperature.

The largest uncertainty of the dehumidification is $3.7 \cdot 10^{-5}$ kg/sm^2 whereas the highest uncertainty of the inlet solution temperature is 0.08 ºC, both for a confidence interval of 95 %.

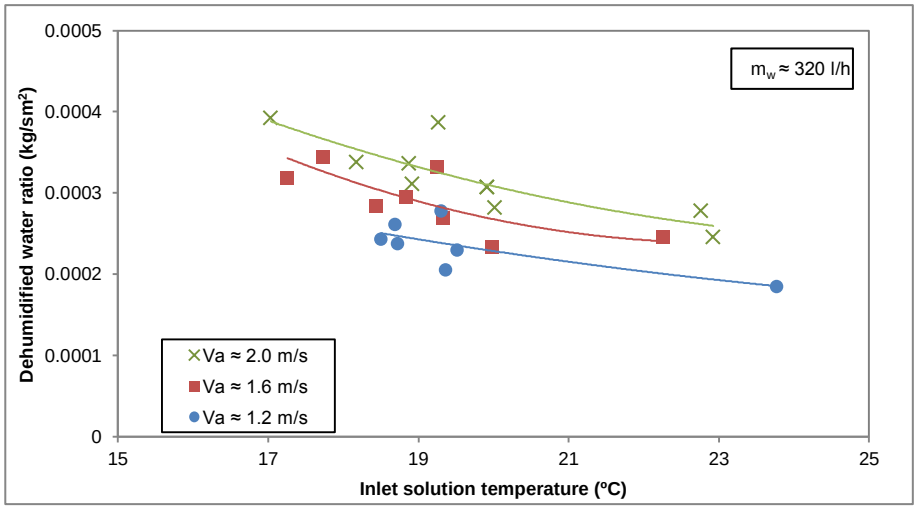

Figure 4.13. Dehumidification of the air-solution contactor with standard PP tubes as function of the inlet solution temperature and the air velocity.

4.5.2. Air-solution contactor with surface treated tubes

4.5.2.1. Heat duty

Figure 4.14 shows the heat duty of the air-solution contactor with treated tubes as function of the difference between the inlet temperature of the solution and the inlet temperature of the water and the air velocities. In general, as in the case of the air-solution contactor with standard polypropylene tubes, the higher difference temperature between water and solution and the higher air velocity, the higher heat duty in the air-solution contactor. The minimum heat duty is in the range of 0.37 kW when the difference temperature is in the range of 6.3 °C and air velocity is about 1.2 m/s. The maximum heat duty is in the range of 0.51 kW when the difference temperature is in the range of 10 °C and air velocity is about 2 m/s. The highest uncertainty of the heat duty is 0.09 kW, moreover, the highest uncertainty of the difference temperature is 0.30 ºC, both for a confidence interval of 95 %.

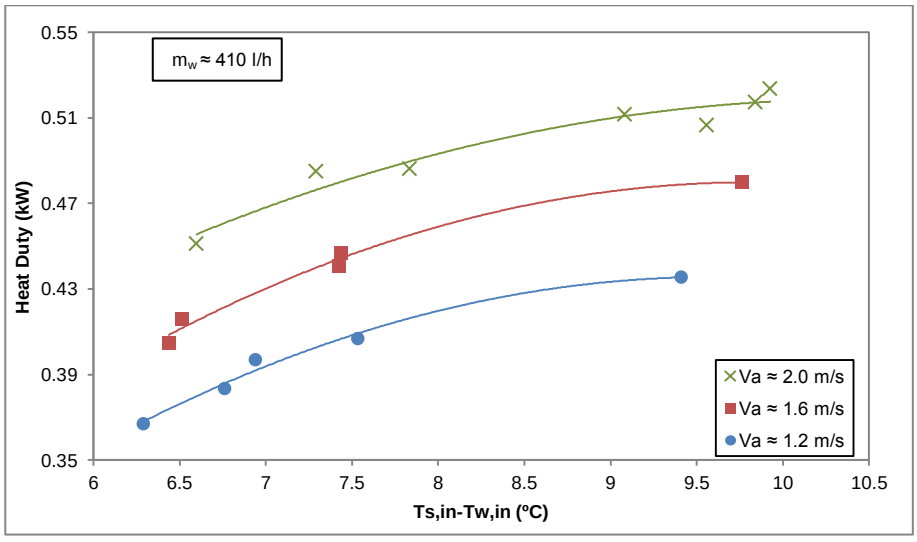

Figure 4.14. Heat duty of the air-solution contactor with treated PP tubes as function of difference temperature between inlet solution and inlet water and air velocity.

4.5.2.2. Air cooling

Figure 4.15 shows the air cooling of the air-solution contactor with standard tubes as function of the air velocity and the Reynolds number of the solution. In general, as it is expected, the higher air velocity and Reynolds number, the higher air cooling in the air-solution contactor. The minimum air cooling is in the range

of 0.62 kW when the air velocity is above 1.2 m/s and the solution Reynolds number is about 10, and the maximum air cooling is above 1.0 kW when the air velocity is about 2 m/s and the Reynolds number is about 18.

In this case, Reynolds number of the solution seems to affect more than with the standard tubes. However, this increasing in the air cooling is not large enough. In fact, despite that tests have been performed at liquid desiccant flow rates higher than the required to fully wet the tubes in Chapter 3, in most of the cases the tubes could not be wetted at all. Probably the main reason that explains this fact is the appearance of little bends on the plastic tubes that created the streams formation in the centre of them.

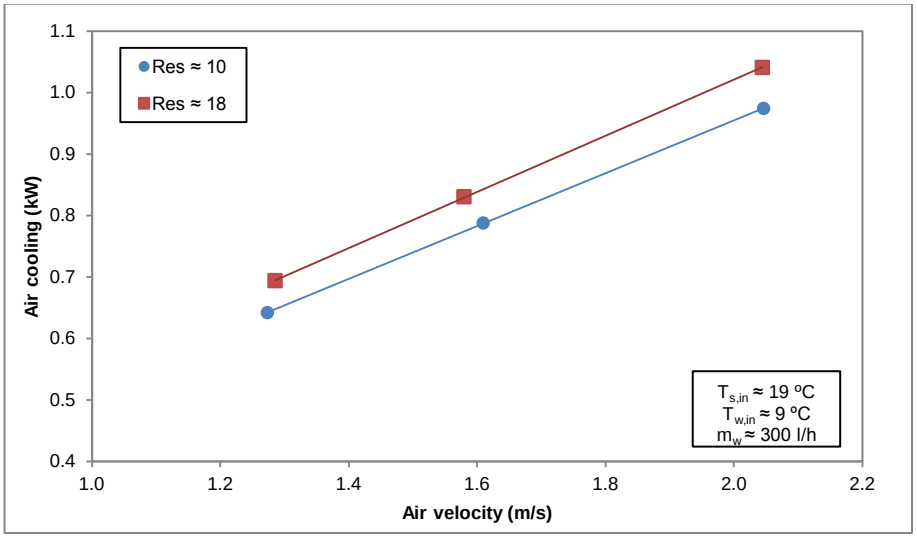

Figure 4.15. Air cooling of the air-solution contactor with treated PP tubes as function of the air velocity and the Reynolds number of the solution.

Figure 4.16 shows the air cooling of the air-solution contactor with treated tubes as function of the air velocity and the inlet water temperature. In this case, the influence of the water temperature on the air cooling is almost negligible (differences are smaller than uncertainties). This happens because illustrated results in Figure 4.16 are achieved when film Reynolds number is about 28. At these conditions the liquid desiccant could wet fully the tubes and, therefore, the air cooling depends much more on the inlet liquid desiccant temperature and the air inlet conditions than on the water temperature. The highest uncertainty of the air cooling is 0.07 kW; moreover, the highest uncertainty of the air velocity is 0.07 m/s, both for a confidence interval of 95 %.

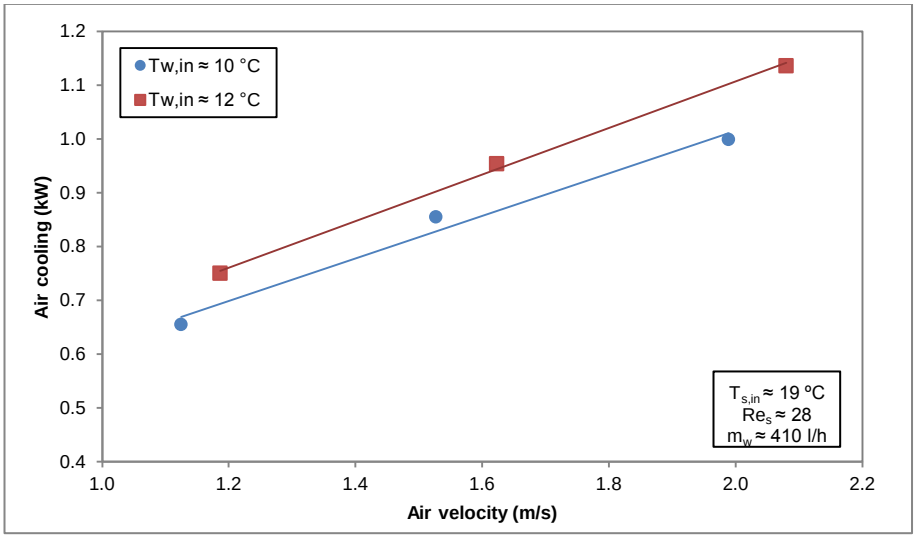

Figure 4.16. Air cooling of the air-solution contactor with treated PP tubes as function of the air velocity and the inlet water temperature.

4.5.2.3. Global heat transfer coefficient

Figure 4.17 shows the global heat transfer coefficient of the air-solution contactor with treated tubes as function of the air velocity and the solution Reynolds number. Higher air velocities and higher liquid desiccant flow rates increase the global heat transfer coefficient of the air-solution contactor. However the global heat transfer coefficient is almost the same when the Reynolds film number is 24 and 88, what could suggest that the tube wetting is not changing in this range and it could be almost fully wetted.

The minimum global heat transfer coefficient is about 0.049 kW/°C when the air velocity is about 1.2 m/s and the film Reynolds number is between 10. The maximum global heat transfer coefficient is in the range of 0.068 kW/°C when the air velocity is above 2 m/s and the film Reynolds number is about 28. The highest uncertainty of the global heat transfer coefficient is 0.008 kW/°C, moreover, the highest uncertainty of the air velocity is 0.07 m/s, both for a confidence interval of 95 %.

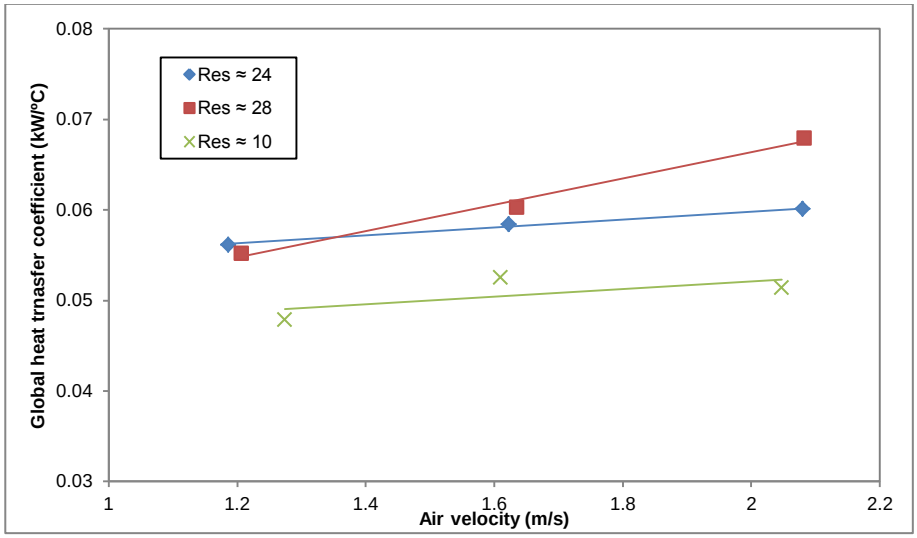

Figure 4.17. Global heat transfer coefficient of the air-solution contactor with treated PP tubes as function of the air velocity and the inlet water temperature.

4.5.2.4. Dehumidified water ratio

Figure 4.18 shows the dehumidified water ratio of the exchanger with treated tubes as function of the inlet solution temperature and the air velocity. In general, the higher air velocity, the higher dehumidified ratio in the exchanger. On the other hand, the higher inlet solution temperature, the lower dehumidification. The minimum dehumidification is in the range of $2.6 \cdot 10^{-4}$ kg/m^{2}s when the air velocity is 1.2 m/s and the inlet solution temperature is 25 °C. The maximum dehumidification is in the range of $4.3 \cdot 10^{-4}$ kg/m^{2}s when the air velocity is 2 m/s and the inlet solution temperature is 19 °C. The largest uncertainty of the dehumidified ratio is $3.1 \cdot 10^{-5}$ kg/sm^2; moreover, the highest uncertainty of the inlet solution temperature is 0.1 °C, both for a confidence interval of 95 %.

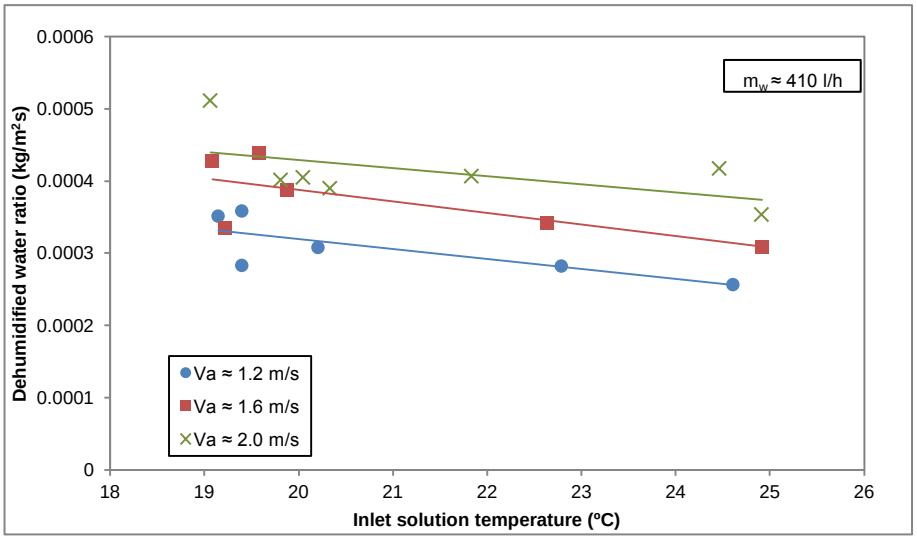

Figure 4.18. Dehumidification of the air-solution contactor with treated PP tubes as function of the inlet solution temperature and the air velocity.

4.6. Standard vs. treated air-solution contactor

One of the main objectives of this chapter is to compare the performance of the air-solution contactors with standard polypropylene tubes and with treated tubes. As in the previous sections, the variables used to do this comparison are the heat duty, the air cooling, the global heat transfer coefficient and the dehumidified water ratio. This comparison is done by using results obtained from similar tested conditions.

4.6.1. Heat duty

Figure 4.19 shows a comparison of the heat duty achieved by the air-solution contactors with standard and treated tubes as function of the air velocity. According to the results obtained from this comparison, the heat duty in the treated air-solution contactor is higher than in the standard at any air velocity. The enhancement achieved with treated tubes is almost constant for the air velocities tested in this study; the average difference for the three cases is 69 W, what means an improvement of about a 17 % with respect the standard polypropylene air-solution contactor.

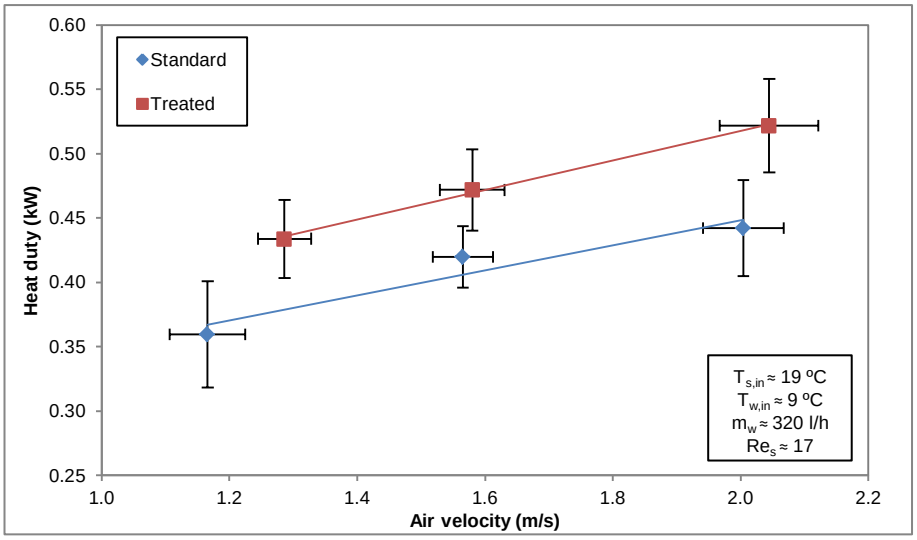

Figure 4.19. Comparison of the heat duty achieved by the standard and the treated exchangers as function of the air velocity.

4.6.2. Air cooling

Figure 4.20 shows a comparison of the air cooling provided through the air-solution contactors with standard and treated tubes as function of the air velocity. According to the results obtained from this comparison, the air cooling in the treated air-solution contactor is higher than in the standard at any air velocity. The enhancement achieved with treated tubes slightly increases at higher air velocities; the maximum difference is 232 W, which is obtained at 2 m/s, what means an improvement of about a 29 % in comparison with the standard polypropylene air-solution contactor.

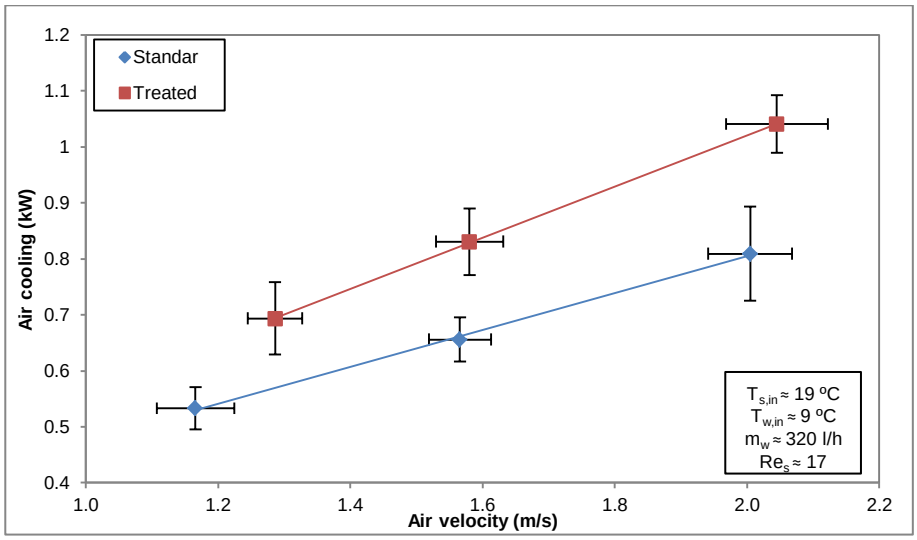

Figure 4.20. Comparison of the air cooling achieved by the standard with the treated exchangers as function of the air velocity.

4.6.3. Global heat transfer coefficient

Figure 4.21 shows a comparison of the global heat transfer coefficient provided through the air-solution contactors with standard and treated tubes as function of the air velocity. According to the results obtained from this comparison the air cooling in the treated exchanger is higher than in the standard exchanger at any air velocity. The enhancement achieved with treated tubes is slightly increasing at higher air velocities; the maximum difference is 0.026 kW/ºC, which is obtained at 2 m/s, what means an improvement of 54 % in comparison with the standard polypropylene exchanger.

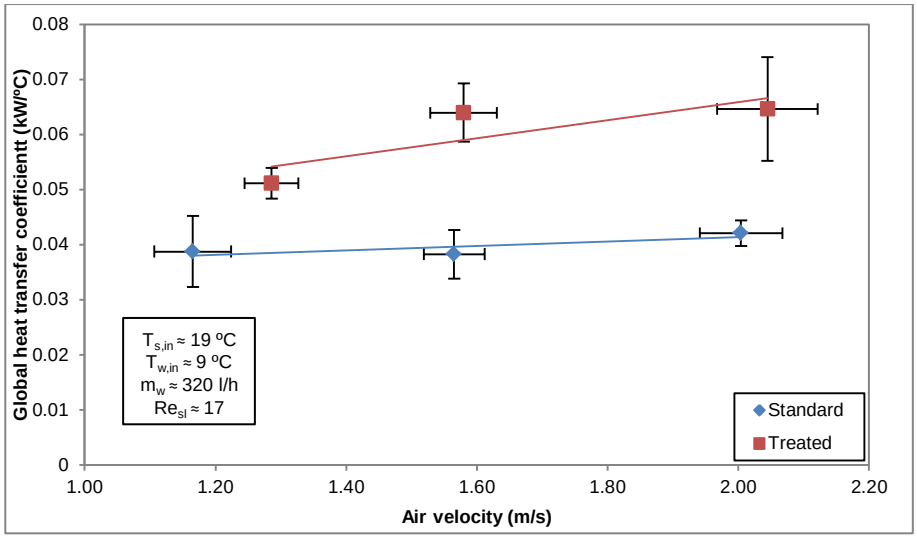

Figure 4.21. Comparison of the global heat transfer coefficient achieved by the standard with the treated exchangers as function of the air velocity.

4.6.4. Dehumidified water ratio

Figure 4.22 shows a comparison of the dehumidified water ratio provided through the air-solution contactors with standard and treated tubes as function of the air velocity. According to the results obtained from this comparison, the dehumidified water ratio in the treated air-solution contactor is higher than in the standard exchanger at any air velocity. The enhancement achieved with treated tubes slightly increases at higher air velocities; the maximum difference is $6.9 \cdot 10^{-5}$ kg/m^{2}s, which is obtained at 2 m/s, what means an improvement of 20 % in comparison with the standard polypropylene exchanger.

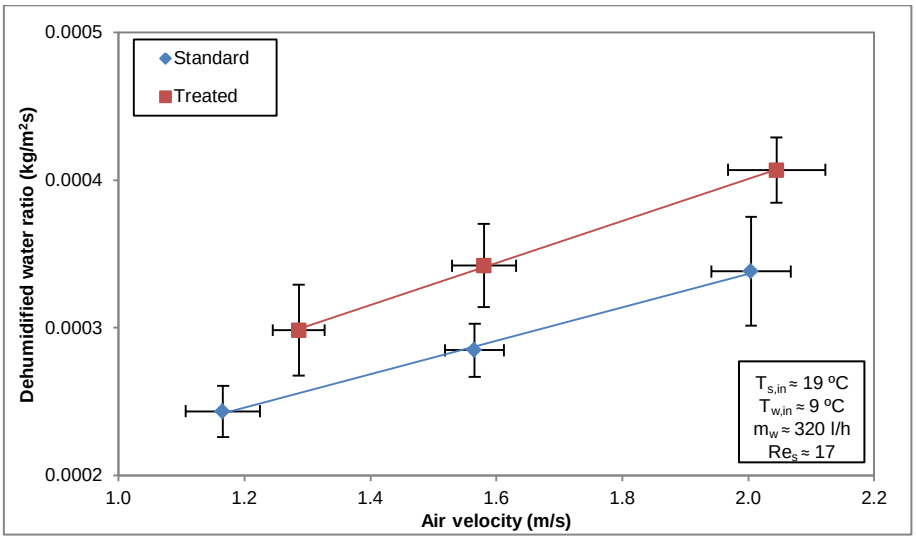

Figure 4.22. Comparison of the dehumidification achieved by the standard and the treated exchangers as function of the air velocity.

4.7. Conclusions

Experimental tests have been carried out at absorber conditions in order to get the performance of two polypropylene air-solution contactors of the falling-film with horizontal tubes type with the same dimensions and features excepting the tube surface. The main difference between them is that tubes in one of them, contains a plasma surface treatment in order to improve its wettability, when it is in contact with LiCl-H_2O. The following conclusions have been obtained from these tests:

- This study has been made at solution Reynolds number above the minimum required to fully wet tubes on the treated polypropylene tubes obtained in Chapter 3. However, full wetting of tubes has not been always reached in the treated air-solution contactor because of a bending of the tubes due to its low rigidity.
- Heat duty, air cooling, global heat transfer coefficient and dehumidified water ratio are the variables that show the performance of the air-solution contactors.
- Air velocity is the variable that has the highest effect on the performance of the air-solution contactors. For the case of the standard polypropylene, the air cooling increases from about 0.5 kW to 0.9 kW when the air velocities is increased from about 1.2 m/s to 2 m/s. For the case of the treated polypropylene, the air cooling increases from about 0.65 kW to 1 kW when the air velocities is increased from about 1.2 m/s to 2 m/s.
- The inlet solution temperature has a high effect on the dehumidified water ratio. In this sense, the higher temperature the lower dehumidification. For the case of the standard polypropylene, the dehumidification achieved is decreased a 35 % when the inlet solution temperature increases from 17 to 23 °C. For the case of the treated polypropylene, the dehumidification achieved is decreased a 25 % when the inlet solution temperature increases from 19 to 25 °C. This effect shows the significance of the heat transfer on the absorber performance.

- Despite tubes were not always fully wetted in the treated air-solution contactor, when comparing them, a better performance of the air-solution contactor with treated tubes has been found. The enhancement is the largest for the global heat transfer coefficient (up to 54 %), but also obvious for the heat duty (about 17 %), air cooling (up to 29 %) and dehumidified water ratio (20 %).

Chapter 5. Sizing and design of the hybrid liquid desiccant system

5.1. Introduction

This chapter deals with the sizing and design of a hybrid liquid desiccant system. The methodology used to perform the objective of this chapter is described below:

- Development of the mathematical model for the absorber and regenerator.
- Development of the mathematical model of other components of the liquid desiccant system.
- Definition of the lay-out of the liquid desiccant system and implementation in a mathematical model.
- Calculation of internal loads and definition of the design conditions.
- Selection of the operational conditions of the system at design conditions.
- Sizing of the system at design conditions.

Results obtained from previous chapters, such as the minimum liquid desiccant flow rate or the maximum air velocity, are used for the sizing and design of the system. In addition, a sensitivity analysis which contains the effect of some of the operational parameters of the hybrid liquid desiccant system on the system performance is included in the end of the chapter.

5.2. Mathematical model for the absorber and regenerator

The absorber and the regenerator are the components that mainly affect to the sizing and design of a liquid desiccant system. A mathematical model of a non-adiabatic air-solution contactor of the falling film type has been implemented in EES [100] (Equation Engineering Solver) for both components.

The thermo-physical properties included in EES for moist air are taken from Hyland and Wexler [90]. The equations are proved for a range of -100 °C to 200 °C. Moreover, the thermo-physical properties for water are assumed from Haar et al. [91]. These correlations are defined up to a pressure of 815 bar. Furthermore, the thermo-physical properties of LiCl-H_2O brine have been adopted from Pátek and Klomfar [24] formulation. These correlations are valid for temperatures between 273 K and 400 K and for mole fractions up to 0.5.

The physical process that occurs in the absorber and the regenerator is very similar, but the inverse. This means that heating is required to regenerate the solution, and cooling is required to dehumidify the air. For this reason the same equations have been used for both exchangers.

Figure 5.1 shows a schematic description of the air-solution contactors. The non-adiabatic air-solution contactors are of the counter-current type between the water and the desiccant. At the same time, the air enters to the exchangers from the bottom to the top.

The mathematical model is based on the model described by Hellmann and Grossman [93], and later improved by Gommed and Grossman [94]. The main reason why this model has been used is the relatively simplicity of it, because it can be modelled with algebraic equations. Moreover, this model is experimentally validated as it has been proved in some of their publications [11], [33].

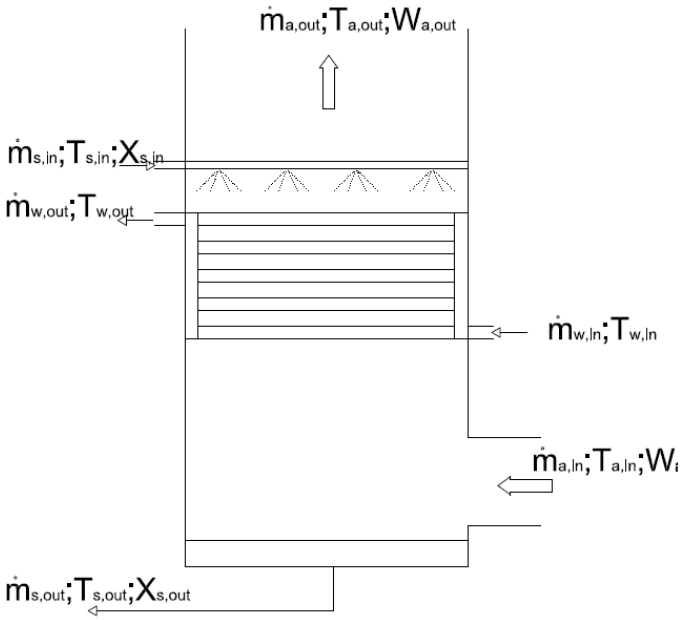

Figure 5.1. Non-adiabatic horizontal tubes falling film air-solution exchanger.

The input values required in the mathematical model are:

- Inlet moist air dry bulb temperature, $T_{a,in}$ (°C) .
- Inlet moist air humidity ratio, $W_{a,in}$ (kg_w/kg_a).
- Inlet moist air mass flow rate, $m_{a,in}$ (kg/s).
- Inlet water temperature, $T_{w,in}$ (°C).
- Inlet water mass flow rate, $m_{w,in}$ (kg/s).
- Inlet solution temperature, $T_{s,in}$ (°C).
- Inlet solution concentration, $X_{s,in}$ (dimensionless), which is the ratio between the liquid desiccant mass and the total solution mass.
- Inlet solution mass flow rate, $m_{s,in}$ (kg/s).

Other parameters related with the physical air-solution contactor characteristics are also required:

- Air-solution contactor width, *Wd* (m).
- Air-solution contactor height, *Hg* (m).
- Tube inside diameter, d_i (m).
- Tube outside diameter, d_o (m).
- Tube length, L_t (m).
- Tube thermal conductivity, k_t (W/m·K).
- Tube pitch, *pitch* (dimensionless).
- Number of tube rows, n_{rows} (dimensionless).
- Number of tube passes, n_p (dimensionless).

Once the exchanger physical characteristics are fixed, heat and mass transfer coefficients can be obtained from correlations. On the other hand, 12 variables are required to be calculated:

- Outlet water temperature, $T_{w,out}$ (°C).

- Outlet moist air humidity ratio, $W_{a,out}$ (kg_w/kg_a).
- Outlet moist air temperature, $T_{a,out}$ (dimensionless).
- Outlet solution mass flow rate, $m_{s,out}$ (kg/s).
- Outlet solution temperature, $T_{s,out}$ (°C).
- Outlet solution concentration, $X_{s,out}$ (dimensionless).
- Air-solution interface temperature at the top, $T_{i,top}$ (°C).
- Air-solution interface concentration at the top, $X_{i,top}$ (dimensionless).
- Air-solution interface humidity ratio at the top, $W_{i,top}$ (dimensionless).
- Air-solution interface temperature at the bottom, $T_{i,b}$ (°C).
- Air-solution interface concentration at the bottom, $X_{i,b}$ (dimensionless).
- Air-solution interface humidity ratio at the bottom, $W_{i,b}$ (kg_w/kg_a).

The same number of equations than outputs is required in order to model the performance of air-solution contactors. The assumptions of the mathematical model are the following:

- The process is in steady-state-conditions.
- Thermal losses to the ambient are not considered.
- The model is one-dimensional.
- Equilibrium in the air-solution interface is reached.
- The heat transfer between the solution and the heating fluid or coolant is approximated by a logarithmic mean temperature difference.
- Both, water content and enthalpy of the air at the air-solution interface change linearly along the interface.

Total water mass balance:

$$\dot{m}_{s,out} \cdot \left(1 - X_{s,out}\right) - \dot{m}_{s,in} \cdot \left(1 - X_{s,in}\right) + \dot{m}_{a,in} \cdot \left(W_{a,out} - W_{a,in}\right) = 0 \tag{5.1}$$

Total lithium chloride mass balance:

$$\dot{m}_{s,out} \cdot X_{s,out} = \dot{m}_{s,in} \cdot X_{s,out} \tag{5.2}$$

Total energy balance:

$$\dot{m}_{w,in} \cdot \left(h_{w,out} - h_{w,in}\right) + \dot{m}_{s,out} \cdot h_{s,out} - \dot{m}_{s,in} \cdot h_{s,in} + \dot{m}_{a,in} \cdot \left(h_{a,out} - h_{a,in}\right) = 0 \tag{5.3}$$

Where enthalpies of water and solution are taken from Hyland and Wexler [90] and Patek and Klomfar [24] respectively.

Interface mass balance at the top:

$$\sigma_{Is} A \cdot \left(X_{s,in} - X_{I,t}\right) - \sigma_a A \cdot \left(W_{a,out} - W_{I,t}\right) = 0 \tag{5.4}$$

Where σ_{IS} and σ_a are the mass transfer coefficients between the solution and the interface, and the air and the interface, respectively, which are both set below. On the other hand, A is the interface contact surface, which is assumed equal to the external tube contact surface, therefore:

$$A(m^2) = \pi \cdot d_o \cdot L_{tube} \cdot n_{rows} \cdot \frac{Lg}{pitch} \tag{5.5}$$

Interface mass balance at the bottom:

$$\sigma_{Is}A\left(X_{s,out} - X_{I,b}\right) - \sigma_a A\left(W_{a,in} - W_{I,b}\right) = 0 \quad (5.6)$$

Interface energy balance at the top:

$$\alpha_a A \cdot \left(T_{a,out} - T_{I,t}\right) - \alpha_{is}A \cdot \left(T_{I,t} - T_{s,in}\right) + \sigma_a A \cdot \left(W_{a,out} - W_{I,t}\right) \cdot h_{WAi,t} - \sigma_{IS}A \cdot (X_{s,in} - X_{I,t}) \cdot h_{WSI,t} = 0 \quad (5.7)$$

Where h_{WA} and h_{WS} are the partial enthalpies of water in the air and the solution respectively.

Interface energy balance at the bottom:

$$\alpha_a A \cdot \left(T_{a,in} - T_{I,b}\right) - \alpha_{Is}A \cdot \left(T_{I,b} - T_{s,out}\right) + \sigma_a A \cdot \left(W_{a,in} - W_{I,b}\right) \cdot h_{WAI,b} - \sigma_{Is}A \cdot \left(X_{s,out} - X_{I,b}\right) \cdot h_{WSI,b} = 0 \quad (5.8)$$

Water vapour pressure equilibrium (interface) at the top:

$$p_{WS}\left(X_{I,top}, T_{I,top}\right) = p_{WA}(W_{I,top}) \quad (5.9)$$

Where p_{WS} and p_{WA} are the vapour pressure of water in solution [24] and moist air, which is calculated as:

$$p_{WA}(kPa) = (W_{I,top} \cdot p)/(W_{I,top} + 0.622) \quad (5.10)$$

Where p is the atmospheric pressure.

Water vapour pressure equilibrium (interface) at the bottom:

$$p_{WS}\left(X_{I,b}, T_{I,b}\right) = p_{WA}(W_{I,b}) \quad (5.11)$$

Internal tube/solution heat transfer:

The heat transfer between the solution and the internal tube water is approximated by a logarithmic mean temperature difference at counter-current conditions.

$$m_{w,in} \cdot c_{p,w,in} \cdot \left(T_{w,out} - T_{w,in}\right) = \frac{UA}{1000} \cdot \frac{(T_{s,in} - T_{w,out}) - (T_{s,out} - T_{w,in})}{\ln\frac{(T_{s,in} - T_{w,out})}{(T_{s,out} - T_{w,in})}} \quad (5.12)$$

Interface/air mass transfer:

The two remaining equations needed are obtained considering the heat and mass transfer coupled processes that take place along the air-solution interface. Two ordinary differential equations describe the local changes of water content and enthalpy:

$$\frac{dW_a}{dA} = -\frac{\sigma_a}{m_{a,in}} \cdot (W_a - W_I) \quad (5.13)$$

$$\frac{dh_a}{dA} = -\frac{\sigma_a}{m_{a,in}} \cdot (h_a - h_I) \quad (5.14)$$

In the following equation, Lewis number of air (Le_a) of one is assumed, which is applicable for it.

$$Le_a = \frac{\alpha_a}{\sigma_a c_{p,a}} \quad (5.15)$$

In order to integrate the differential equations, it is assumed that both, water content and enthalpy of the air-solution interface, change linearly along the interface. Under these assumptions, the equations can be integrated analytically to give the following equations:

$$W_{a,out} - W_{a,in} - (W_{l,b} - W_{a,in}) \cdot \left(1 - e^{-\frac{\sigma_a A}{m_{a,in}}}\right) - (W_{l,top} - W_{l,b}) \cdot \left(1 - \frac{m_{a,in}}{\sigma_a A}\left(1 - e^{-\sigma_a \frac{A}{m_{a,in}}}\right)\right) = 0 \quad (5.16)$$

$$h_{a,out} - h_{a,in} - (h_{l,b} - h_{a,in}) \cdot \left(1 - e^{-\frac{\sigma_a A}{m_{a,in}}}\right) - (h_{l,top} - h_{l,b}) \cdot \left(1 - \frac{m_{a,in}}{\sigma_a A} \cdot \left(1 - e^{-\sigma_a \frac{A}{m_{a,in}}}\right)\right) = 0 \quad (5.17)$$

However, in some cases, these assumptions do not hold. To overcome this problem, Gommed and Grossman [105] suggested dividing the single exchanger unit into several sub-exchangers. They have found that the number of required sub-units *n* depends on the dimensionless ratio of mass transfer coefficient in air times-area divided by the air flow rate:

$$n = \frac{\sigma_a A}{m_{a,in}} \quad (5.18)$$

Heat and mass transfer coefficients:

The global heat transfer coefficient between the water and the film is calculated considering the thermal resistance of water inside the tubes (R_{wt}), the thermal resistance of the tube wall (R_t) and the thermal resistance of film outside the tubes (R_{ts}):

$$U\left(\frac{kW}{m^{2\circ}C}\right) = \frac{1}{R_{wt}+R_t+R_{ts}} \quad (5.19)$$

Thermal resistance between the water and the tube wall:

The thermal resistance between the water and the tube wall is obtained as:

$$R_{wt}\left(\frac{m^{2\circ}C}{kW}\right) = \frac{1}{\alpha_{wt}} \quad (5.20)$$

$$\alpha_{wt}\left(\frac{kW}{m^{2\circ}C}\right) = \frac{Nu_{wt} \cdot \lambda_{wt}}{\phi_i} \quad (5.21)$$

Thermal conductivity of the water λ_{wt} (kW/m°C) is obtained using correlations from [106].

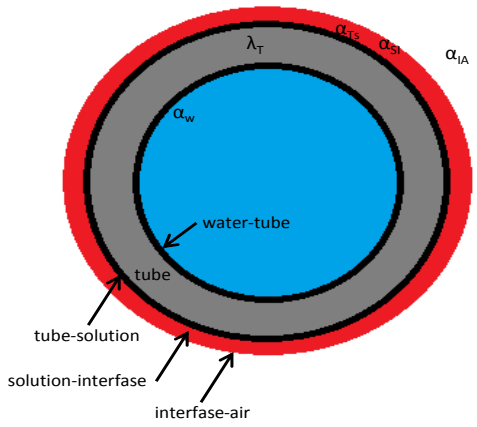

Figure 5.2. Interface and heat/mass transfer coefficients for each tube.

Depending on the water flow regime, the Nusselt number is calculated according with the empirical correlations for internal forced convention in cylindrical pipes available in Nellis and Klein book [107] and referred to [108], [109] and [110]:

$$Nu_{wt} = \begin{cases} 2300 > Re_w \rightarrow 4.36 + \frac{\left(0.1156 + \frac{0.08569}{Pr^{0.4}}\right) Gz_w}{1 + 0.1158 Gz_w^{0.6}} \\ 2300 < Re_w < 10000 \rightarrow \frac{\varepsilon}{8} \cdot (Re_w - 1000) \cdot \frac{Pr_w}{1 + 12.7 \cdot \left(\frac{\varepsilon}{8}\right)^{1/2} \cdot \left(Pr_w^{2/3} - 1\right)} \\ Re_w \geq 10000 \rightarrow 0.023 \cdot Re_w^{0.8} \cdot Pr_w^n \end{cases} \quad (5.22)$$

Where P_{rw} is the Prandtl number for water, defined as:

$$Pr_w = \frac{c_{p,w} \mu_w}{k_w} \quad (5.23)$$

Re_w is the Reynolds number for water, calculated as:

$$Re_w = \frac{V_w \cdot d_i}{\nu_w} \quad (5.24)$$

Where V_w is the water velocity inside the tube (m/s), and ν_w is the Kinematic viscosity (m^2/s) of water [106]. Gz_w is the Graetz number for water, defined as:

$$Gz_w = \frac{d_i Pr_w Re_w}{L_t} \quad (5.25)$$

ε is the pipe friction coefficient which is calculated as:

$$\varepsilon = (0.79 \cdot lnRe_w - 1.64)^{-2} \quad (5.26)$$

n is a constant that is equal to 0.4 for heating of the water (absorber conditions) and 0.3 for cooling of the water (for regenerator conditions).

Tube wall thermal resistance:

The thermal resistance of the tube wall R_t is calculated with the following expression:

$$R_t \left(\frac{m^{2\circ}C}{kW}\right) = \frac{d_o}{2\lambda_t} \cdot ln\left(\frac{d_o}{d_i}\right) \quad (5.27)$$

Thermal resistance between the tube wall and the LiCl-H_2O solution:

The thermal resistance between the tube wall and the LiCl-H_2O solution film is assumed constant and equal to the values obtained by Gommed et al. [11] when full wettability is reached, this is for the titanium air-solution contactor. The heat transfer coefficient obtained in that case was 0.676 $kW/m^{2\circ}C$.

$$R_{ts} \left(\frac{m^{2\circ}C}{kW}\right) = \frac{1}{\alpha_{ts}} \quad (5.28)$$

$$\alpha_{ts} \left(\frac{kW}{m^{2\circ}C}\right) = 0.676 \quad (5.29)$$

This value was achieved with titanium tubes completely wetted and with a droplet flow mode. These are the same conditions than expected.

Mass transfer coefficient between air-solution interface and moist air:

The mass transfer coefficient between the air-solution interface and moist air is assumed constant and equal to the values obtained from the experimental tests developed in Chapter 4. Among the different results achieved with these experiments, the chosen value was considered the obtained from the treated air-solution contactor with the lowest solution flow rate and velocity. The chosen value is 0.05 $kg/m^2 \cdot s$.

Heat transfer coefficient between air-solution interface and moist air:

The heat transfer coefficient between air-solution interface and moist air is obtained by using the Chilton-Colburn analogy, in which heat transfer and the mass transfer coefficients are related by the Lewis number according the following expression:

$$Le^{2/3} = \frac{\alpha}{\sigma c_p} \tag{5.30}$$

And, therefore, heat transfer coefficient is equal to:

$$\alpha_a \left(\frac{kW}{m^{2\circ}C}\right) = c_{p,a} \cdot \sigma_a \cdot Le_a^{2/3} \tag{5.31}$$

Heat and mass transfer coefficient between the LiCl-H_2O solution and the air-solution interface:

Because of Lewis number is much higher in the solution film than in the air, the thermal resistance between the interface and the solution can be neglected. According with Hellman and Grossman [104], heat transfer coefficient between the LiCl-H_2O solution and the air-solution interface has been set as 500 times bigger than heat transfer coefficient between air-solution interface and moist air. In addition, they verified that the mass transfer coefficient between air-solution interface and the solution can be assumed three times lower than the mass transfer coefficient of the solution.

5.3. Mathematical model for other components

Three more heat exchangers are required in the hybrid liquid desiccant system:

- A solution heat exchanger in order to improve the COP of the liquid desiccant system.
- A cooling coil in order to reach the supply air temperature.
- An air heat exchanger (heat recovery) in order to increase the air inlet temperature at the entrance of the regenerator.

The mathematical model of each heat exchanger is described below.

5.3.1. Mathematical model of the heat exchangers

Figure 5.3 shows a schematic description of a counter-current heat exchanger model which is the arrangement of the three heat exchangers. The main difference between them is related with the fluid properties. Thermo-physical properties for moist air, water and LiCl-H_2O are the same than used for absorber and regenerator.

This model requires 7 parameters given by the user or calculated from other equations of the full model:

- Inlet cold fluid temperature, $T_{c,in}$ (°C).
- Cold fluid specific heat capacity, $c_{p,c}$ (kJ/kg·°C).
- Inlet cold fluid mass flow rate, $m_{c,in}$ (kg/s).
- Inlet hot fluid temperature $T_{h,in}$ (°C)
- Hot fluid specific heat capacity, $c_{p,h}$ (kJ/kg·°C).
- Inlet hot fluid mass flow rate, $m_{,h,in}$ (kg/s).
- Heat transfer coefficient, UA_{HX} (kW/°C).

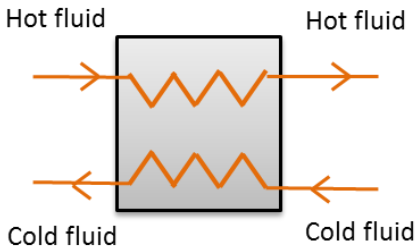

Figure 5.3. Counter-current heat exchanger.

The mathematical model is based on ε-NTU method for counter-current heat exchangers, 10 equations are required to calculate 10 parameters:

Heat capacity rate in hot fluid:

$$C_h\left(\frac{kW}{^\circ C}\right) = \dot{m}_h c_{p,h} \tag{5.32}$$

Heat capacity rate in cold fluid:

$$C_{co}\left(\frac{kW}{^\circ C}\right) = \dot{m}_c c_{p,co} \tag{5.33}$$

Minimum heat capacity rate:

$$C_{min}\left(\frac{kW}{^\circ C}\right) = Minimum(C_h, C_{co}) \tag{5.34}$$

Maximum heat capacity rate:

$$C_{max}\left(\frac{kW}{^\circ C}\right) = Maximum(C_h, C_{co}) \tag{5.35}$$

Heat capacity ratio:

$$HC_{HX} = \frac{C_{min}}{C_{max}} \tag{5.36}$$

Number of heat transfer units:

$$NTU_{HX} = \frac{UA_{HX}}{C_{min}} \tag{5.37}$$

Heat exchanger effectiveness:

$$\varepsilon_{HX} = \frac{1-e^{-(1-HC_{HXl})NTU_{HX}}}{1-R_{HX}e^{-(1-HC_{HX})NTU_{HX}}} \tag{5.38}$$

Heat exchanged in the solution heat exchanger:

$$\dot{Q}_{HX}(kW) = \varepsilon_{sol} C_{min}(T_{in} - T_{out}) \tag{5.39}$$

Outlet cold fluid temperature:

$$T_{co,out} = T_{co,in} + \frac{\dot{Q}_{HX}}{C_{co}} \tag{5.40}$$

Outlet strong solution temperature:

$$T_{h,out} = T_{h,in} + \frac{\dot{Q}_{HX}}{C_h} \tag{5.41}$$

5.4. Definition of the lay-out of the liquid desiccant system and implementation in a mathematical model

The lay-out of the hybrid liquid desiccant system is shown in Figure 5.4. The system consists in three different subsystems:

- A liquid desiccant system, whose absorber and regenerator are of the internally-cooled type and made of polypropylene with plasma surface treatment. A solution heat exchanger is also included in order to improve the performance of the system.
- An air handling unit, which controls the supply air temperature (with a cooling/heating coil) and the air flow rate. Return air is used to regenerate the water through the regenerator. The air is pre-heated before passing the regenerator in order to improve the water desorption.
- A flexible heat pump that, depending on the energy requirements, is able to condensate with water or with air. It supplies the chilled and hot water to the absorber and regenerator respectively.

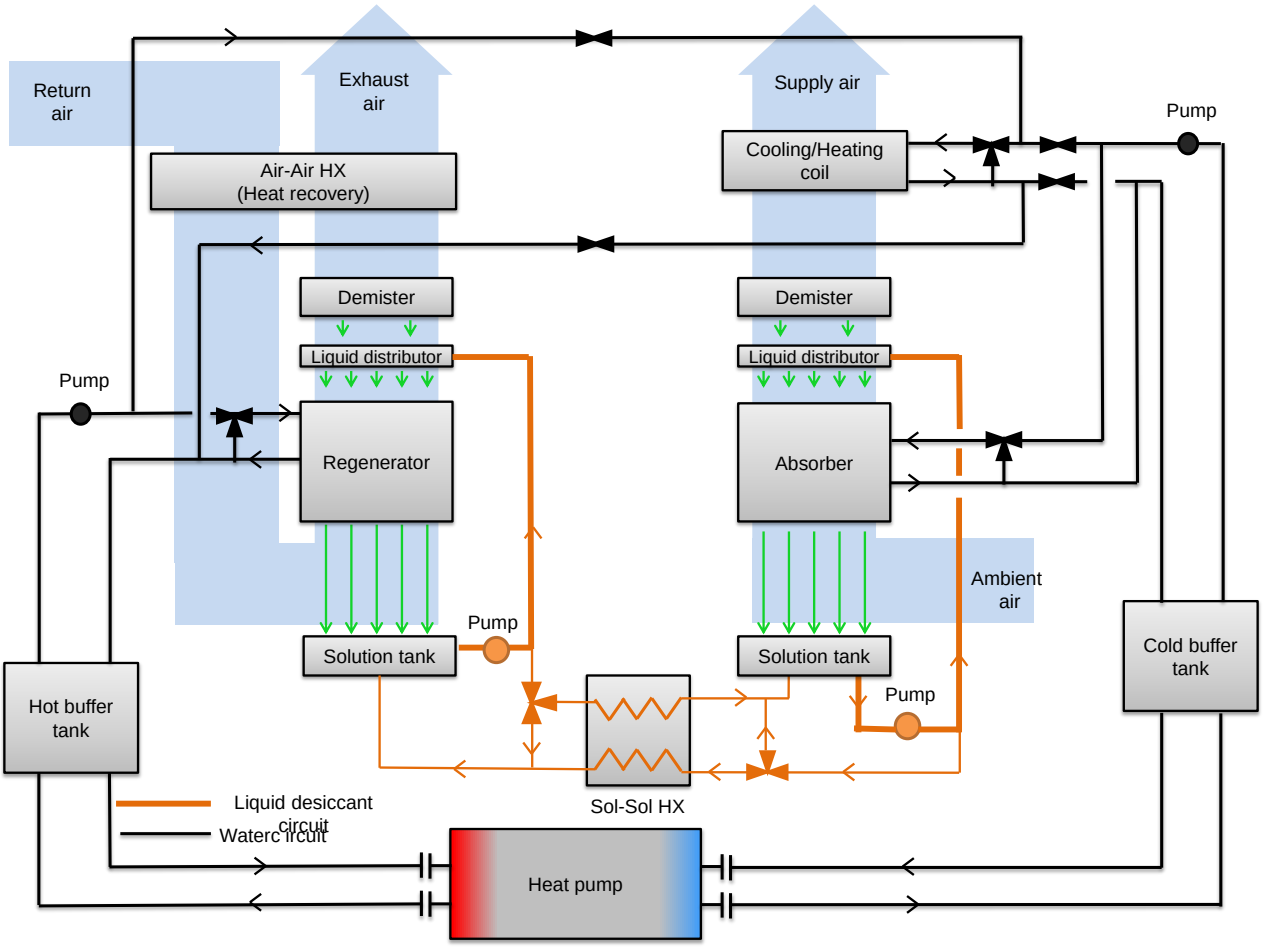

Figure 5.4. Schematic figure of the proposed hybrid liquid desiccant system.

5.5. Calculation of internal loads and definition of the internal and external air conditions

The hybrid liquid desiccant system must operate in Taiwan, where ambient conditions are warm and humid during almost ten months of a year. Moreover, the system has to climate two locker rooms of a swimming-pool, where high latent loads must be handled.

In order to calculate the size of the hybrid liquid desiccant system internal loads, internal temperature and humidity and external air conditions must be defined before.

5.5.1. External and internal air conditions

Ambient conditions of Taipei are warm and humid for the most part of the year as it is pointed out in Table 5.1, where average high temperature are above 25 °C from April to October. Table 5.2 contains the ambient conditions of Taipei based on dew-point temperatures (which are typically considered for dehumidification purposes). The values highlighted in red colour, that corresponds to a percentile 1 %, are the used for the sizing of the system. Weather Data has been taken from 2009 ASHRAE Handbook Fundamentals [111].

On the other hand, taking into account the suggestions given by the European Standards [112] the dry bulb temperature selected in the locker rooms is 25 °C and the relative humidity taken as reference is 60 %.

Table 5.1. Average monthly values of some climatic parameters of Taipei [113].

	Month												
	Jan	**Feb**	**Mar**	**Apr**	**May**	**Jun**	**Jul**	**Ago**	**Sep**	**Oct**	**Nov**	**Dec**	**Annual**
Average high temperature (°C)	18.9	19.1	21.8	25.8	28.7	31.9	34.0	33.4	31.2	27.6	23.9	20.7	26.4
Daily mean temperature (°C)	15.8	15.9	18.0	21.7	24.7	27.5	29.2	28.8	27.1	24.3	20.9	17.6	22.6
Average low temperature (°C)	13.3	13.5	15.3	18.7	21.8	24.3	25.8	25.6	24.3	21.9	18.7	15.2	19.9
% humidity	79.4	81.1	81.0	78.7	78.8	78.3	74.0	75.2	76.0	76.3	76.5	76.5	77.7

Table 5.2. External design condition for Taipei based on dew point temperature [111].

Station	**Dehumidification design conditions**					
Percentile	**0.4 %**			**1 %**		
Parameter	**Dew point Temperature (ºC)**	**Humidity Ratio (kg_w/kg_{da})**	**Mean coincident dry bulb temperature (ºC)**	**Dew point Temperature (ºC)**	**Humidity Ratio (kg_w/kg_{da})**	**Mean coincident dry bulb temperature (ºC)**
Sungshan/ Taipei	27.0	0.0227	30.5	**26.2**	**0.0217**	**29.9**

5.5.2. Internal loads

Since the two locker rooms do not have any exterior floor, wall or roof, all the internal loads are positive. The main internal gains of these rooms are lightings, people and showers.
Results obtained from internal load calculations at design conditions are shown in Table 5.3.

Table 5.3. Sensible and latent loads for the locker rooms.

Loads	**Sensible (kW)**	**Latent (kW)**	**Total (kW)**
Lights	1.28	0.00	1.28
People	2.25	1.65	3.90
Showers	0.29	10.73	11.02
Total	3.82	12.38	16.20

5.6. Selection of the operational conditions of the system at design conditions

The operational conditions of the system at design conditions must be set before doing the sizing of it. In this way, operational conditions depends not only on the internal loads and ambient conditions, but also on the air flow rate, which determines the supply air conditions, and other constrictions related to the system, such as working conditions in some of the main variables of the system, and physical constrictions. The selection of the operational conditions required for the sizing of the hybrid liquid desiccant system is contained and explained in detail in this section.

5.6.1. Air flow rate and calculation of supply air conditions and ventilation loads

Since all the return air of the locker rooms is discharged to the ambient, the supply air flow rate is calculated with the ventilation requirements. Figure 5.5 shows the conditioned space distribution and area. Moreover, the height of the locker rooms is 3 m and therefore, the zone volume is 386.25 m^3. On the other hand, ventilation requirements for locker rooms are in the range of 6 air changes per hour. For this reason, a volumetric air flow rate of 2500 m^3/h has been chosen, which supposes about 6.5 air changes per hour.

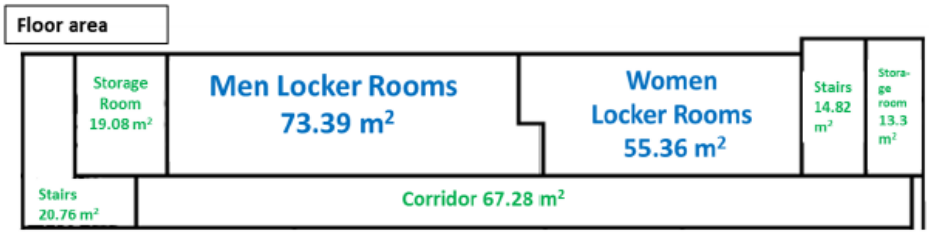

Figure 5.5. Conditioned space distribution and area.

Once the supply air flow rate and internal loads are calculated, supply air conditions can be obtained. If steady-state conditions are reached inside the locker rooms, the internal gains and internal moisture generation must be the same that the energy and the water removed by the supply air. That means that supply air conditions can be calculated at design conditions by considering the following expressions obtained from the energy balance and the water mass balance inside the locker rooms.

$$T_{supply}(°C) = T_{room} - \frac{\dot{Q}_{sen}}{\dot{m}_{supply} \cdot c_{p,a}} \tag{5.42}$$

$$W_{supply}(\frac{kg_w}{kg_{da}}) = W_{room} - \frac{\dot{Q}_{lat}}{\dot{m}_{supply} \cdot h_{cp}} \tag{5.43}$$

On the other hand, since ambient conditions are not the same as internal conditions, ventilation loads must be also handled by the hybrid liquid desiccant system. In this case, sensible and latent loads related to ventilation are calculated as:

$$\dot{Q}_{sen,vent}\ (kW) = \dot{m}_{supply} \cdot c_{p,a} \cdot (T_{amb} - T_{room}) \tag{5.44}$$

$$\dot{Q}_{lat,vent}\ (kW) = \dot{m}_{supply} \cdot h_{cp} \cdot (W_{amb} - W_{room}) \tag{5.45}$$

Finally, total load is calculated with the addition of the internal loads and the calculation loads. Table 5.4 contains the results of the calculations of this section.

Table 5.4. Air flow rate, supply air conditions, ventilation loads and total loads at design conditions.

Supply air flow rate (m^3/h)	2500
Supply air temperature (ºC)	19.0
Supply air humidity ratio (kg_w/kg_a)	0.0069
Sensible ventilation load (kW)	4.16
Latent ventilation load (kW)	19.48
Total load (kW)	39.84

5.6.2. Water temperatures, flow rates and heat pump selection

Liquid desiccant temperature is a key parameter for the behaviour of both the absorber and the regenerator. In general, the higher temperature in the regenerator, the more regeneration of water. On the other hand, the lower temperature in the absorber, the more dehumidification of moist air.

However, since both hot and cold water are provided by a water-to-water heat pump, there are some limitations that must be taken into consideration. The performance of a heat pump depends much on the hot water temperature in the condenser and the cold water temperature in the evaporator. In general, the effect is the opposite than for a liquid desiccant system: the higher temperature in the condenser and the lower temperature in the evaporator, the lower thermal capacity and COP.

Moreover, according to the manufacturer of the heat pump, the maximum suitable temperature for the heat pump is 55 °C. At this water temperature in the condenser, the minimum suitable temperature in the evaporator is 10 °C [114].

Finally, taking into consideration these constrictions, the chosen water temperatures to be provided by the heat pump are 55 °C for the condenser of the heat pump, which is the inlet hot water temperature for the regenerator; and 15 °C for the evaporator of the heat pump which is the inlet cold water temperature for the absorber.

The water flow rate in the absorber can be obtained from the total load calculated in the previous section, and defining a difference temperature of water by using the following equation:

$$\dot{m}_w\left(\frac{kg}{s}\right) = \frac{\dot{Q}_{abs}}{c_{p,w} \cdot \Delta T_w} \tag{5.46}$$

In this case, it is important to try to reduce the difference temperature of water in order to minimize the average temperature in the absorber and increase the capacity of it. For this reason, ΔT_w has been chosen equal to 2.9 °C. With this assumption, the required water mass flow rate is 3.3 kg/s.

In the same way, the water flow rate in the regenerator is calculated, but considering a COP of the LDS equal to 0.75 in order to obtain the thermal capacity required in it. By considering the same difference temperature, the required water mass flow rate is 4.4 kg/s.

The thermal capacity of the selected water-to-water heat pump has been oversized because it will operate far from nominal conditions in the condenser side. The selected heat pump is the NRP 280 [114], which is manufactured by Aermec. The main performance parameters of it are shown in Table 5.5.

Table 5.5. Main performance parameters of the selected heat pump

Nominal heat pump cooling capacity (kW)	58.0
Nominal heat pump heating capacity (kW)	75.0
Nominal COP	2.96

*Nominal conditions: 7 °C in the evaporator and 45 °C in the condenser; difference temperature of 5 °C in both sides.

5.6.3. Air-solution contactor constrictions and desiccant flow rate

For the size of the absorber and the regenerator, there are additional constrictions related to the place they will be placed, as well as the manufacturing process of themselves.

Figure 5.6 shows the towers and their dimensions that will be used to contain the absorber and the regenerator. Cross section of the tower permits achieving an air velocity smaller than 2 m/s, which is the maximum air velocity to avoid dragging of liquid desiccant and deflection of the film, at design conditions. Two towers will be required, one for the regeneration process and another for the absorption process. They should be made off fiberglass, instead of the standard galvanized steel, because of its resistance to corrosion. In addition, there is a collector for the liquid desiccant at the bottom of each tower with a volume of about 200 l.

The selected material for the two air-solution contactors is polypropylene. Moreover, as it was concluded in Chapter 3 and Chapter 4, the tubes will contain a surface plasma treatment in order to improve its wettability when LiCl-H_2O is in contact with the outer surface of the horizontal tubes. Each air-solution contactor will be

comprised by smaller modules that have an in-line configuration of tubes that can be changed to staggered configuration during the manufacturing process of the module, as it is shown in Figure 5.7.
These modules can be joined in order to obtain air-solution contactors with a bigger contact surface. According to the cross section of the towers, the maximum tube length of each module is 680 mm. More specifications of the modules are detailed in Table 5.6. In total, three modules fit in the cross section of the towers. Special endings for the headers of the modules are made in order to connect each other and to make the connections between different passes. The connections between passes must be placed in opposite edges in order to assure a proper distribution of the water flow through each pass. In order to have the inlet and outlet of the bundle in the same edge, an even number of passes must be used.

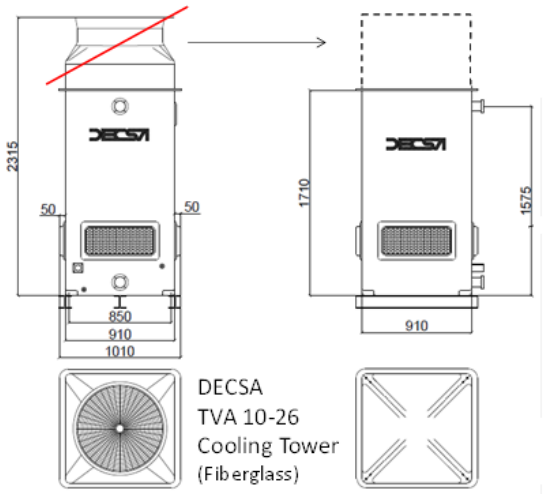

Figure 5.6. Fiberglass tower from DECSA that will be used to build the absorber and regenerator towers.

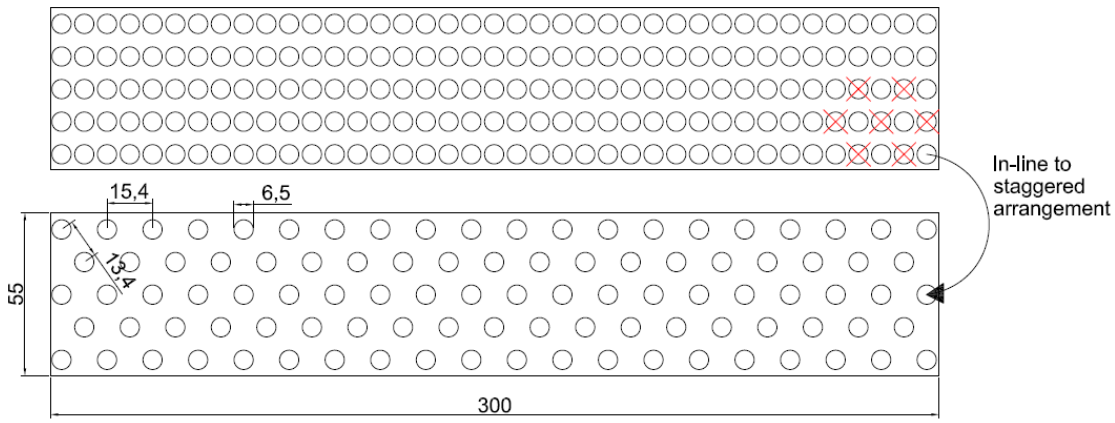

Figure 5.7. Layout of each module, in-line configuration to staggered configuration

Table 5.6. Specification of the modules for the air-solution contactors.

Number of rows	5
Total number of tubes	98
Tube length (mm)	680
Outlet tube diameter (mm)	6.5
Inlet tube diameter (mm)	5.1
Column distance (mm)	14.4
Row distance (mm)	10.5
Tube arrangement	Staggered
Material	Polypropylene with continuous plasma treatment II

5.6.3.1. Desiccant flow rate

The minimum LiCl-H_2O flow rate for the air-solution contactors is the obtained from wettability tests of the tubes presented in Chapter 3. The material used for the air-solution contactors is polypropylene with the second continuous plasma treatment. As reminder, the equation that was determined in Chapter 3 for the minimum film Reynolds number required to completely wet the tube surface is the following:

$$Re_s = 0.0552 \cdot Ga_s^{0.2768} \tag{5.47}$$

Where solution Reynolds number and Galileo number are calculated as:

$$Re_s = \frac{2\Gamma_s}{\mu_s} \tag{5.48}$$

$$Ga_s = \frac{\rho_s \sigma_s^3}{\mu_s^4 g} \tag{5.49}$$

With solution Reynolds number and the physical properties of the LiCl-H_2O at absorber and regenerator conditions the minimum required flow rate to achieve full wetting of tubes can be calculated. The minimum solution mass flow rate per unit of length of tube is $2.083 \cdot 10^{-2}$ kg/m·s for the absorber and $2.167 \cdot 10^{-2}$ kg/m·s for the regenerator. This means that the minimum mass flow rate of liquid desiccant is given by the regenerator calculation. If 117 tubes of 0.68 m are considered, the minimum solution mass flow rate must be 1.72 kg/s. Therefore 1.8 kg/s will be considered as the liquid desiccant mass flow rate at design conditions for both air-solution contactors.

5.6.3.2. Liquid desiccant distribution

Nozzles (Figure 5.8) have been proposed for the distribution of the LiCl-H_2O solution because these elements are typically installed in cooling towers. These sorts of nozzles produce an empty cone; for this reason, they must be placed in a way where the cones are overlapped and covering at the same time the whole cross section surface of the bundle.

According to the provider, these nozzles have never been used with LiCl-H_2O solution. For this reason, four nozzles were tested in the small wettability setup (see Chapter 3) in order to determine the flow rate and the minimum operating pressure of the nozzles when they are used with LiCl-H_2O. The diameters of the nozzles tested were 14, 18, 20, 22 mm (Figure 5.8). The objective of the tests was to assess the correct diameter of the nozzles to be used for the air-solution contactors considering the solution flow rate required and propose the number of nozzles to be used.

Figure 5.8. Nozzles tested (A = 14 mm, B = 18 mm, C = 20mm and D = 22 mm)

The methodology adopted to obtain the minimum operating pressure and flow rate was the following:

- Test the four nozzles at different available pressures at the inlet of it and at different liquid desiccant concentrations.
- Measure the flow rate and pressures and take pictures of the cone in order to obtain the cone angle.
- Obtain the minimum working pressure given by the pressure at which the cone angle is stable.

- Calculate the number of nozzles required to supply the solution mass flow rate set in the previous Section.

Figure 5.9 shows the 14 mm nozzle tested. Figure 5.10 and Figure 5.11 show the cone angle and flow rate, respectively, as a function of the available pressure before the nozzle and de liquid desiccant mass concentration for the 14 mm nozzle. As it can be seen from Figure 5.10, the output angle is quite stable (~90°) for pressures higher than 0.25 bar, for lower pressures the output angle oscillates and is not stable. The output flow rate is quite linear as a function of the pressure and ranges from 300 l/h up to 855 l/h. At 0.25 bar, the liquid desiccant flow rate is about 550 l/h.

Taking into consideration the above methodology, the required number of nozzles to supply 1.8 kg/s of desiccant to the air-solution contactors is shown in Table **5.7**. Since a good distribution of the liquid desiccant is required, at least 9 nozzles are required to cover the cross section of the two towers. Therefore the nozzle with the diameter of 14 mm is chosen.

Moreover the working pressure chosen for this nozzle is 0.25 bar. At this working pressure the liquid desiccant flow rate is 550 l/h (see Figure 5.11) and the required number of nozzles is 10.

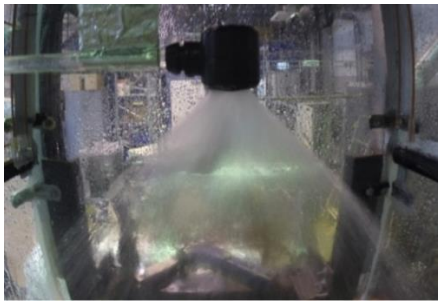

Figure 5.9. 14 mm nozzle tested at 0.36 bar.

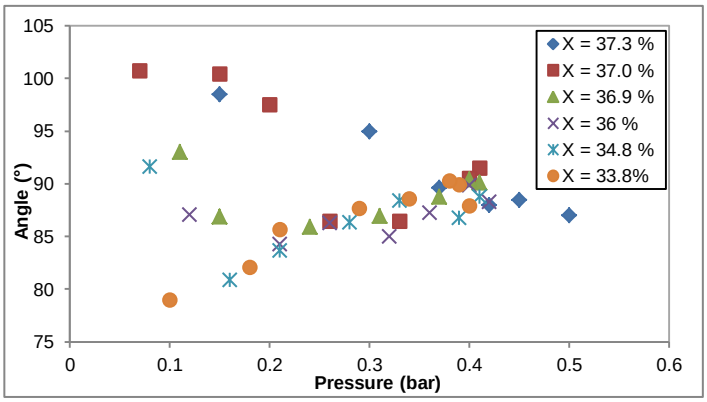

Figure 5.10. Output angle as a function of the pressure for the 14 mm nozzle.

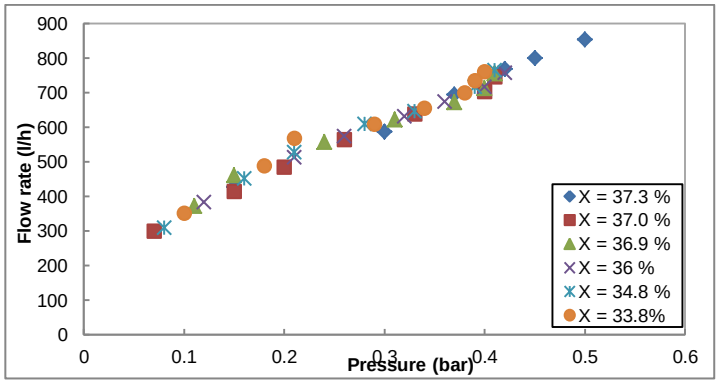

Figure 5.11. Flow rate as a function of the pressure for the 14 mm nozzle

Table 5.7. Results of the experimental tests for the nozzles.

Nozzle diameter	Minimum working pressure (bar)	Minimum flow rate (l/h)	Number of nozzles
14 mm	0.25	550	10
18 mm	0.21	850	7
20 mm	0.21	900	6
22 mm	0.20	950	6

5.6.4. Summary of operational conditions

Table 5.8 contains a summary of the design conditions to size the absorber and the regenerator. Solution mass flow rate is calculated from Section 5.6.3.1; water mass flow rates and temperatures are fixed in Section 5.6.2; inlet air temperature and humidity ratio are the calculated for the design ambient conditions and the room conditions in Section 5.5.1. Air flow rate is set from ventilation requirement selected in Section 5.6.1; supply air humidity ratio and temperature are set from design loads described in Section 5.6.1; and tube material and surface treatment were selected based on the results obtained from Chapters 3 and 4. Inside and outside diameter are the available from the polypropylene tube supplier. In addition Figure 5.12 illustrates the operational conditions of the hybrid liquid desiccant system set in order to size the absorber and regenerator.

Since the simulation have to be carried out not only with the absorber and regenerator but with the complete hybrid liquid desiccant system, it is necessary to set parameters related with other components of the system.

Table **5.9** includes the other parameters set to size them. Regenerator size and materials are assumed equal to the absorber size; this assumption will be justified in Section 5.8. On the other hand, solution heat exchanger effectiveness affects much to the system performance. Moreover, the air heat exchanger effectiveness is essential for better water desorption, the effect of its effectiveness will be explained in Section 5.8.

The split solution ratio is defined as the amount of liquid desiccant recirculated to the air-solution contactors divided by the total liquid desiccant flow rate, this is:

$$split = \frac{\dot{m}_{rec}}{\dot{m}_{rec}+\dot{m}_{s,in}} \tag{5.50}$$

The reason why split ratio has been chosen as 0.9 is explained in Section 5.8.3.

Table 5.8. Summary of the design conditions for the absorber and regenerator sizing.

Solution mass flow rate (kg/s)	1.8
Absorber water flow rate (kg/s)	3.3
Regenerator water flow rate (kg/s)	4.4
Absorber water temperature (°C)	15.0
Regenerator water temperature (°C)	55.0
Air flow rate (m^3/h)	2500
Inlet air temperature (°C)	30.0
Inlet air humidity ratio (kg_w/kg_a)	0.0215
Supply air humidity ratio (kg_w/kg_a)	0.0069
Tube Material	PP tubes, continuous treatment II
Arrangement	Staggered
Tube therm. conductivity (W/m·°C)	0.21
Tube length (m)	0.68
Tower width (m)	0.90
Inside tube diameter (mm)	5.10
Outside tube diameter (mm)	6.50

Table 5.9. Summary of the LDS set parameters for the air-solution contactors sizing.

Regenerator size and material	Equal to absorber
Solution heat exchanger effectiveness (-)	0.85
Air heat exchanger effectiveness (-)	0.65
Split ratio	0.90

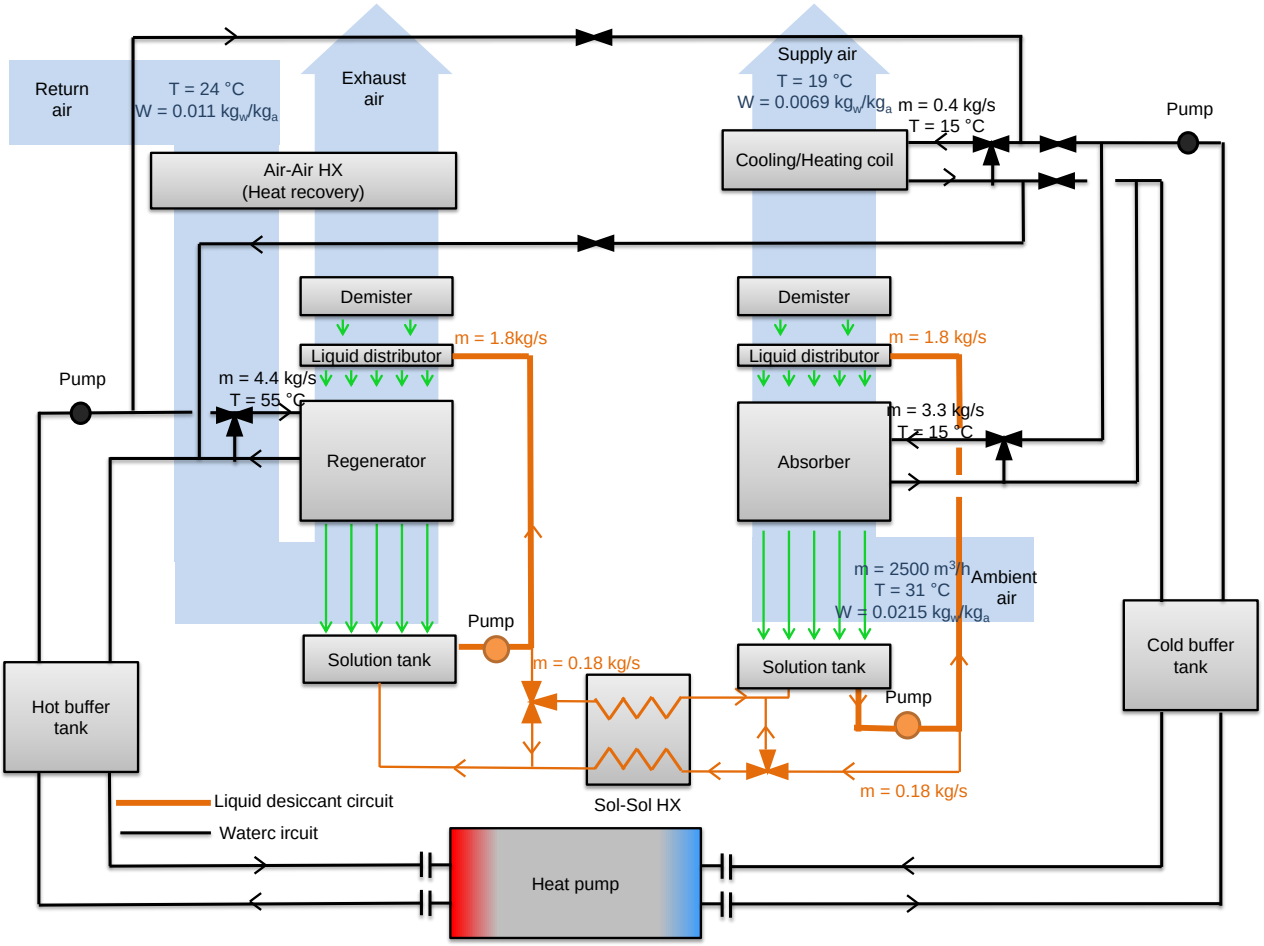

Figure 5.12. Operational conditions of the proposed hybrid liquid desiccant system.

5.7. Sizing Results

From simulations it is possible to obtain directly the required contact surface of both air-solution contactors and therefore the required tube rows. Because of the absorber bundle will be composed by modules of 5 rows and it is necessary to install an even number of modules, the final number of rows has to be a number multiple of 10. According to the simulations carried out and with the restrictions, the number of tube rows in the absorber necessary to achieve the design conditions is 70; other important results are summarized in Table 5.10. Figure 5.13 shows a top and side view of the fiberglass tower from that will be used to build the liquid desiccant system.

Table 5.10. Summary of air-solution contactors sizing results obtained from simulations.

Total absorber surface contact (m^2)	59.29
Tube rows in the absorber (-)	70
Number of passes in the absorber (-)	14
Number of modules in the absorber (-)	42
Total required tube length (m)	2771

On the other hand, based on the previous calculations, Figure 5.14 shows the design proposed by the supplier of the plastic air-solution contactors (MAGEN) for a complete heat exchanger, with 3 complete modules per pass and 14 passes. Each header has a section area of 50 x 50 mm and the connection between passes is made with an elbow connected to an adapter with a diameter of 40 mm. Due to the welding of the adaptors, a maximum space of 1 mm will be required between passes; for that reason, total height will vary between 770 and 785 mm. Including the elbows, the maximum width is 1094 mm requiring a special frame in order to assemble the bundles in the towers. The frame must be able to allocate around 100 mm at each side in order to place the elbows outside the limits of the tower.

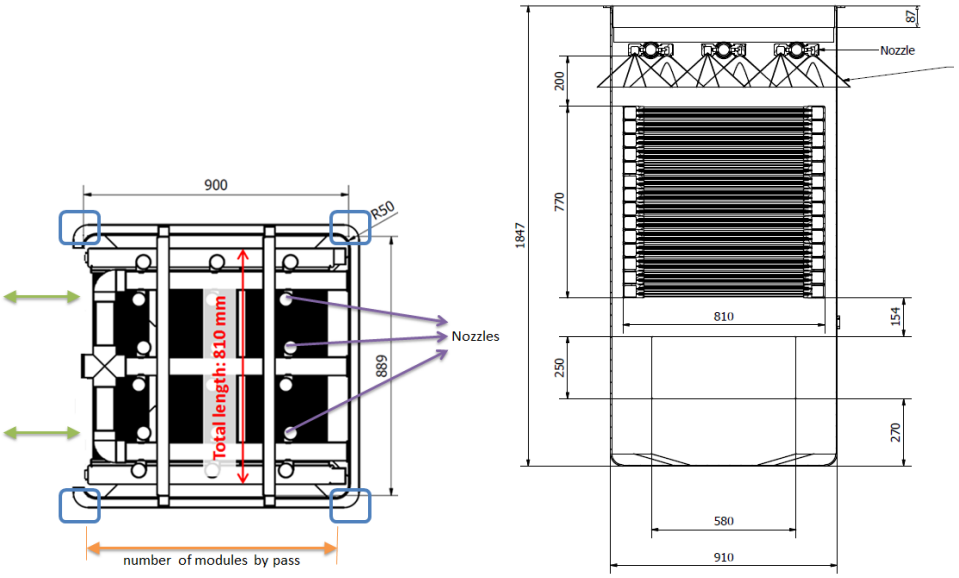

Figure 5.13. Top and side view of the fiberglass tower.

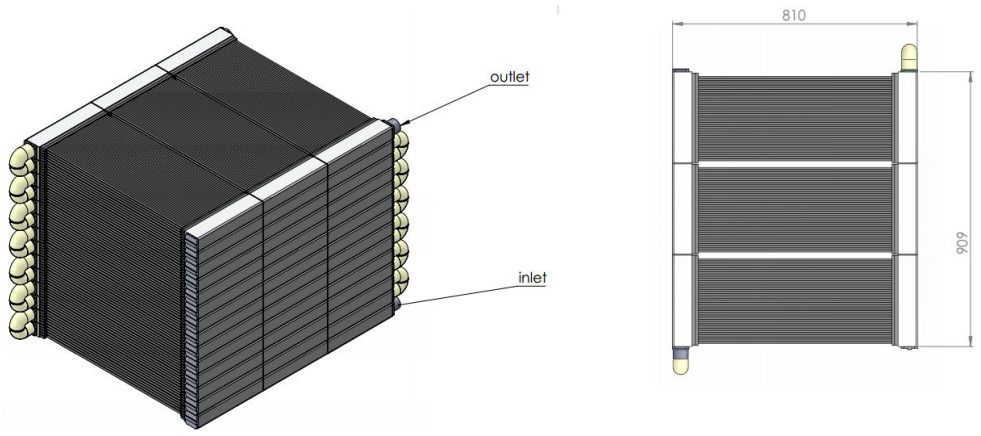

Figure 5.14. Complete heat exchanger proposed by MAGEN

5.8. Sensitivity analysis

Several decisions have been taken in order to size the system. Among them, three of the most important are: equal size for the absorber and regenerator, the addition of an air-to-air heat exchanger in the return air and the split ratio value for the liquid desiccant.

A sensitivity analysis using the model described in this chapter has been carried out in order to evaluate how these decisions affect to the size of the system. Several simulations have been done with respect to the

design conditions. In the simulations, three variables have been varied separately: the air-air heat exchanger effectiveness, the inlet water temperature to the regenerator and the split ratio. All the others parameters required for the simulations have been kept constant at design conditions.

5.8.1. Effect of the air-air heat exchanger effectiveness

The capacity to contain vapour in the air directly depends on the air temperature. In this sense, the regeneration rate and the mass concentration of LiCl in the regenerator increase when the inlet air temperature in the regenerator increases (increasing also the whole system performance). Moreover, a higher inlet air temperature decreases the heat that has to be provided through the regenerator decreasing the energy that must be provided by the heat pump. A way to increase the inlet temperature of the air to the regenerator is including an air-air heat exchanger that pre-heats the moist air at room conditions by cooling the outlet air from the regenerator.

Figure 5.15 shows the supply air humidity ratio and the required heating rate in the regenerator as function of the air-air heat exchanger effectiveness. The humidity ratio slightly decreases when the exchanger effectiveness increases due to the better regeneration of water. When the effectiveness is increased the inlet air temperature also increases reaching a higher LiCl concentration. On the other hand, the required heating rate in the regenerator is reduced due to less energy is used to increase the air temperature through the regenerator.

Therefore, it remains clear from this sensitivity analysis that the inclusion of an air-air heat exchanger to pre-heat the air before entering the regenerator improves not only the regenerator performance but the system performance because it is possible to achieve a better dehumidification.

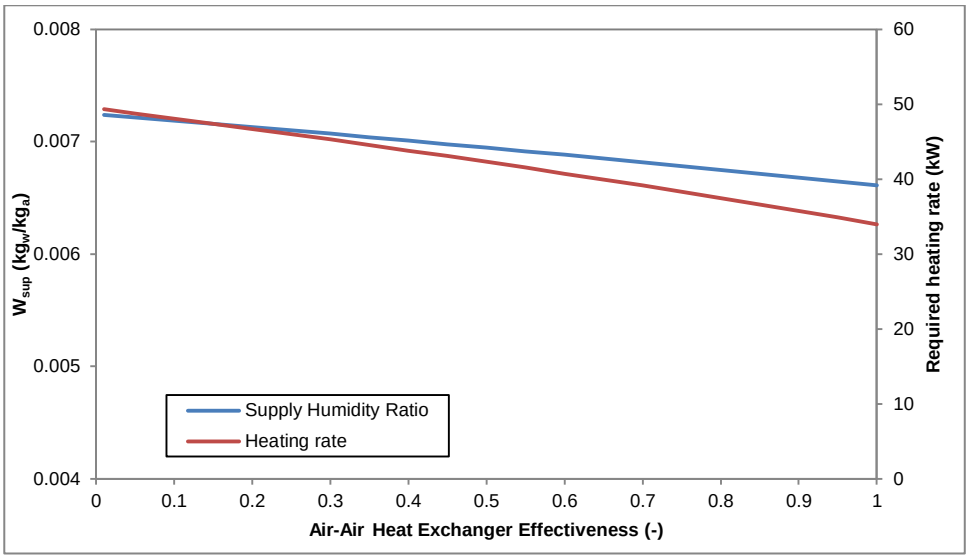

Figure 5.15. Supply humidity ratio in the absorber and heating rate required in the regenerator as function of the air to air heat exchanger effectiveness.

5.8.2. Effect of the inlet water temperature on the regenerator thermal capacity

Because of the water vapour pressure in the LiCl-H_2O solution increases with its temperature, the regenerator performance depends on the inlet liquid desiccant temperature and, therefore, on the inlet water temperature. The higher the inlet solution temperature is the easier to desorb the water and concentrate the solution. A sensitivity analysis to estimate the effect of the inlet hot water temperature on the regenerator thermal capacity has been carried out considering two cases: constant size for the regenerator and variable size for the regenerator to fulfil design conditions. For the first case, Figure 5.16 shows the outlet air humidity ratio from the absorber and the required heating rate in the regenerator as function of the inlet water

temperature in the regenerator. The outlet air humidity ratio decreases when the water temperature increases due to the increasing of the water desorbed in the regenerator that permits reaching a higher LiCl concentration. This means that capacity of the liquid desiccant system increases with the inlet water temperature in the regenerator. On the other hand, the required heating rate in the regenerator is also increased because of the higher temperature reached in the regenerator.

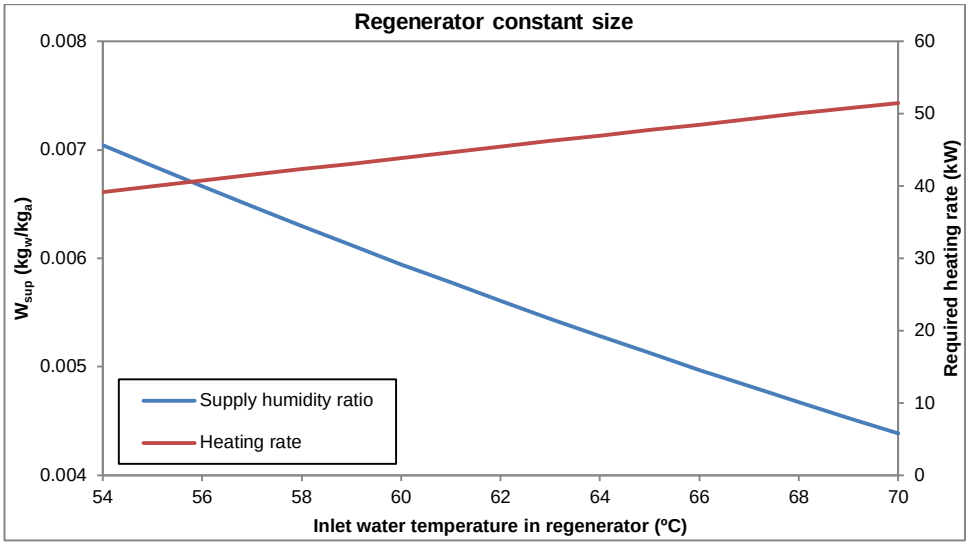

Figure 5.16. Supply humidity ratio in the absorber and regenerator heating rate as function of the inlet water temperature in the regenerator.

For the second case, Figure 5.17 shows the required contact surface of the regenerator and the required heating rate in the regenerator as function of the inlet hot water temperature in order to reach the design air humidity. The regenerator required surface roughly decreases when the temperature decreases, this effect is even bigger when the temperature is smaller than 55 °C. On the other hand, the required heating rate in the regenerator almost remains constant because the amount of water to be evaporated is almost the same.

Therefore, it remains clear from this sensitivity analysis that the higher inlet water temperature in the regenerator the higher the regenerator thermal capacity. However, the maximum hot water temperature that can be provided by the heat pump is 55 °C and therefore, the regenerator size has to be at least with the same size that the absorber, as it was considered in the in the sizing simulations.

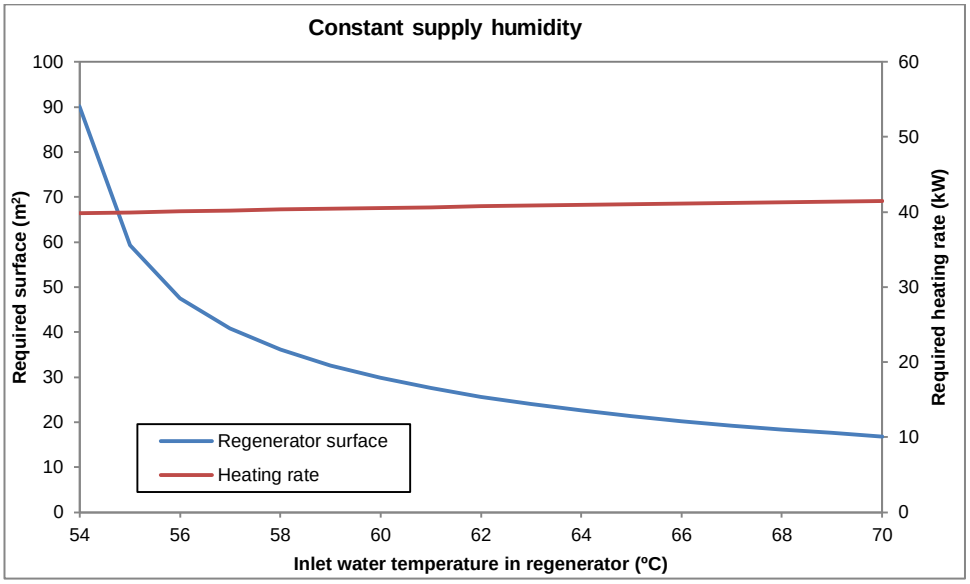

Figure 5.17. Regenerator required contact surface and regenerator thermal capacity as function of the regenerator inlet water temperature.

5.8.3. Effect of the split ratio on the system performance

The main reason that explains the effect of the split ratio is the average liquid desiccant in both air-solution contactors. In general, the higher split ratio, the higher difference temperature between absorber and regenerator; this means the lower temperature in the absorber and the higher temperature in the regenerator.

Figure 5.18 shows the influence of the heating rate required in the regenerator and the LiCl mass fraction at the inlet of the absorber as function of the split ratio. From this Figure itis deducted that the heating water required in the regenerator decreases with the split ratio. This is due to less energy provided by the hot water is in charge of heating the liquid desiccant when split ratio is close to 1.

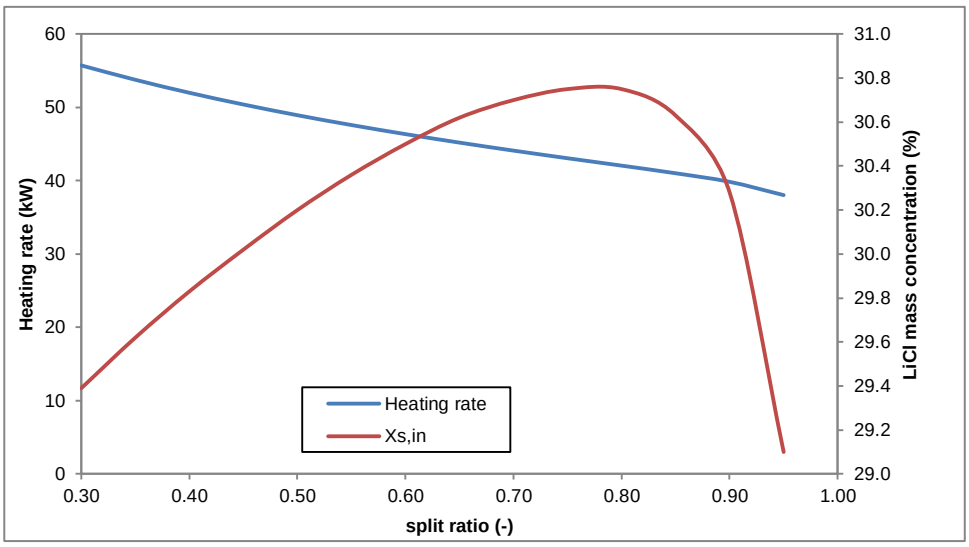

Figure 5.18. Heating rate required in the regenerator and LiCl mass fraction at the inlet of the absorber as function of the split ratio.

On the other hand, the absorber inlet LiCl mass concentration mainly depends on two variables: the water regeneration through the regenerator and the liquid desiccant flow rate from the regenerator to the absorber; the more regeneration and the more liquid desiccant flow rate, the more LiCl mass concentration. In this sense split ratio has an opposite effect on water regeneration and liquid desiccant flow rate: the higher split ratio the more regeneration because of temperatures and the less liquid desiccant flow rate from the regenerator to the absorber. This explains the fact that there is a maximum in the LiCl mass concentration that happens when split ratio is about 0.8.

Figure 5.19 shows the influence of the cooling rate required and cooling rate provided to the air in the absorber as function of the split ratio. From this figure it is deduced that the cooling rate required in the absorber decreases when split ratio is higher. This is due to less energy removed by the cooling water is in charge of cooling the liquid desiccant when split ratio is higher because liquid desiccant temperature is lower.

On the other hand, the cooling rate provided to the air increases when the split ratio is higher up to 0.9, where the maximum is reached. In this case, there are two opposite effects that make to get a maximum at this value: liquid desiccant temperature and mass concentration. The higher split ratio, the lower liquid desiccant temperature and the more sensible load (because of temperature) and latent load (because of vapour pressure) is handled in the absorber. Moreover, the higher LiCl mass concentration the more dehumidification and therefore the more latent load handled. However, since LiCl mass concentration drastically drops when split ratio is higher than 0.9 (see Figure 5.18) it is in that point where the cooling provided to the air starts to decrease.

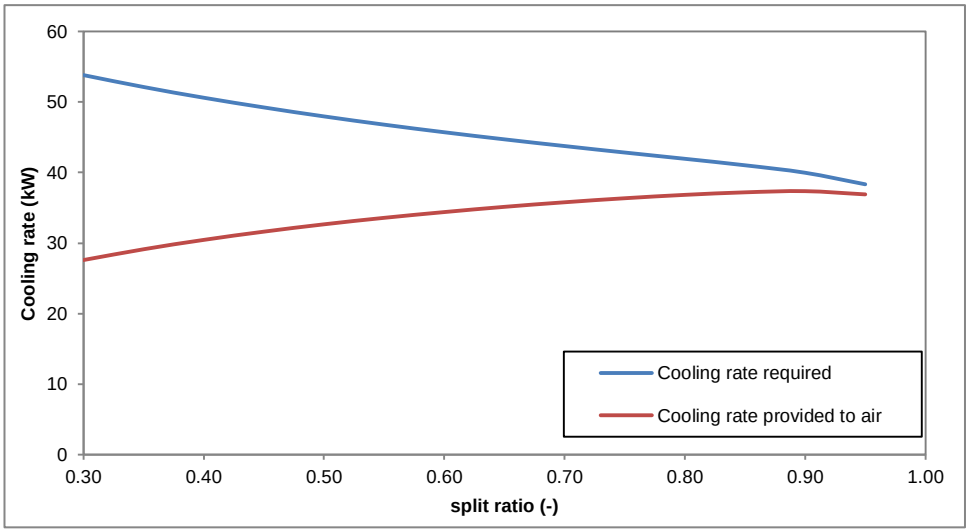

Figure 5.19. Cooling water required and cooling provided to the air in the absorber as function of the split ratio.

Therefore, from results obtained with this sensitivity analysis it is shown that the most suitable split ratio is in the range of 0.80 - 0.95 because it allows achieving the maximum cooling rate provided to the air with a low heating rate and cooling rate required in the regenerator and the absorber, respectively.

5.9. Conclusions

The hybrid liquid desiccant system has been designed and sized in order to be operated in two locker rooms of a swimming-pool in Taipei (Taiwan). Although the whole system has been designed, the sizing has been mainly focused on the two air-solution contactors. Moreover, the operational conditions of the system have been established at design conditions.

A mathematical model of the liquid desiccant system has been developed on EES in order to obtain the sizing of the system. Three main decisions were considered in advance: equal size for the absorber and regenerator, the addition of an air-to-air heat exchanger in the return air and the value of the split ratio for the liquid desiccant flow. These decisions have been evaluated with a sensitivity analysis from which the following conclusions can be taken:

- By adding an air-to-air heat exchanger before the regenerator both, the heating rate required in the regenerator and the supply humidity ratio decreases. A reduction of 8.8 kW is found in the heating rate required when an air-to-air with an effectiveness of 0.65 is added to the system. The supplied humidity ratio is reduced from 0.00722 to 0.00685 kg_w/kg_a if the heat exchanger is added.
- The regenerator size is limited by the inlet water temperature within itself; due to the maximum inlet water temperature that can be provided to the regenerator by the condenser of the heat pump is 55 °C. For instance, with an inlet water temperature equal to 70 °C, the regenerator size could be almost three times smaller than with and inlet water temperature equal to 55 °C.
- Finally, the optimum split ratio is found at about 0.90 because it allows achieving the maximum cooling rate provided to the air with a low heating rate and cooling rate required in the regenerator and the absorber, respectively.

Chapter 6. Description and set-up of the hybrid liquid desiccant system with treated polypropylene air-solution contactors

6.1. Introduction

After being manufactured and before being brought to Taiwan, the hybrid liquid desiccant system was tried and set-up at the Universitat Rovira i Virgili facilities (see Figure 6.1). Since it is a system with many devices and parts, many difficulties appeared during this stage. In addition, the test bench was required to be adapted in order to simulate tropical conditions of air.

Therefore, this chapter is distributed in the following sections:

- Description of the hybrid liquid desiccant system, where the main parts of the system as well as the moist air cycle and the liquid desiccant cycle at design conditions are described.
- Description of the control algorithm of the hybrid liquid desiccant system. In this section, the control strategy, that it is not only focused on the air humidity and temperature, but also on the liquid desiccant regeneration and the air flow control, is described in a simplified way.
- Description of the test bench that had to provide moist air at two conditions: tropical conditions for the supply air circuit, and room conditions to the return air circuit. Moreover, the electrical connections were adapted to supply the electrical energy at Taiwanese conditions.
- Set-up of the hybrid liquid desiccant system. The set-up of the system, from the installations and first checking to the operation of the system in manual and automatic mode, is described in this section.
- Conclusions taken from this chapter are summarised in the end of it.

Figure 6.1. Picture of the hybrid liquid desiccant system during its set-up phase in Tarragona.

6.2. Description of the hybrid liquid desiccant system

As it is mentioned in Section 5.4, the hybrid liquid desiccant system consists of three subsystems:

- The liquid desiccant subsystem.
- The air subsystem, which is basically an air handling unit.
- A heat pump that supplies hot water and chilled water to the regenerator, the absorber and the coil.

A hydraulic circuit that distributes the water from the heat pump to the regenerator, the absorber and the coils is also needed.

This section contains a description of the three main subsystems.

6.2.1. Air subsystem

The air subsystem is in charge of supplying the moist air at the required conditions to the locker rooms. These conditions are the air temperature, the air humidity and the air flow rate. Moreover, this subsystem uses the return air to regenerate the liquid desiccant through the regenerator. It is divided into two circuits:

- Supply air circuit that is in charge of achieving the supply air temperature and water content.
- Return air circuit that is in charge of regenerating the liquid desiccant.

Figure 6.2 illustrates a 3D view of the hybrid liquid desiccant system focusing on the supply air circuit. In addition to this figure, Figure 6.4 shows, in a psychrometric chart, the air processes that moist air suffers when it is passing through the supply air circuit.

As it can be observed from these two figures, moist air at ambient conditions is firstly dehumidified within the absorber until the required supply air humidity ratio is reached. In this process, moist air is also slightly cooled. Outlet air temperature in the absorber mostly depends on the inlet liquid desiccant temperature. After being dehumidified in the absorber, moist air is cooled through a coil until the required supply air temperature is reached.

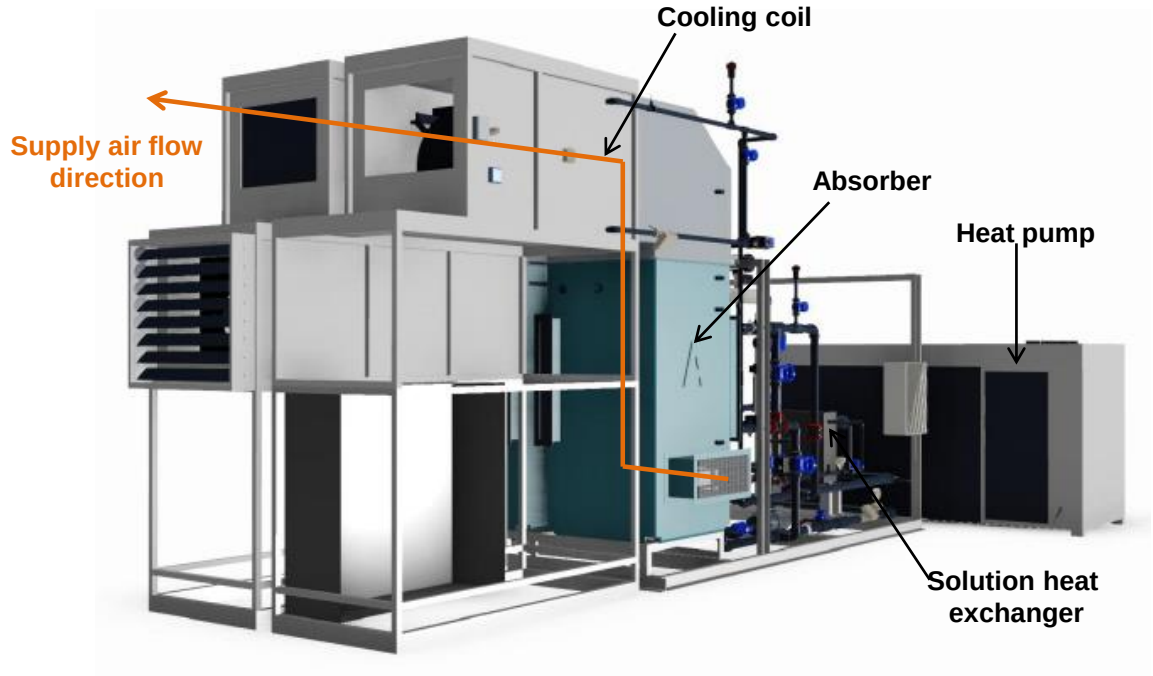

Figure 6.2. 3D view of the hybrid liquid desiccant system focused on the supply air circuit.

Figure 6.3 illustrates a 3D view of the hybrid liquid desiccant system focusing on the return air circuit. As well as in the supply air circuit, Figure 6.4 shows, in a psychrometric chart, the air processes that moist air suffers when it is passing through the return air circuit.

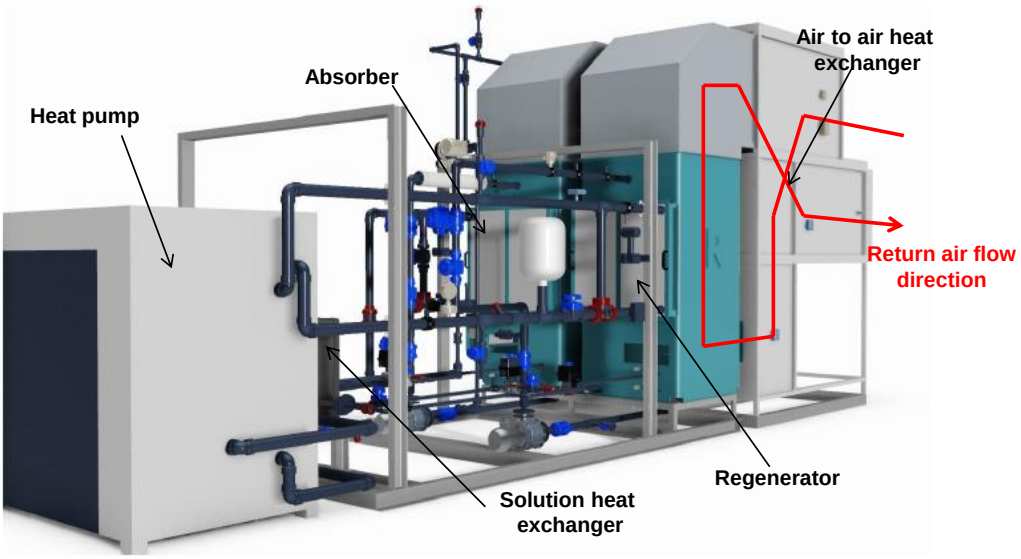

Figure 6.3. 3D view of the hybrid liquid desiccant system focused on the return air circuit.

As it can be observed from these two figures, moist air at room conditions is firstly heated within the air to air heat exchanger by using as heating source the hot air after regenerator. This sensible heating enhances the regeneration process that occurs in the regenerator. Then, the moist air is passed through the regenerator where liquid desiccant is regenerated. Therefore, at the outlet of the regenerator, moist air is more humid, but also hotter due to the regenerator is internally heated. In the same way that in the absorber, outlet air temperature in the regenerator mostly depends on the inlet liquid desiccant temperature. Points represented in the psychrometric chart are, approximately, in agreement with the design conditions.

Finally, supply air flow rate is provided by both, a supply fan placed after the cooling coil, and a return fan placed after the air to air heat exchanger.

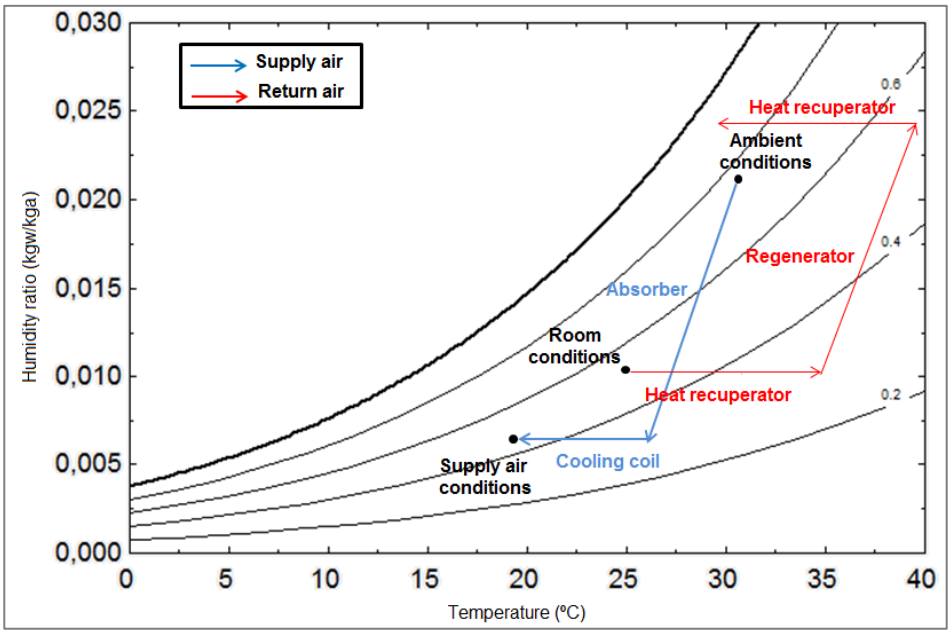

Figure 6.4. Moist air cycle of the hybrid liquid desiccant system.

6.2.2. Liquid desiccant subsystem

Figure 6.5 illustrates a simplified scheme of the liquid desiccant subsystem. Moreover, Figure 6.6 shows, in a chart with the LiCl-H_2O properties, the processes that liquid desiccant suffers in this cycle. Numbers represent the same points in both figures.

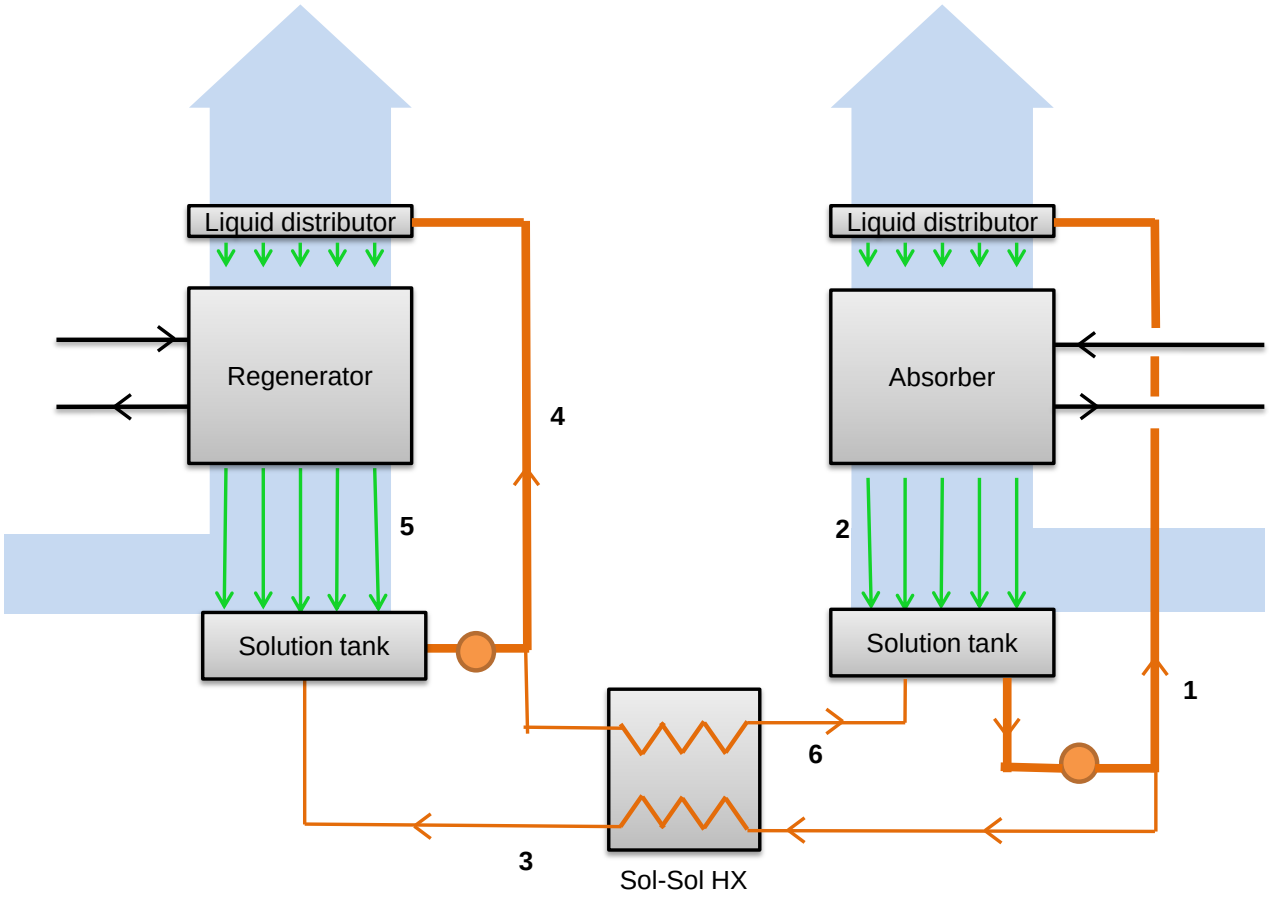

Figure 6.5. Simplified scheme of the liquid desiccant subsystem.

The liquid desiccant is taken from the tank of the absorber at conditions of point 1. Approximately, the 90 % of this flow rate is brought to the absorber, where the liquid desiccant is cooled and absorbs water up to the conditions of point 2. The rest of the liquid desiccant (approximately, the 10 %) is brought to the regenerator tank by passing through the solution heat exchanger. At the outlet of the exchanger, point 3 conditions are reached. In this point, the liquid desiccant is hotter and with the same LiCl mass concentration than in point 1. In the regenerator tank, which is at point 4 conditions, the liquid desiccant at point 3 conditions is mixed with the liquid desiccant that comes from the regenerator at conditions of point 5. The liquid desiccant is taken from the regenerator tank at conditions of point 4. Again, the 90 % of this flow rate is brought to the regenerator, where the liquid desiccant is heated and desorbs water up to the conditions of point 5. The rest of the liquid desiccant (approximately the 10 %) is brought to the absorber tank by passing through the solution heat exchanger. At the outlet of the exchanger, point 6 conditions are reached. In this point, the liquid desiccant is colder and with the same LiCl mass concentration than in point 4. In the absorber tank, which is at point 1 conditions, the liquid desiccant at point 6 conditions is mixed with the liquid desiccant that comes from the absorber at conditions of point 2.
Points represented in Figure 6.6 are, approximately, in agreement with the design conditions.

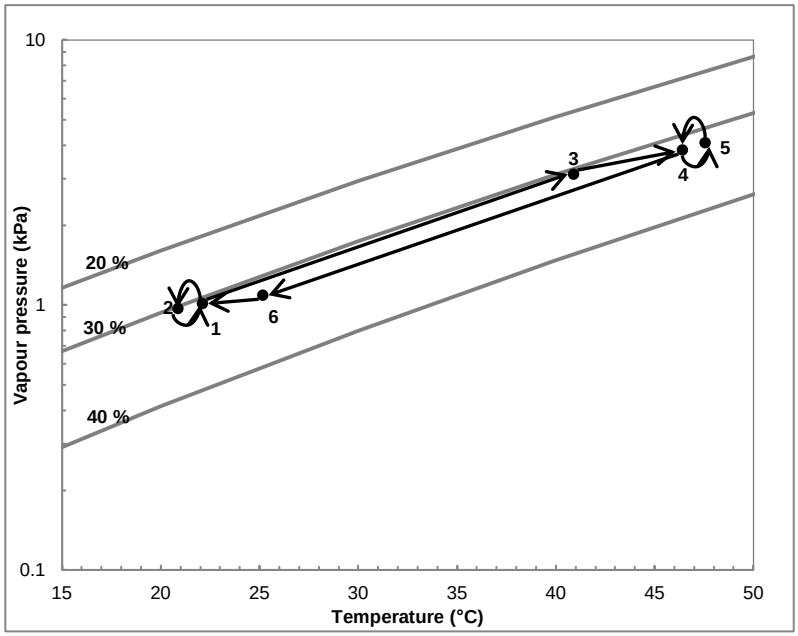

Figure 6.6. Liquid desiccant cycle of the hybrid liquid desiccant system.

6.2.3. Heat pump

Since chilled water is required for the absorber and the cooling coil (if the system is working in summer conditions) and hot water is required for the regenerator (or the coil if the system is operating in winter conditions), a water-to-water heat pump was decided to be used to provide both. The main problem while using a standard water-to-water heat pump is to manage the different energy loads that will appear when the system is operating.

In order to solve this problem, a flexible heat pump was chosen. This heat pump contains two compressors, two evaporators and two condensers. One of the evaporators and the condensers are water cooled/heated and the others are air cooled/heated. In this way, the compressors of the heat pump operate to follow the maximum load. This means that if the maximum load is cooling, the compressors will operate to handle it and the water cooled condenser will transfer part of the heating and the air cooled condenser will transfer the rest to the ambient. The opposite occurs if the maximum load is heating, this is, the compressors will operate to handle it and the water heated evaporator will transfer part of the cooling and the air heated evaporator will transfer the rest to the ambient.

The operational conditions of the hybrid liquid desiccant system were chosen taking into consideration the working constrictions of the heat pump. Section 5.6.2 contains the main specifications of the selected heat pump.

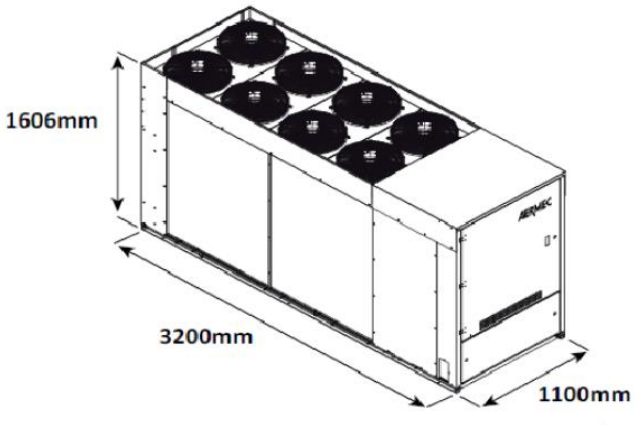

Figure 6.7. Water-to-water heat pump [114].

6.3. Description of the control algorithm of the hybrid liquid desiccant system

One of the main objectives to be reached by the hybrid liquid desiccant system is the independent control of the temperature and humidity of the two locker rooms. Therefore, the control strategy of the system must focus on this objective.

The control of the system can be divided into four subsystems:

- Absorber, for the humidity control.
- Regenerator, for the liquid desiccant regeneration control.
- Coil, for the supply air temperature control.
- Fans of the air handling unit, for the air flow control.

Figure 6.8 illustrates a scheme of the hybrid liquid desiccant system with the main sensors and actuators used for the control strategy of the system. In addition to this, the system is equipped with security sensors and actuators, such as release valves, pressure sensors or level sensors, as well as manual valves used for the equilibrium of the hydraulic circuits. Moreover, additional sensors are included on the system for the analysis of the performance of it.

On the other hand, the heat pump is equipped with its own control algorithm, which tries to handle the cooling and heating demand in and independent way. The only possible parameters of the heat pump that can be modified by the control algorithm of the system are the set point temperatures and the start and stop of it.

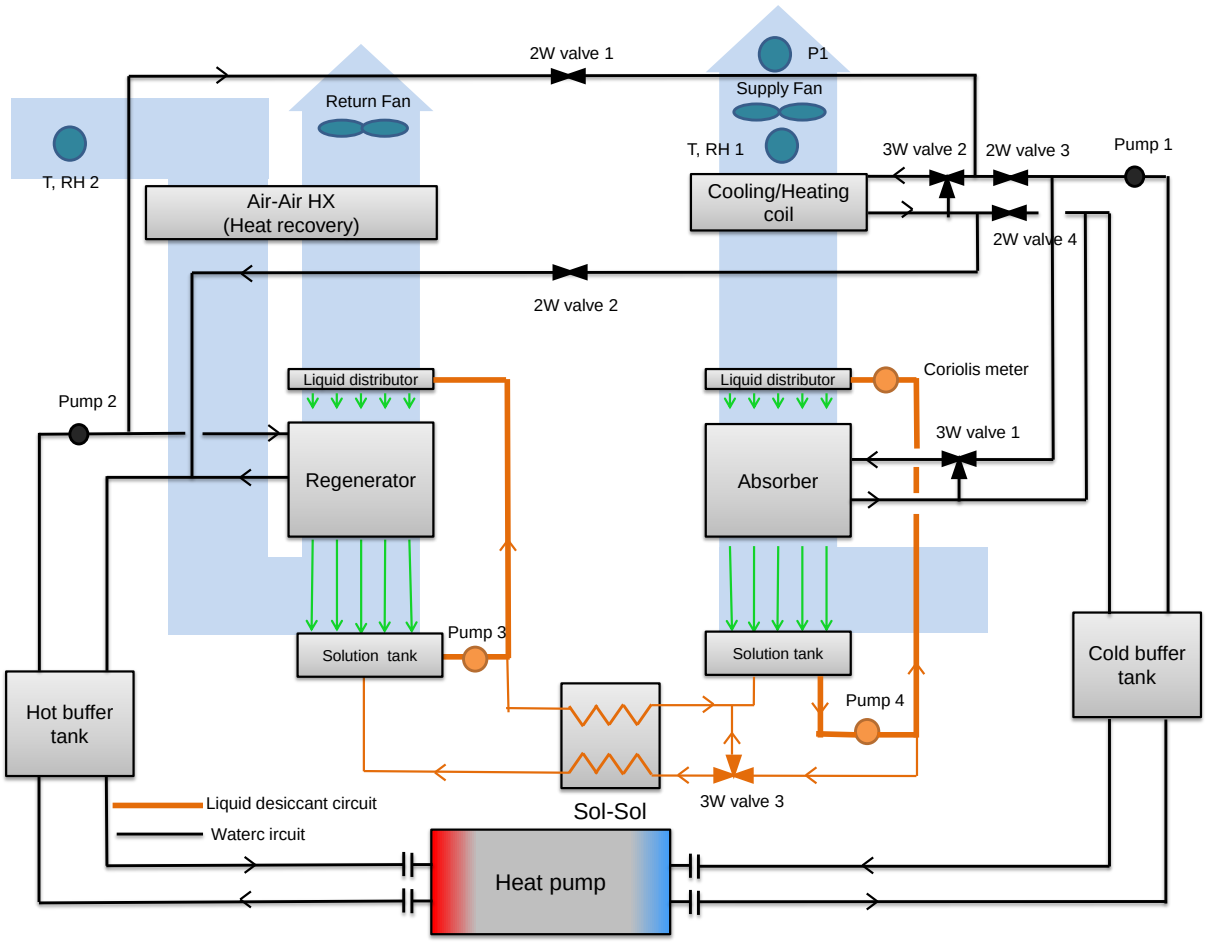

Figure 6.8. Schematic of the hybrid liquid desiccant system with the main sensors and actuators.

This section explains, in a simple way, the strategies used to operate the hybrid liquid desiccant system. In addition to this, other strategies were thought to be used in the system but most of them were discarded after the set-up of it. Therefore, only the selected control strategies are explained in this Section.

Control of the air flow with the fans of the air handling unit

A variable air flow system has been decided to be used in order to control the temperature of the two locker rooms. Each locker room contains two dampers, one before the supply air diffusers and the other in the return ducts. These dampers regulate the air flow rate as a function of the locker room temperature. A minimum value of opening has to be set in order to guarantee a good air distribution and a proper control for the air fans.

Both supply and return fans contain a frequency driver that permits regulating the air flow rate as function of the supply air pressure that is measured from P1 of Figure 6.8.

Control of the humidity with the absorber

The absorber is the component in charge of controlling the humidity of the locker rooms. The return relative humidity, measured from RH 2 sensor, is controlled by regulating the water flow rate in the absorber with the three-way valve 1.

If return relative humidity achieves a value bellow a minimum set by the user, pumps 3 and 4 are stopped and the three-way valve 1 is fully closed to the absorber. These pumps will not start operating again and three-way valve 1 will not start regulating the flow to the absorber again, unless a maximum value of relative humidity in RH 2 is not reached.

Control of the liquid desiccant regeneration with the regenerator

The regenerator is the component in charge of controlling it. There are two options to control the operation of the regenerator:

- To operate it whenever the absorber is operating. This mode is called *Regenerator ON*.
- To operate it as function of the LiCl mass concentration at the entrance of the absorber. LiCl mass concentration is calculated from measurements of temperature and density of the liquid desiccant with the coriolis meter. In this case, a maximum and a minimum value of density must be provided by the user. If regenerator is operating, Pump 3 is stopped and three-way valve 3 is closed towards the regenerator whenever the maximum value of density is reached. On the other side, if regenerator is not operating, Pump 3 is switched on and three-way valve 3 is opened towards the regenerator when the minimum value of density is reached.

In both cases, water flow rate in the regenerator is constant. Moreover, these two control strategies for the regeneration will be analysed with dynamic simulations in Chapter 8.

Control of the supply air temperature with the coil

The coil is the device in charge of controlling the temperature of the locker rooms. There are two different controls for the coil:

- Constant supply air temperature: this control occurs whenever the position of the dampers of the two locker rooms are more opened than the minimum position. The value of the supply air temperature is set by the user.
- Variable supply air temperature: this control occurs whenever at least one of the dampers of the two locker rooms are opened at the minimum position. The value of the supply air temperature is calculated from the average return temperature sensor T2.

Supply air temperature is controlled by regulating the water flow rate in the coil with the three-way valve 2.

On the other hand, if one of the locker rooms achieves a value of temperature bellow a minimum set by the user, the coil changes its mode from cooling to heating mode. This means that hot water from the condenser of the heat pump is circulated inside the coil instead of chilled water from the evaporator of it. To do that, two-way valves 1 and 2 open and 3 and 4 close. The opposite occurs if one of the two locker rooms achieves a value of temperature above a maximum set by the user.

6.4. Description of the test bench

In order to make a previous evaluation of the hybrid liquid desiccant system during its set-up period in Tarragona, it was necessary to fit it together to a test bench able to produce tropical conditions to be supplied to the absorber. Moreover, room air conditions were required to be supplied in the return line, before the regenerator.

Figure 6.9 illustrates a simplified scheme of the hybrid liquid desiccant system coupled with the test bench. As it can be observed, there are two loops well distinguished:

- A closed loop to provide the moist air at tropical conditions to the hybrid liquid desiccant system (represented in blue tones).
- An opened loop that takes the air at outdoor conditions to provide the moist air at room conditions (represented in orange tones).

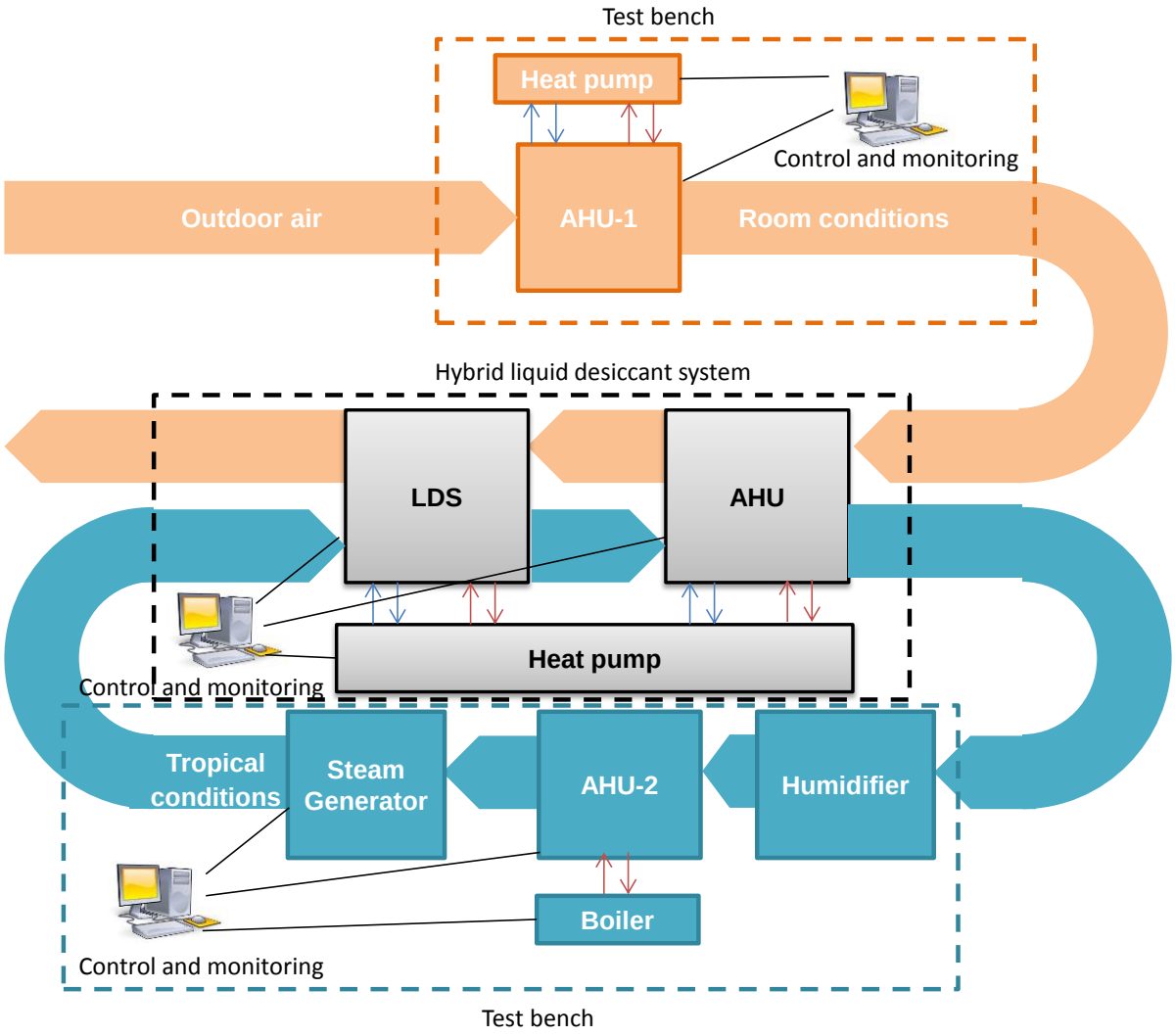

Figure 6.9. Schematic of the test bench coupled with the hybrid liquid desiccant system.

In this section, the processes, in which the moist air is changed to achieve these two conditions, are explained in detail. In addition, the electrical equipment required to feed the hybrid liquid desiccant system is included.

6.4.1. Air ducts, sensors and actuators

Figure 6.10 illustrates the cycle that the moist air follows when passing through the closed loop of the test bench and the hybrid liquid desiccant system. In this figure, the process through the test bench is represented with blue arrows and the process through the hybrid liquid desiccant system is represented with red arrows.

The moist air arrives at the test bench (after the air handling unit of the hybrid liquid desiccant system) at supply air conditions, which are approximately, 19 °C and 0.0069 kg_w/kg_a. Air at these conditions is firstly humidified in an, approximately, adiabatic process through a humidifier. At the outlet of the humidifier air is cooler and more humid (near saturation conditions). Then, it is heated in a sensible way throughout an air handling unit that takes the heating from a gas boiler. Air temperature after this device is above 30 °C. Finally, the moist air is humidified in an almost isothermal way through a steam generator. At the outlet of this device, the moist air achieves tropical conditions (about 31 °C and 0.021 kg_w/kg_a) required for the testing of the hybrid liquid desiccant system.

Both, moist air temperature and humidity ratio at the outlet of the test bench can be regulated. Temperature is regulated with a three-way valve of the water at the entrance of the coil of the air handling unit. Humidity ratio is internally controlled by the steam generator. The air flow rate is controlled by the fan of the hybrid liquid desiccant system.

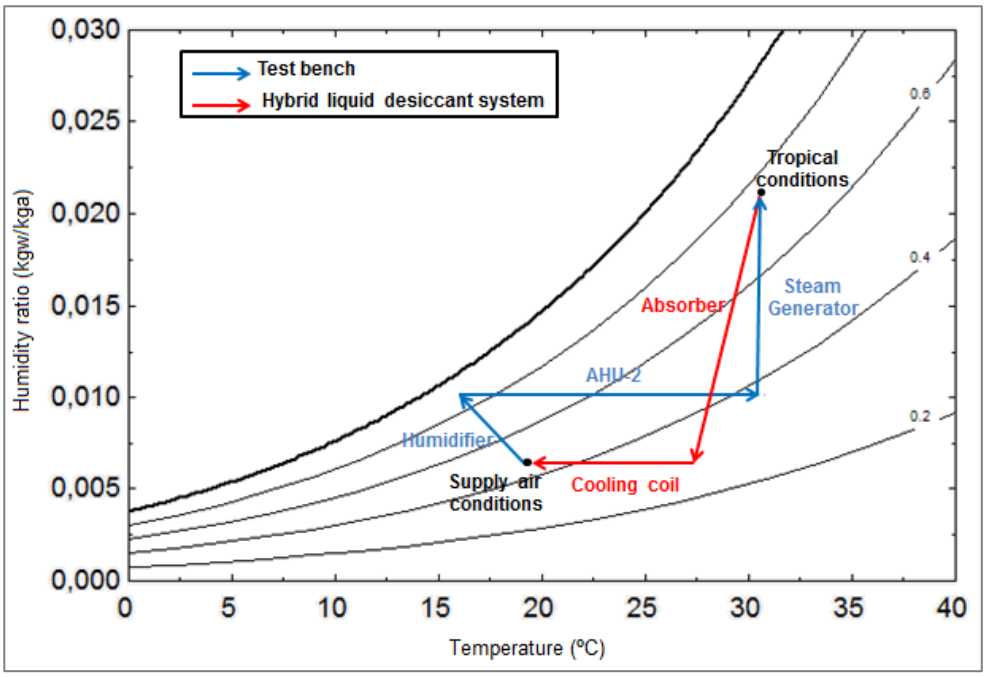

Figure 6.10. Moist air cycle for the achievement of tropical conditions with the test bench.

The total humidification capacity of the test bench is 45 kg/h, from which 30 kg/h are provided by the steam generator. The gas boiler can modulate the sensible heating provided to the air from 20 kW to 135 kW. Air temperature and relative humidity sensors as well as air velocity sensors were used to both, control the air conditions and validate the air measurements of the hybrid liquid desiccant system.

Figure 6.11 illustrates the cycle that the moist air follows when passing through the opened loop of the test bench and the hybrid liquid desiccant system. In the same way than in the closed loop, the process through

the test bench is represented with blue arrows and the process through the hybrid liquid desiccant system is represented with red arrows.

The moist air arrives at the test bench at outdoor conditions that, at design conditions in Tarragona, are approximately, 30 °C and 0.013 kg_w/kg_a. Air is then cooled and dehumidified in an air handling unit that receives chilling water from a heat pump. At the outlet of the air handling unit, air is cooler and less humid in order to achieve room conditions (25 °C and 0.010 kg_w/kg_a).

In this case, only air temperature can be regulated by the test bench. However, humidity ratio is free and mostly depends on the average water temperature inside the coil. Temperature is regulated with a three-way valve of the water at the entrance of the coil of the air handling unit. The total cooling capacity of the cooling coil of this air handling unit is 21.8 kW. Air temperature sensors were used to control the air conditions and validate the air measurements of the hybrid liquid desiccant system. Additional air relative humidity sensors and differential pressure sensors were used just to validate the air measurements of the hybrid liquid desiccant system.

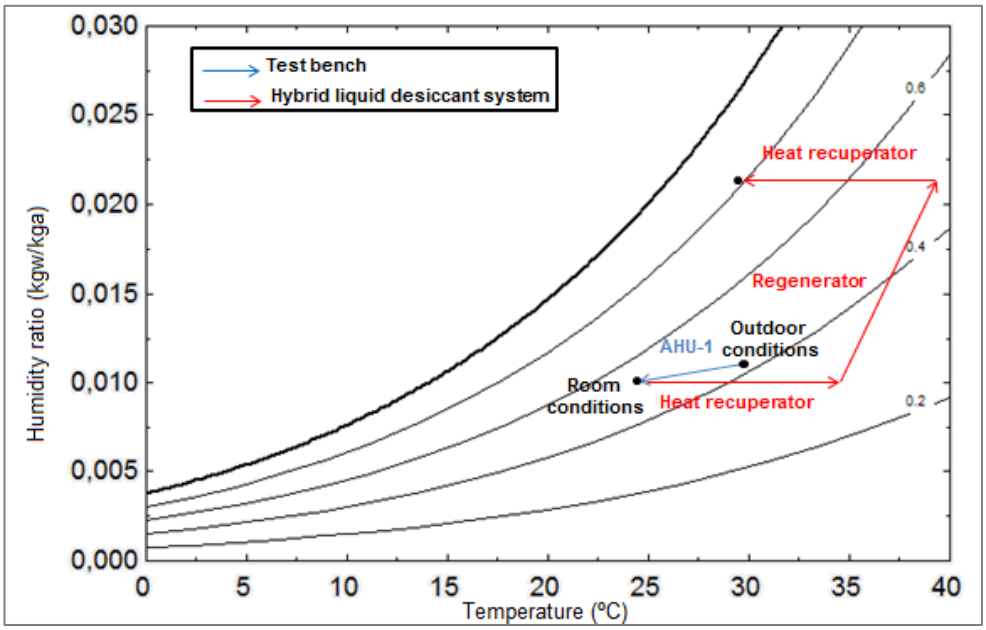

Figure 6.11. Moist air cycle for the achievement of room conditions with the test bench.

6.4.2. Electrical connections

One of the main problems to be solved during the tests in Tarragona was the electrical connections. Since the hybrid liquid desiccant system was designed to operate in Taiwan, where electric supply at three-phase is 230 V and 60 Hz, and the Spanish electric supply at three-phase is 400 V and 50 Hz, frequency inverters that are able to make the change of voltage and frequency, should be installed.

For that purpose two frequency drivers were required. These frequency drivers were selected from Toshiba [115]. The smallest frequency driver is the 4110PL and it has an output capacity of 21 kVA. The biggest frequency driver is the 4550PL and it has an output capacity of 88 kVA. When frequency drivers have to operate with different systems at the same time, it is necessary to incorporate wave filters in order to avoid critical problems such as burning of the components. For this reason, two wave filters were also needed. In this case wave filters were selected from Mitsubishi [116]. The smallest wave filter is the FFR-SI-62A-SS1 and it can provide a capacity of 41 kVA. The biggest wave filter is the FFR-SI-260A-SS1 and it can provide a capacity of 179 kVA.

Both, frequency drivers and wave filters, are oversized in order to handle the peak currents during the starting periods. Frequency drivers, filters and the system were put in serial disposition as it is shown in

Figure 6.12. This is the way that Mitsubishi suggested to place it. The biggest frequency driver and filter were connected to the heat pump, whereas the smallest devices were connected to the rest of the system.

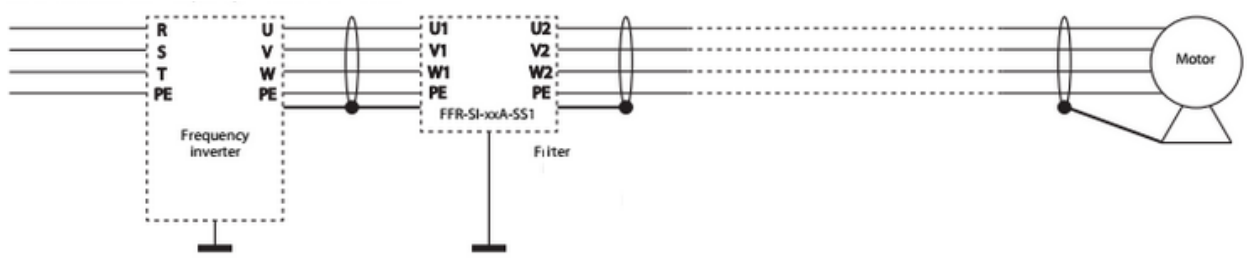

Figure 6.12. Simple scheme of the connection on the frequency driver and wave filter connected to an electric motor in serial disposition.

Figure 6.13. Frequency drivers (left and centre) and wave filters (right).

6.5. Set-up of the hybrid liquid desiccant system

In order to prepare the system and minimize the problems when it operates in Taiwan, a set-up and a tune-up of the hybrid liquid desiccant system was performed in Tarragona. This preparation can be divided into three phases:

- Installation and first checking of the system.
- Operation of the system in manual mode.
- Operation of the system in automatic mode.

6.5.1. Installation, assembling and first checking of the system

Due to the big dimensions of the hybrid liquid desiccant system, it had to arrive in three parts: the air handling unit with the main electrical panel, the liquid desiccant system with the hydraulic circuit, and the heat pump. Liquid desiccant system and heat pump arrived as a unique part. However, the air handling unit and the electrical panel arrived divided into 6 boxes (see Figure 6.14).

After joining of the different parts and making the electrical connections, the system was checked in order to verify that all the components were like the expected in the design phase. Several discrepancies were found in the system, most of these discrepancies were minor problems that could be solved in an easy way. However, two main problems that affected to the system performance were found:

Figure 6.14. Delivery of the air handling unit and the electrical panel.

- The air-solution contactors were made with in-line arrangement instead of the staggered arrangement. The different arrangement of the tubes of the air-solution contactors may change the performance of them.
- The hydraulic circuit, that joins the heat pump with the air-solution contactors and the coil, was constructed without following the 3D design. As a result a more complex circuit was done, what increased the pressure drops of water along it. Therefore, water flow rates were smaller than expected.

In the meantime these two problems were solved the system could be tested in both, manual and automatic mode. In this sense, the performance of the air-solution contactors with in-line arrangement could be compared with the one with staggered arrangement. Chapter 7 contains these results.

Other works done during this period were the connection of the system to the test bench, the filling of the hydraulic circuit and the liquid desiccant circuit, the sealing of the leakages and removing of air bubbles, the checking and learning of the monitoring system, and the calibration of sensors.

6.5.2. Operation of the system in manual mode

Once the system was checked and most of the found problems were solved, the system was operated in manual mode. In this sense, the system was thought to operate all the actuators from the control and monitoring system in manual mode with the following objectives:

- To verify that all the actuators, such as pumps, electronic valves or fans, operated in a proper way.
- To equilibrate the hydraulic circuit in order to avoid pressure problems and to ensure a good distribution of water. Since the maximum pressure inside the air-solution contactors is about 4 bars (manufacturer suggestion), this was a key point at this stage. Manual valves thought for this purpose were adjusted.
- To verify that security alarms appeared in the required moments.
- To obtain the maximum water and liquid desiccant flow rates available in the system.
- To check that plastic tubes of the air-solution contactors were fully wetted by the liquid desiccant.
- To operate the system in manual mode in order to get its performance at different operational conditions.
- To obtain the required time to achieve steady-state conditions. This is very useful for the fine-tuning of the control of the system.

After doing the manual tests, some problems that affect to the system performance were found:

- Maximum water flow rates obtained inside both, the absorber and the regenerator, were lower than the expected in Chapter 5. Even when the hydraulic circuit was replaced for the one that follows the 3D design, the maximum water flow rate inside them was almost half than expected at the design stage. More details about this issue are explained in Section 7.6.5.
- Plastic tubes of the air-solution contactors were not fully wetted by the liquid desiccant. This non-wetting happened for bot arrangements. However, the wetting was better for the in-line arrangement. This effect is explained in more detail in Section 7.4.

In addition, the effect of the lower water flow rates and the lack of wettability of plastic tubes are studied in a separated way in Section 7.7. The performance results on the absorber, the regenerator and the whole system obtained in the manual mode are included in Chapter 7.

6.5.3. Operation of the system in automatic mode

After the system was tested in manual mode, the last phase of the set-up, in which the system is operated in automatic mode, was performed. The objectives at this stage were the following:

- To verify that the system starts operating in the proper way and time. In this sense, the fans of the air handling unit should work first. Once the two fans are running, the heat pump should start. Finally, the two pumps of the liquid desiccant subsystem are operated.
- To check that the regenerator operates when it should do it when it operates as function of the LiCl mass concentration. This was done by varying the maximum and minimum LiCl density set point at the entrance of the absorber.
- To check that a proper control of the temperature and humidity is done by the system. In this case, instead of using the return humidity ratio and the room temperature, the system had to control the supply air temperature and humidity ratio. Fine adjustment of the PID controllers of the 3-way valves was also performed at this stage. Different set point temperatures and humidity ratios were tried in order to know the reaction time of the system.
- To adjust the PID controller for a proper control of the supply air flow rate.
- To verify that the system was able to change from summer mode, in which the coil cools the air, to winter mode, in which the coil heats the air.

Some modifications to the control algorithm programming were required in order to success with a proper control. At the end of the tests, the system was ready to be brought to Taiwan.

6.6. Conclusions

After being manufactured and before being sent to Taiwan, the hybrid liquid desiccant system has been assembled and set-up at the Universitat Rovira i Virgili. Moreover, the test bench had to be modified in order to achieve tropical conditions required to make the first tests to the system.

After trying the system during this period, the following main conclusions have been taken:

- Due to a mistake of the air-solution contactor manufacturer, the two air solution contactors were made with in-line arrangement instead of staggered arrangement. Therefore, the system was firstly tested with in-line arrangement air-solution contactors and, once the new air-solution contactors were replaced, the system was then tested with the staggered arrangement. The results of these tests and a comparison between both air-solution contactors are included in Chapter 7.
- Several discrepancies with the designed system were found when the system arrived. Most of them were solved.
- Two problems appeared in the air-solution contactors that affect to the performance of the system:
    - Maximum water flow rates obtained inside both, the absorber and the regenerator, were lower than the expected in Chapter 5.
    - Plastic tubes of the air-solution contactors were not fully wetted by the liquid desiccant.

- When operating the system in automatic mode, all the controllers were adjusted and the system was finally ready to be sent to Taiwan. Moreover, different control strategies were tested and compared. Among them, the selected strategies are the described in Section 6.3

Chapter 7. Experimental performance of the hybrid liquid desiccant system

7.1. Introduction

The experimental results obtained from the hybrid liquid desiccant system are shown in this chapter. Results were taken during its operation at the Universitat Rovira i Virgili (Tarragona, Spain) for three months and at the National Taiwan University of Science and Technology (Taipei, Taiwan) since November 2015.

Two different air-solution contactors have been tried within the system: one with in-line arrangement, which was tried firstly during the setting-up of the system in Tarragona, and another with staggered arrangement, that has been tried, firstly, in Tarragona and, secondly, in Taipei. All the experimental values shown in this chapter are available in Annex D.

Specific results of the air-solution contactors as well as global results of the hybrid liquid desiccant system are included in this chapter. Moreover, the performance of the air-solution contactors with different arrangements is compared. In addition, the mathematical model of the air-solution contactors presented in Chapter 5 is used in order to obtain the tube-solution heat transfer coefficient and the mass transfer coefficient in the air side of the air-solution contactors with staggered arrangement.

Finally, operational conditions of three complete days are included in this chapter in order to show both: the performance of the system at different ambient conditions, and the capability of the system of controlling separately the room humidity and temperature.

7.2. Results with air-solution contactors with in-line arrangement

As it has been mentioned in Chapter 6, despite the air-solution contactors were designed to be of the staggered arrangement, the manufacturer made a mistake and provided them with an in-line arrangement. In the meantime, the new air-solution contactors with the right arrangement were coming, a first setting-up of the system was done and some interesting results of the absorber with in-line arrangement could be taken.

However, enough representative results for the regenerator with in-line arrangement could not be taken due to finding steady-state conditions for it was much more difficult than for the absorber. The main reason that explains this is that the coriolis meter, which measures the density of the LiCl-H_2O, is placed at the entrance of the absorber and, therefore, steady-state conditions must be reached in the whole system in order to be able to measure the steady-state conditions in the regenerator. Table D.1 in Annex D contains the experimental measurements taken for the absorber with in-line arrangement.

Left graph in Figure 7.1 shows the supply humidity ratio of the moist air as function of the ambient humidity when the air flow rate is higher than 1800 m^3/h. As it is expected, the higher inlet humidity ratio, the higher supply humidity ratio (from about 0.006 kg_w/kg_a when ambient humidity is in the range of 0.011 kg_w/kg_a, to 0.011 kg_w/kg_a when ambient humidity ratio is about 0.023 kg_w/kg_a). The slope of the tendency line is lower than 1, what means that the dehumidification achieved by the absorber is higher when the ambient humidity is higher too.

On the other hand, right graph in Figure 7.1 shows the supply humidity ratio as function of the inlet liquid desiccant temperature in the absorber. As it can be observed from this graph, the inlet liquid desiccant temperature in the absorber affects much to the supply humidity ratio, due to the decreasing of the water vapour pressure when the desiccant temperature is decreased. In this case supply humidity ratio is about 0.006 kg_w/kg_a when inlet liquid desiccant temperature is about 21 °C and in the range of 0.011 kg_w/kg_a when inlet liquid desiccant temperature is about 26.5 °C. In these two graphs, the highest uncertainty for the

supply humidity ratio is 0.00052 kg_w/kg_a, for the ambient humidity ratio is 0.00085 kg_w/kg_a and for the inlet liquid desiccant temperature is 0.25 °C.

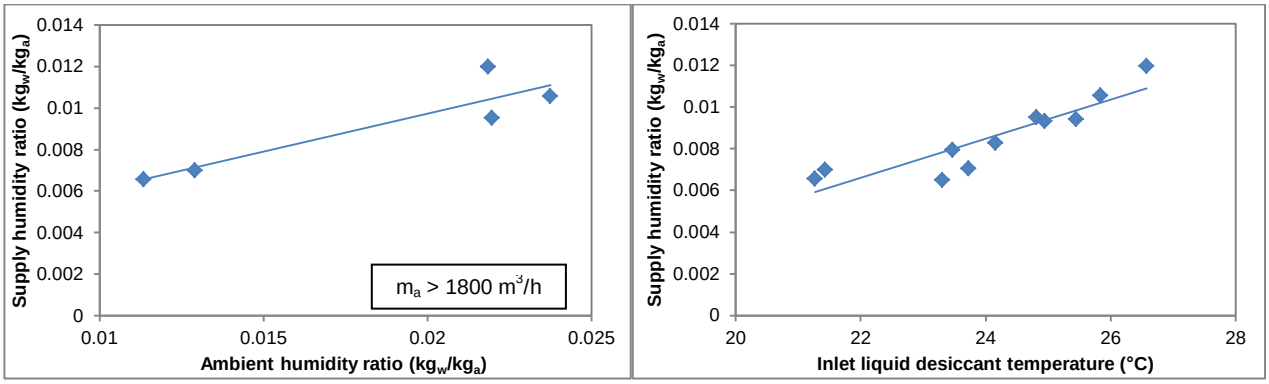

Figure 7.1. Supply humidity ratio in the absorber with in-line arrangement as function of the ambient humidity ratio (left) and inlet liquid desiccant temperature (right).

However, the liquid desiccant temperature not only affects to the supply humidity, but also to the outlet air temperature in the absorber, as it is shown in Figure 7.2. The outlet air temperature is about 0.5 °C higher than the inlet liquid desiccant temperature, what demonstrates that sensible load handled by the absorber mostly depends on the liquid desiccant temperature. Moreover, Figure 7.2 also illustrates the heat duty in the absorber as function of the inlet liquid desiccant temperature. As it is expected, the higher liquid desiccant temperature, the higher heat duty in the absorber. In this case, the heat duty increases from 20 kW to 26 kW when inlet liquid desiccant temperature increases from 21 °C to 26 °C. In this figure, the highest uncertainty for the supply air temperature is 0.28 °C, for the heat duty is 1.6 kW and for the inlet liquid desiccant temperature is 0.25 °C.

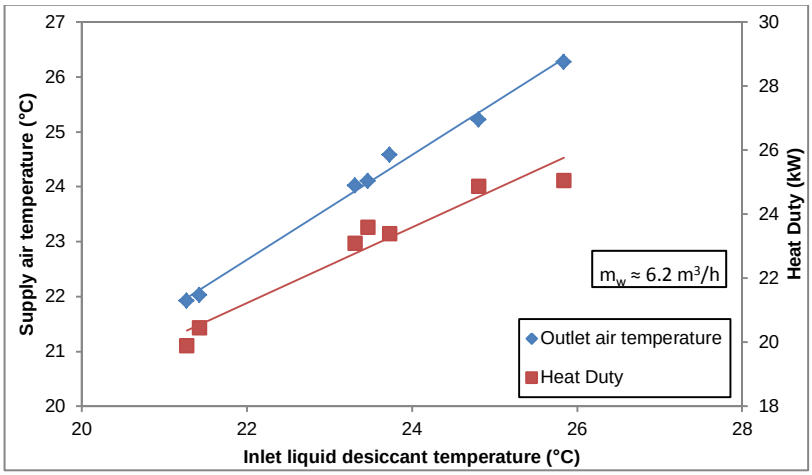

Figure 7.2. Supply air temperature and heat duty in the absorber with in-line arrangement as function of the inlet liquid desiccant temperature.

From Figure 7.1 and Figure 7.2, it is shown the importance of the inlet liquid desiccant temperature in the dehumidification achieved, in the supply air temperature and in the heat duty. In this sense, since most of the liquid desiccant taken from the collector of the absorber is recirculated again to the absorber (because split ratio is about 0.9), the inlet liquid desiccant temperature depends much on the inlet water temperature in the absorber. This effect is shown in Figure 7.3, where inlet liquid desiccant temperature as function of the inlet water temperature in the absorber is illustrated for water flow rates in the range of 6.2 m^3/h. As it can be observed from this figure, the inlet liquid desiccant temperature increases from about 21 °C to 26 °C when inlet water temperature is about 15 °C and 19 °C, respectively. In this figure, the highest uncertainty for the inlet water temperature is 0.26 °C and for the inlet liquid desiccant temperature is 0.25 °C.

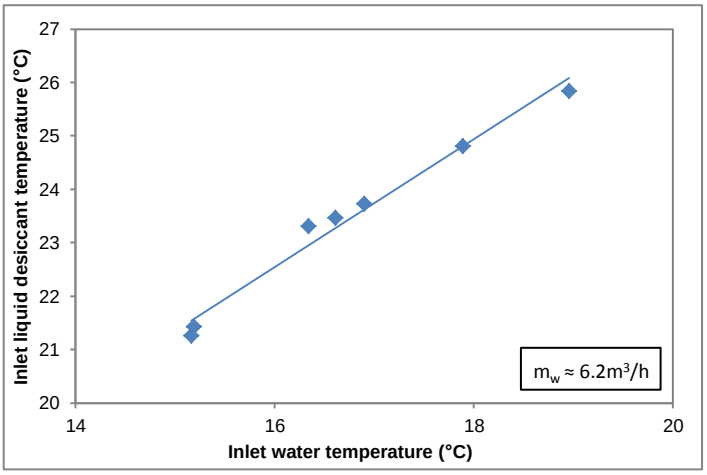

Figure 7.3. Inlet liquid desiccant temperature in the absorber with in-line arrangement as function of the inlet water temperature.

Therefore, the overall heat transfer coefficient of the absorber (defined as in the Equation 7.1) is a key parameter for the performance of it:

$$UA_{abs}\left(\frac{kW}{°C}\right) = \frac{\dot{Q}_{w,abs}}{\Delta T_{LM}} \tag{7.1}$$

Where Q_w is calculated from Equation 4.3 and ΔT_{LM} from Equation 4.6.

Figure 7.4 shows the global heat transfer coefficient of this absorber as function of the liquid desiccant mass flow rate and water flow rate (left), and the air flow rate (right). The higher water flow rate, liquid desiccant mass flow rate and air flow rate, the higher global heat transfer coefficient. The three effects were expected because an increasing on the water flow rate enhances the water-tube heat transfer coefficient and higher liquid desiccant flow rate, and an increasing on the air flow rate enhances the solution-tube heat transfer coefficient. However, full wetting of tubes was not reached. This fact is explained in detail in Section 7.4. In these two graphs, the highest uncertainty for the global heat transfer coefficient is 0.13 kW/°C, for the liquid desiccant mass flow rate is 0.01 kg/s and for the air flow rate is 7 m^3/h.

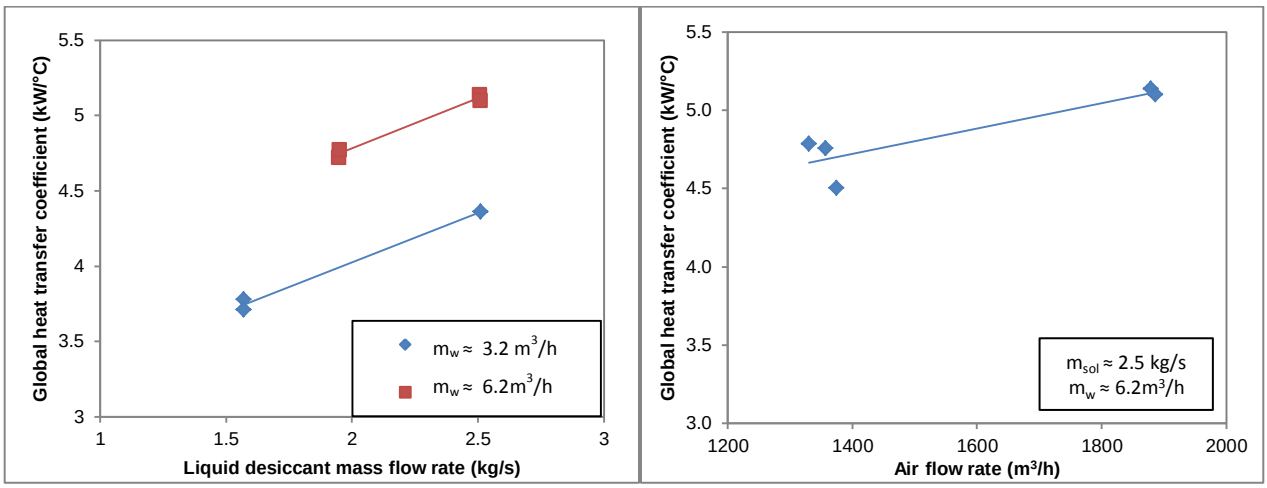

Figure 7.4. Global heat transfer coefficient of the absorber with in-line arrangement as function of the liquid desiccant mass flow rate and water flow rate (left) and air flow rate (right).

Figure 7.5 illustrates the mass transfer coefficient in the air side as function of the air flow rate (left) and the liquid desiccant mass flow rate (right). An increasing in both, the air flow rate and the liquid desiccant mass flow rate, makes to rise the mass transfer coefficient in the air side. For the case of the air flow rate, minimum mass transfer coefficient in the air side rises from 0.021 kg/m^2·s, when the air flow rate is about 1350 m^3/h, to 0.027 kg/m^2·s, when the air flow rate is almost 2500 m^3/h. For the case of the liquid desiccant flow rate, minimum mass transfer coefficient in the air side rises from 0.018 kg/m^2·s, when the liquid

desiccant mass flow rate is about 1.5 kg/s, to 0.021 kg/m^2·s, when the liquid desiccant mass flow rate is about 2.5 kg/s. In these two graphs, the highest uncertainty for the mass transfer coefficient in the air side is 0.003 kg/m^2·s, for the liquid desiccant mass flow rate is 0.01 kg/s and for the air flow rate is 7 m^3/h.

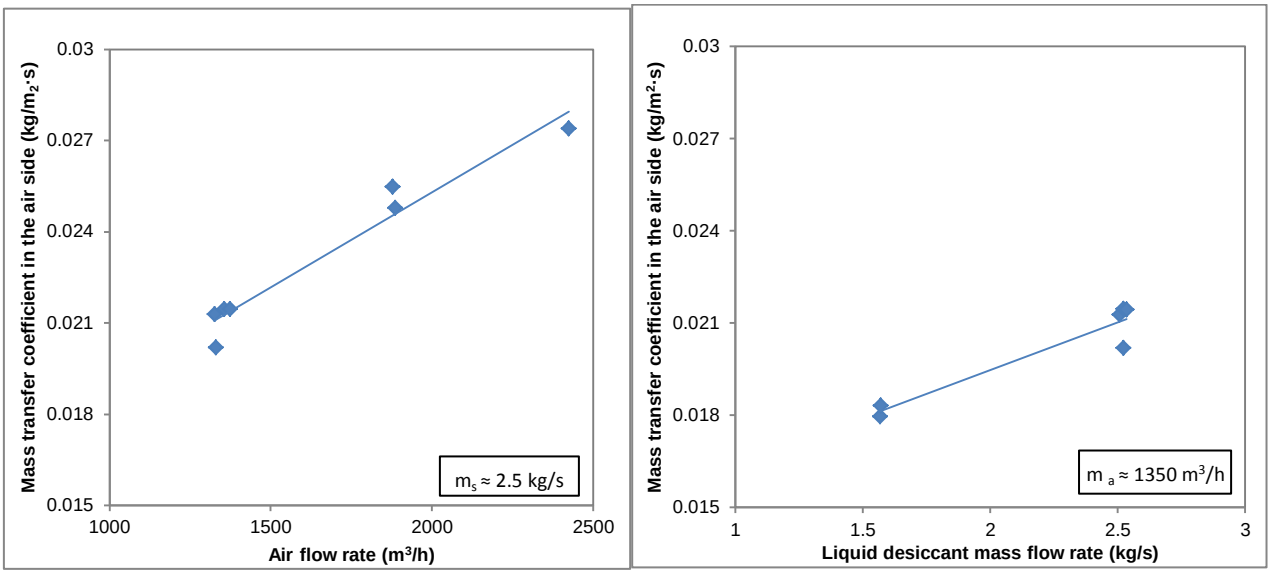

Figure 7.5. Mass transfer coefficient in the air side of the absorber with in-line arrangement as function of the air flow rate (left) and the liquid desiccant mass flow rate (right).

Since both, overall heat transfer coefficient and mass transfer coefficient in the air side are higher when liquid desiccant mass flow rate is 2.5 kg/s, it has been decided to operate the system at this flow rate.

7.3. Results air-solution contactors with staggered arrangement

Once the required air-solution contactors with staggered arrangement were placed within the fiberglass towers, new experimental results were taken from the hybrid liquid desiccant system during its operation in Tarragona and Taipei. In this case, both, absorber and regenerator, results could be taken. Although, less steady-state points for the regenerator than for the absorber could be obtained.

As it was concluded in Section 7.2, the best liquid desiccant mass flow rate is 2.5 kg/s, which is, actually, the maximum liquid desiccant mass flow rate that can be provided by the solution pumps. Therefore, all the results showed above for the air-solution contactors with staggered configuration are taken for this liquid desiccant mass flow rate. Since the system has been operating with these air-solution contactors during a longer period than with the air-solution contactors with in-line disposition, a higher amount of experimental data has been collected. Table D.2 and Table D.3 in Annex D contain the experimental measurements taken for the absorber and the regenerator with staggered arrangement.

7.3.1. Absorber

Left graph of Figure 7.6 shows the supply air humidity ratio as function of the ambient humidity and the air flow rate. As it is expected the higher inlet humidity ratio and the higher air flow rate, the higher supply humidity ratio (from about 0.008 $kg_w/kg_{a,}$ when ambient humidity is about 0.017 kg_w/kg_a and air flow is about 2070 m^3/h, to 0.010 kg_w/kg_a, when ambient humidity ratio is higher than 0.020 kg_w/kg_a and the air flow is about 2720 m^3/h).

On the other hand, right graph of Figure 7.6 shows the supply air humidity ratio as function of the inlet liquid desiccant temperature and the inlet liquid desiccant density in the absorber. As it can be observed from this graph, the lower inlet liquid desiccant temperature and the higher liquid desiccant density, the lower supply air humidity ratio. This behaviour is because of the low vapour pressure of the liquid desiccant at those

conditions. The effect of the liquid desiccant temperature is even, at this range, more important than the liquid desiccant density (and hence, LiCl mass concentration), because, for instance, the supply humidity ratio achieved at about 1208 kg/m^3 and 26 °C is about the achieved at 1172 kg/m^3 and 24 °C. In these two graphs, the highest uncertainty for the supply humidity ratio is 0.00049 kg_w/kg_a, for the ambient humidity ratio is 0.00051 kg_w/kg_a and for the inlet liquid desiccant temperature is 0.21 °C.

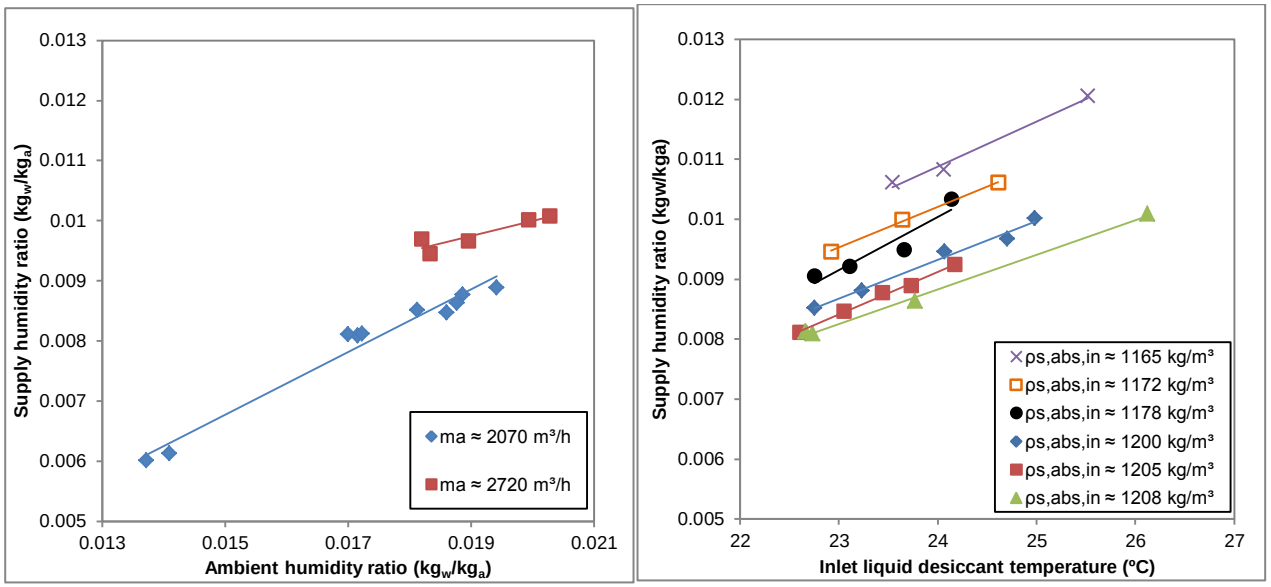

Figure 7.6. Supply air humidity ratio as function of the ambient humidity and the air flow rate (left), and as a function of the liquid desiccant temperature and density (right).

As in the case of the absorber with in-line arrangement, the liquid desiccant temperature not only affects to the supply humidity ratio, but also to the outlet air temperature in the absorber, as it is shown in Figure 7.7. The outlet air temperature is about 0.5 °C higher than the inlet liquid desiccant temperature what demonstrates again that sensible load handled by the absorber mostly depends on the inlet liquid desiccant temperature. Moreover, Figure 7.7 also illustrates the heat duty in the absorber as function of the inlet liquid desiccant temperature. As it happens with the absorber with in-line arrangement, the higher liquid desiccant temperature, the higher heat duty in the absorber. In this case, the heat duty increases from 19 kW to 27 kW when inlet liquid desiccant temperature increases from 22.5 °C to 26 °C. In this figure, the highest uncertainty for the supply air temperature is 0.33 °C, for the heat duty is 2.2 kW and for the inlet liquid desiccant temperature is 0.31 °C.

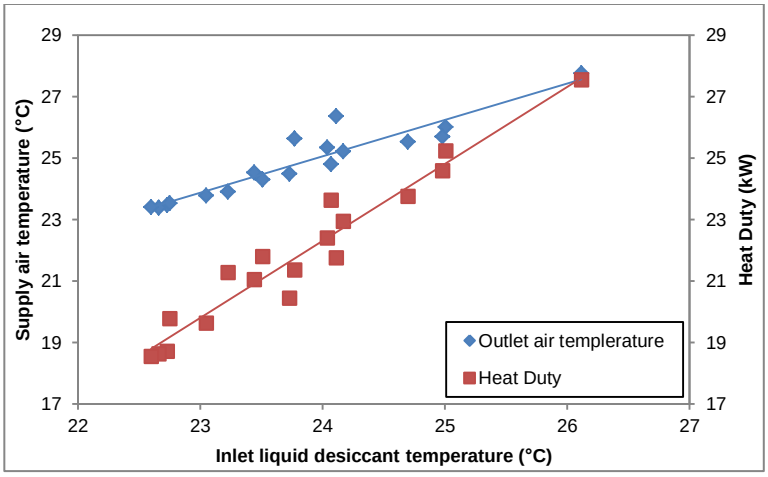

Figure 7.7. Supply air temperature and heat duty in the absorber with staggered arrangement as function of the inlet liquid desiccant temperature.

Again, inlet liquid desiccant temperature is shown as a key parameter of the performance of the absorber. For the same reason as it was explained in Section 7.2 (split ratio is about 0.90), the inlet liquid desiccant temperature depends much on the inlet water temperature in the absorber. This effect is shown in Figure 7.8, where inlet liquid desiccant temperature is illustrated as function of the inlet water temperature in the absorber, for water flow rates in the range of 6.0 m^3/h. As it can be observed from this figure, the inlet liquid desiccant temperature increases from about 22.5 °C to 25 °C when inlet water temperature is about 16.6 °C and 17.4 °C, respectively. In this figure, the highest uncertainty for the inlet water temperature is 0.31 °C and for the inlet liquid desiccant temperature is 0.11 °C.

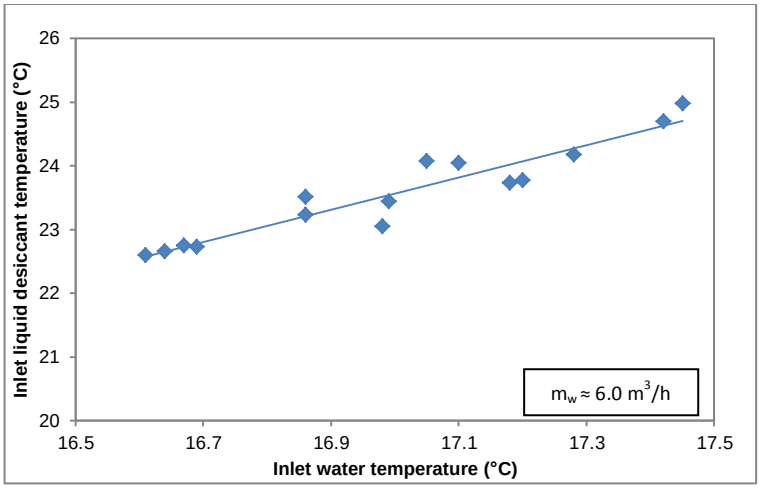

Figure 7.8. Inlet liquid desiccant temperature in the absorber with staggered arrangement as function of the inlet water temperature.

Figure 7.9 shows the global heat transfer coefficient of this absorber as function of the water flow rate (left), and the air flow rate (right). Both, the higher water flow rate and the higher air flow rate, the higher global heat transfer coefficient. Both effects were expected because an increasing on the water flow rates enhances the water-tube heat transfer coefficient, and an increasing on the air flow rate enhances the solution-tube heat transfer coefficient. However, as it happens with the absorber with in-line arrangement, full wetting of tubes is not reached. This fact is explained in detail in Section 7.4. In these two graphs, the highest uncertainty for the global heat transfer coefficient is 0.16 kW/°C, for the water flow rate is 0.06 m^3/h and for the air flow rate is 8 m^3/h.

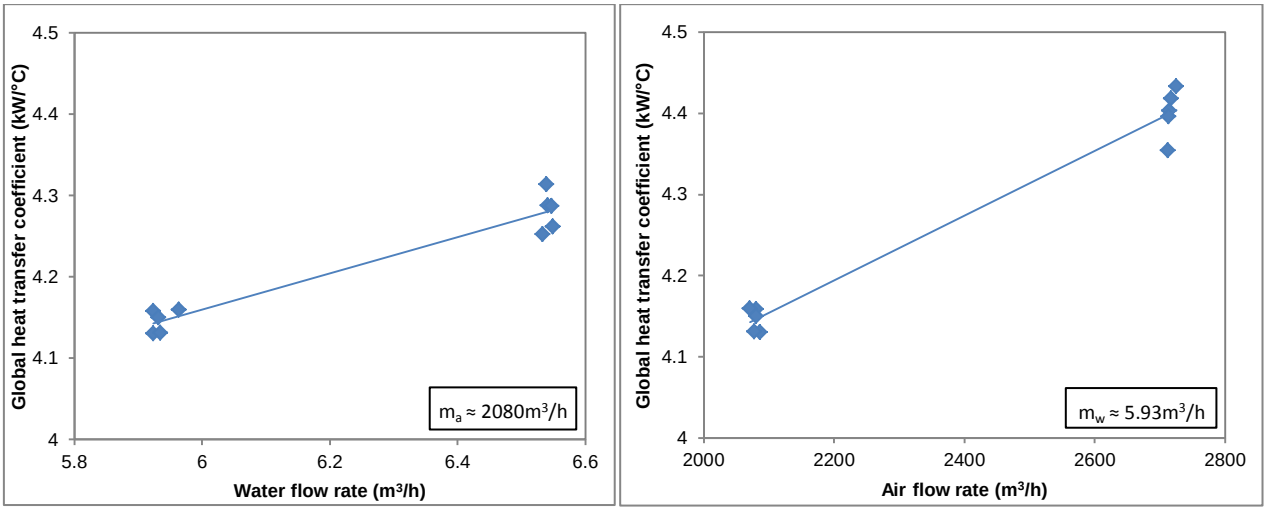

Figure 7.9. Overall heat transfer coefficient of the absorber with staggered arrangement as function of the water flow rate (left) and air flow rate (right).

Figure 7.10 illustrates the mass transfer coefficient in the air side as function of the air flow rate. An increasing of the air flow rate makes to rise the mass transfer coefficient in the air side. In this case, from

0.019 kg/m^2·s, when the air flow rate is about 1950 m^3/h, to 0.023 kg/m^2·s, when the air flow rate is about 2700 m^3/h. In this figure, the highest uncertainty for the mass transfer coefficient in the air side is 0.004 kg/m^2·s and for the air flow rate is 8 m^3/h.

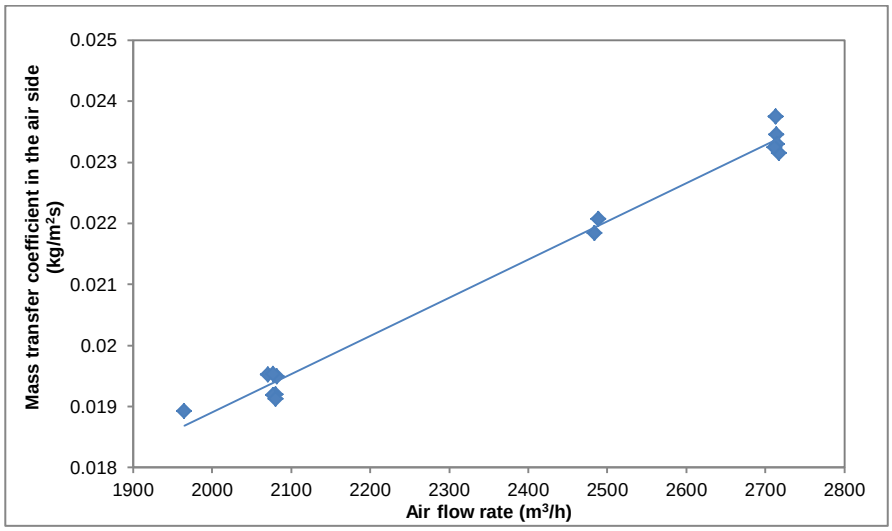

Figure 7.10. Mass transfer coefficient in the air side of the absorber with staggered arrangement as function of the liquid desiccant mass flow rate.

7.3.2. Regenerator

Left graph of Figure 7.11 shows the outlet air humidity ratio as function of the inlet air humidity ratio (when air flow rate is about 2600 m^3/h). As it is expected, the higher inlet humidity ratio the higher outlet humidity ratio (from about 0.019 kg_w/kg_a when ambient humidity is in the range of 0.0010 kg_w/kg_a, to 0.023 kg_w/kg_a when ambient humidity ratio is about 0.014 kg_w/kg_a).

On the other hand, right graph of Figure 7.11 shows the difference between the outlet and the intlet air humidity ratio in the regenerator as function of the inlet liquid desiccant temperature in the regenerator. As it can be observed from this graph, the lower inlet liquid desiccant temperature, the lower difference of the air humidity ratio. In addition, the difference of the air humidity ratio increases from about 0.006 kg_w/kg_a to 0.011 kg_w/kg_a when the inlet desiccant temperature is about 39 °C and 47 °C respectively, which means that regeneration of the liquid desiccant is enhanced when the inlet liquid desiccant temperature is high. In these two graphs, the highest uncertainty for the outlet humidity ratio is 0.00082 kg_w/kg_a, for the inlet humidity ratio is 0.00071 kg_w/kg_a, for the inlet liquid desiccant temperature is 0.24 °C and for the difference humidity ratio 0.00121 kg_w/kg_a.

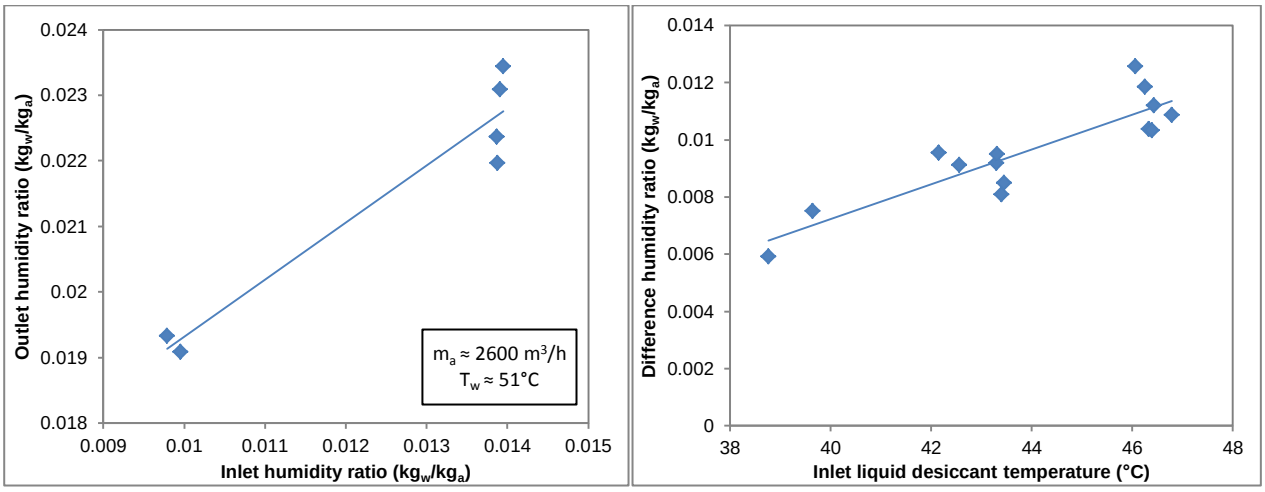

Figure 7.11. Outlet humidity ratio in the regenerator as function of the inlet humidity ratio (left) and difference humidity ratio in the regenerator as function of the inlet solution temperature (right).

Furthermore, the liquid desiccant temperature not only affects to the outlet humidity, but also to the outlet air temperature in the regenerator. In this sense, left graph of Figure 7.12 shows that the outlet air temperature is about 1 °C lower than the inlet liquid desiccant temperature.

On the other side, right graph of Figure 7.12 illustrates the water heating rate provided in the regenerator as function of the inlet liquid desiccant temperature. In the opposite way that happened in the absorber with the heat duty, the higher liquid desiccant temperature, the lower water heating rate in the regenerator. In this case, the water heating rate provided in the regenerator decreases from 27 kW to 17 kW when inlet liquid desiccant temperature increases from 42 °C to 47 °C. In these two graphs, the highest uncertainty for the outlet air temperature is 0.48 °C, for the water heating rate is 2.2 kW and for the inlet liquid desiccant temperature is 0.24 °C.

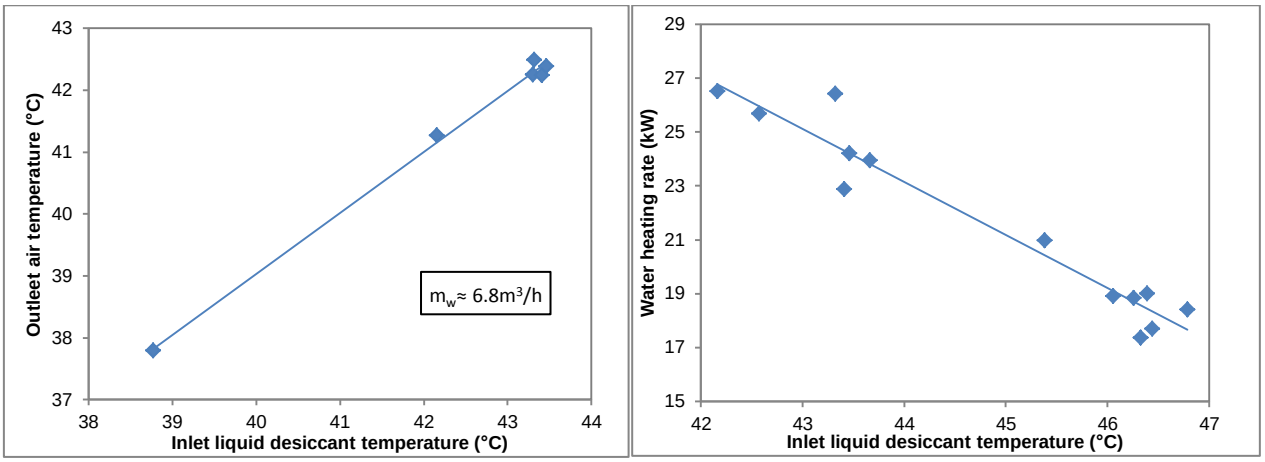

Figure 7.12.Outlet air temperature (left) and water heating rate (right) in the regenerator as function of the inlet liquid desiccant temperature.

From Figure 7.11 and Figure 7.12 it is shown the importance of the inlet liquid desiccant temperature in the regeneration achieved in the regenerator and in the water heating rate in it. In this sense, since most of the liquid desiccant taken from the collector of the regenerator is recirculated again to the regenerator (because split ratio is about 0.9), the inlet liquid desiccant temperature depends much on the inlet water temperature in the regenerator. This effect is shown in Figure 7.13, where inlet liquid desiccant temperature as function of the inlet water temperature in the regenerator is illustrated. As it can be observed from this figure, the inlet liquid desiccant temperature increases from about 38 °C to 43 °C when inlet water temperature is about 45 °C and 51 °C, respectively. In this figure, the highest uncertainty for the inlet water temperature is 0.37 °C and for the inlet liquid desiccant temperature is 0.24 °C.

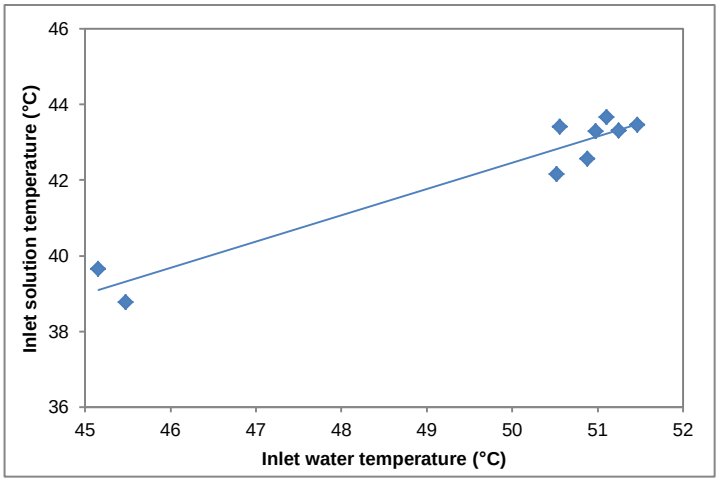

Figure 7.13. Inlet solution temperature in the regenerator as function of the inlet water temperature.

Figure 7.14 shows the global heat transfer coefficient of the regenerator as function the water flow rate (left), and the air flow rate (right). Since water flow rate in the regenerator is constant, the operational range of this variable is small, and therefore, the influence on the global heat transfer coefficient is not perceptible. On the other side, according to results showed in the right graph of Figure 7.14, only a small increasing of the overall heat transfer coefficient is detected for higher air flow rates. This increasing is smaller than the obtained with the absorber. In any case, the global heat transfer coefficient of the regenerator is nearly 4.1 kW/°C, which is in the range of the obtained with the absorber. In these two graphs, the highest uncertainty for the global heat transfer coefficient is 0.27 kW/°C, for the water flow rate is 0.10 m^3/h and for the air flow rate is 8 m^3/h.

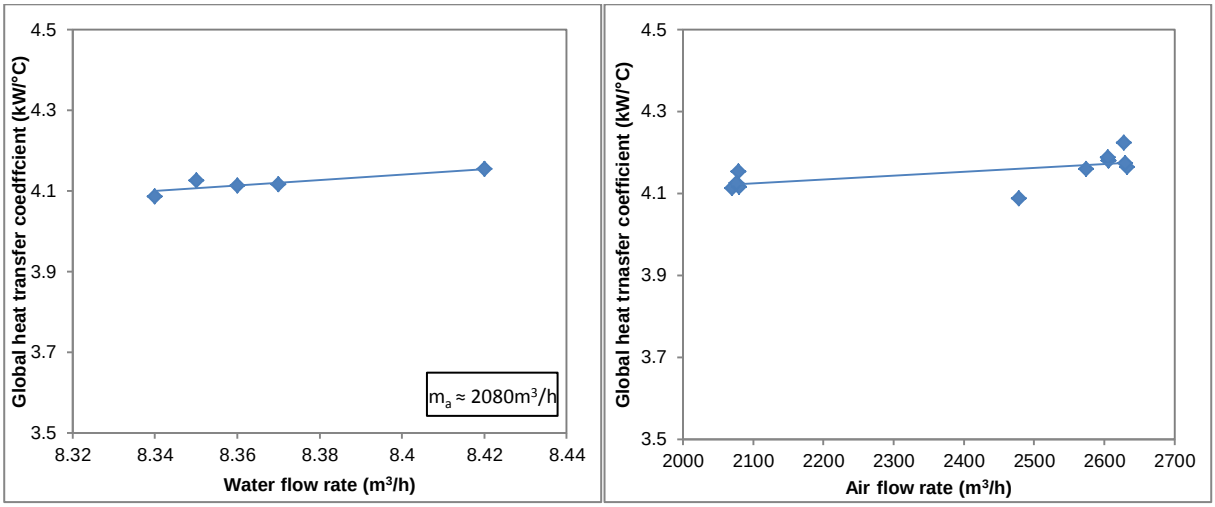

Figure 7.14. Overall heat transfer coefficient in the regenerator as function of the water flow rate (left) and the air flow rate (right).

Finally, Figure 7.15 shows the mass transfer coefficient in the air side as function of the air flow rate. An increasing in the air flow rate makes to rise the mass transfer coefficient in the air side. In this case, the air flow rate increases from 0.033 kg/m^2·s when the air flow rate is about almost 2100 m^3/h to nearly 0.070 kg/m^2·s when the air flow rate is higher than 2600 m^3/h. These values of mass transfer coefficient are much higher than the obtained with the absorber. In this figure, the highest uncertainty for the mass transfer coefficient in the air side is 0.006 kg/m^2·s and for the air flow rate is 8 m^3/h.

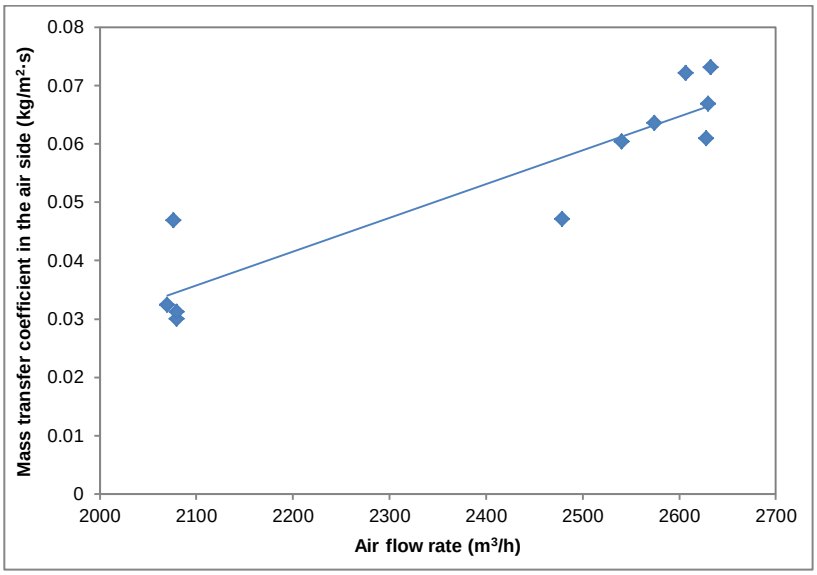

Figure 7.15. Mass transfer coefficient in the air side in the regenerator as function of the air flow rate.

7.4. Comparison between air-solution contactors

7.4.1. Results

Figure 7.16 shows the overall heat transfer coefficient (left) and mass transfer coefficient in the air side (right) of the two tested absorbers as function of the air flow rate. Both, global heat transfer coefficient and mass transfer coefficient in the air side are higher in the absorber with in-line arrangement. In fact, absorber with in-line arrangement provides a global heat transfer coefficient and a mass transfer coefficient in the air side about 9 % and 20 %, respectively, higher than the absorber with staggered arrangement.

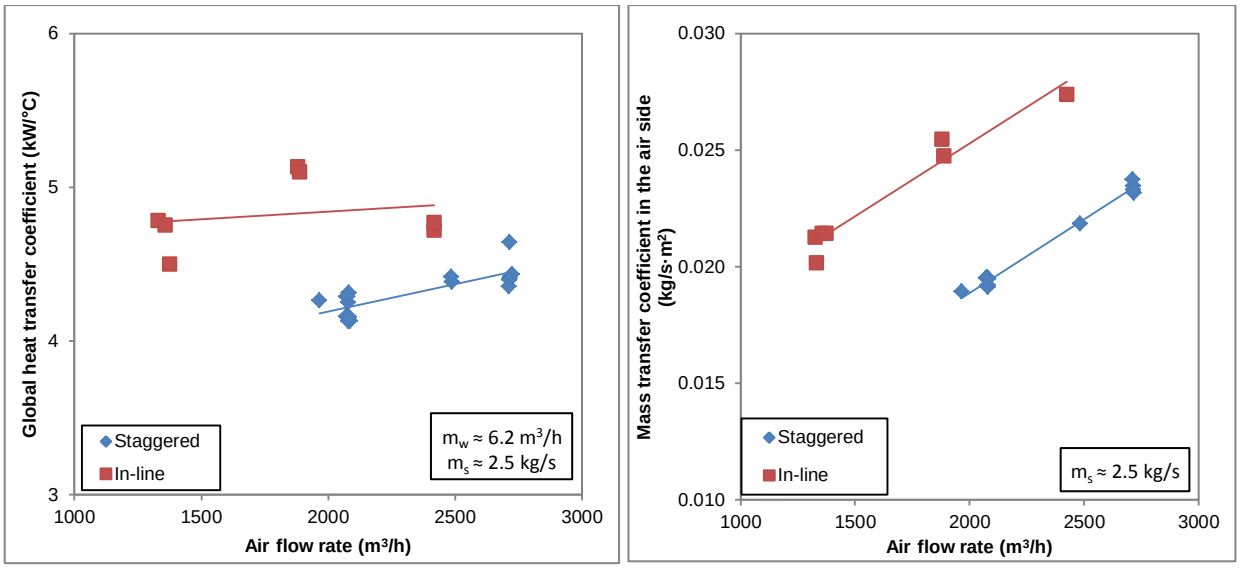

Figure 7.16. Comparison of the overall heat transfer coefficient (left) and the mass transfer coefficient in the air side (right) achieved in the absorber with staggered and in-line configuration.

7.4.2. Discussion

Although the absorber with staggered arrangement was the designed and the definitive one, the absorber with in-line arrangement has achieved a better performance. The main reason why air-solution contactors with staggered arrangement were chosen in the design phase in favour of the in-line arrangement air-solution contactors was because usually the staggered arrangement provides a better performance in the air side, due to the circulation of the air throughout the tube bundle. However, in this case, the achieved results show an opposite behaviour.

When trying to find an explanation for this fact, we realized that tube wetting in the air-solution contactors with in-line arrangement was better than in the one with staggered arrangement. Although, a wettability study was done in order to determine the minimum liquid desiccant flow rate to fully wet the plastic tubes (see Chapter 3), an unexpected bend along the tubes was formed in both air-solution contactors due to the low rigidity of plastic tubes, and a big number of dry patches appeared around them, as Figure 7.17 shows, especially, in both extremes of the tubes.

But, why tubes are more wetted in in-line than in staggered arrangement? Figure 7.18 shows one module section of the in-line and the staggered disposition. When both air-solution contactors are working with the same liquid desiccant flow rate, the linear mass flow rate in the in-line disposition is higher than in the staggered arrangement, because the liquid desiccant is distributed in almost the double of them, permitting achieve a better wetting and therefore a better heat and mass transfer. Moreover, the liquid desiccant passes around 5 tubes per module in the case of the in-line and around 2 or 3 tubes in the case of the staggered, what allows for achieving a better cooling/heating of it. In any case, this study should be studied in detail with CFD software in order to verify that this justification is valid. Other reasons, such as a worst

plasma deposition on the polypropylene tubes in the case of the staggered arrangement or a bigger tube bending, may lead to similar behaviour.

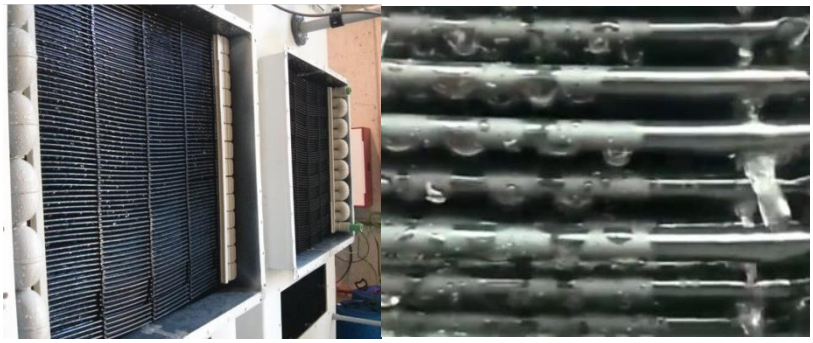

Figure 7.17. Absorber and regenerator with staggered arrangement (left) and picture of the falling-film in the absorber with staggered arrangement (right).

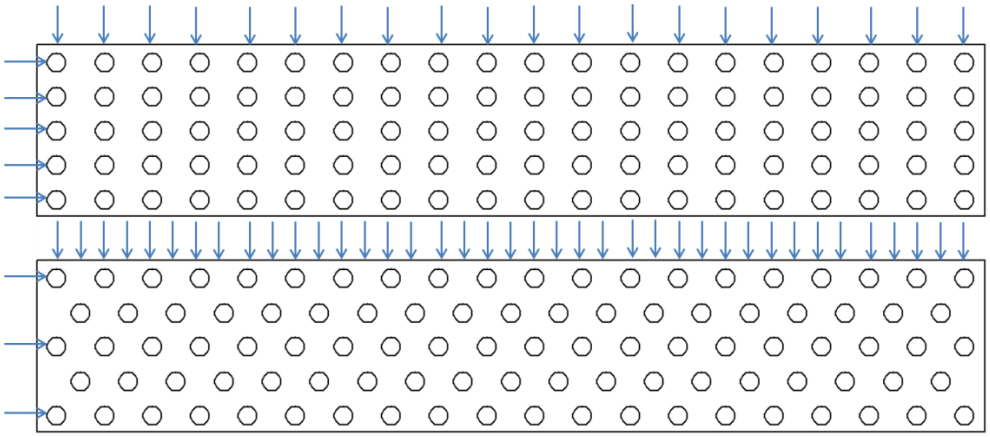

Figure 7.18. Section of the in-line and staggered arrangement of the air-solution contactors.

7.5. Modelling of the air-solution contactors

In order to model the air-solution contactors, both, solution-tube heat transfer coefficient and mass transfer coefficient in the air side, are needed to be calculated. Since, liquid desiccant flow rate is constant in the absorber and the regenerator with staggered arrangement, the solution-tube heat transfer coefficient and the mass transfer coefficient in the air side can be just correlated as function of the air flow rate.

The methodology used to calculate the heat and mass transfer coefficients is the following:

- Experimental values obtained from the air-solution contactors were implemented in the EES model that was developed for the system design (it is described in Chapter 5). In this case, both, outlet air and water conditions were given by measurements, and solution-tube heat transfer coefficient and mass transfer coefficient in the air side were calculated.
- Once heat and mass transfer coefficients were calculated for each measurement, potential regressions as function of the air flow rate were obtained by minimizing the quadratic mean error of the heat and mass transfer coefficients. This means that the correlated equations have the following structure:

$$H = P \cdot \dot{m}_a{}^N \tag{7.2}$$

Where

H is either the solution-tube heat transfer coefficient (W/m^2·°C) or the mass transfer coefficient in the air side (kg/m^2·s),

P and *N* are empirical parameters calculated from the previous methodology.
$\dot{m}_a$ (m^3/h) is the air flow rate.

Table 7.1 contains the calculated empirical values for the solution-tube heat transfer coefficient and the mass transfer coefficient in the air side of the absorber and the regenerator with staggered arrangement.

Table 7.1. Empirical parameters for the solution-tube heat transfer coefficient and the mass transfer coefficient in the air side for the absorber and the regenerator with staggered arrangement.

Air-solution contactor	Solution-tube heat transfer coefficient		Mass transfer coefficient in the air side	
	P	N	P	N
Absorber	3.264	0.510	$7.89 \cdot 10^{-6}$	1.021
Regenerator	189.0	0.000	$1.56 \cdot 10^{-5}$	1.046

Left graph of Figure 7.19 shows a comparison between the dehumidification achieved by the absorber with staggered arrangement and the dehumidification calculated by using the above correlations for heat and mass transfer coefficients. According to this graph, the deviations between measured and calculated dehumidification are always below the 10 %.

On the other hand, right graph of Figure 7.19 shows a comparison between the heat duty achieved by the absorber with staggered arrangement and the heat duty calculated by using the above correlations for heat and mass transfer coefficients. According to this graph, the deviations between measured and calculated heat are always below the 5 %.

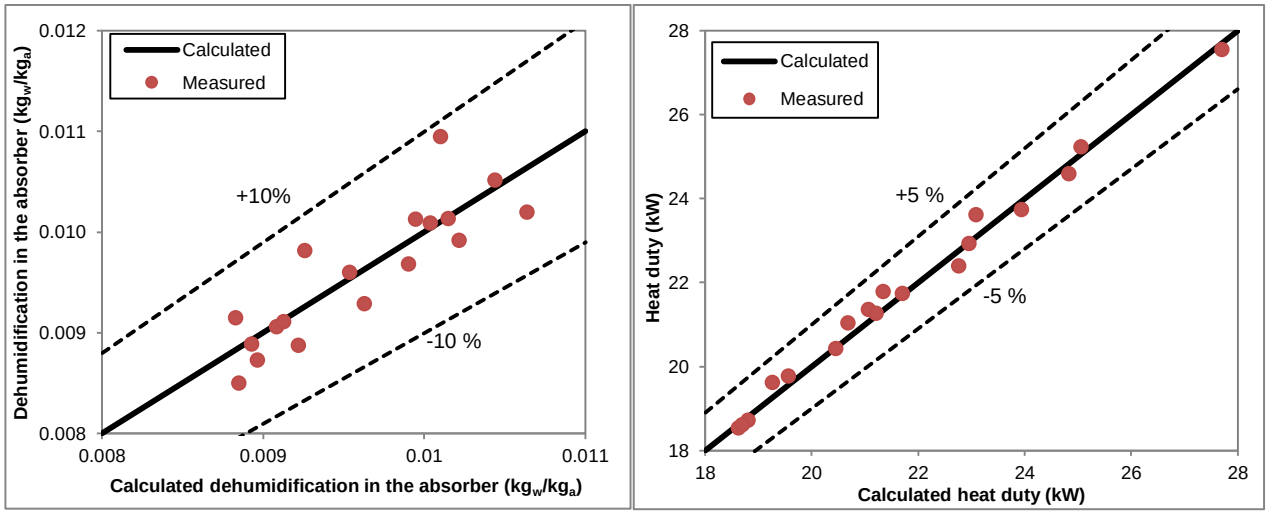

Figure 7.19. Calculated and measured dehumidification (left) and heat duty (right) in the absorber.

Therefore, small deviations are achieved between the calculated and the measured values for the absorber. Consequently, the empirical parameters contained in Table 7.1 as well as the equations that have been described in Chapter 5 can be validated for the absorber.

Left graph of Figure 7.20 shows a comparison between the difference air humidity ratio achieved by the regenerator with staggered arrangement and the difference air humidity ratio calculated by using the above correlations for heat and mass transfer coefficients. According to this graph, the deviations between measured and calculated difference air humidity ratio are always below the 10 %.

On the other hand, right graph of Figure 7.20 shows a comparison between the heat provided by the regenerator with staggered arrangement, and the heat calculated by using the above correlations for heat and mass transfer coefficients. According to this graph, the deviations between measured and calculated heat are always below the 10 %.

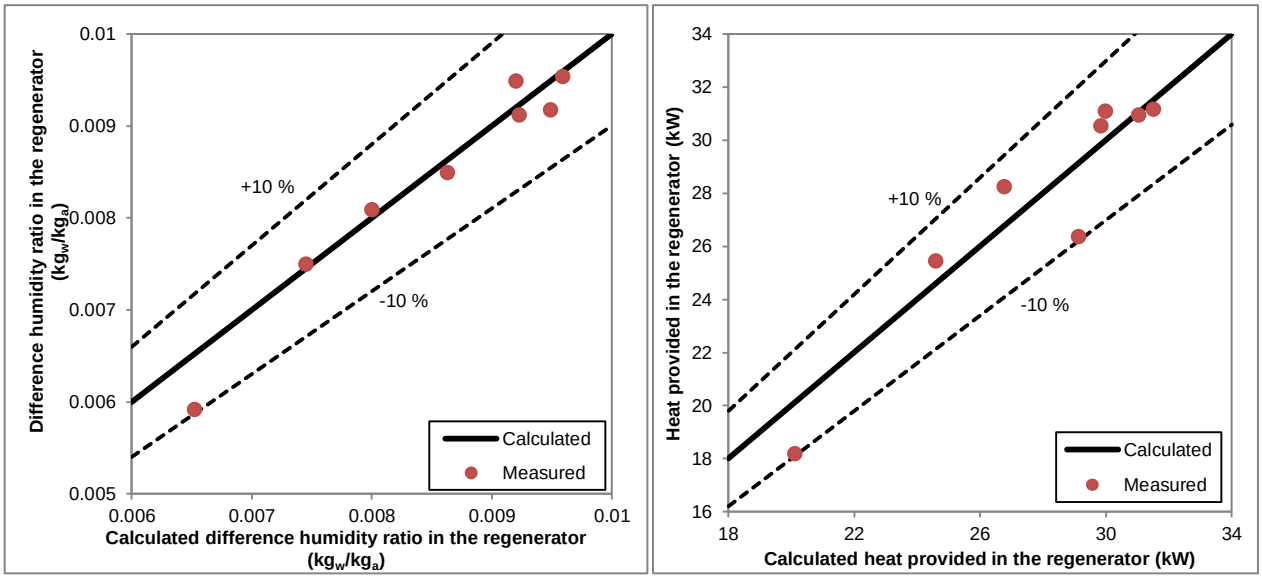

Figure 7.20. Calculated and measured difference humidity ratio (left) and heat provided (right) in the regenerator.

Therefore, small deviations are achieved between the calculated and the measured values for the regenerator. Consequently, the empirical parameters contained in Table 7.1 as well as the equations that have been described in Chapter 5 can be validated for the regenerator.

7.6. Global results of the hybrid liquid desiccant system

Once the performance of the air-solution contactors has been presented, global results of the liquid desiccant system are described in this section. The hybrid liquid desiccant system has been fully operational at National Taiwan University of Science and Technology since November 2015, and its operation has been monitored since that moment. Although, the system has been specially designed for warm and humid conditions, it was kept running along the winter months providing also comfort conditions to the locker rooms.

7.6.1. Performance at design operation conditions

Figure 7.21 shows a schematic description of the system with the values of the main experimental variables when it operates at ambient conditions and internal loads near the design conditions. Comparing with the values given in Figure 5.12, where design conditions were estimated, supply air conditions are warmer and more humid, due mainly to water flow rates are lower, and inlet water temperature in the absorber and the regenerator are higher and lower, respectively, than expected. Furthermore, tubes were not fully wetted. These conditions lead to decrease the cooling capacity of the system. Moreover, air flow rate is increased from 2500 m^3/h to 2714 m^3/h. The temperature problem can be solved by adjusting the set point temperatures of the heat pump. However, water flow rates cannot be increased due to high pressure drops inside the air-solution contactors in the water side, and the bending of tubes is an issue not easy to be solved.

Figure 7.22 illustrates the evolution of the heating rates of the main components of the hybrid liquid desiccant system as well as the ventilation and internal loads during the warmest and most humid day. As it can be observed from this figure, ventilation loads were higher (from 20 to 25 kW) than internal loads (from 10 to 15 kW) under those conditions. On the other hand, cooling provided by the absorber was in the range of 30 kW (not only latent cooling, but also sensible cooling) and the provided by the cooling coil was in the range of 4 kW. Moreover, the required heating rate in the regenerator is more or less the same than in the absorber, this is about 30 kW along the day.

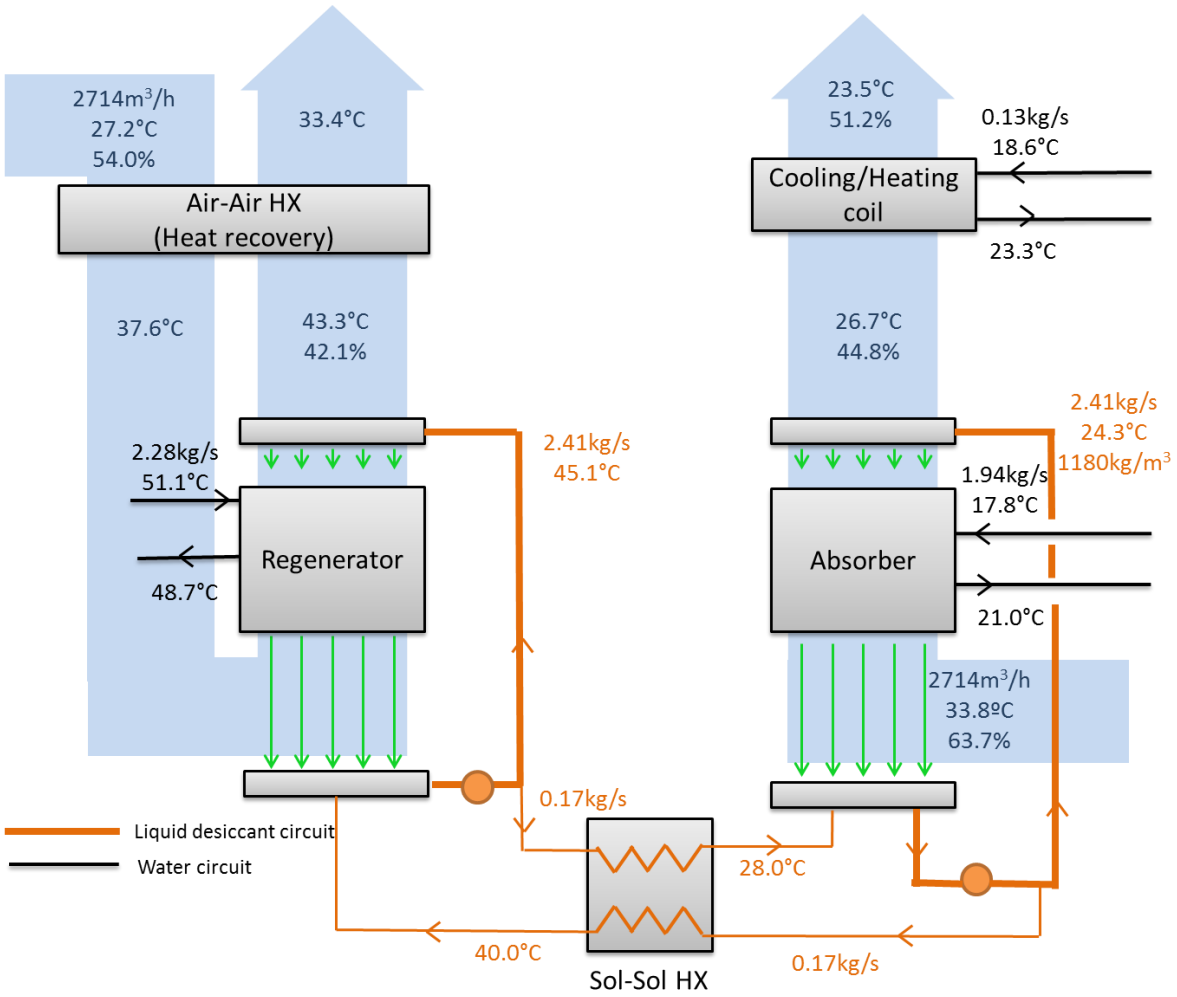

Figure 7.21. Schematic description of the system with the experimental values of the main variables when it operates at high ambient temperature and humidity.

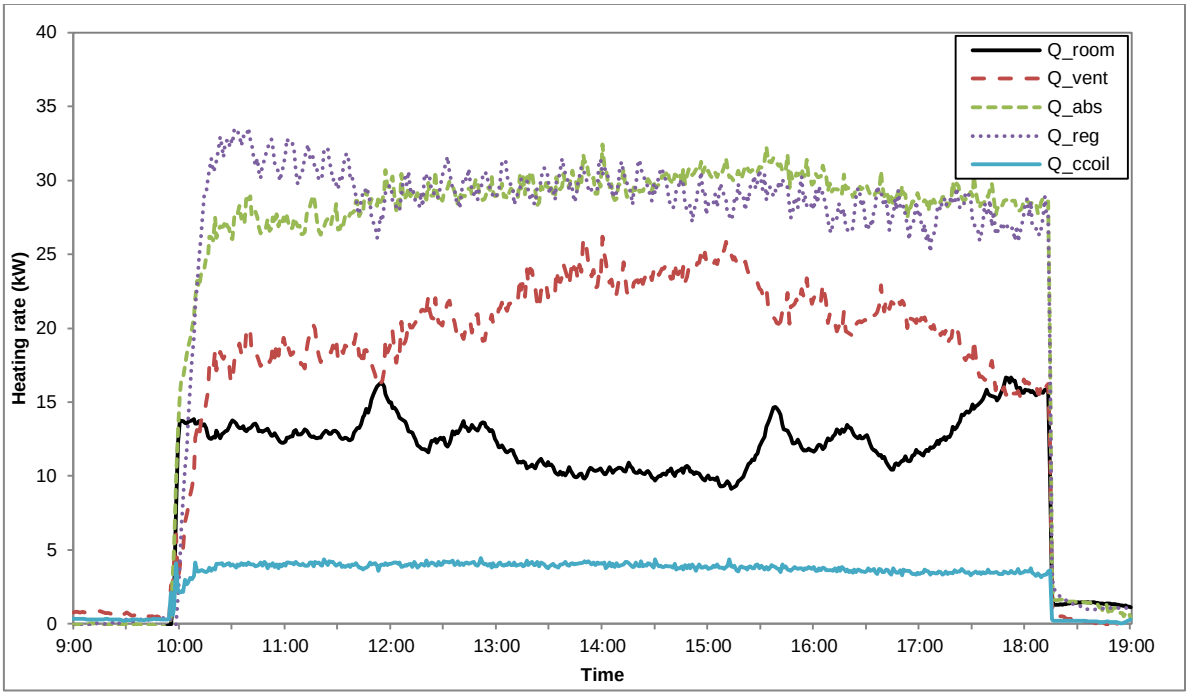

Figure 7.22. Heating rates of the main components of the hybrid liquid desiccant system and ventilation and internal loads for the warmest and most humid day.

7.6.2. Performance of the system at different ambient conditions

Since the hybrid liquid desiccant system started to operate at the National Taiwan University of Science and Technology (Taipei, Taiwan) in November 2015. Last measurements collected and analysed were taken in February 2016. During most of that time, the system operated at colder air temperatures and smaller humidity ratios than at design conditions. However, during a significant number of hours of November the system was working at full load because the internal loads were high.

For this reason, 23 points at steady-state conditions could be taken from the measurements during its operation in Taiwan. These 23 steady-state points are illustrated in Figure 7.23 in a psychrometric chart that contains the ambient air conditions, the outlet air conditions in the absorber and the air-solution equilibrium conditions that represent the minimum air temperature and humidity ratio that the moist air could achieve under these operational conditions. The air-solution interface temperature is assumed as:

$$T_{a-s,I} = T_{s,in} \tag{7.3}$$

Whereas the air-solution interface humidity ratio is assumed as:

$$W_{a-s,I} = \frac{0.622}{\frac{p}{p_{WA}}-1} \tag{7.4}$$

Where p is the atmospheric pressure and p_{WA} is the vapour pressure of the water in air that, at equilibrium conditions, can be considered equal to vapour pressure of water in the liquid desiccant in the interface. This variable is calculated by using the Patek and Klomfar [24] correlations. For this case, the liquid desiccant conditions at the interface have been considered equal to the absorber inlet liquid desiccant conditions.

According to the results, outlet air temperature and humidity ratio in the absorber are next to the air-solution equilibrium conditions in most of the cases what means that the absorber efficiency is good. Again, these results show how important are the inlet liquid desiccant conditions in the performance of the system, especially the inlet liquid desiccant temperature and, therefore, the global heat transfer coefficient of the absorber.

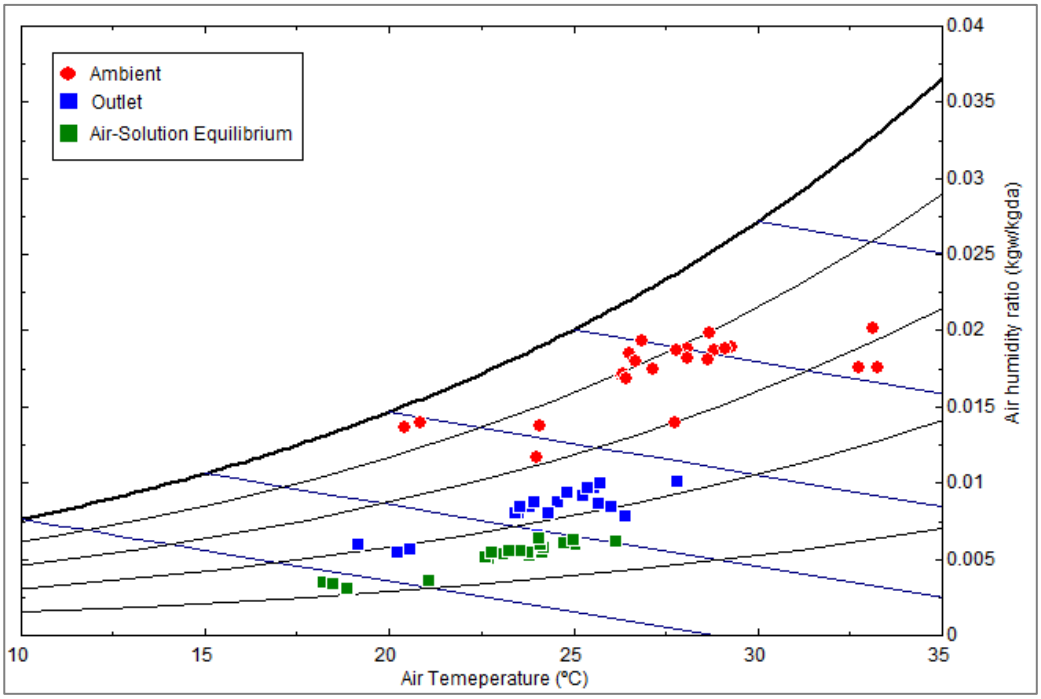

Figure 7.23. Psychrometric chart with the ambient air conditions, the supply air conditions and air-solution equilibrium during the operation of the system in Taiwan.

7.6.3. COP of the liquid desiccant system

COP of the liquid desiccant system has been defined as the cooling provided to the air in the absorber divided by the heating provided by the hot water to the regenerator, this means:

$$COP_{LDS} = \frac{\int_0^t \dot{m}_a \cdot (h_{a,in,abs} - h_{a,out,abs})dt}{\int_0^t \dot{m}_w \cdot (c_{p,w,in,reg} \cdot T_{w,in,reg} - c_{p,w,out,reg} \cdot T_{w,out,reg})dt} \quad (7.5)$$

Where *t* is a period of time that always is always longer than 1 hour. This definition of COP of the liquid desiccant system only takes into account the heating in the regenerator, but it does not consider the cooling in the absorber. This definition has been chosen to be in agreement with most of the authors that evaluate the COP of other liquid desiccant system, who only consider the heating in the regenerator due to, in their case, cooling is provided by a cooling tower. In any case, in this liquid desiccant system cooling and heating are provided by the same heat pump, this is the same energy source.

According to the data taken from measurements, the parameters that mainly affect the COP of the liquid desiccant system are the air flow rate, the cooling rate in the absorber and the hot water temperature. Left graph of Figure 7.24 illustrates the COP of the liquid desiccant system as function of the air flow rate and the cooling rate in the absorber. Measured values show that the higher cooling rate in the absorber the higher COP of the liquid desiccant system. However, the lower air flow rate the higher COP of the liquid desiccant system. Minimum COP of the liquid desiccant system is about 0.9 when cooling rate in the absorber is about 13 kW and air flow rate is about 2700 m^3/h. Maximum COP of the liquid desiccant system is about 1.5 when cooling rate in the absorber is about 20 kW and air flow rate is about 2000 m^3/h.

In addition, right graph of Figure 7.24 illustrates the COP of the liquid desiccant system as function of the hot water temperature at the inlet of the regenerator. The measured values show that the higher hot water temperature, the lower COP of the liquid desiccant system. Maximum COP of the liquid desiccant is about 1.1 when hot water temperature is about 42.5 °C and the minimum is about 0.9 when ambient hot water temperature is about 52 °C.

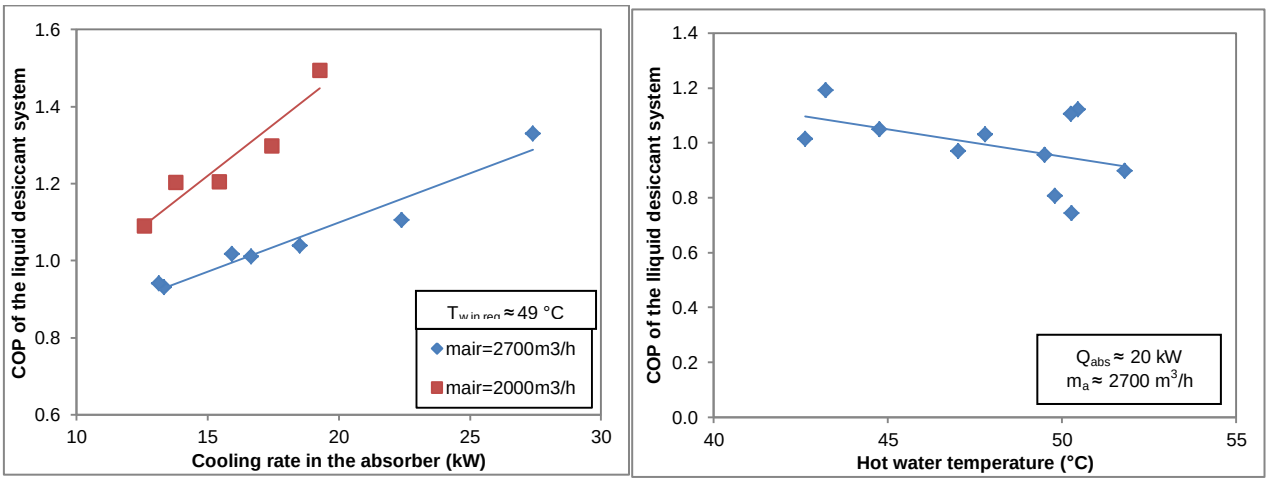

Figure 7.24. COP of the liquid desiccant system as function of the cooling ratio in the absorber and the air flow rate (left) and as function of the water temperature at the inlet of the regenerator (right).

All these values have been taken at steady-state conditions of the liquid desiccant system, what means that the density of the liquid desiccant is constant, and the water absorbed and regenerated in that period is the same. Therefore, the only reason that explains why COP of the liquid desiccant system is higher than 1 is because the absorber is cooling the moist air more than regenerator is heating it, this is possible when ambient temperature is very high. This explanation is well illustrated in Figure 7.25, which shows the heating provided by the regenerator as function of the air cooling in the absorber. As expected, the higher air cooling in the absorber, the higher heating provided in the regenerator. However, the slope of the curve is decreasing with the air cooling in the absorber because more sensible load is handled by the absorber. With

an air flow rate of about 2700 m^3/h the heating provided in the regenerator is about 14 kW when the air cooling in the absorber is about 13 kW and about 21 kW when the cooling rate is about 27 kW.

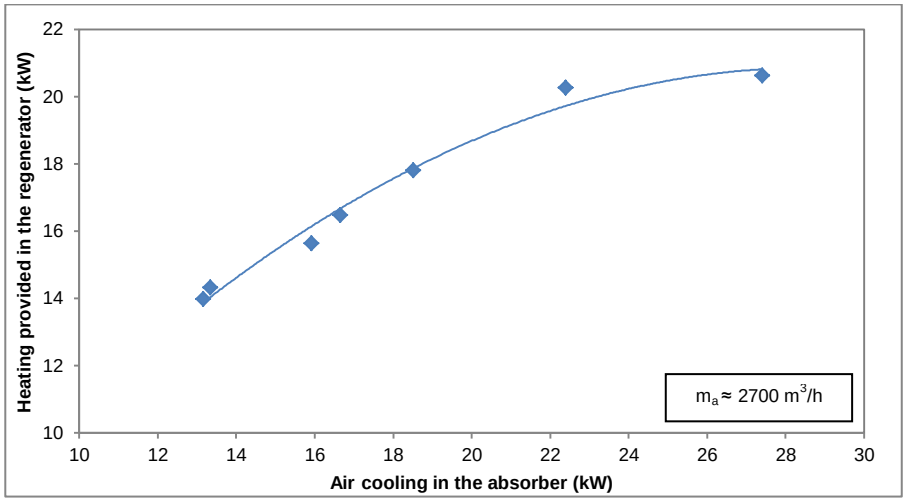

Figure 7.25. Heating provided in the regenerator as function of the cooling capacity in the absorber.

7.6.4. Global COP of the hybrid liquid desiccant system

Global COP of the hybrid liquid desiccant system has been defined as the cooling provided to the air in the absorber and the cooling coil divided by the electrical consumption of the compressor of the heat pump ($P_{el,comp}$), this means:

$$COP_{Gl} = \frac{\int_0^t \dot{m}_a \cdot (h_{a,in,abs} - h_{a,out,cc})dt}{\int_0^t \dot{P}_{el,comp}dt} \quad (7.6)$$

Where *t* is a period that is always longer than 1 hour.

After analysing the measured data, the parameters that mainly affects to the global COP of the hybrid liquid desiccant system are the water temperature at the outlet of the condenser and the cooling capacity provided by the system. Left graph of Figure 7.26 illustrates the global COP of the hybrid liquid desiccant system as function of the water temperature at the outlet of the condenser. The measured values show that the higher water temperature, the lower the global COP of the hybrid liquid desiccant system. Minimum COP is about 3.2 when water temperature is about 52 °C and the maximum is about 3.9 when water temperature is about 42 °C.

Right graph of Figure 7.26 illustrates the global COP of the hybrid liquid desiccant system as function of the cooling provided by the system. The measured values show that the higher the cooling provided the higher the global COP of the hybrid liquid desiccant system. Minimum COP is about 1.7 when the cooling provided is about 11 kW and the maximum is about 3.8 when the cooling provided is about 21 kW.

These effects on the global COP are quite similar to the obtained for a conventional vapour compression chiller. This happens because the liquid desiccant system COP is close to 1 in most of the cases and it is affected in the same way than the COP of a chiller, this is, for higher hot water temperatures and lower cooling demands the COP is lower (see Section 7.6.3)

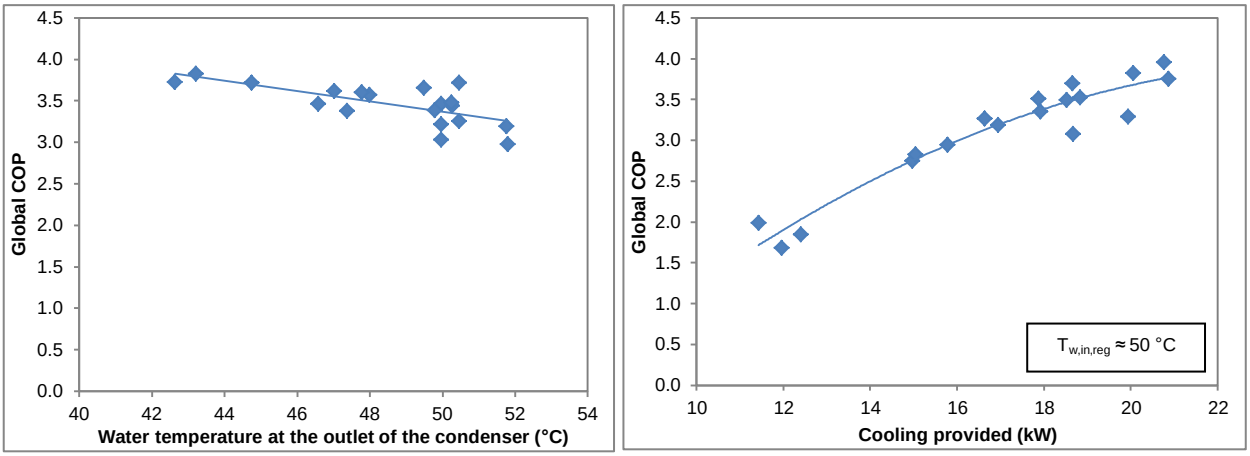

Figure 7.26. Global COP of the hybrid liquid desiccant system as function of the water temperature at the outlet of the condenser (left) and as function of the cooling provided by the system (right).

7.6.5. Other performance results

Despite a detailed design of the system was performed in Chapter 5, some discrepancies between the expected performance and the measured performance have been found, not only in the air-solution contactors, but also in the solution heat exchanger, the air heat exchanger, and the liquid desiccant and water flow rates of the hybrid liquid desiccant system.

Table 7.2 shows the expected results at design stage and the measured results achieved of the heat exchangers effectiveness, the water and liquid desiccant mass flow rates and the split ratio.

In one hand, measured results of the effectiveness of both, air and solution heat exchangers, are in the range of the expected results. However, maximum water flow rate inside the air-solution contactors does not achieve the expected values because the water pressure drops inside them are much higher than the specified by the manufacturer. Even after including two new water pumps in the hydraulic circuit, these flow rates are still low due to pressure drops inside the air-solution contactors at the expected flow rates are higher than the maximum static pressure that they can support, which is 4 bars. Although, according to the provider, the pressure drops at design water flow rates should have been lower than 1.5 bars, pressure drops higher than 2 bars were measured at 50 % of the designed water flow rates. Therefore, flow rates were about half of the expected, what reduces the performance of the system as it is explained in detail in Section 7.7.

On the other hand, since full wetting of tubes was not reached, as it is explained in Section 7.4.2, the solution mass flow rate in both, the absorber and the regenerator, was set as the maximum that the solution pumps could provide. This increasing also enhances the heat and mass transfer coefficient of the air-solution contactors. This means that the solution flow rate was about 35 % higher than the expected at design conditions. Due to the increasing of the liquid desiccant flow rate in the air-solution contactors and higher pressure drops than expected in the solution-solution heat exchanger, split ratio measured is 0.93 instead of the 0.9 expected at the design stage.

Table 7.2. Expected results vs. measured results of the main parameters of the system.

Parameter	Expected	Measured
Air to air heat exchanger effectiveness (-)	0.65	0.67±0.02
Solution heat exchanger effectiveness (-)	0.85	0.83±0.06
Maximum water flow rate in the absorber (kg/s)	3.30	1.73±0.08
Maximum water flow rate in the regenerator (kg/s)	4.40	2.24±0.01
Split ratio (-)	0.90	0.93±0.01
Solution mass flow rate in the absorber (kg/s)	1.80	2.42±0.03
Solution mass flow rate in the regenerator (kg/s)	1.80	2.47±0.02

7.7. Comparison of measured results with the designed results

According to the results shown and described in previous sections, the performance of the hybrid liquid desiccant system has been decreased for two main reasons:

- Wetting of tubes has not been as expected, due mainly to the bending of the tubes produced by the low rigidity of polypropylene.
- Water flow rates inside the air-solution contactors have been nearly 50 % lower than the expected because of high pressure drops of water inside them.

The first problem affects to the tube-solution heat transfer coefficient and to the mass transfer as it is detailed in Section 7.4.2. On the other hand, the second problem affects to the water-tube heat transfer coefficient because of both, the decreasing of the Reynolds number of water, and the average water temperature of the absorber and regenerator.

Therefore, the liquid desiccant temperature in the absorber is higher and in the liquid desiccant temperature in the regenerator is lower than expected. Since liquid desiccant temperatures affect much to the performance of the system (as it is shown in Sections 7.2, 7.3.1 and 7.3.2) dehumidification capacity of the system is reduced as well as the total load handled by the system. Moreover, since mass transfer is also reduced, dehumidification capacity is decreased even more.

In order to know how big is the decreasing of the performance of the hybrid liquid desiccant system, the dehumidification and the heat duty of the system have been compared for three different cases:

- Experimental results obtained from measurements.
- Results calculated by simulations taking into consideration heat and mass transfer coefficients at design conditions when full wettability was assumed and when the system operates at the designed flow rates.
- Results calculated by simulations taking into consideration tube-solution heat transfer coefficient and mass transfer coefficient at design conditions when full wettability was assumed, but with the measured flow rates.

These three different cases have been chosen in order to understand in a separate way the effect of the poorer wettability of tubes and the effect of the lower water flow rates. Left graph of Figure 7.27 illustrates a comparison of the dehumidification obtained in these three cases, whereas right graph of the same figure shows the comparison of the heat duty.

As expected, both, dehumidification and heat duty are the highest when assuming full wetting and designed flow rates. In addition, measured dehumidification and heat duty are the lowest of these three cases. The differences among the three cases are almost linear along the measured range.

When comparing dehumidification achieved at design conditions with the calculated with lower water flow rates a decreasing of about 5 % is obtained, whereas a decreasing of about 16 % is found when comparing design conditions with the measured dehumidification.

On the other hand, when comparing heat duty achieved at design conditions with the calculated with lower water flow rates a decreasing of about 7 % is obtained, whereas a decreasing of about 23 % is found when comparing design conditions with the measured heat duty.

Therefore, wettability problem has a higher effect on the dehumidification and the heat duty of the hybrid liquid desiccant system than lower water flow rates.

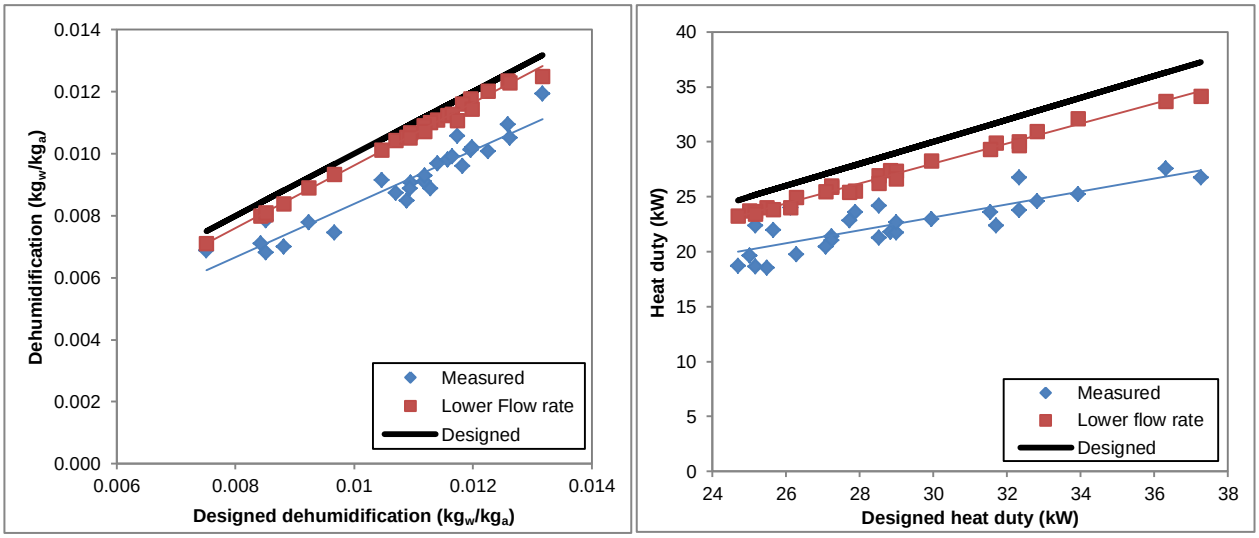

Figure 7.27. Comparison between the measured and the designed dehumidification (left) and heat duty (right) achieved in the hybrid liquid desiccant system.

7.8. Analysis of the independent control of temperature and humidity

One of the main objectives to be achieved by the hybrid liquid desiccant system is the independent control of the temperature and humidity of the locker rooms. In this section, the operational performance of three different typical days are analysed from the point of view of the air temperature and humidity ratio in order to verify that the independent control of both of them is gotten.

Among all the days when the system has been working in Taiwan, three very different days have been chosen to make this analysis:

- A very humid and warm day when ventilation loads are high.
- A cooler a dryer day when ventilation loads are medium.
- A cool and dry air when ventilation loads are low.

In total, 6 figures that contain the evolution during the day of the most relevant humidity ratios and temperatures are included:

- Ambient humidity ratio and temperature (W_{amb}, T_{amb}).
- Air temperature after the absorber (T_{abs}).
- Supply air humidity ratio and temperature (W_{sup}, T_{sup}).
- Return air humidity ratio and temperature (W_{room}, T_{room}).
- Room air set humidity ratio and air temperature (W_{set}, T_{set}).

In addition, blue bands in these figures represent the range between the maximum and the minimum values that room humidity ratio and room temperature were set in the control parameters.

Figure 7.28 illustrates the evolution of the humidity ratios (left) and air temperatures (right) of the warmest (up to 34 °C) and most humid measured day (up to 0.021 kg_w/kg_a). During this day, the hybrid liquid desiccant system had to operate at full load during the whole day. Under these conditions, neither the room temperature nor the room humidity ratio achieved the set point conditions along the day. However, they were kept below or near the maximum values assigned in most of the time (27 °C for the temperature and 0.014 kg_w/kg_a for the humidity ratio). In addition, absorber was able to dehumidify the air below 0.010 kg_w/kg_{da} and cool it down up to 26 ºC.

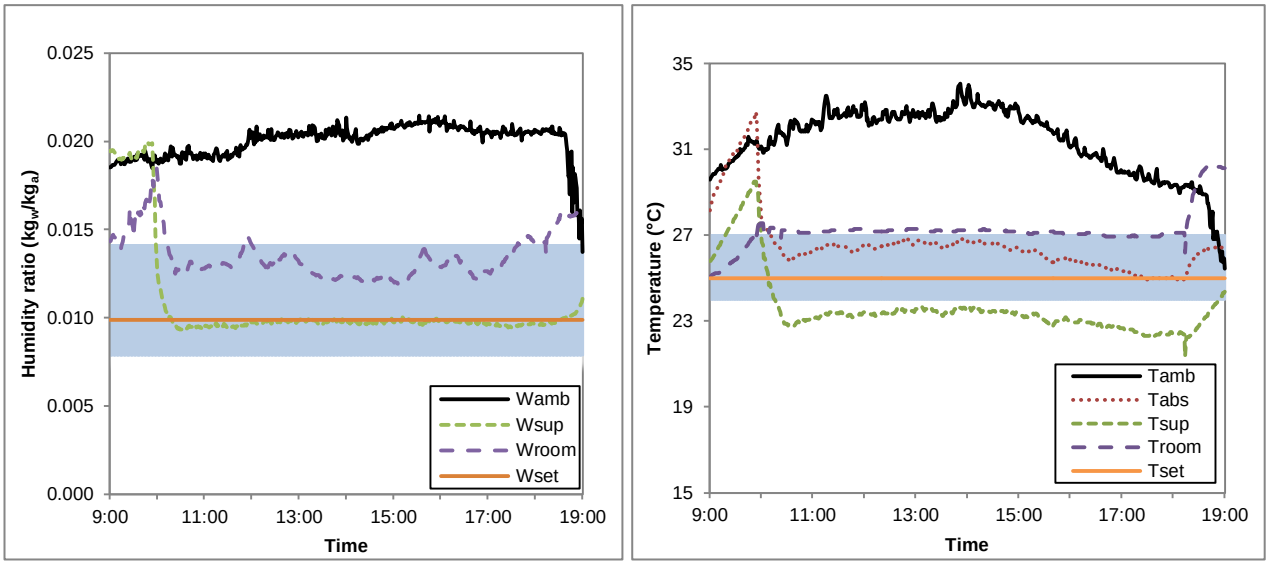

Figure 7.28. Temperatures and humidity ratios in the hybrid liquid desiccant system during a warm and humid day.

Comparing to the design conditions, ambient conditions in this day were warmer and with the same humidity ratio. On the other hand, internal loads were in the same range than expected at design conditions (about 16 kW). Therefore, the system was not able to reach expected results from design stage. This poorer behaviour is explained in detail in Section 7.7.

In any case, according to conditions of the locker rooms the results obtained during that day suggest that the system was able to keep acceptable comfort conditions. Probably, a higher capacity could have been achieved by the system, if it had operated with higher air flow rate and higher water flow rates in the absorber and the cooling coil.

Figure 7.29 illustrates a day when ambient temperature was about 24 °C and ambient humidity ratio was 0.016 kg_w/kg_a. During this day, the system was able to achieve the set point conditions in the locker room after 40 minutes of operation. After 14:30 h, it can be observed from the supply air conditions that, the system started to work at partial load trying to control and achieving the room temperature and humidity ratio (25 °C and 0.010 kg_w/kg_a, respectively). At the beginning of the day, under full load conditions, the absorber was able to dehumidify the air down to 0.007 kg_w/kg_a.

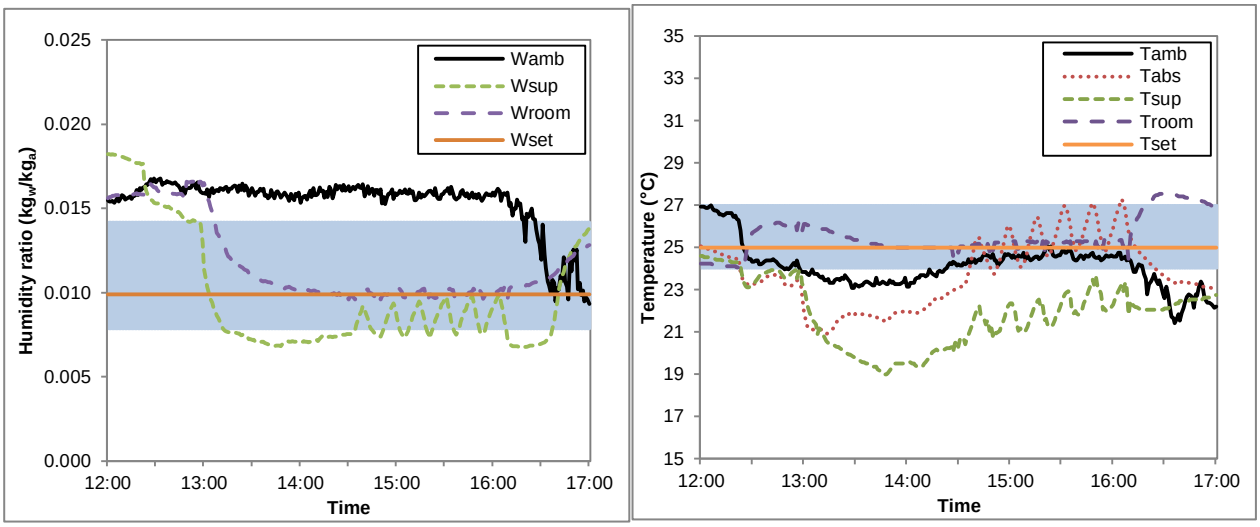

Figure 7.29. Temperatures and humidity ratios in the hybrid liquid desiccant system during a day with medium humidities and temperatures.

Finally, Figure 7.30 shows a day when ambient temperature was always below 23 °C and ambient humidity ratio was between 0.011 and 0.013 kg_w/kg_a. In this figure, it can be clearly observed that the hybrid liquid desiccant system controls separately the room humidity and temperature.

Under these dry ambient conditions, the system tried to control the set point humidity ratio. However, once the minimum value assigned for the humidity (0.008 kg_w/kg_a) was reached after 17:00 h the dehumidification of the system was stopped. After that moment, room humidity increased very fast and reached the maximum humidity in less than 15 minutes, when the dehumidification system started to operate again, being able to reach the set humidity ratio. Supply humidity ratio achieved by the absorber was below 0.005 kg_w/kg_a for some moments of the day.

On the other hand, in order to control the room temperature during this day, the coil in charge of controlling the temperature was operating in both, heating and cooling mode. Whenever the minimum set temperature inside the room (24 °C) was achieved, the coil changed from cooling to heating mode (this happened at 14:30 h, at 15:30 h, at 18:30 h and at 20:30 h). The opposite thing happened when the maximum set temperature inside the room (26 °C) was gotten (this happened at 14:00 h, at 15:00 h, at 18:00 h and at 19:30 h).

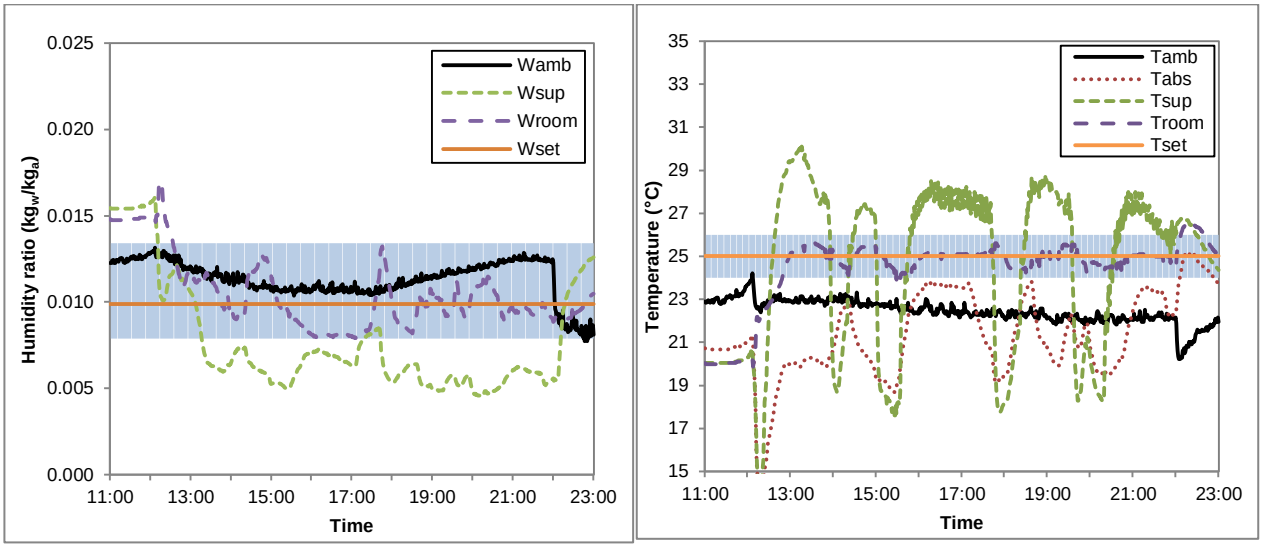

Figure 7.30. Temperatures and humidity ratios in the hybrid liquid desiccant system during a cool and dry day.

As conclusion, the hybrid liquid desiccant system shows an adequate independent control of the humidity and temperature of the locker rooms at different operational conditions.

7.9. Conclusions

The hybrid liquid desiccant system has been tested during its setting-up at Universitat Rovira i Virgili in Tarragona (Spain) and during its demonstration period at the National Taiwan University of Science and Technology (Taipei, Taiwan). Moreover, the performance of two different falling film air-solution contactors typologies has been tested: air-solution contactors with the in-line arrangement firstly, and air-solution contactors with the staggered arrangement secondly.

In both cases, liquid desiccant temperature has been shown as one of the most important parameters of the system behaviour, what shows that heat transfer in the air-solution contactors is crucial on the performance of the system.

When comparing the two typologies of air-solution contactors, the results show that in-line arrangement provides a higher mass transfer coefficient (about 20 % higher) and global heat transfer coefficient (about 9 %) than the staggered arrangement, which is contradictory with the expected results. The most likely

reasons that explain this fact are: tube wetting was much better in the in-line arrangement because the linear liquid desiccant flow rate is higher, and liquid desiccant is more cooled/heated because it has to pass around more tubes. Moreover, a poorer wettability of tubes due to a bad surface treatment on them could also explain this unexpected performance.

On the other hand, mass transfer coefficient in the air side and solution-tube heat transfer coefficient have been correlated as function of the air flow rate for the absorber and the regenerator with staggered arrangement. Small deviations of heat duty and dehumidification (below 10%) are obtained with these correlations when they are compared to the measured results.

During the demonstration period, the maximum cooling production of the hybrid liquid desiccant system has been about 34 kW and the maximum dehumidification nearly 0.012 $kg_w/kg_{a.}$ These results are about a 23 % and a 16 % lower than expected at design conditions because fully wetting of tubes was not reached and because air-solution contactors operated with lower water flow rates than it was expected at the design stage.

Both, the liquid desiccant COP and the global COP of the system mainly depends on the inlet water temperature in the regenerator and on the cooling load. The lower the water temperature in the regenerator and the higher the cooling load, the higher the liquid desiccant and the global COPs. The maximum COP of the liquid desiccant system is almost 1.5 and the maximum COP of the hybrid liquid desiccant system is about 3.8.

Finally, the presented hybrid liquid desiccant system shows an adequate independent control of the humidity and temperature of the locker rooms at different operational ambient conditions, either at warm and humid or at cool and dry air conditions.

Chapter 8. Modelling, validation and dynamic simulation of the hybrid liquid desiccant system

8.1. Introduction

Liquid desiccant systems are typically analysed by discrete steady-state simulations, which show how the system behaves for particular conditions. These are the cases of Ahmed et al. [117], Dai et al. [62] or Gommed and Grossman [105]. With these simulations, sensitivity analysis about the system performance as function of some key parameters, such as ambient conditions or working temperatures, can be achieved.

However, dynamic simulations offer the possibility of obtaining the seasonal performance as well as making a deep study of the control strategies that permits a better use of these systems in terms of energy savings or comfort. In particular for liquid desiccant systems, dynamic simulations are very useful because the operation of these systems is, during most of the time, in transient conditions.

In this sense, Yamaguchi et al. [43] used the Simulink tool to dynamically simulate a hybrid liquid desiccant system. More recently, Coca et al. [118] modelled and dynamically simulated a liquid desiccant system activated by solar energy by using TRNSYS. Instead of creating a new component on TRNSYS for the air-solution contactors, they obtained the performance of the absorber and the regenerator of a liquid desiccant system by using parametric tables generated from EES. Crofoot [119] also modelled and dynamically simulated a validated solar liquid desiccant system on TRNSYS. In this case, a new component for the absorber and the regenerator was conducted.

With the objective of improving the performance of the hybrid liquid desiccant system along the year, a model of the hybrid liquid desiccant system has been developed on TRNSYS. Therefore, the modelling of the system is firstly presented in this chapter. Then, the results obtained from the model are compared with real measurements in order to validate it. Once the model is validated, it is used to optimize the performance of the system by varying the operational conditions of the system and trying two different control strategies. Finally, a sensitivity analysis of the system is conducted in order to understand in a deeper way how three of the main operational parameters of the system affect to the seasonal performance of it.

8.2. Modelling of the hybrid liquid desiccant system

Figure 8.1 illustrates a simplified scheme of the system modelled for the dynamic simulations. As it can be observed from this figure, the main components of the hybrid liquid desiccant system are included in the model with the exception of the heat pump. This device is not included in the model because it is a quite complicate element to be modelled due to its internal control which has to manage how much energy is transferred to the hot circuit, the cold circuit and wasted to the air. Moreover, values of temperatures and flow rates of the hydraulic circuit of the system are taken from measurements. Therefore, these values can be directly used for the validation of the rest of the system without the need of including the heat pump.

On the other hand, zone has been required to be modelled due to the return air is used for the regeneration of the LiCl-H_2O through the regenerator. Most of the components are available either in the standard libraries of TRNSYS [120] or in the TESS libraries, with the exception of the solution tanks and the air-solution contactors. For this reason new types for the solution tanks and the air-solution contactors have been created for this purpose.

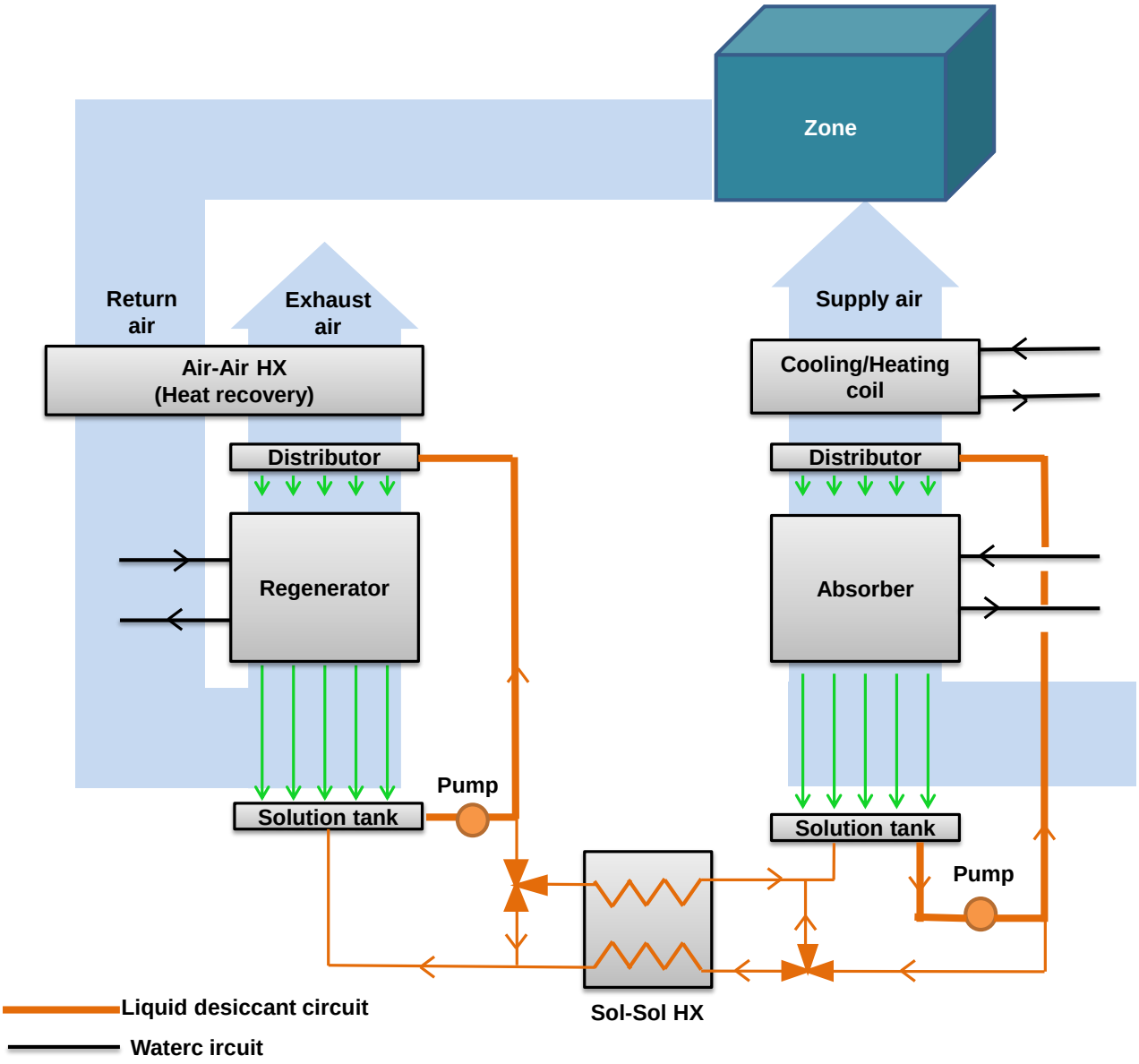

Figure 8.1. Schematic with the elements modelled for the dynamic simulations.

8.2.1. Modelling of the air-solution contactors

Since there were not available components on the standard libraries of TRNSYS of air-solution contactors for liquid desiccant systems, a component of internally cooled/heated air-solution contactor has been developed on FORTRAN. Table 8.1 contains the parameters (variables that do not change with time), inputs (variables that can change with time) and outputs of the developed component on TRNSYS with their corresponding units.

The model developed on FORTRAN is based on the equations explained in Chapter 5. In the same way that in that chapter, 12 variables are required to be calculated, and therefore, 12 equations are needed to be solved. These equations are the same that the given in Chapter 5 (equations 5.1-5.4, 5.6-5.11, 5.16 and 5.17). Multivariable Newton-Raphson method has been used to solve this system of equations.

On the other hand, LiCl-H_2O correlations for the properties given by Conde [23] have been used instead of the properties given by Pátek and Klomfar [24]. The main reason to use the correlations given by Conde is that not iterations are needed to calculate them, what makes easier the development of the model and reduces the simulation time.

As it can be observed from Table 8.1, heat and mass transfer coefficients of the air-solution contactors are required as inputs by the model. This means that they can change along the time, as it happens on the real system, where heat and mass transfer coefficients depend on the air flow rate (see Section 7.5). Correlations of the solution-tube heat transfer coefficient and of the mass transfer coefficient in the air side obtained from the experimental measurements of the hybrid liquid desiccant system (see Table 7.1) are taken into consideration for the calculation of the heat and mass transfer coefficients required in the air-solution contactors model.

Table 8.1. Parameters, inputs and outputs of the developed component on TRNSYS for the air-solution contactors.

Parameters	Inputs	Outputs
Inside pipe diameter (m)	Inlet solution mass flow rate (kg/s)	Outlet solution mass flow rate (kg/s)
Outside pipe diameter (m)	Inlet water mass flow rate (kg/s)	Outlet air temperature (K)
Height (m)	Inlet air mass flow rate (kg/s)	Outlet water temperature (K)
Length (m)	Inlet solution temperature (K)	Outlet solution temperature (K)
Number of rows (-)	Inlet water temperature (K)	Top air-solution interface temperature (K)
Width (m)	Inlet air temperature (K)	Bottom air-solution interface temperature (K)
	Inlet air humidity ratio (kg_w/kg_a)	Outlet air humidity ratio (kg_w/kg_a)
	Inlet LiCl mass fraction (-)	Top air-solution interface humidity ratio (kg_w/kg_a)
	Air-solution heat transfer coefficient (kW/K)	Bottom air-solution interface humidity ratio (kg_w/kg_a)
	Solution mass transfer coefficient (kg/s)	Outlet solution mass fraction (-)
	Air mass transfer coefficient (kg/s)	Top air-solution interface mass fraction (-)
	Overall heat transfer coefficient (kW/K)	Bottom air-solution interface mass fraction (-)
		Outlet water mass flow rate
		Number of iterations (-)
		Norm of the solution vector (-)

8.2.2. Modelling of the liquid desiccant tanks

Since the storage capacity of the solution tanks is related not only by the temperature of the liquid desiccant, but also by the concentration of the liquid desiccant, the model of the liquid desiccant tanks must take into account a changeable mass inside them, as well as a variable liquid desiccant concentration. However, there are not types available in the standard libraries on TRNSYS with these features. For this reason, a model of the solution tanks had to be modelled.

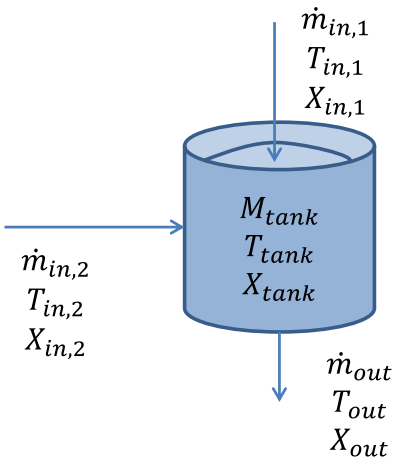

Figure 8.2. Schematic picture of the liquid desiccant tank model.

Energy and mass balance equations have been used in this model. Moreover, complete mixing has been assumed for it. Therefore, the equations that model the solution tanks are:

Tank mass balance

$$M_{tank}(kg) = M_{LiCL} + M_w \tag{8.1}$$

Liquid desiccant mass balance:

$$M_{LiCL}(kg) = M_{LiCL,-1} \tag{8.2}$$

Water mass balance:

$$M_w(kg) = M_{w,-1} + [\dot{m}_{in,1} \cdot (1 - X_{in,1}) + \dot{m}_{in,2} \cdot (1 - X_{in,2}) - \dot{m}_{out} \cdot (1 - X_{tank,-1})] \cdot timestep \tag{8.3}$$

Tank LiCl mass concentration:

$$X_{tank} = \frac{M_{LiCL}}{M_{tank}} \tag{8.4}$$

Tank energy balance:

Tank energy balance has been approximated with temperatures:

$$T_{tank}(°C) = T_{tank,-1} + \left[\frac{\dot{m}_{in,1} \cdot T_{in,1}}{M_{tank}} + \frac{\dot{m}_{in,2} \cdot T_{in,2}}{M_{tank}} - \frac{\dot{m}_{out} \cdot T_{out}}{M_{tank}} - \frac{UA_{tank} \cdot (T_{tank,-1} - T_{amb})}{M_{tank} \cdot c_{p,tank,-1}}\right] \cdot timestep \tag{8.5}$$

Where $c_{p,tank}$ is the specific heat of the liquid desiccant calculated from Conde correlations [23].

In the above equations subscript *-1* means the value of the variable in the previous time step. The standard component Type 93 has been used in order to recall the variables of the previous time step. In order to achieve convergence along the simulation and accurate results, time step of the simulation has been set very short (6 seconds).

Table 8.2 contains the parameters of the liquid desiccant tanks set for the simulations. Starting mass of the solution tanks corresponds with the amount of liquid desiccant added to the system during its operation in Taipei. Global heat transfer coefficient of the solution tanks has been adjusted by evaluating the evolution of the measured liquid desiccant temperature inside the solution and the ambient temperature.

Table 8.2. Parameters of the liquid desiccant tanks simulated on TRNSYS.

Parameter	Value
Starting mass (kg)	200
Starting LiCl mass concentration (-)	0.35
Starting temperature (°C)	25
Starting specific heat of the solution (kJ/kg·°C)	2.71
Global heat transfer coefficient (kW/°C)	0.021

8.2.3. Modelling of other components

Apart from the air-solution contactors and the solution tanks, there are additional components that must be included for the modelling of the liquid desiccant system. All the components described in this section are taken from standard libraries of TRNSYS or from libraries available from TESS models.

8.2.3.1. Heat exchangers

Two of the three heat exchangers of the hybrid liquid desiccant system (the solution heat exchanger and the air-air heat exchanger) have been modelled with the standard component of TRNSYS Type91 [120]. In this component, the following assumptions are taken into account:

- Only sensible heat takes place within it.
- Constant effectiveness.
- Zero capacitance of the heat exchanger.
- Constant specific heat of the fluids along the time.

The cooling/heating coil has been modelled with the standard component of TRNSYS Type5d [120]. In this component, the following assumptions are taken into account:

- Only sensible heat takes place within it.
- Zero capacitance of the heat exchanger.
- Constant specific heat of the fluids along the time.
- Overall heat transfer coefficient is given as an input.

Table 8.3 contains the parameters set for the simulations. Effectiveness of the solution heat exchanger and the air-air heat exchanger are the obtained during the operation of the system in Taipei (see Table 7.2). Global heat transfer coefficient is calculated from the measured values of the supply air conditions (temperature and air flow rate) and the water temperature and flow rate inside the cooling/heating coil.

Table 8.3. Parameters of the heat exchangers simulated on TRNSYS.

Parameter	Solution heat exchanger	Air-air heat exchanger	Cooling/Heating coil
Cold side specific heat (kJ/kg·°C)	2.72	1.02	4.19
Hot side specific heat (kJ/kg·°C)	2.66	1.02	1.02
Effectiveness (-)	0.83	0.67	-
Overall heat transfer coefficient (kW/°C)	-	-	4.00

8.2.3.2. Pumps and diverting valves

The hydraulic components of the liquid desiccant system are two pumps that take the liquid desiccant from the solution tanks, and two diverting valves that distribute the liquid desiccant flow through the different branches of the circuit.

Pumps are modelled with the Type3b from the standard libraries of TRNSYS [121]. This is a pump with a constant flow rate. The liquid desiccant flow rate has been set at 2.5 kg/s, which is in agreement with the measured values of the system in Taipei.

On the other hand, diverting valves are modelled with the Type647 from the TESS libraries. The split ratio set for the two diverting valves of the circuit is 0.93, which is in agreement with the measured values of the system in Taipei (see Table 7.2).

8.2.3.3. Zone

It is necessary to model the internal loads of the two locker rooms for the following reasons:

- Because the return air is used to regenerate the liquid desiccant.
- In order to evaluate the comfort achieved with the system.
- In order to use room conditions as variables to be controlled for the control components.

The model used for the locker rooms is Type759 from the TESS libraries. This model calculates the air temperature and humidity ratio of the room with heat and mass balances at each time step. Moreover, it takes into account the infiltration effects, ventilation effects, wall losses, internal heat and mass gains and exchanges with adjacent zones.

In this case, since total loads are known from measurements of the supply air conditions and return air conditions, infiltration, ventilation, wall effects and exchanges with adjacent zones have been set as 0. For each measured time step, real internal heat gains have been calculated from equation 5.42.On the other hand, water gains have been calculated from the equation 5.43.

For the validation of the model the capacitance of the zone has been chosen 0 because it is included in the measured heat and mass gains. However, for the annual simulations thermal capacitance of the room has been set as 5000 kJ/°C and moisture capacitance of the room as the double of the air capacitance.

8.2.3.4. Control components

One of the main advantages of dynamic simulations is the possibility of including the control in the model. This is very useful in order to identify the most efficient control strategy or operational conditions. In this sense, two control strategies for the regeneration process have been designed and experimentally evaluated (see section 6.3).

Moreover, different set point temperatures for both, chilled and hot water, as well as different operational values for the concentration of the liquid desiccant have been experimentally compared during the operation of the system in Taipei and Tarragona.

Two different standard components have been used for the implementation of the control in the liquid desiccant system:

- Type2d, which is a generic differential controller. This component has been used to start or stop operating the regeneration process as function of the LiCl mass concentration at the inlet of the absorber.
- Type2b, which is a temperature differential controlled. This component has been used to set if the system is operating in heating or cooling mode as function of the room temperature.

8.2.4. Integration of all the components

Figure 8.3 is a screenshot with the modelled liquid desiccant system taken from the Simulation Studio tool of TRNSYS.

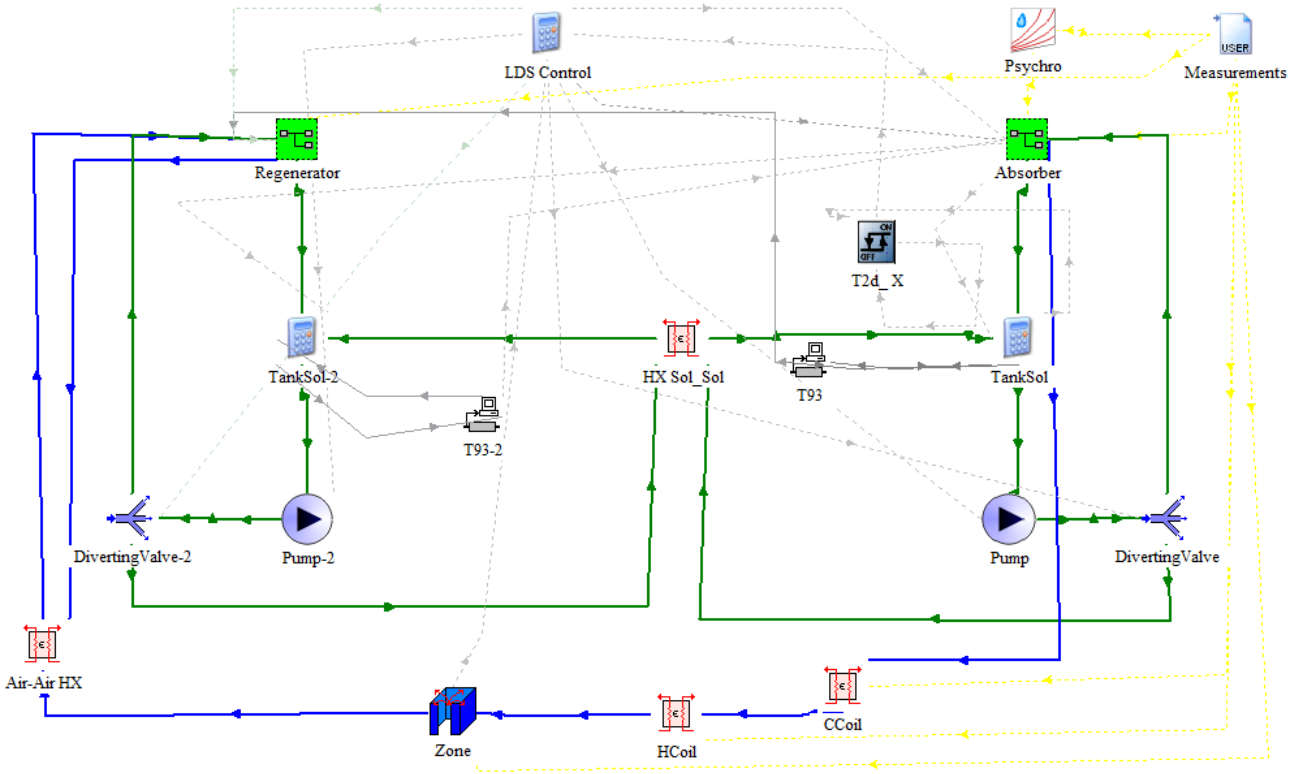

Figure 8.3. Screenshot from of the modelled liquid desiccant system.

For the validation of the system, measurements taken from the system during its operation in Taiwan have been used as inputs of the system. These measurements are:

- Ambient temperature.
- Ambient humidity ratio.
- Supply air mass flow rate.

- Inlet water temperature in the absorber.
- Water flow rate in the absorber.
- Inlet water temperature in the regenerator.
- Water flow rate in the regenerator.
- Inlet water temperature in the coil.
- Inlet water mass flow rate in the coil
- Internal sensible load (kW).
- Internal moisture generation (kg/h).

These measurements are given with a time step of 1 minute.

8.3. Validation of the model

In order to validate the developed model, outputs calculated from simulations are compared with real measurements of the system. In this sense, the comparison is done for two days when the control strategy of the real system was different.

Figure 8.4 shows the comparison of the air humidity ratios between the calculated with the dynamic simulation and the measured values of the real system. Very low discrepancies are found in both, supply and room humidity ratios. Moreover, these good results are gotten for the two control strategies studied in this case.

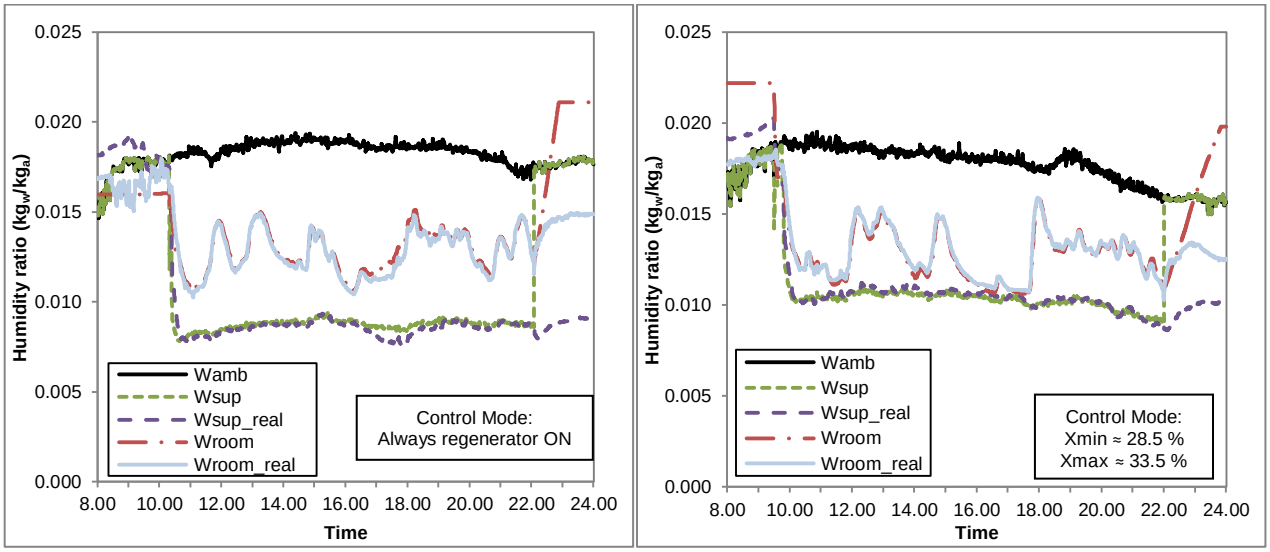

Figure 8.4. Comparison between calculated and measured air humidity ratios for a typical day.

Figure 8.5 shows the comparison of the air temperatures between the calculated with the dynamic simulation and the measured values of the real system. Calculated temperatures are slightly lower than measured for both, supply and room conditions. Moreover, these good results are gotten for both control strategies.

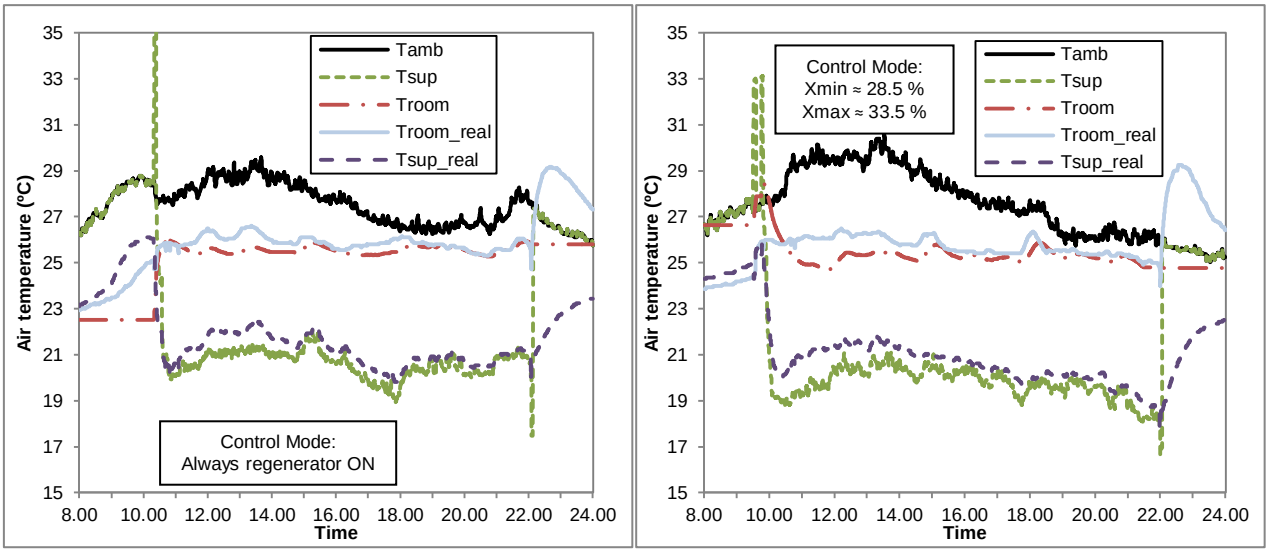

Figure 8.5. Comparison between calculated and measured air temperatures for a typical day.

Figure 8.6 shows the comparison of the outlet water temperature and the inlet solution temperature in the absorber calculated with the dynamic simulation and the measured values of the real system. Very low discrepancies are found in both outlet water temperature and inlet solution temperature. As in the previous comparisons, these good results are gotten for the two control strategies.

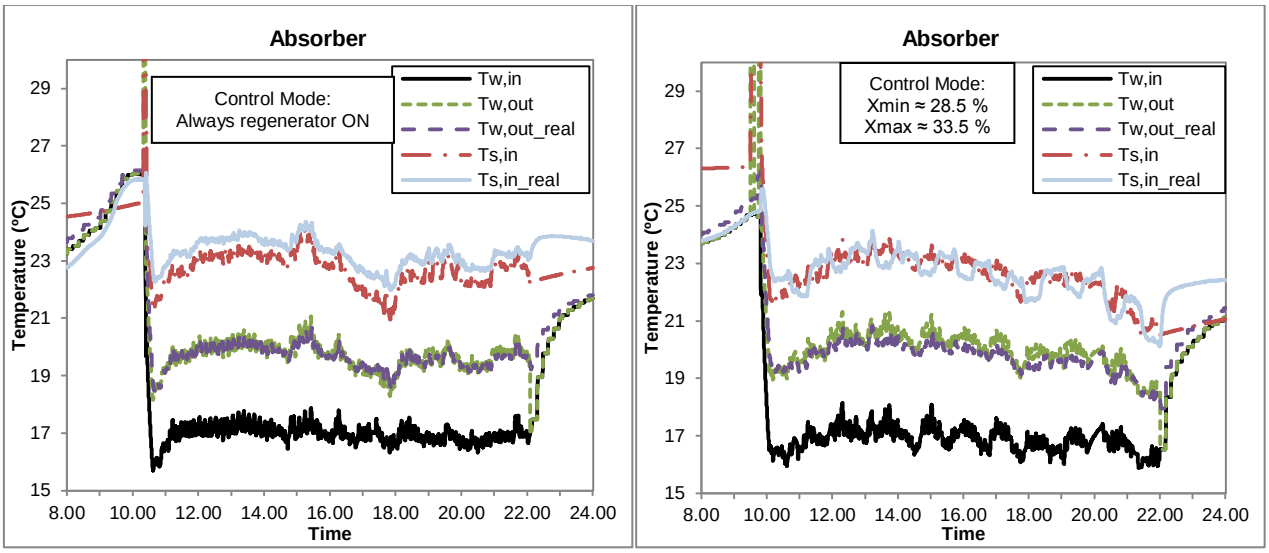

Figure 8.6. Comparison between calculated and measured absorber temperatures for a typical day.

Finally, Figure 8.7 shows the comparison of the outlet water temperature and in the inlet solution temperature in the regenerator between the calculated with the dynamic simulation and the measured values of the real system. Very low discrepancies are found in both, the outlet water temperature and the inlet solution temperature when the regenerator is always ON. However, having a first look at the other control strategy, it seems that there are higher discrepancies between the measured and the calculated results. The reason why this happens is that with this control strategy, the regenerator is not always operating, and therefore, if initial conditions of the LiCl mass concentration are not exactly the same for the real and the simulated case, or if the total mass of the liquid desiccant is not exactly the same, the regenerator will operate at different moments in simulated and in real system. In any case, the number of starts/stops and the average temperature of outlet water and inlet solution are almost the same for the calculated and the measured results when regeneration of the desiccant is happening. This suggests that these discrepancies could not be due to a problem with the equations of the model or the correlations.

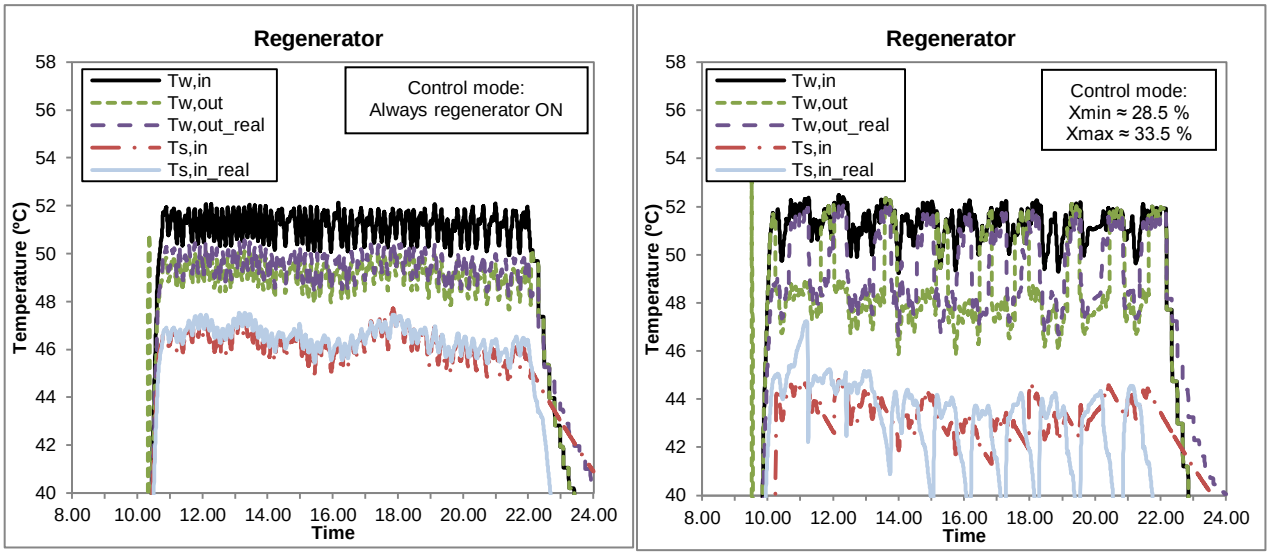

Figure 8.7. Comparison between calculated and measured regenerator temperatures for a typical day.

Table 8.4 shows a statistical comparison between the results obtained in the simulated model and the measured data taken during the two compared days. In the same way than in the previous figures, good approximation of the compared variables are achieved with the modeled liquid desiccant system. Only higher discrepancies are taken on the outlet water temperature in the regenerator when the regenerator operates as function of the LiCl mass concentration. However, the average outlet water temperature in the regenerator in both, the measured and the simulated results, are quite similar, what suggests that this deviation could be due to the regenerator is not operating at the same time in the simulated and in the real system.

Table 8.4. Statistical comparison between measured and simulated data.

Variable		Regenerator ON	By LiCl mass concentration
W_{sup}	**Standard deviation**	0.00039	0.00017
	Average calculated	0.00876	0.01025
	Average measured	0.00861	0.01035
W_{room}	**Standard deviation**	0.00029	0.00019
	Average calculated	0.01285	0.01266
	Average measured	0.01269	0.01275
T_{sup}	**Standard deviation**	0.30	0.41
	Average calculated	20.62	19.76
	Average measured	21.15	20.50
T_{room}	**Standard deviation**	0.29	0.42
	Average calculated	25.56	25.27
	Average measured	25.88	25.72
$T_{w,out,abs}$	**Standard deviation**	0.23	0.40
	Average calculated	19.68	19.94
	Average measured	19.66	19.81
$T_{w,out,reg}$	**Standard deviation**	0.13	2.39
	Average calculated	49.34	48.49
	Average measured	49.52	48.71

8.4. Selection of the best control strategy and operational conditions

Once the model is validated with real measurements, it can be used in order to optimize the operation of the system. In this sense, it is interesting to figure out which are the optimal control strategy and the operational conditions of the system that improve its performance along the year.

8.4.1. Modifications to the base case

For the annual simulation of the system, it is necessary to add new components to the model in order to provide an independent control that regulates the water and air flow rates. For this reason, a PID component (Type23 of standard libraries) has been included to the model of the system three times:

- To set the air flow rate as function of the room temperature.
- To set the water flow rate at the inlet of the absorber as function of the room humidity ratio.
- To set the water flow rate at the inlet of the cooling/heating coil as function of the supply air temperature.

Both, gain constant and integral time have been separately tuned in order to improve the actuation of the PID controllers. Moreover, maximum and minimum values for the flow rates are in agreement with the obtained in the real system.

8.4.2. Definition of the objectives and description of the simulated cases

In order to select the best control strategy and the operational conditions of the hybrid liquid desiccant system, two parameters have been used to be optimized: the annual heating transferred in the condensers of the heat pump (to the system or dissipated to the ambient) and the number of hours out of comfort conditions inside the rooms. The annual heating transferred in the condensers has been chosen because of the way that the heat pump is controlled: the two compressors operate to follow the maximum load either in the evaporator or in the condenser. If cooling required in the evaporator is higher than in the condenser, a parallel air-condenser dissipates the waste heat to the ambient. If heating required in the condenser is higher than in the evaporator, a parallel air-evaporator dissipates the waste cold to the ambient.

The annual heating transferred in the condensers has been calculated as the integration along the year of the maximum of the heating rate required by the system or the heating rate produced by the heat pump because of the cooling rate required by the system in each time step. This means:

$$Q_{cond} = \int_0^{8760} \max\left(\left(\dot{Q}_{w,abs} + \dot{Q}_{w,cc}\right) \cdot \left(1 + \frac{1}{COP_{HP}}\right), \dot{Q}_{w,reg} + \dot{Q}_{w,hc}\right) \cdot dt \tag{8.6}$$

The COP has been considered as the given of the catalogue of the heat pump, which depends on the set points of the water at the outlet of the evaporator and the condenser. The following equation gives the COP of the heat pump:

$$COP_{HP} = \frac{2.96}{1.01 \cdot \left[1.16 + 0.01 \cdot \left(T_{evap} - 12\right) + 0.02 \cdot \left(T_{cond} - 51\right)\right]} \tag{8.7}$$

Where 2.96 is the COP of the heat pump at nominal conditions and the denominator of the fraction is the correcting equation as function of the evaporator and condenser set point temperatures.

Comfort conditions have been taken into account for both, the room air temperature and the relative humidity. For the air temperature, the minimum and the maximum values are 24 °C and 27 °C respectively. For the air relative humidity, the minimum and the maximum values are 45 % and 65 %, respectively. Every time step that the system is operating and one of these conditions are not reached, is considered as out of comfort conditions.

In total, 45 operational conditions and control strategies have been simulated in order to choose the optimal of them: 36 operational conditions for the control strategy in which regenerator operation is controlled by the LiCl mass concentration at the inlet of the absorber, and 9 operational conditions for the control strategy in which regenerator operates if absorber operates too. Table 8.5 shows the operational conditions and control strategies simulated. Maximum LiCl mass concentration has been 5 % higher than minimum in all the cases.

These operation variables have been chosen because they are easily changeable from the configuration and the system and they are expected to affect the performance of the system.

Table 8.5. Operational conditions and control strategies simulated.

Operational conditions	Control strategy	
	Regenerator controlled by LiCl mass concentration (%)	Regenerator is ON if absorber is ON
Minimum LiCl mass concentration at the inlet of the absorber (%)	27.5, 30.0, 32.5, 35.0	-
Absorber inlet water temperature (°C)	12, 14, 16	12, 14, 16
Regenerator inlet water temperature (°C)	51, 53, 55	51, 53, 55

Since the use of the locker rooms is, approximately, constant along the year, the internal loads have been modelled from 14 measured days when the hybrid liquid desiccant system is operating at real conditions. For the annual simulations, these days have been repeated along the 365 days of the year. Figure 8.8 illustrates both internal moisture gain and internal sensible load of these 14 days. The internal loads values are given with a time step of 1 minute.

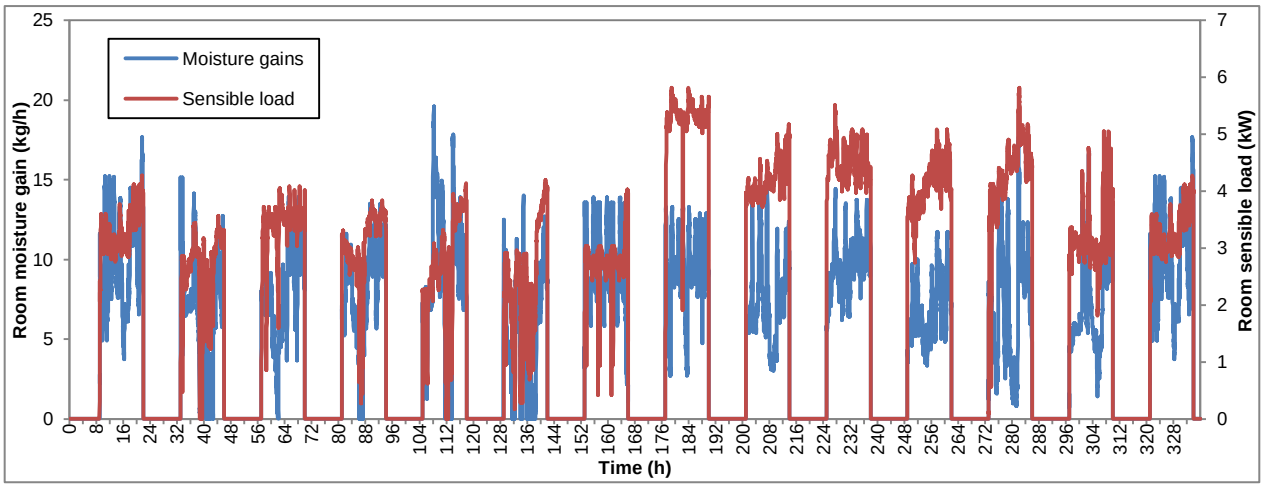

Figure 8.8. Defined internal loads on TRNSYS.

8.4.3. Annual optimization

Since this is a multi-objective optimization, the optimal solution is one of the points of the Pareto front. Depending on the relative significance of the number hours out of comfort or the heating transferred in the condenser, the selected point could be in one of the extremes of the Pareto front or in the middle of it. Figure 8.9 shows the annual heating required from the condenser and the hours out of comfort of the 45 simulations. In this figure, Pareto front is highlighted with a darker colour.

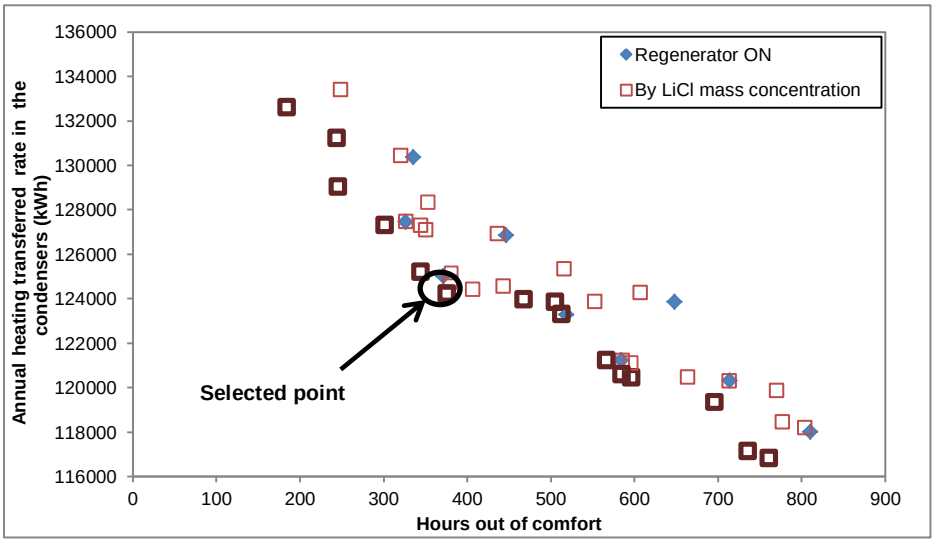

Figure 8.9. Annual heating transferred in the condensers vs. hours out of comfort of the 45 simulated cases.

The selected point corresponds to an inlet water temperature in the absorber of 12 °C, an inlet water temperature in the regenerator of 51 °C and a minimum LiCl mass concentration of 32.5 %. In general, the control strategy in which the operation of the regenerator is controlled by the LiCl mass concentration presents better results than the other, in which regenerator is operating whenever the absorber is operating too.

8.4.4. Monthly optimization

Table 8.6 contains a summary of the ambient temperature and humidity ratio taken from the hourly weather data file of Taipei used for the simulation. As it can be observed from this table, ambient conditions are quite different from winter to summer conditions, what suggests that there could not be an only control strategy and operational conditions that is the best along the whole year, but these could change with time.

Table 8.6. Summary of the ambient conditions of Taipei used for the simulations.

	Average temperature (°C)	Minimum temperature (°C)	Maximum temperature (°C)	Average humidity ratio (kg_w/kg_a)	Minimum humidity ratio (kg_w/kg_a)	Maximum humidity ratio (kg_w/kg_a)
January	16.09	6.00	27.60	0.00903	0.00484	0.01376
February	16.16	10.00	25.30	0.00983	0.00614	0.01458
March	18.10	11.85	31.40	0.01082	0.00596	0.01761
April	21.78	14.90	31.50	0.01404	0.00804	0.02042
May	24.69	16.85	34.30	0.01651	0.01110	0.02250
June	27.15	20.90	34.15	0.01860	0.01469	0.02237
July	29.53	24.50	37.90	0.02063	0.01409	0.02417
August	28.94	23.00	36.95	0.01945	0.01419	0.02288
September	27.00	21.15	32.95	0.01844	0.01209	0.02235
October	23.70	17.00	32.00	0.01417	0.00894	0.01920
November	21.93	10.00	30.00	0.01332	0.00658	0.01770
December	17.82	9.50	28.20	0.00994	0.00528	0.01720

For this reason, results from the 45 simulations have been analysed month by month in order to obtain the best control strategy and operational conditions that minimize the hours out of comfort and the heat transferred in the condensers of the heat pump. Table 8.7 contains the selected control strategy and operational conditions of the system that optimized these two variables month by month.

In general, according to results of this optimization, when the ambient humidity ratio is high, the inlet water temperature in the regenerator and the absorber that optimize the operation of the hybrid liquid desiccant system must be more separated. It is more difficult to try to find a relationship for the LiCl mass concentration values.

Table 8.7. Selected control strategy and operational conditions of the system in each month.

	Control strategy	Inlet temperature in the regenerator (°C)	Inlet temperature in the absorber (°C)	Minimum LiCl mass concentration at the inlet of the absorber (%)
January	By LiCl mass concentration	51	14	30.0
February	By LiCl mass concentration	51	14	32.5
March	By LiCl mass concentration	51	14	30.0
April	By LiCl mass concentration	53	16	30.0
May	By LiCl mass concentration	53	12	30.0
June	By LiCl mass concentration	53	14	35.0
July	By LiCl mass concentration	55	12	27.5
August	By LiCl mass concentration	53	12	27.5
September	By LiCl mass concentration	53	12	27.5
October	By LiCl mass concentration	51	16	30.0
November	By LiCl mass concentration	51	16	27.5
December	By LiCl mass concentration	51	16	27.5

8.4.5. Annual vs. monthly optimization

Figure 8.10 illustrates, in the same way that Figure 8.9, the annual heating transferred in the condensers and the number of hours out of comfort. However, this figure also includes the result obtained from the simulation with the monthly optimization. Compared to the selected point with the annual optimization, there is a reduction of both, heating transferred in the condenser and number of hours out of comfort. In terms of heating transferred in the condenser, the reduction with the monthly optimization is almost 1.5 %. On the other side, in terms of hours out of comfort, the reduction is higher than 19 %.

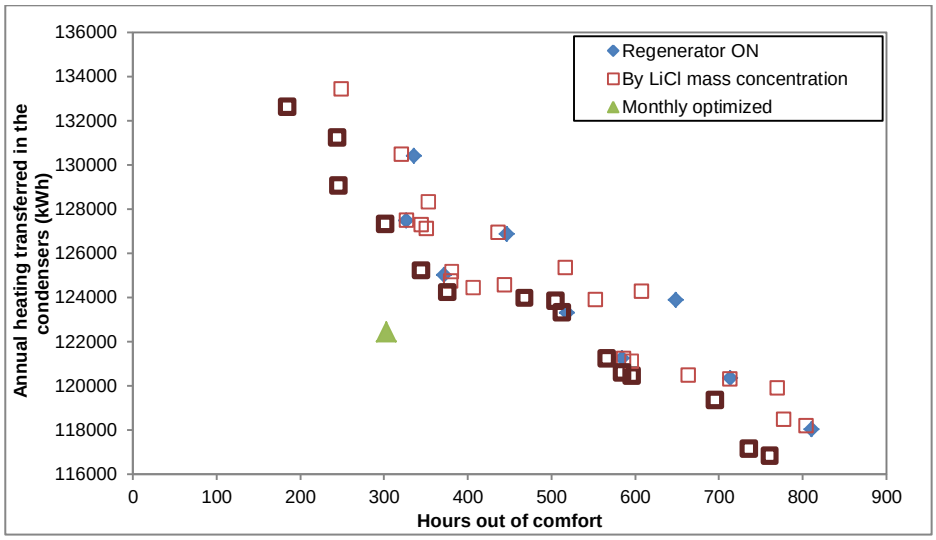

Figure 8.10. Annual heating transferred in the condensers vs. hours out of comfort of the 45 simulated cases and the monthly optimized case.

Figure 8.11 contains the monthly results of the number of hours out of comfort conditions for both, the simulation with the monthly optimized control strategy and the annual optimized operation conditions. In the same way, Figure 8.12 illustrates the monthly results of the heating transferred in the condensers in both simulations. It can be observed that the number of hours out of comfort conditions is much higher during warm and humid months due to the lack of thermal capacity of the system. In addition, in most of the months the hours out of comfort are reduced with the monthly optimization without increasing much the heat transferred in the condensers. Moreover, some months (like from October to December), both, hours out of comfort and heat transferred in the condensers, are reduced with the monthly optimization.

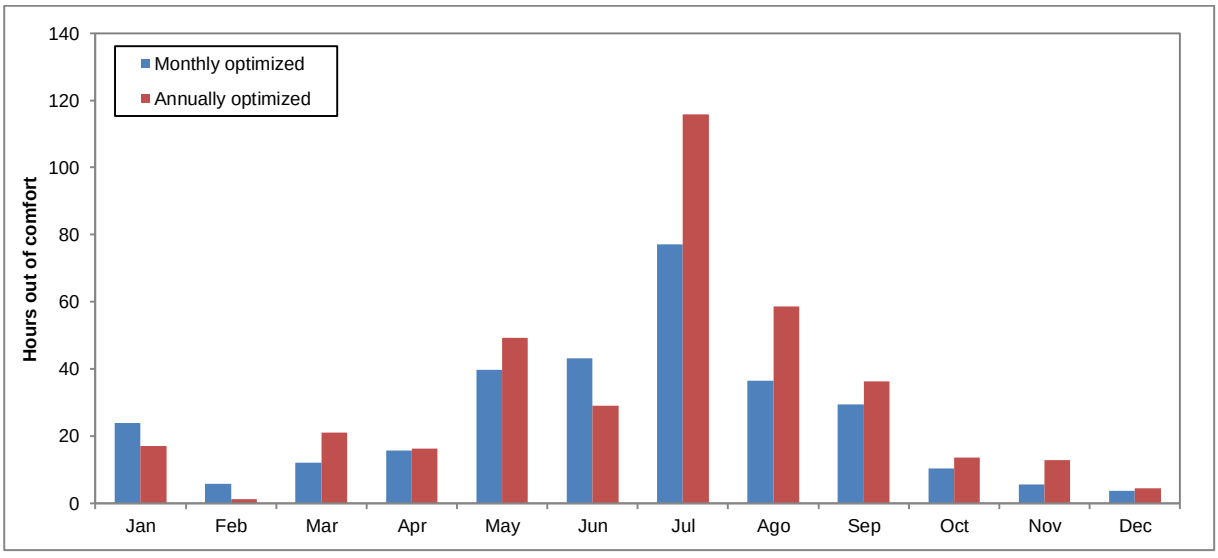

Figure 8.11. Monthly results of the hours out of comfort achieved with the hybrid liquid desiccant system monthly optimized and annually optimized.

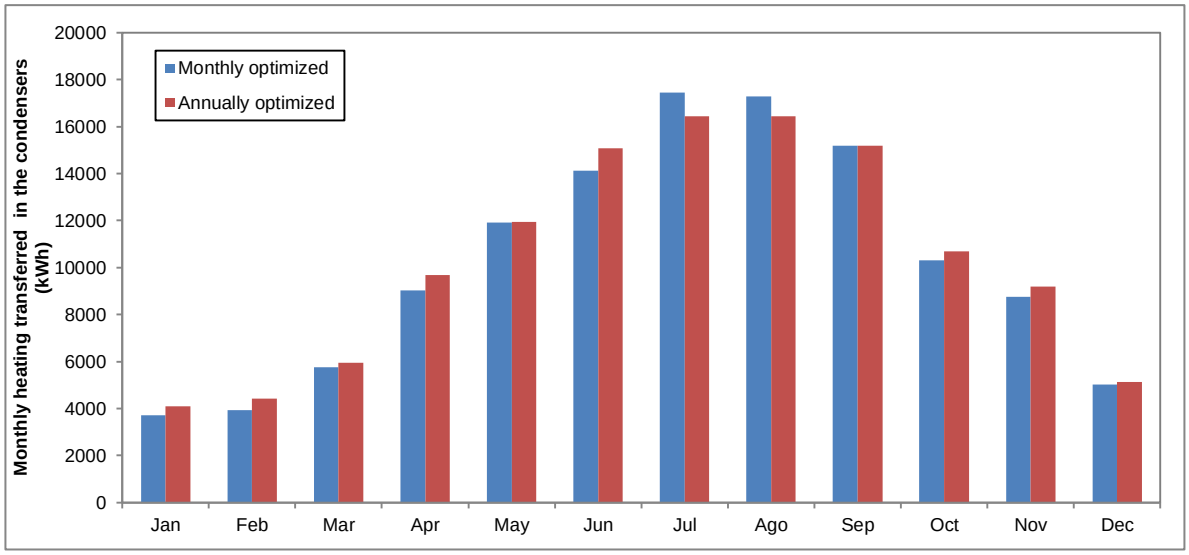

Figure 8.12. Monthly results of the heating transferred from the condensers with the hybrid liquid desiccant system monthly optimized and annually optimized.

8.4.6. Annual results of the system

Figure 8.13 shows the seasonal performance of the hybrid liquid desiccant system calculated from the monthly optimized strategy. Since the system does not recirculate any air from the room, the thermal loads are very affected by the ambient conditions. This can be observed from this figure because room load is almost constant along the year, but the other thermal loads change much with time.

During summer, the total cooling required by the liquid desiccant system is almost the same that the total heating required. However, during winter, the total heating is about the double than the total cooling. This difference is not only due to the heating in the coil, but also to the heating in the regenerator that is higher in winter months that the heat duty in the absorber. This effect is explained because the COP of the liquid desiccant system decreases whit the cooling load, as it was detailed in Section 7.6.3.

Finally, absorber provides most of the total cooling to the air because of two reasons: latent cooling is high in comparison with sensible cooling, and part of the sensible cooling is provided by the absorber.

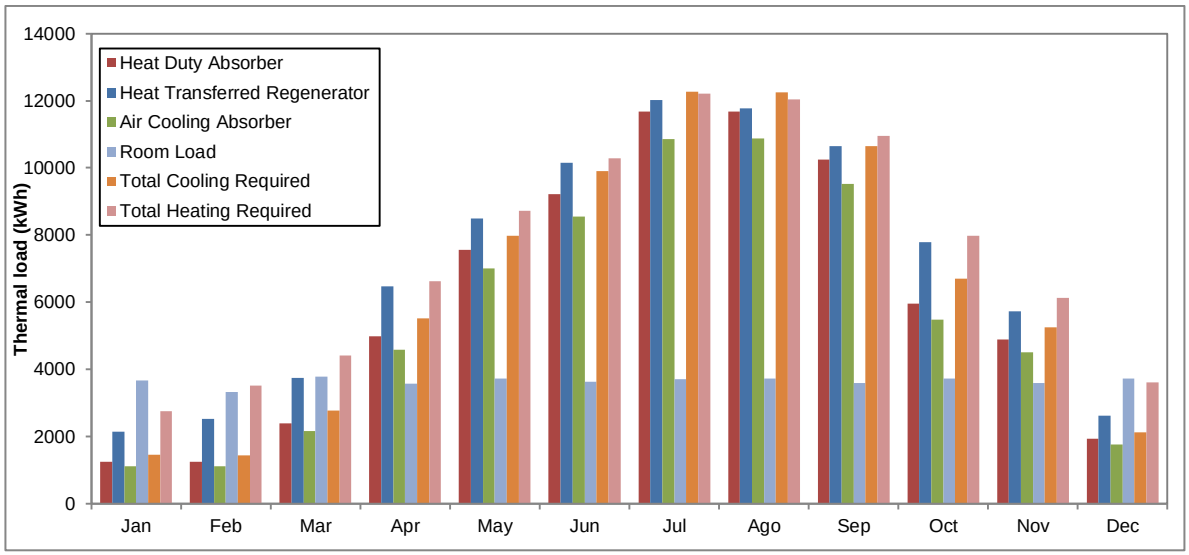

Figure 8.13. Monthly results of the different thermal loads calculated from the monthly optimized control strategy.

Table 8.8 contains the results of the annual thermal loads of the system calculated from the monthly optimized case. The difference between the heat duty in the absorber and the air cooling in the absorber is the cooling energy to the liquid desiccant in the absorber.

Table 8.8. Annual thermal loads of the system calculated from the simulation of the monthly optimized case.

Thermal load	Value
Heat duty in the absorber (kWh)	72086
Heat transferred in the regenerator (kWh)	91357
Air cooling in the absorber (kWh)	66708
Locker rooms internal load (kWh)	43766
Total cooling required (absorber + coil) (kWh)	79647
Total heating required (regenerator + coil) (kWh)	95407

8.5. Sensitivity analysis

The validated model can be also used to perform a sensitivity analysis to different variables of the system. In this sense, the system is analysed from the 36 simulations operational conditions simulated when the system operates with the control strategy, in which the regenerator is activated as function of the LiCl mass concentration at the entrance of the absorber. The following five variables are analysed:

- Annual hours out of comfort.
- Annual air cooling (sensible + latent) in the absorber.
- Annual cooling required in the absorber and the coil.
- Annual heating required in the regenerator and the coil.
- Annual heating transferred in the condensers of the heat pump.

Figure 8.14 shows the effect of the inlet water temperature in the absorber and the regenerator and the minimum LiCl mass concentration at the entrance of the absorber on the annual hours out of comfort. The higher is the temperature in the regenerator and the lower is the temperature in the absorber; the lower is number of hours out of comfort. This is due to the thermal capacity and dehumidification capacity of the system increase at these conditions.

On the other hand, medium LiCl mass concentrations provide better comfort levels. This could be explained by two contradictory reasons: at low LiCl mass concentrations, the dehumidification capacity is low. However, at high LiCl mass concentrations, the sensible capacity of the system is low too.

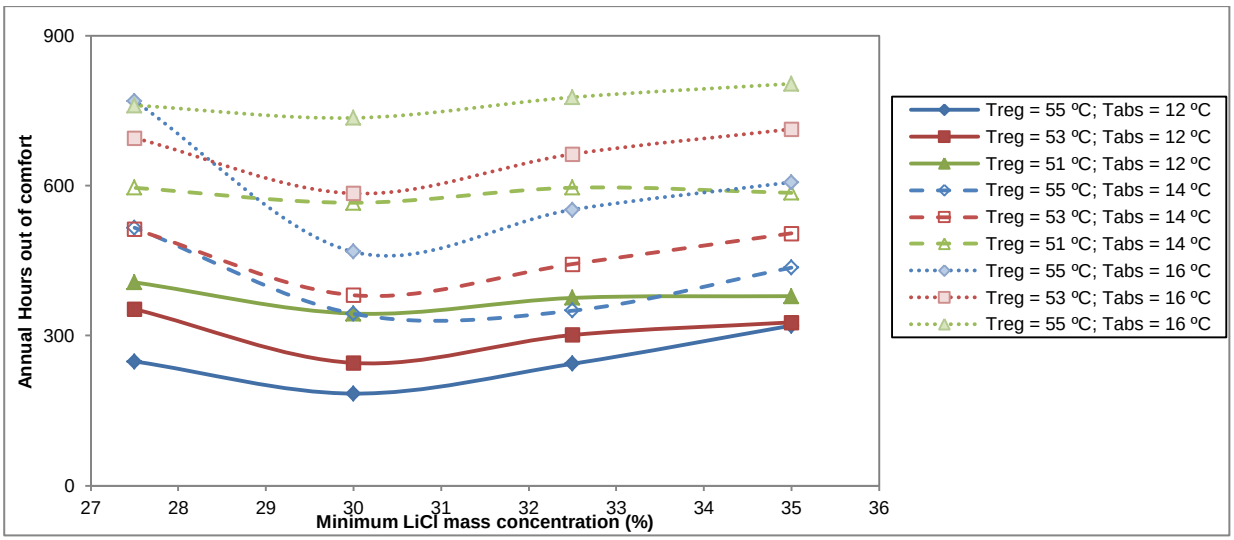

Figure 8.14. Sensitivity analysis of the number of hours out of comfort.

Figure 8.15 shows the effect of the inlet water temperature in the absorber and regenerator and the minimum LiCl mass concentration at the entrance of the absorber on the annual air cooling in the absorber. As it is expected, the inlet water temperature in the absorber is the variable with the highest effect on the air cooling in the absorber. In this case, the lower is the inlet water temperature in the absorber, the higher is the air cooling.

On the other hand, low LiCl mass concentrations provide more cooling to the air than high, because liquid desiccant temperature has to be lower in order to achieve the same dehumidification than at high LiCl mass concentrations. This low temperature of the liquid desiccant makes decreasing the air temperature when it passes through the absorber.

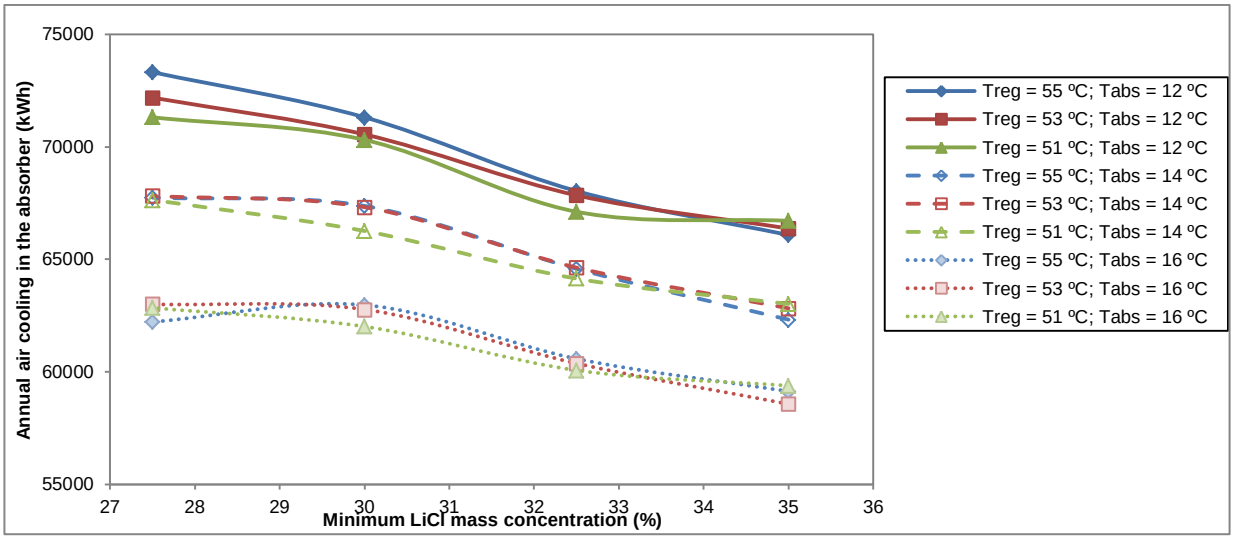

Figure 8.15. Sensitivity analysis of the annual air cooling in the absorber.

Figure 8.16 shows the effect of the inlet water temperature in the absorber and regenerator and the minimum LiCl mass concentration at the entrance of the absorber on the annual cooling provided by the evaporator of the heat pump to the absorber and the coil. In general, the higher is the temperature in the regenerator and the lower is the temperature in the absorber; the higher is the cooling provided by the heat pump. This is due to the dehumidification capacity the system at these conditions increases with them.

On the other hand, the effect of the LiCl mass concentration on the cooling provided by the heat pump is not easy to be understood. Cooling provided by the heat pump decreases at LiCl mass concentrations lower than 30 % because, under these conditions, the dehumidification capacity is reduced. However, for LiCl mass concentrations higher than 30 % cooling provided by the heat pump does not follow always the same behaviour.

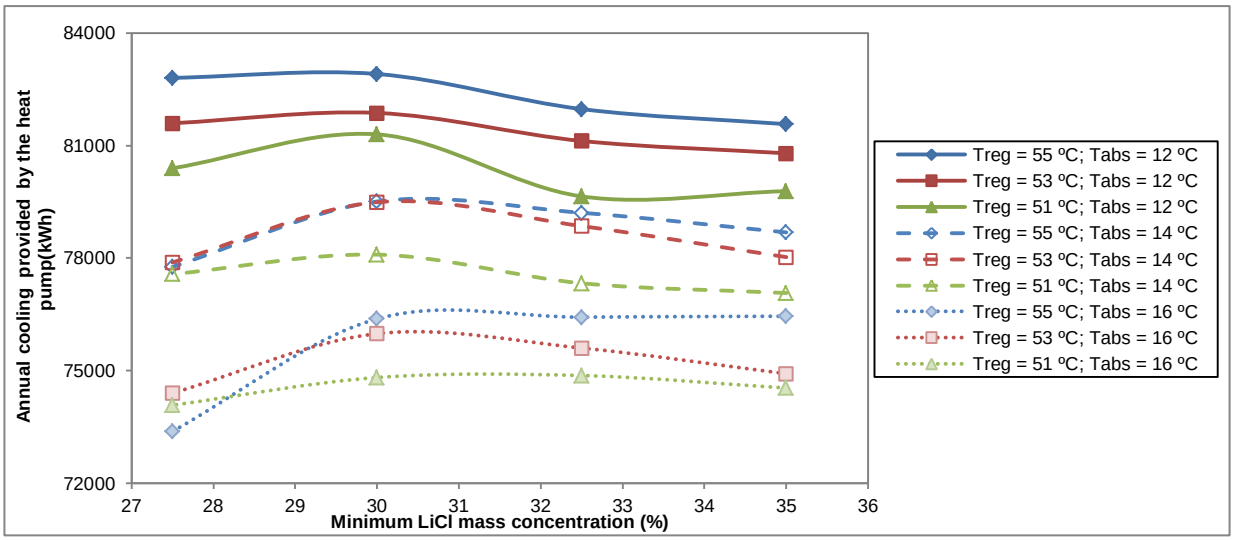

Figure 8.16. Sensitivity analysis of the annual cooling provided by the heat pump.

Figure 8.17 shows the effect of the inlet water temperature in the absorber and regenerator and the minimum LiCl mass concentration at the entrance of the absorber on the annual heating required by the regenerator and the coil. The higher is the temperature in the regenerator, and the lower is the temperature in the

absorber; the higher is the annual heating required. The effect of the temperature on the heating required in the regenerator is due to an increasing of the water desorption at high water temperatures. The effect of the low temperature in the absorber is due to a decreasing on the heating required in the coil and the low temperature of the desiccant at the entrance of the regenerator.

On the other hand, the higher LiCl mass concentration, the higher annual heating required. This effect is due to the large amount of energy required to keep the desiccant at high concentrations.

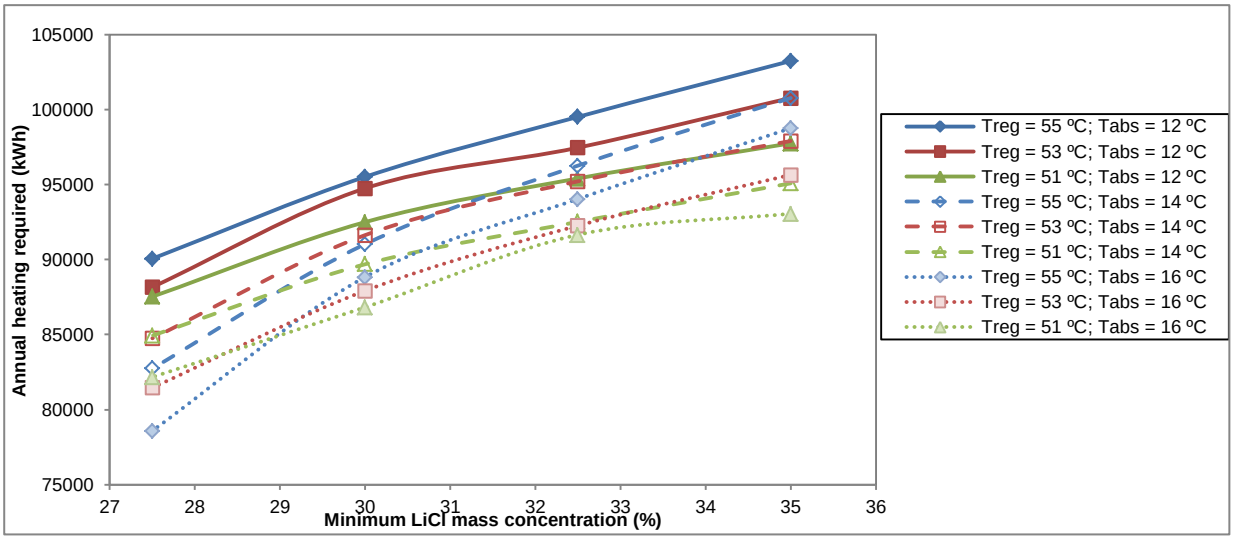

Figure 8.17. Sensitivity analysis of the annual heating required.

Finally, Figure 8.18 shows the effect of the inlet water temperature in the absorber and regenerator and the minimum LiCl mass concentration at the entrance of the absorber on the annual heating transferred in the condensers of the heat pump. The higher is the temperature in the regenerator and the lower is the temperature in the absorber, the higher is the heating transferred in the condensers. This effect is due to both, an increasing on dehumidification capacity of the system and a decreasing on the COP of the heat pump.

However, LiCl mass concentration does not seem to affect much to this heating. This effect is due to the heating required by the regenerator and the coil is, during most of the time, lower than the heating transferred in the condenser. This permits to use the excess of the energy to keep high LiCl mass concentration in the system by using the energy from the condenser that, otherwise, it would be removed to the ambient.

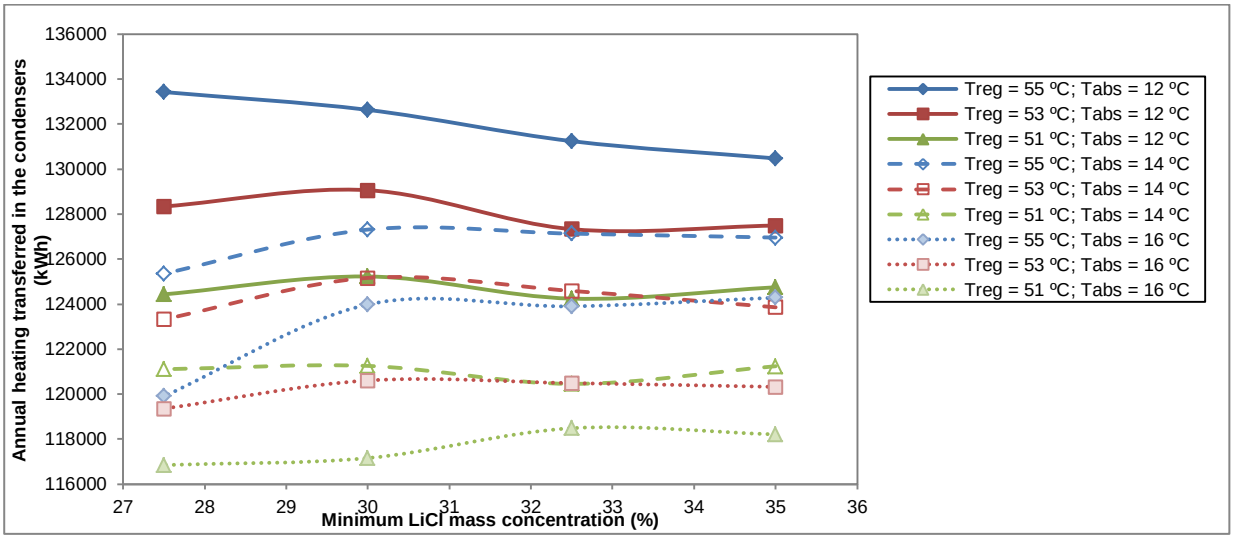

Figure 8.18. Sensitivity analysis of the annual heating transferred in the condensers.

8.6. Conclusions

The hybrid liquid desiccant system has been modelled for being dynamically simulated. For this purpose, new components for the air-solution contactors and the solution tanks have been developed on TRNSYS. Simulated results of the outlet conditions of the main devices of the system have been compared with measurements of the system when it operates in Taiwan. Very small deviations have been found between them and, therefore, the model has been considered as validated.

In order to optimize the control and the operation of the real hybrid liquid desiccant system, a multi-objective optimization has been performed after simulating 45 different cases, where two different control strategies as well as 3 different operational conditions were taken into account. The following conclusions have been obtained from these simulations:

- When the regeneration of the liquid desiccant is activated as function of the LiCl mass concentration at the entrance of the absorber, the performance of the hybrid liquid desiccant system has been, generally, better than when it is activated always than the absorber is in operation.
- Inlet water temperature in the absorber should be 12 °C, inlet water temperature in the regenerator should be 51 °C, and minimum LiCl mass concentration should be 32.5 %.

Since the ambient conditions vary from winter to summer, a monthly optimization was decided to be done in order to set the best control strategy month by month.

Table 8.7 contains the selection of the control strategy and the operational conditions that optimize the performance of the system in each month. When comparing the results of the monthly optimization with the previous optimization, an improvement is found in both, the number of hours out of comfort and the heating energy transferred in the condenser. The reduction on the number of hours out of comfort is higher than 19 % and the reduction on the heating energy transferred in the condenser is almost 1.5 %.

From the results obtained with the 36 simulations performed with the control strategy in which the regenerator operates as function of the LiCl mass concentration at the entrance of the absorber, a sensitivity analysis of 5 different variables has been done. These variables are evaluated as function of the inlet water temperature in the absorber, the inlet water temperature in the regenerator and the minimum LiCl mass concentration has been done. The following conclusions are obtained from this analysis:

- When the inlet water temperature in the regenerator is increased; the number of hours out of comfort is reduced, the air cooling in the absorber is increased, the cooling required be the absorber and the coil is increased, the heating required by the regenerator and coil is increased, and the heating transferred in the condensers of the heat pump is increased too.
- When the inlet water temperature in the absorber is decreased; the number of hours out of comfort is reduced, the air cooling in the absorber is increased, the cooling required be the absorber and the coil is increased, the heating required by the regenerator and coil is increased, and the heating transferred in the condensers of the heat pump is increased too.
- The minimum LiCl mass concentration mostly affects to the air cooling in the absorber and the heating required in the regenerator and the coil. When the minimum LiCl mass concentration is increased, the air cooling in the absorber is decreased, and the heating required by the regenerator and the coil is increased.

Chapter 9. General conclusions and future work

9.2. General conclusions

Despite liquid desiccant systems seemed to be a promising HVAC technology when latent load is high with respect to the sensible load, this technology had not been deeply used due to two main reasons: corrosiveness of the liquid desiccant materials and carry-over. The work developed in this thesis overcomes these two issues in the following way:

- Corrosiveness is solved by using plastic materials in the air-solution contactors, and
- Carry-over is tried to be solved by reducing the liquid desiccant flow without affecting the heat and mass transfer performance. This is done by using internally-cooled air-solution contactors of the falling-film with horizontal tubes type. Moreover, plastic tubes with a surface treatment that improves their wettability have been used.

This thesis contains all the stages to develop, analyse and optimize a hybrid liquid desiccant system. In this sense, the study started from the state-of-the-art of the liquid desiccant technology, to continue, then, with the selection of the air-solution contactor materials and typology, the sizing and design of the system, the set-up of the system, the experimental tests, the analysis of results, the modelling of the system and finally, the operational optimization of it. The following main conclusions can be taken from it:

- According to the hydrodynamic study carried out with ten different tube materials and surface treatments, the standard plastic tubes needs, at least, a jet flow mode to be fully wetted, with the exception of polyamide, that is able to be fully wetted at droplet mode.
- Plasma surface treatment improves the wettability of plastic tubes. In this sense, all the tubes with plasma treatment on their surface can be fully wetted at droplet mode.
- Film Reynolds number to achieve full wettability increases with increasing film Galileo number.
- Potential equation for the film Galileo number correlates properly the film Reynolds number to obtain full wettability. These correlations have been obtained for each tube with deviations lower than 10 %.
- Among the different tube materials compared in this thesis, polypropylene with a surface continuous plasma treatment II is the most suitable material to be used for the non-adiabatic air-solution contactors of a liquid desiccant system that uses LiCl-H_2O as liquid desiccant material. The reasons that support this election are: good wettability, low-cost of the material, easiness of being manufactured, and it is a rustproof material.
- When using polypropylene with the surface treatment, improvements of almost 29 % in the air cooling and 20 % in the dehumidification were obtained with respect to the standard polypropylene tubes.
- A hybrid liquid desiccant system has been designed and sized to handle the thermal loads for two locker rooms of a swimming-pool in Taipei (Taiwan). The system was expected to cool an air flow rate of 2500 m^3/h from 31 °C and 0.0215 kg_w/kg_a to 19 °C and 0.0069 kg_w/kg_a.
- Once the system was manufactured, the assembling of the whole system as well as the set-up and the fine-tuning of it was done, before being sent to Taiwan.
- The air-solution contactor with in-line arrangement achieved a 20 % mass transfer coefficient higher and a 9 % global heat transfer coefficient higher than the air-solution contactor with the staggered arrangement. This better performance can be due to both, the higher linear liquid desiccant flow rate and the higher number of tubes on which the liquid desiccant passes around.
- Air flow rate and liquid desiccant inlet temperature are the key variables for a higher performance of the air-solution contactors. In this sense, the higher air flow rate and the lower inlet desiccant temperature in the absorber, the higher dehumidification. The effect of the lower inlet desiccant temperature shows the importance of the heat transfer on the air-solution contactor performance.

- Cooling load and inlet hot water temperature in the regenerator seem to have the highest effect on the COP of the hybrid liquid desiccant system. In this sense, the lower the water temperature in the regenerator and the higher the cooling load, the higher the liquid desiccant and the global COPs.
- The maximum cooling rate of the absorber has been about 30 kW and the maximum dehumidification about 0.011 $kg_w/kg_{a.}$ These results are around 23 % and 16 %, respectively, lower than expected at design conditions because full wetting of tubes was not reached, and air-solution contactors operated with lower water flow rates than expected.
- The system achieves an adequate control of humidity and temperature, either at warm and humid or at cool and dry conditions.
- Air flow rate affects to both, tube-solution heat transfer coefficient and mass transfer coefficient in the air side for the absorber and the regenerator.
- Potential equation of the air flow rate correlates properly the tube-solution heat transfer coefficient and the mass transfer coefficient in the air side for the absorber and the regenerator. With these correlations for the absorber, deviations lower than 10 % for the dehumidification and lower than 5 % for the heat duty have been achieved. In addition, deviations lower than 10 % for both, the humidity ratio difference and the heating provided in the regenerator have been achieved.
- When using these correlations in a dynamic model of the hybrid liquid desiccant system, results obtained from simulations show small discrepancies in comparison with real measurements of the system.
- If number of hours out of comfort and energy consumption of the heat pump are required to be minimized, the regenerator should be operated as function of the LiCl mass concentration at the entrance of the absorber. Moreover, the system has to operate with an inlet water temperature in the absorber of 12 °C, an inlet water temperature in the regenerator of 51 °C, and a minimum LiCl mass concentration of 32.5 %.
- Monthly optimization of the operational conditions of the system reduces the number of hours out of comfort in a 19 % and the heating energy transferred in the condenser in almost 1.5 % in comparison with the annual optimization.
- According to the results obtained in the sensitivity analysis carried out, inlet water temperatures affect more to the seasonal system performance than LiCl mass concentration. In this sense, when the inlet water temperature in the regenerator is increased and the inlet water temperature in the absorber is reduced: the number of hours out of comfort is reduced, the air cooling in the absorber is increased, the cooling required be the absorber and the coil is increased, the heating required by the regenerator and coil is increased, and the heating transferred in the condensers of the heat pump is increased too.

9.3. Future work

The results and conclusions obtained in this thesis open new researches on liquid desiccant systems from both, experimental and theoretical points of view:

- Overall heat transfer coefficient in the air-solution contactors has been found as a key parameter to enhance the performance of the liquid desiccant systems. In this sense, higher overall heat transfer coefficients will lead to a lower size of these systems and a better performance of the system. The improvement of the overall heat transfer coefficient could be done in the following ways:
    - By avoiding the bend formation of plastic tubes what will improve the tube wetting and, therefore, the tube-solution heat transfer coefficient. This could be done by increasing the rigidity of plastic tubes.
    - By increasing the contact surface of the air-solution contactors. This could be done by adding fins to the tubes, by reducing the tube diameter or by increasing the number of tubes.
    - By using a material with a higher thermal conductivity than standard plastics. Corrosion must be considered in the selection of the material.

In this sense, titanium tubes with fins could be a good alternative to increase the performance of the air-solution contactors due to its high rigidity, wettability, thermal conductivity and non-corrosiveness with LiCl-H_2O.

- The development of validated CFD models for the air-solution contactors could help to verify if the poorer performance of the air-solution contactor with staggered arrangement is due to the lower linear liquid desiccant flow rate and the lower number of tubes for which the liquid desiccant passes around. Moreover, with these models it could be found the tube arrangement and the tube dimensions that maximize the heat and the mass transfer without increasing much the air pressure drops.
- To try different control strategies on the hybrid liquid desiccant system in order to optimize their seasonal performance. In this sense, it could be interesting to try a control strategy that regulates the set point temperature in the absorber and the regenerator as function of the return humidity ratio, and the dehumidification and the amount of water regenerated, respectively. Other interesting control strategy could be to regulate the water flow rate at the entrance of the regenerator as function of the same parameters.
- Once air-solution contactors and solution tanks have been modelled on TRNSYS, it could be useful to use them for other dynamic simulation studies. For instant, it could be used:
    - In order to compare the seasonal performance of the hybrid liquid desiccant system with other desiccant systems, such as solid desiccant systems, liquid desiccant systems with evaporation cooling or conventional air handling units. This comparison could be also done from an economical point of view.
    - In order to try the hybrid liquid desiccant systems in other climates and kind of buildings.
    - In order to try the system coupled to other heating and cooling sources, such as solar energy, cooling towers, geothermal heat pumps, polygeneration systems, waste heat, etc.

References

[1] J. Adnot and P. Waide, “Energy Efficiency and Certification of Central Air Conditioners.” 2003.

[2] “Technology Roadmap. Energy-efficient Buildings: Heating and Cooling Equipment,” 2011.

[3] M. A. McNeil and V. E. Letschert, “Future air conditioning energy consumption in developing countries and what can be done about it: the potential of efficiency in the residential sector,” 2007.

[4] A. Pesaran, T. Penney, and A. W. Czanderna, *Desiccant Cooling State-of-the-Art Assessment*. Golden, Colorado: National Renewable Energy Laboratory, 1992.

[5] K. Systems, “Kathabar Systems http://www.kathabar.com/index.php/liquid-desiccant/liquid-literature,” 2015. .

[6] A. Systems, “Advantix Systems http://www.advantixsystems.com/downloads.php,” 2014. .

[7] J. L. McNab and M. Bank, “U.S. Patent 4910971. Indirect Air Conditining System,” 1990.

[8] C. Dyna Air ltd, “Dyna-air dryer system,” *http://www.dyna-air.jp/*, May 2016. .

[9] A. Lowenstein, S. Slayzak, J. Ryan, and A. Pesaran, *Advanced Commercial Liquid-Desiccant Technology Development Study*. Golden, Colorado: National Renewable Energy Laboratory, 1998.

[10] Y. Chen, Y. Yin, and X. Zhang, “Performance analysis of a hybrid air-conditioning system dehumidified by liquid desiccant with low temperature and low concentration,” *Energy Build.*, vol. 77, pp. 91–102, Jul. 2014.

[11] K. Gommed, G. Grossman, J. Prieto, J. Ortiga, and A. Coronas, “Experimental comparison between internally and externally cooled air-solution contactors,” *Sci. Technol. Built Environ.*, vol. 21, pp. 267–274, 2015.

[12] V. Mei, F. Chen, Z. Lavan, R. Collier Jr., and G. Meckler, *An Assessment of desiccant cooling and dehumidification technology*. Oak Ridge, Tennessee: OAK RIDGE NATIONAL LABORATORY, 1992.

[13] F. R. Bichowsky and G. A. Kelley, “Concentrated solution in air-conditioning,” *Ind. Eng. Chem.*, vol. 27, no. (8), pp. 880–882, 1935.

[14] M. Conde, “Open Absorption Systems for Air-Conditioning using Membrane Contactors,” 2008.

[15] G. O. G. Löf, “House Heating and Cooling with Solar Energy.” F. Daniels ed., Wisconsin University Press, Madison, USA, pp. 33–46, 1955.

[16] A. Kakabaev and M. Golaev, “Glazed flat surface as a Solution Regenerator for Use in an Absorption Cooling System,” *Geliotekhnika*, vol. 7, no. 4, pp. 44–49, 1971.

[17] H. I. Robinson, “Open cycle chemical heat pump and energy storage system.” Annual DOE Active Solar Heating and Cooling Contractors Review Meeting: Proceedings and Project Summaries, Washington, DC, USA, pp. 3.26–3.27, 1982.

[18] G. Meckler, “Solar cooling system reduces summer utility demand and HVAC systems life-cycle cost in commercial and institutional buildings.” American Chemical Society, Washington, DC, USA, pp. 1194 – 1197, 1986.

[19] A. H. Abdel-Salam and C. J. Simonson, "State-of-the-art in liquid desiccant air conditioning equipment and systems," *Renew. Sustain. Energy Rev.*, vol. 58, pp. 1152–1183, May 2016.

[20] A. Lowenstein, "Review of Liquid Desiccant technology for HVAC Applications," *HVAC&R Res.*, vol. 14, no. 6, pp. 819–839, 2008.

[21] M. Krause, "State of the art - Survey on new solar cooling developments," 2009.

[22] A. Al-Farayedhi, P. Gandhidasan, A. Antar, and M. Abdul Gafar, "Experimental study of an aqueous desiccant mixture system: air dehumidification and desiccant regeneration," *Proc. Inst. Mech. Eng. Part. A; J. Power Energy*, vol. 219 (A8), pp. 669–680, 2005.

[23] M. R. Conde, "Properties of aqueous solutions of lithium and calcium chloride: formulations for use in air conditioning equipment design.," *Conde Eng.*, 2009.

[24] J. Pátek and J. Klomfar, "Thermodynamic properties of the LiCl-H2O system at vapor-liquid equilibrium from 273 K to 400 K," *Int. J. Refrig.*, vol. 31, pp. 287–303, 2008.

[25] A. L. McNeely, "Thermodynamic properties of aqueous solution lithium bromide," 1979.

[26] R. and A.-C. E. American Society of Heating Inc., "F32 Sorbents and Desiccants," in in *ASHRAE Handbook Fundamentals (SI)*, 2009, p. 32.1.

[27] V. Öberg and Y. Goswami, "A Review of Liquid Desiccant Cooling," *Adv. Sol. Energy*, vol. 12, 1998.

[28] T. W. Chung, T. K. Ghosh, A. L. Hines, and D. Novosel, "Dehumidification of moist air with simultaneous removal of selected indoor pollutants by tiethylene glycol solution in packed-ped absorber," *Sep. Sci. Technol.*, vol. 30, pp. 1807–1832, 1995.

[29] L. Mei and Y. J. Dai, "A technical review on use of liquid-desiccant dehumidification for air conditioning application," *Renew. Sustain. Energy Rev.*, vol. 12, pp. 662–689, 2008.

[30] G. A. Longo and A. Gasparella, "Experimental analysis on desiccant regeneration in a packed column with structured and random packing," *Sol. Energy*, vol. 83, pp. 511–521, 2009.

[31] "Koch-Glitsch, Intalox Packed Tower System, Plastic Random Packing, Wichita, Kansas." 2012.

[32] "Koch-Glitsch, Intalox Packed Tower System, High performance Structured Packing, Wichita, Kansas." 2012.

[33] K. Gommed, G. Grossman, and F. Ziegler, "Experimental Investigation of a LiCl-Water Open Absorption System for Cooling and Dehumidification," *J. Sol. Energy Eng.*, vol. 126, pp. 710–715, 2004.

[34] P. Bansal, S. Jain, and C. Moon, "Performance comparison of an adiabatic and an internally cooled structured packed-bed dehumidifier," *Appl. Therm. Eng.*, vol. 31, pp. 14–19, 2011.

[35] E. Lävemann and M. Peltzer, "Distributor for micro-quantities of liquid," 2006.

[36] W. Kessling, E. Lävemann, and C. Kapfhammer, "Energy storage for desiccant cooling systems component development," *Sol. Energy*, vol. 64, pp. 209–221, 1998.

[37] A. Lowenstein, M. Sibilia, J. Miller, and T. S. Tonon, "Heat exchanger assembly," 2004.

[38] Y. Yonggao, Z. Xiaosong, W. Geng, and L. Lei, "Experimental study on a new internally cooled/heated dehumidifier/regenerator of liquid desiccant systems," *Int. J. Refrig.*, vol. 31, pp. 857–866, 2008.

[39] J. Liu, T. Zhang, X. Liu, and J. Jiang, "Experimental analysis of an internally-cooled/heated liquid desiccant dehumidifier/regenerator made of thermally conductive plastic," *Energy Build.*, vol. 99, pp. 75–86, Jul. 2015.

[40] E. Lävemann, M. Peltzer, A. Hublitz, A. Kroenauer, U. Raab, and A. Hauer, "Thermochemical Storage for Air-Conditioning using Open Cycle Liquid Desiccant Technology," in *ECOSTOCK*, 2006, vol. Stockton C.

[41] A. Y. Khan and F. J. Sulsona, "Modelling and parametric analysis of heat and mass transfer performance of refrigerant cooled liquid desiccant absorbers," *Int. J. Energy Res.*, vol. 22, pp. 813–832, 1998.

[42] T. W. Chung and H. Wu, "Comparison between spray towers with and without fin coils for air dehumidification using triethylen glycol solutions and development on the mass-transfer correlations," *Ind. Eng. Chem. Res*, vol. 39, pp. 2076–2084, 2000.

[43] S. Yamaguchi, J. Jeong, K. Saito, H. Miyauchi, and M. Harada, "Hybrid liquid desiccant air-conditioning system: Experiments and simulations," *SET 2010 Spec. Issue*, vol. 31, no. 17–18, pp. 3741–3747, 2011.

[44] A. Kakabaev, A.; Khandurdyev, "Absorption solar refrigeration unit with open regeneration of solution," *Appl. Sol. Energy*, vol. 5, no. 4, 1968.

[45] R. K. Collier, "The analysis and simulation of an open cycle absorption refrigeration system," *Sol. Energy*, vol. 23, no. 4, pp. 357–366, Jan. 1979.

[46] P. Gandhidasan, "A simple analysis of an open regeneration system," *Sol. Energy*, vol. 31, no. 3, pp. 343–345, Jan. 1983.

[47] P. Gandhidasan, "Theoretical study of tilted solar still as a regenerator for liquid desiccants," *Energy Convers. Manag.*, vol. 23, no. 2, pp. 97–101, Jan. 1983.

[48] R. Yang and P.-L. Wang, "The optimum glazing height of a glazed solar collector/regenerator for open-cycle absorption cooling," *Energy*, vol. 19, no. 9, pp. 925–931, Sep. 1994.

[49] S. Alizadeh and W. . Saman, "An experimental study of a forced flow solar collector/regenerator using liquid desiccant," *Sol. Energy*, vol. 73, no. 5, pp. 345–362, Nov. 2002.

[50] P. Agarwal, R.S.; Aggarwal, M.K.; Das Gupta, "Solar Powered Space Conditioning System using LiBr as a Desiccant," *INTERSOL 85, Proc. 9th Bienn. Congr. Int. Sol. Energy Soc.*, vol. 1, no. 1, pp. 674–681, 1985.

[51] W. C. Griffiths, "Solar Energy Asisted Air-Conditioning Apparatus and Method," U.S. Patent No. 4,164,1251979.

[52] Y. Yin, B. Zheng, C. Yang, and X. Zhang, "A proposed compressed air drying method using pressurized liquid desiccant and experimental verification," *Appl. Energy*, vol. 141, pp. 80–89, Mar. 2015.

[53] K. Gommed and G. Grossman, "Liquid desiccant dehumidification system and heat/mass exchanger therefor," US Patent No. 20110132027A1.

[54] K. Gommed and G. Grossman, “Investigation of an improved solar-powered open absorption system for cooling, dehumidification and air conditioning,” *Int. J. Refrig.*, vol. 35, no. 3, pp. 676–684, 2012.

[55] K. Gommed and G. Grossman, “Experimental investigation of a liquid desiccant system for solar cooling and dehumidificaion,” *Sol. Energy*, vol. 81, pp. 131–138, 2007.

[56] A. Chebbah, “Analysis and Design of a Solar-Powered Liquid Desiccant Air COnditioner for Use in Hot and Humid Climates,” phD Thesis, University of Florida, Gainesville, FL., 1987.

[57] A. T. Mohammad, S. Bin Mat, M. Y. Sulaiman, K. Sopian, and A. A. Al-abidi, “Historical review of liquid desiccant evaporation cooling technology,” *Energy Build.*, vol. 67, pp. 22–33, Dec. 2013.

[58] J. L. . Peterson and J. R. Howell, “Hybrid Vapor-Compression/Liquid Desiccant Air Conditioner,” U.S. Patent 4,941,3241990.

[59] Y. K. Yadav, “Vapour-compression and liquid-desiccant hybrid solar space-canditioning system for energy conservation,” *Renew. Energy*, vol. 6 (7), pp. 719–723, 1995.

[60] F. Sick, “Analysis of the seasonal performance of hybrid liquid desiccant cooling systems,” University of Wisconsin, Madison, 1986.

[61] M. Thornbloom and B. Ninmo, “An Economic Analisys of a Solar Open Cycle Desiccant Dehumidification System,” in *Solar Engineering 1995, Proceedings of the 13th Annual ASME Conference*, 1995, pp. 705–709.

[62] Y. . Dai, R. . Wang, H. . Zhang, and J. . Yu, “Use of liquid desiccant cooling to improve the performance of vapor compression air conditioning,” *Appl. Therm. Eng.*, vol. 21, no. 12, pp. 1185–1202, Aug. 2001.

[63] X. Niu, F. Xiao, and Z. Ma, “Investigation on capacity matching in liquid desiccant and heat pump hybrid air-conditioning systems,” *Int. J. Refrig.*, vol. 35, no. 1, pp. 160–170, Jan. 2012.

[64] W. H. Wilkinson, “Hybrid Air Conditioning System,” U.S. Patent 4,905,4791990.

[65] H. R. . Hernández, J. E. . González, and A. Y. Khan, “Modeling of a Solar-Assisted Absorption/Desiccant System for Applications in Puerto Rico and the Caribbean,” in *SOLAR 96, Proceedings of 1996 Annual Conference of the American Solar Energy Society*, 1996, pp. 124–132.

[66] C. S. Khalid Ahmed, P. Gandhidasan, and A. Al-Farayedhi, “Simulation of a hybrid liquid desiccant based air-conditioning system,” *Appl. Therm. Eng.*, vol. 17, pp. 125–134, 1997.

[67] M. Conde, “Liquid Desiccant-based air-conditioning systems-LDACS,” in *1st European Conference on Polygeneration*, 2007, vol. Tarragona,.

[68] “AIL Research, Inc http://www.ailr.com/liquid_desiccants.htm, May 2016.” .

[69] Menerga, “Comfort air conditioning - Sorpsolair 72 and 73.” 2016.

[70] “LDC-s Technology http://www.l-dcs.com/applications/index.html, June 2014.” .

[71] H. Miyauchi, “Practical study on liquid desiccant processor in medical facilities,” in *The 24th IIR International Congress of Refrigeration ICR2015*, 2015.

[72] David A. Thompson, “Enthalpy pump,” US Patent 6684649 B1,2004.

[73] G. Ribatski and A. M. Jacobi, “Falling-film evaporation on horizontal tubes-a critical review,” *Int. J. Refrig.*, vol. 28, pp. 635–653, 2005.

[74] U. Gross, “Falling Film Evaporation Inside a Closed Thermosyphon,” *Proc. 10th Int. Heat Transf. Conf. Bright. U.K.*, vol. 7, pp. 443–448, 1994.

[75] M. S. El-Genk and H. H. Saber, “Minimum thickness of a flowing down liquid film on a vertical surface,” *Int. J. Heat Mass Transf.*, vol. 44, no. 15, pp. 2809–2825, 2001.

[76] P.-G. de Gennes, F. Brochard-Wyart, and D. Quéré, *Capillarity and Wetting Phenomena*. Berlin, Germany, 2003.

[77] M. R. Conde, “Properties of aqueous solutions of lithium and calcium chlorides: formulations for use in air conditioning equipment design,” *Int. J. Therm. Sci.*, vol. 43, pp. 367–382, 2004.

[78] V. Konduru, “Static and Dynamic Contact Angle Measurement on Rough Surfaces Using Sessile Drop Profile Analysis with Application to Water Management in Low Temperature Fuel Cells,” Michigan Technological University, 2010.

[79] R. Qi, L. Lu, and Y. Jiang, “Investigation on the liquid contact angle and its influence for liquid desiccant dehumidification system,” *Int. J. Heat Mass Transf.*, vol. 88, pp. 210–217, Sep. 2015.

[80] A. Doniec, “Flow of a laminar liquid film down a vertical surface,” *Chem. Eng. Sci.*, vol. 43, pp. 847–854, 1988.

[81] D. E. Hartley and W. Murgatroyd, “Criteria for the Breakup of Thin Liquid Layers Flowing Isothermally over Solid Surfaces,” *Int. J. Heat Mass Transf.*, vol. 7, pp. 1003–1015, 1964.

[82] K. R. Morison, Q. A. G. Worth, and N. P. O’Dea, “Minimum wetting and distribution rates in falling film evaporators,” *Food Bioprod. Process.*, vol. 84, pp. 302–310, 2006.

[83] S. Paramalingam, J. Winchester, and C. Marsh, “On the Fouling of Falling Film Evaporators Due to Film Break-Up,” *Food Bioprod. Process.*, vol. 78, no. 2, pp. 79–84, Jun. 2000.

[84] H. Zhang, J. Yue, G. Chen, and Q. Yuan, “Flow pattern and break-up of liquid film single-channel falling film microreactors,” *Chem. Eng. J.*, vol. 163, pp. 126–132, 2010.

[85] J. R. Thome, “Chapter 14. Falling film evaporation,” in in *Engineering Data Book III*, I. Wolverine tube, Ed. 2004, pp. 1–39.

[86] X. Hu and A. M. Jacobi, “The Intertube Falling-Film Modes: Transition, Hysteresis, and Effects on Heat Transfer.” Urbana, IL, pp. 1–138, 1995.

[87] D. Gstöhl, J. F. Roques, and J. R. Thome, “Falling film transitions on plain and enhanced tubes,” *J. Heat Transfer*, vol. 124, pp. 491–499, 2002.

[88] R. Armbruster and J. Mitrovic, “Evaporative cooling of a falling water film on horizontal tubes,” *Exp. Therm. Fluid Sci.*, vol. 18, no. 3, pp. 183–194, 1998.

[89] R. O. Parker and R. E. Treybal, “The heat, mass transfer characteristics of evaporative coolers,” *Chem. Eng. Prog. Symp. Ser.*, vol. 57, no. 32, pp. 138–149, 1961.

[90] T. Mizushima, H. Ito, and H. Miyashita, “Experimental study of an evaporative cooler,” *Int. Chem. Eng.*, vol. 7, no. 4, pp. 727–732, 1967.

[91] V. Charan and M. E. Wasekar, “Heat and mass transfer in an evaporative dissipator,” in *Proceedings of XVth International Congress of Refrigeration*, 1979, pp. 373–379.

[92] R. S. Rana and V. Charan, “Heat and mass transfer from a single horizontal tube of an evaporative tubular heat exchanger,” *Int. Commun. Heat Mass Transf.*, vol. 10, pp. 403–412, 1983.

[93] R. S. Rana, V. Charan, and H. K. Varma, “Hear and mass transfer from a horizontal tube of an evaporative heat dissipator,” *Int. J. Heat Mass Transf.*, vol. 29, no. 4, pp. 555–562, 1986.

[94] R. Armbruster and J. Mitrovic, “Heat transfer in falling film flow on a horizontal tube,” in *Proceedings of 30th National Heat Transfer Conference of ASME*, 1995, pp. 13–21.

[95] Y. H. Wei and A. M. Jacobi, “Vapor shear, geometric and bundle-depth effects on the Intertube falling-film modes,” in *1st Int. Conference Heat Transfer, Fluid Mechanics, and Thermodynamics,*, 2002, vol. 1, pp. 40–60.

[96] B. Ruan, A. M. Jacobi, and L. Li, “vapor Shear Effects on Falling-Film Mode Transitions Between Horizontal Tubes,” in *International Refrigeration and Air Conditioning Conference*, 2008, p. Paper 983.

[97] Argal, “Argal pumps catalogue.” 2014.

[98] REGIN, “Products and Systems for Building Automation.” 2013.

[99] A. Technologies, “Agilent data logger cathalogue.” 2013.

[100] EES, “Engineering Equation Solver,” *F-Chart Softw.*

[101] R. W. Hyland and A. Wexler, “Formulations for the Thermodynamic Properties of the Saturated Phases of H20 from 173.15 K to 473.15 K,” 1983.

[102] L. Haar, J. S. Gallagher, and G. S. Kell, *Thermodynamic and Trnasport Properties and Computer Programs for Vapor and Liquid of Water in S.I. Units.*, vol. NBSC/NRC. Washington, D.C.: Hemisphere, 1984.

[103] W. M. Bowman, R.A.; Mueller, A.C.; Nagle, “Mean Temperature Diference in Design,” *Trans. ASME*, vol. 62, p. 283, 1940.

[104] H. M. Hellmann and G. Grossman, “Simulation and analysis of an open-cycle dehumidifier-evaporator-regenerator (DER) absorption chiller for low-grade heat utilization,” *Int. J. Refrig.*, vol. 18, pp. 177–189, 1995.

[105] K. Gommed and G. Grossman, “Improved Simulation Model for Air-Liquid Contactors in Open Absorption Air Conditioning Systems,” in *International Sorption Heat Pump Conference*, 2014.

[106] K. R. Patil, A. D. Tripathi, G. Pathak, and S. S. Katti, “Thermodynamic properties of aqueous electrolyte Solutions. 1. Vapor pressure of aqueous solutions of LiCl, LiBr, and LiI.,” *J. Chem. Eng. Data*, vol. 35, pp. 166–168, 1990.

[107] S. Nellis, G.; Klein, *Heat Transfer*. New York: Cambridge Uniervity Press, 2009.

[108] L. M. K. Dittus, P.W.; Boelter, “Heat Transfer in Automobile Radiators of the Tubular Type,” *Publ. Eng.*, vol. 2, p. 443, 1930.

[109] R. K. Shah and A. L. London, “Laminar Flow Forced Convection in Ducts,” *Suppl. 1 to Adv. Heat Transf.*, vol. Academic P, 1978.

[110] V. Gnielinski, “New equations for heat and mass transfer in turbulent pipe and channel flow,” *Int. Chem. Eng.*, vol. 16, pp. 359–367, 1976.

[111] R. and A.-C. E. American Society of Heating Inc., “F14 Climatic Design Information,” in in *ASHRAE Handbook Fundamentals (SI)*, 2009.

[112] P. 15251, “Indoor environmental input parameters for design and assessment of energy performance of buildings-addressing indoor air quality, thermal environment, lighting and acoustics.” 2007.

[113] C. W. Bureau, “Statistics Monthly Mean Taipei,” 2015. .

[114] Aermec, “Unidades polivalentes para instalaciones con 2/4 tubos - Manual Técnico.” 2015.

[115] Toshiba, “Industrial inverter (for 3-phase induction motors), simplified manual.” 2015.

[116] Mitsubishi, “Sine wave output filter for 400 V Inverter, product information.” 2015.

[117] S. Y. Ahmed, P. Gandhidasan, and A. Al-Farayedhi, “Thermodynamic analysis of liquid desiccants,” *Sol. Energy*, vol. 62, pp. 11–18, 1998.

[118] A. Coca-Ortegón, J. Prieto, and A. Coronas, “Modelling and dynamic simulation of a hybrid liquid desiccant system regenerated with solar energy,” *Appl. Therm. Eng.*, vol. 97, pp. 109–117, Nov. 2015.

[119] L. Crofoot, “Experimental Evaluation and modeling of solar liquid desiccant air conditioner (Master thesis),” Department of Mechanical and Materials Engineering , Queen’s University, 2012.

[120] “GmbH, TRANSSOLAR Energietechnik, TRNSYS 16: A TRaNsient SYstem Simulation program, Volume 5: Mathematical Reference,” 2007.

[121] TRNSYS, “Transient System Simulation Tool, Program Manual. Solar Energy Labratory, University of Wisconsin.” Madison, USA, 2004.

Annex A. Dimensional analysis of wettability

There are 7 parameters which may affect the wettability and the flow mode transitions for the falling film flow on horizontal tubes. They are the flow rate per unit length on the tube Γ_s (kg/s-m), solution viscosity μ_s (N·s/m^2), solution density ρ_s (kg/m^3), surface tension σ (N/m), tube diameter *d* (m), tube spacing *s* (m), gravity *g* (m/s^2). Applying the Buckingham Pi theorem there are four dimensionless groups for the seven physical parameters governing the falling-film modes.

In order to obtain these four dimensionless groups the following combination of parameters is examined:

$$\Pi = \Gamma_s^{C_1} \mu_s^{C_2} \rho_s^{C_3} \sigma^{C_4} d^{C_5} s^{C_6} g^{C_7} \tag{A.1}$$

Which written in terms of the basic dimensions is:

$$(kgs^{-1}m^{-1})^{C_1}(kgs^{-1}m^{-1})^{C_2}(kgm^{-3})^{C_3}(kgs^{-2})^{C_4}(m)^{C_5}(m)^{C_6}(ms^{-2})^{C_7} \tag{A.2}$$

If Π is dimensionless we have the following equations:

$$\begin{cases} c_1 + c_2 + c_3 + c_4 = 0 \\ -c_1 - c_2 - 3c_3 + c_5 + c_6 + c_7 = 0 \\ -c_1 - c_2 - 2c_4 - 2c_7 = 0 \end{cases} \tag{A.3}$$

Choosing Γ_s, d, s, g, to appear once in the dimensionless groups, the seven dimensionless groups are made up by:

$$\begin{pmatrix} c_1 \\ c_5 \\ c_6 \\ c_7 \end{pmatrix} = \begin{pmatrix} 1 \\ 0 \\ 0 \\ 0 \end{pmatrix}, \begin{pmatrix} 0 \\ 1 \\ 0 \\ 0 \end{pmatrix}, \begin{pmatrix} 0 \\ 0 \\ 1 \\ 0 \end{pmatrix}, \begin{pmatrix} 0 \\ 0 \\ 0 \\ 1 \end{pmatrix} \tag{A.4}$$

The solution obtained for equations (*,*) are:

$$\begin{pmatrix} c_1 \\ c_2 \\ c_3 \\ c_4 \\ c_5 \\ c_6 \\ c_7 \end{pmatrix} = \begin{pmatrix} 1 \\ -1 \\ 0 \\ 0 \\ 0 \\ 0 \\ 0 \end{pmatrix}, \begin{pmatrix} 0 \\ -2 \\ 1 \\ 1 \\ 1 \\ 0 \\ 0 \end{pmatrix}, \begin{pmatrix} 0 \\ -2 \\ 1 \\ 1 \\ 0 \\ 1 \\ 0 \end{pmatrix}, \begin{pmatrix} 0 \\ 4 \\ -1 \\ -3 \\ 0 \\ 0 \\ 1 \end{pmatrix} \tag{A.5}$$

The four dimensionless variables can be then written as:

$$\frac{\Gamma_s}{\mu_s}, \frac{\rho_s \sigma_s d}{\mu_s^2}, \frac{\rho_s \sigma_s s}{\mu_s^2}, \frac{\mu_s^4 g}{\rho_s \sigma_s^3} \tag{A.6}$$

These parameters can be reorganized as:

$$\Pi_1 = \frac{2\Gamma_s}{\mu_s} = Re_s \tag{A.7}$$

$$\Pi_2 = \frac{\rho_s \sigma_s d}{\mu_s^2} = Oh_s \tag{A.8}$$

$$\Pi_3 = \frac{s}{d} \tag{A.9}$$

$$\Pi_4 = \frac{\rho_s \sigma_s^3}{\mu_s^4 g} = Ga_s \tag{A.10}$$

Consequently the wettability depends on:

$$Wettability = function(Re, Oh_1, \frac{s}{d}, Ga) \quad \text{(A.11)}$$

Annex B. Experimental results of the hydrodynamic study on the horizontal tubes

Table B.1. Experimental results of the hydrodynamic study on the horizontal tubes.

Tube material	d_t (m)	s (m)	L_t (m)	$T_{s,in}$ (°C)	$X_{s,in}$ (%)	$m_{s,in}$ (l/h)
Standard polypropylene	0.0061	0.035	0.44	18.7	37.6	165.0
Standard polypropylene	0.0061	0.035	0.44	33.0	37.6	213.0
Standard polypropylene	0.0061	0.035	0.44	28.9	37.6	173.0
Standard polypropylene	0.0061	0.035	0.44	47.5	37.6	235.0
Standard polypropylene	0.0061	0.037	0.44	17.5	37.6	178.3
Standard polypropylene	0.0061	0.037	0.44	27.0	37.6	182.3
Standard polypropylene	0.0061	0.037	0.44	32.0	37.6	198.0
Standard polypropylene	0.0061	0.037	0.44	45.0	37.6	194.0
Polypropylene + batch plasma nano-layer deposition	0.0061	0.038	0.32	20.1	37.5	28.1
Polypropylene + batch plasma nano-layer deposition	0.0061	0.038	0.32	56.3	37.5	28.0
Polypropylene + batch plasma nano-layer deposition	0.0061	0.038	0.32	51.4	37.5	28.0
Polypropylene + batch plasma nano-layer deposition	0.0061	0.038	0.32	46.9	37.5	28.8
Polypropylene + batch plasma nano-layer deposition	0.0061	0.038	0.32	42.2	37.5	28.6
Polypropylene + batch plasma nano-layer deposition	0.0061	0.038	0.32	39.0	37.5	27.7
Polypropylene + batch plasma nano-layer deposition	0.0061	0.038	0.32	36.2	37.5	28.2
Polypropylene + batch plasma nano-layer deposition	0.0061	0.038	0.32	31.3	37.5	28.0
Polypropylene + batch plasma nano-layer deposition	0.0061	0.038	0.32	28.3	37.5	27.8
Polypropylene + continuous deposition I	0.0061	0.037	0.32	51.6	37.5	40.2
Polypropylene + continuous deposition I	0.0061	0.037	0.32	44.9	37.5	43.4
Polypropylene + continuous deposition I	0.0061	0.037	0.32	39.3	37.5	44.2
Polypropylene + continuous deposition I	0.0061	0.037	0.32	35.9	37.5	39.9
Polypropylene + continuous deposition I	0.0061	0.037	0.32	33.2	37.5	37.1
Polypropylene + continuous deposition I	0.0061	0.037	0.32	31.3	37.5	36.6
Polypropylene + continuous deposition I	0.0061	0.037	0.32	29.1	37.5	34.4
Polypropylene + continuous deposition I	0.0061	0.037	0.32	25.5	37.5	34.1
Polypropylene + continuous deposition I	0.0061	0.037	0.32	23.7	37.5	33.4
Polypropylene + continuous deposition II	0.0061	0.037	0.32	19.3	37.5	22.3
Polypropylene + continuous deposition II	0.0061	0.037	0.32	55.7	37.5	24.2
Polypropylene + continuous deposition II	0.0061	0.037	0.32	47.0	37.5	24.8
Polypropylene + continuous deposition II	0.0061	0.037	0.32	43.7	37.5	24.6
Polypropylene + continuous deposition II	0.0061	0.037	0.32	42.0	37.5	23.8
Polypropylene + continuous deposition II	0.0061	0.037	0.32	37.5	37.5	24.4
Polypropylene + continuous deposition II	0.0061	0.037	0.32	34.1	37.5	24.6
Polypropylene + continuous deposition II	0.0061	0.037	0.32	29.9	37.5	24.5
Polypropylene + continuous deposition II	0.0061	0.037	0.32	27.3	37.5	24.6
Low density polyethylene	0.0061	0.038	0.32	18.6	37.6	213.7
Low density polyethylene	0.0061	0.038	0.32	36.6	37.6	181.0
Low density polyethylene	0.0061	0.042	0.32	27.5	37.3	222.0
Low density polyethylene	0.0061	0.042	0.32	44.0	37.3	213.0
Low density polyethylene	0.0061	0.042	0.32	51.4	37.3	202.0
Low density polyethylene + batch plasma nano-layer deposition	0.0061	0.042	0.32	51.8	37.6	27.7
Low density polyethylene + batch plasma nano-layer deposition	0.0061	0.038	0.32	18.6	37.6	27.8
Low density polyethylene + batch plasma nano-layer deposition	0.0061	0.038	0.32	53.0	37.6	26.0
Low density polyethylene + batch plasma nano-layer deposition	0.0061	0.038	0.32	48.5	37.6	26.6
Low density polyethylene + batch plasma nano-layer deposition	0.0061	0.038	0.32	43.8	37.6	27.4
Low density polyethylene + batch plasma nano-layer deposition	0.0061	0.038	0.32	38.7	37.6	27.0
Low density polyethylene + batch plasma nano-layer deposition	0.0061	0.038	0.32	32.0	37.6	27.2
Low density polyethylene + batch plasma nano-layer deposition	0.0061	0.038	0.32	28.9	37.6	27.4
Polyamide	0.0061	0.040	0.32	18.0	37.6	36.1
Polyamide	0.0061	0.040	0.32	35.0	37.6	33.4
Polyamide	0.0061	0.040	0.32	51.3	37.6	28.7
Polyamide	0.0061	0.040	0.32	46.0	37.6	30.8

Polyamide	0.0061	0.047	0.32	17.5	37.6	37.5
Polyamide	0.0061	0.047	0.32	37.5	37.6	31.5
Polyamide	0.0061	0.047	0.32	52.0	37.6	25.8
Polyamide	0.0061	0.047	0.32	46.0	37.6	27.6
Polyamide + batch plasma nano-layer deposition	0.0061	0.042	0.32	18.2	37.4	32.0
Polyamide + batch plasma nano-layer deposition	0.0061	0.042	0.32	18.8	37.4	40.3
Polyamide + batch plasma nano-layer deposition	0.0061	0.042	0.32	26.0	37.4	36.0
Polyamide + batch plasma nano-layer deposition	0.0061	0.042	0.32	41.3	37.4	31.7
Polyamide + batch plasma nano-layer deposition	0.0061	0.042	0.32	52.0	37.4	31.7
Polyamide + batch plasma nano-layer deposition	0.0061	0.033	0.32	19.9	37.4	42.2
Polyamide + batch plasma nano-layer deposition	0.0061	0.033	0.32	32.9	37.4	35.1
Polyamide + batch plasma nano-layer deposition	0.0061	0.033	0.32	45.9	37.4	33.1
Polyamide + batch plasma nano-layer deposition	0.0061	0.033	0.32	56.0	37.4	30.0
High density polyethylene	0.0061	0.038	0.44	18.7	37.6	225.0
High density polyethylene	0.0061	0.038	0.44	26.9	37.6	217.0
High density polyethylene	0.0061	0.038	0.44	36.0	37.6	197.0
High density polyethylene	0.0061	0.034	0.44	18.7	37.6	229.5
High density polyethylene	0.0061	0.034	0.44	42.8	37.6	175.0
High density polyethylene	0.0061	0.034	0.44	34.0	37.6	203.5
Graphite	0.0254	0.030	0.44	19.6	37.5	43.7
Graphite	0.0254	0.030	0.44	33.6	37.5	39.3
Graphite	0.0254	0.030	0.44	43.0	37.5	36.0
Graphite	0.0254	0.041	0.44	19.2	37.6	38.2
Graphite	0.0254	0.041	0.44	34.6	37.6	35.5
Graphite	0.0254	0.041	0.44	42.4	37.6	32.8
Graphite	0.0254	0.041	0.44	56.1	37.6	31.2

Annex C. Experimental results of the small-scale internally cooled air-solution contactor

Table C.1. Experimental results with the standard air-solution contactor.

No.	$T_{s,in}$ (ºC)	$T_{s,out}$ (ºC)	$H_{a,in}$ (%)	V_a (m/s)	$T_{a,in}$ (ºC)	$H_{a,out}$ (%)	$T_{a,out}$ (ºC)	$v_{s,in}$ (l/h)	$T_{w,in}$ (ºC)	$T_{w,out}$ (ºC)	v_w (l/h)	$X_{s,in}$ (%)
1	17.74	20.44	48.5	1.78	27.03	42.9	21.78	222.9	13.25	14.29	220.4	35.9
2	19.92	22.79	39.4	2.06	28.22	39.2	21.96	221.7	8.83	10.26	276.3	35.7
3	17.03	19.39	35.5	2.10	32.56	37.9	24.16	313.7	10.16	11.24	321.5	35.9
4	17.26	19.22	42.2	1.62	29.53	40.8	22.62	310.8	9.51	10.55	318.8	35.9
5	18.69	19.88	46.3	1.20	28.16	41.5	21.71	314.7	8.87	9.89	311.7	35.9
6	18.18	20.76	43.1	2.00	29.19	40.4	24.03	215.1	9.57	10.74	323.9	35.8
7	18.44	20.28	41.1	1.57	29.89	41.2	22.89	212.9	8.70	9.82	321.9	35.9
8	18.50	20.11	44.7	1.17	28.81	42.6	21.69	212.0	9.25	10.22	321.1	35.8
9	18.72	20.42	44.3	1.17	29.09	43.1	21.98	159.4	9.66	10.62	323.4	35.9
10	18.84	20.89	42.0	1.59	29.83	42.8	22.55	158.5	10.08	11.12	322.4	35.8
11	18.87	21.34	38.4	1.99	30.88	41.0	23.29	158.1	8.65	9.92	320.9	35.9
12	18.92	21.50	39.1	2.01	30.80	41.7	23.98	156.2	13.03	13.97	325.2	35.7
13	19.33	21.64	41.2	1.56	30.38	42.0	23.71	155.3	13.52	14.39	322.1	35.6
14	19.52	20.77	44.7	1.15	29.59	42.9	23.21	154.8	14.13	14.89	319.6	35.8
15	19.36	20.50	44.6	0.99	29.20	41.3	22.81	220.6	14.51	15.19	322.1	35.9
16	19.26	21.21	39.4	2.00	31.61	39.9	24.31	299.7	13.65	14.58	316.0	35.7
17	19.25	21.18	41.0	1.59	31.14	40.3	23.85	298.0	14.01	14.85	309.8	35.8
18	19.30	20.75	43.7	1.18	30.42	40.1	23.36	297.0	14.32	15.07	310.7	35.8
19	20.02	22.13	35.8	2.07	29.24	37.0	22.68	230.5	10.17	11.41	321.5	35.7
20	22.93	24.40	36.7	2.06	29.38	38.9	23.45	134.2	12.50	13.66	322.0	35.7
21	19.97	22.05	39.2	1.63	28.86	39.1	23.06	133.7	13.08	14.00	322.8	35.7
22	23.77	25.00	41.7	1.21	28.41	39.6	23.21	133.3	13.47	14.49	316.4	35.7
23	22.26	23.33	39.5	1.60	29.33	38.1	23.81	303.8	14.86	15.85	325.7	35.8
24	22.76	24.10	37.2	2.08	30.08	37.4	24.61	300.8	15.34	16.40	325.4	35.7

Table C.2. Experimental results of treated air-solution contactor.

No.	$T_{s,in}$ (ºC)	$T_{s,out}$ (ºC)	$H_{a,in}$ (%)	V_a (m/s)	$T_{a,in}$ (ºC)	$H_{a,out}$ (%)	$T_{a,out}$ (ºC)	$v_{s,in}$ (l/h)	$T_{w,in}$ (ºC)	$T_{w,out}$ (ºC)	v_w (l/h)	$X_{s,in}$ (%)
1	17.90	18.70	42.6	1.27	29.50	41.7	21.20	123.3	9.58	10.62	322.2	35.6
2	18.29	19.45	39.7	1.61	30.12	42.1	21.22	122.5	10.09	11.23	321.9	35.7
3	18.48	19.93	37.0	2.05	30.86	41.3	21.62	122.6	8.82	10.14	321.7	35.6
4	17.99	18.34	36.5	2.04	31.19	39.6	21.54	233.9	9.36	10.75	322.4	35.7
5	17.91	18.07	38.6	1.58	30.68	39.9	21.28	233.2	9.94	11.20	322.5	35.7
6	17.92	17.78	40.4	1.29	30.20	39.7	21.05	232.1	8.73	9.89	322.9	35.6
7	19.07	20.95	44.6	2.08	31.52	46.0	22.79	343.8	11.23	12.25	411.6	35.7
8	19.09	20.66	43.7	1.62	32.05	45.1	22.60	342.0	11.66	12.59	412.3	35.7
9	19.15	20,41	45.4	1,19	31.82	44.2	22.28	340,3	12.21	13,04	411,6	35.7
10	19,40	20,75	46.6	1,20	31.51	44.9	22.21	259.1	12.64	13.44	410.3	35.7
11	19.58	21.29	44.7	1.64	31.89	45.2	22.79	255.1	13.07	13.93	412.5	35.7
12	19.88	21.76	43.8	1.63	32.08	46.6	23.27	171.3	13.44	14.29	412.0	35.7
13	20.21	21.69	45.9	1.21	31.56	46.6	23.10	170.9	13.92	14.69	413.5	35.7
14	24.99	26.07	36.1	2.09	31.89	39.5	24.37	172.2	15.85	16.80	423.5	35.4
15	24.61	25.21	40.6	1.21	31.39	38.5	24.46	257.1	17.08	17.92	417.5	35.5
16	24.92	25.67	37.9	1.63	32.30	38.2	25.19	256.4	17.49	18.39	421.8	35.6
17	24.47	25.68	35.2	2.08	33.18	37.1	25.89	255.8	17.87	18.79	423.0	35.6
18	18.91	20.79	33.2	2.07	33.60	39.1	22.65	345.4	8.98	10.08	409.8	35.3
19	19.22	20.84	35.7	1.53	32.80	40.0	22.20	343.3	9.46	10.48	405.4	35.5
20	19.40	20.45	40.1	1.12	31.50	40.3	21.66	341.5	9.99	10.91	406.7	35.5
21	19.81	21.48	38.3	1.99	31.78	42.1	22.52	343.7	10.73	11.80	410.8	35.5
22	20.05	21.23	38.6	1.99	31.67	42.0	22.52	232.4	10.21	11.30	408.9	35.4
23	20.34	21.66	38.9	2.00	31.67	43.2	22.70	160.6	10.78	11.84	411.0	35.5
24	21.84	23.96	41.4	2.09	31.16	42.6	23.81	330.9	14.55	15.53	423.2	35.4
25	22.64	24.97	43.0	1.64	30.88	42.0	23.95	329.6	14.93	15.91	423.5	35.4
26	22.79	25.36	45.7	1.21	30.38	42.0	23.77	328.4	15.33	16.23	423.5	35.3

Annex D. Experimental results of the hybrid liquid desiccant system

Table D.1. Experimental results of the absorber with in-line arrangement.

No.	$H_{a,in}$ (%)	$T_{a,in}$ (ºC)	$H_{a,out}$ (%)	$T_{a,out}$ (ºC)	Δp_a (Pa)	$m_{s,in}$ (kg/s)	$T_{s,in}$ (ºC)	$\rho_{s,in}$ (kg/m^3)	v_w (m^3/h)	$T_{w,in}$ (ºC)	$T_{w,out}$ (ºC)
1	73.2	31.77	53.3	27.12	650.8	2.51	26.58	1168.3	4.62	19.16	23.68
2	75.6	32.62	49.6	26.26	391.1	2.50	25.84	1175.8	6.21	18.96	22.43
3	78.9	30.56	47.6	25.21	394.4	2.51	24.81	1182.6	6.22	17.89	21.33
4	77.7	32.37	46.8	25.17	194.2	1.57	24.95	1187.0	3.21	15.77	21.50
5	76.2	32.75	46.3	25.49	194.4	1.57	25.45	1187.4	3.21	16.13	21.88
6	86.3	30.65	42.8	24.72	194.7	2.51	24.16	1189.3	3.20	15.73	21.51
7	89.4	30.44	42.6	24.10	196.2	2.52	23.47	1194.5	6.19	16.61	19.89
8	54.6	27.98	42.5	22.02	647.2	1.95	21.43	1195.9	6.09	15.19	18.08
9	44.8	29.16	40.3	21.92	647.5	1.95	21.27	1199.7	6.11	15.16	17.96
10	97.7	28.36	36.8	24.57	203.9	2.52	23.73	1207.0	6.17	16.90	20.16
11	95.6	28.25	35.2	24.02	209.2	2.54	23.31	1214.4	6.19	16.34	19.55

Table D.2. Experimental results of the absorber with staggered arrangement.

No.	$H_{a,in}$ (%)	$T_{a,in}$ (ºC)	$H_{a,out}$ (%)	$T_{a,out}$ (ºC)	Δp_a (Pa)	$m_{s,in}$ (kg/s)	$T_{s,in}$ (ºC)	$\rho_{s,in}$ (kg/m^3)	V_w (m^3/h)	$T_{w,in}$ (ºC)	$T_{w,out}$ (ºC)
1	74.8	28.83	42.1	25.64	475.7	2.39	24.17	1209.1	6.54	17.20	20.01
2	63.2	33.11	43.3	27.77	818.3	2.41	23.44	1208.4	5.94	17.69	21.68
3	56.5	32.76	36.9	26.37	482.4	2.40	23.51	1207.8	5.92	17.12	20.28
4	79.4	26.30	45.0	23.46	479.8	2.40	22.75	1207.4	5.92	16.69	19.41
5	79.5	26.36	45.4	23.39	478.4	2.40	24.70	1206.7	5.94	16.64	19.34
6	86.8	26.84	46.4	24.49	475.3	2.41	23.23	1205.9	5.96	17.18	20.13
7	78.2	26.42	45.3	23.41	479.8	2.40	24.98	1205.7	5.93	16.61	19.30
8	54.9	33.24	40.7	26.00	822.8	2.40	24.07	1204.7	5.94	17.37	21.03
9	84.8	26.53	46.2	23.78	427.8	2.40	24.04	1204.4	6.55	16.98	19.56
10	78.7	28.08	46.2	25.21	686.4	2.39	18.20	1204.2	6.54	17.28	20.30
11	79.8	27.78	45.7	24.53	480.5	2.39	18.45	1204.0	6.54	16.99	19.76
12	73.7	29.29	42.7	24.29	479.4	2.41	18.87	1202.9	6.53	16.86	19.73
13	82.0	26.67	47.2	23.53	478.2	2.40	21.04	1201.6	6.55	16.67	19.27
14	74.2	29.13	47.4	25.52	816.3	2.40	18.85	1201.4	5.95	17.42	20.86
15	77.2	27.16	47.7	23.90	684.0	2.40	18.11	1201.2	6.56	16.86	19.65
16	79.9	28.70	48.6	25.70	816.1	2.41	20.39	1200.6	5.95	17.45	21.01
17	76.3	28.09	48.4	24.81	817.1	2.40	25.03	1199.2	5.94	17.05	20.47
18	73.3	28.65	48.1	25.34	815.1	2.38	23.66	1193.8	5.93	17.10	20.35
19	91.1	20.84	44.5	19.18	472.3	2.44	20.19	1215.6	6.29	13.38	15.46
20	91.3	20.39	43.8	19.14	493.8	2.44	24.14	1218.1	6.48	13.84	15.79
21	63.1	23.98	37.4	20.18	838.9	2.45	23.11	1233.2	6.54	13.48	15.81
22	60.1	27.73	35.9	24.00	850.1	2.46	22.75	1228.3	6.32	14.44	17.35
23	73.6	24.09	38.2	20.56	460.2	2.46	22.92	1229.9	6.54	13.44	15.69
24	77.6	22.92	39.2	19.55	459.2	2.45	23.64	1229.3	6.54	12.67	14.91
25	58.0	27.05	44.9	22.31	755.7	2.45	24.61	1183.3	5.39	13.66	17.19
26	70.5	31.53	50.5	26.05	687.8	2.47	25.52	1180.4	5.36	15.78	20.13
27	55.5	30.88	48.1	24.96	769.4	2.40	24.06	1178.7	5.21	16.32	20.28
28	47.1	30.40	46.7	22.37	746.3	2.44	23.54	1177.4	5.40	12.95	16.65
29	76.6	30.61	51.4	25.28	725.5	2.42	24.17	1177.3	5.42	14.75	18.99
30	57.1	30.82	47.7	24.62	485.5	2.40	23.44	1177.3	5.29	16.06	19.63
31	57.4	30.91	47.0	24.58	485.5	2.40	23.51	1177.1	5.29	15.42	19.06
32	53.7	31.30	51.4	23.82	707.9	2.45	22.75	1173.0	5.31	15.44	18.87
33	56.5	31.02	50.6	24.98	768.1	2.40	24.70	1172.3	5.31	16.15	20.07
34	58.1	31.41	50.5	26.00	768.9	2.39	23.23	1170.8	5.30	17.31	21.02
35	73.3	31.49	55.5	26.55	692.6	2.45	24.98	1165.1	5.38	17.03	21.31
36	58.9	31.20	53.0	25.52	767.8	2.38	24.07	1164.2	5.33	16.48	20.14

37	62.7	30.79	54.3	24.79	762.2	2.38	24.04	1163.2	5.28	16.13	19.97

Table D.3. Experimental results of the regenerator with staggered arrangement.

No.	$W_{a,in}$ (kg_w/kg_a)	$T_{a,in}$ (ºC)	$H_{a,out}$ (%)	$T_{a,out}$ (ºC)	Δp_a (Pa)	$v_{s,in}$ (l/min)	$T_{s,in}$ (ºC)	v_w (m^3/h)	$T_{w,in}$ (ºC)	$T_{w,out}$ (ºC)
1	0.0127	33.39	42.1	42.91	479.2	126.6	46.33	7.47	51.35	49.35
2	0.0131	35.71	43.2	43.15	479.2	128.3	46.79	8.42	51.79	49.91
3	0.0106	33.32	42.3	42.34	474.7	126.9	46.26	8.36	51.68	49.74
4	0.0117	34.18	42.5	42.54	479.3	126.8	46.44	8.37	51.60	49.78
5	0.0115	33.61	42.0	43.74	477.8	127.3	46.06	8.35	51.37	49.42
6	0.0145	36.28	42.8	43.93	681.0	127.5	46.39	8.34	51.70	49.74
7	0.0130	34.49	50.1	38.99	713.0	133.3	39.65	6.07	45.16	42.58
8	0.0139	36.23	49.3	42.25	715.3	134.0	43.30	6.94	50.98	47.71
9	0.0098	34.07	44.2	41.27	753.0	132.7	42.16	6.81	50.52	46.58
10	0.0100	34.28	43.6	41.59	752.2	132.8	42.57	6.83	50.88	46.98
11	0.0139	35.24	45.8	42.24	734.2	131.2	43.41	6.83	50.56	47.00
12	0.0139	33.11	53.7	37.79	765.3	134.7	38.77	6.78	45.48	42.25
13	0.0140	35.48	47.8	42.49	768.2	132.4	43.32	6.92	51.25	47.45
14	0.0139	35.42	47.6	42.38	766.5	132.0	43.46	6.95	51.47	47.62

Annex E. Uncertainty analysis

E.1. Introduction

A measurement is an approximation or estimation of a real value. The uncertainty of a measurement is an associated parameter that specifies a range that could reasonably be attributed to this approximation of the measured value. Therefore, the uncertainty is a random result and is expressed in the form of an interval which must be associated to a confidence level.

An experimental result whose value can be obtained directly from a specific measurement device is a direct measurement. On the other hand, an experimental result whose value is obtained from indirect measurements of other quantities is an indirect measurement.

A measurement can be mathematically described as:

$$y = f(x_1, x_2, \dots x_n) \tag{E.1}$$

Where a set of observations (x_1, x_2,…x_n) are related to the resulting value of the measurement (y).

The combined standard uncertainty is the standard deviation that can be attributed to the measurement. This can be calculated as:

$$u_c(y) = \sqrt{\sum_{i=1}^{n} \left(\frac{\partial f}{\partial x_i}\right)^2 u^2(x_i)} \tag{E.2}$$

This equation is known as uncertainty propagation law, where $u(x_i)$ is the standard uncertainty of each source, if y is a direct measurement. If y is an indirect measurement $u(x_i)$ is the standard uncertainty of direct measurements. $\left(\frac{\partial f}{\partial x_i}\right)^2$ is the sensitivity coefficient associated with each input x_i. This means that is the partial derivative of the model function f with respect to x_i.

The expanded uncertainty, U, is calculated by using the recommended coverage factor of $k = 1.96$. This will give a coverage probability of 95 %, assuming a normal distribution.

$$U = k \cdot u_c(y) \tag{E.3}$$

E.2. Uncertainty calculation for the performance parameters of the small-scale air-solution contactors

E.2.1. Heat duty

The estimation of the uncertainty of the heat duty has been done by constructing the uncertainty budgets for each of the derived variables. The heat duty is a function of the chilled water inlet and outlet temperatures, as well as the water volumetric flow rate, water density and water specific heat. This means:

$$Q_w = v_w \cdot (\rho_{w,out} \cdot c_{p,w,out} \cdot T_{w,out} - \rho_{w,in} \cdot c_{p,w,in} \cdot T_{w,in}) \tag{E.4}$$

Thermodynamic properties of water depend on temperature.

Table E.1. Uncertainty budget for heat duty of the small-scale air-solution contactors.

Variable X_i	Estimate x_i	Repeatability $u_1(x_i)$	Probability distribution p_1	Accuracy $u_2(x_i)$	Probability distribution p_2	Resolution $u_3(x_i)$	Probability distribution p_3	Reference data $u_4(x_i)$	Probability distribution p_4	Sensitivity coefficient ci	Uncertainty contribution $u_i(y)$
v_w	Value	Std. Dev.	1	0.3 % v_w	$\frac{1}{2\sqrt{3}}$	0.1	$\frac{1}{2\sqrt{3}}$			$\frac{\partial Q_w}{\partial v_w}$	$\sqrt{\sum_{i=1}^{n} p_i^2 u_i^2(x_i)}$
$T_{w,out}$	Value	Std. Dev.	1	0.01	$\frac{1}{\sqrt{3}}$	0.01	$\frac{1}{2\sqrt{3}}$			$\frac{\partial Q_w}{\partial T_{w,out}}$	$\sqrt{\sum_{i=1}^{n} p_i^2 u_i^2(x_i)}$
$T_{w,in}$	Value	Std. Dev.	1	0.01	$\frac{1}{\sqrt{3}}$	0.01	$\frac{1}{2\sqrt{3}}$			$\frac{\partial Q_w}{\partial T_{w,in}}$	$\sqrt{\sum_{i=1}^{n} p_i^2 u_i^2(x_i)}$
$c_{p,w,out}$	Value							0.1 % $c_{p,w,out}$	$\frac{1}{\sqrt{3}}$	$\frac{\partial Q_w}{\partial c_{p,w,out}}$	$\sqrt{\sum_{i=1}^{n} p_i^2 u_i^2(x_i)}$
$c_{p,w,in}$	Value							0.1 % $c_{p,w,in}$	$\frac{1}{\sqrt{3}}$	$\frac{\partial Q_w}{\partial c_{p,w,in}}$	$\sqrt{\sum_{i=1}^{n} p_i^2 u_i^2(x_i)}$
$\rho_{w,out}$	Value							0.001 % $\rho_{w,out}$	$\frac{1}{\sqrt{3}}$	$\frac{\partial Q_w}{\partial \rho_{w,out}}$	$\sqrt{\sum_{i=1}^{n} p_i^2 u_i^2(x_i)}$
$\rho_{w,in}$	Value							0.001 % $\rho_{w,in}$	$\frac{1}{\sqrt{3}}$	$\frac{\partial Q_w}{\partial \rho_{w,in}}$	$\sqrt{\sum_{i=1}^{n} p_i^2 u_i^2(x_i)}$
Combined Uncertainty											$u_c(y) = \sqrt{\sum_{i=1}^{n} {c_i}^2 u^2(x_i)}$
Expanded Uncertainty											$U = k \cdot u_c(y)$

E.2.2. Air cooling

The estimation of the uncertainty of the air cooling has been done by constructing the uncertainty budgets for each of the derived variables. The air cooling is a function of the air volumetric flow rate, air density and air enthalpy. This means:

$$Q_a = v_a \cdot (\rho_{a,in} \cdot h_{a,in} - \rho_{a,out} \cdot h_{a,out}) \quad \text{(E.5)}$$

Both, moist air density and enthalpy depend on its temperature and relative humidity. Volumetric flow rate is a function of the air velocity and the diameter of the air duct.

Therefore (D.5) equation can be written as:

$$Q_a = V_a \cdot \frac{\pi \cdot d_{ad}^2}{4} \cdot (\rho_{a,in} \cdot h_{a,in} - \rho_{a,out} \cdot h_{a,out}) \quad \text{(E.6)}$$

Table E.2. Uncertainty budget for the air cooling of the small-scale air-solution contactors.

Variable X_i	Estimate x_i	Repeatability $u_1(x_i)$	Probability distribution p_1	Accuracy $u_2(x_i)$	Probability distribution p_2	Resolution $u_3(x_i)$	Probability distribution p_3	Reference data $u_4(x_i)$	Probability distribution p_4	Sensitivity coefficient ci	Uncertainty contribution $u_1(y_i)$
V_a	Value	Std. Dev.	1	3 % v_a	$\frac{1}{\sqrt{3}}$	0.01	$\frac{1}{2\sqrt{3}}$			$\frac{\partial Q_a}{\partial V_a}$	$\sqrt{\sum_{i=1}^{n} p_i^2 u_i^2(x_i)}$
d_{ad}	Value	Std. Dev.	1	0.001	$\frac{1}{\sqrt{3}}$	0.001	$\frac{1}{2\sqrt{3}}$			$\frac{\partial Q_a}{\partial d_{ad}}$	$\sqrt{\sum_{i=1}^{n} p_i^2 u_i^2(x_i)}$
$T_{a,in}$	Value	Std. Dev.	1	0.2	$\frac{1}{2}$	0.01	$\frac{1}{2\sqrt{3}}$			$\frac{\partial Q_a}{\partial T_{a,in}}$	$\sqrt{\sum_{i=1}^{n} p_i^2 u_i^2(x_i)}$
$T_{a,out}$	Value	Std. Dev.	1	0.2	$\frac{1}{2}$	0.01	$\frac{1}{2\sqrt{3}}$			$\frac{\partial Q_a}{\partial T_{a,out}}$	$\sqrt{\sum_{i=1}^{n} p_i^2 u_i^2(x_i)}$
$H_{a,in}$	Value	Std. Dev.	1	2 % $H_{a,in}$	$\frac{1}{2}$	0.01	$\frac{1}{2\sqrt{3}}$			$\frac{\partial Q_a}{\partial H_{a,in}}$	$\sqrt{\sum_{i=1}^{n} p_i^2 u_i^2(x_i)}$
$H_{a,out}$	Value	Std. Dev.	1	2 % $H_{a,out}$	$\frac{1}{2}$	0.01	$\frac{1}{2\sqrt{3}}$			$\frac{\partial Q_a}{\partial H_{a,out}}$	$\sqrt{\sum_{i=1}^{n} p_i^2 u_i^2(x_i)}$
$\rho_{a,in}$	Value							0.001 % $\rho_{a,in}$	$\frac{1}{\sqrt{3}}$	$\frac{\partial Q_a}{\partial \rho_{a,in}}$	$\sqrt{\sum_{i=1}^{n} p_i^2 u_i^2(x_i)}$
$\rho_{a,out}$	Value							0.001 % $\rho_{a,out}$	$\frac{1}{\sqrt{3}}$	$\frac{\partial Q_a}{\partial \rho_{a,out}}$	$\sqrt{\sum_{i=1}^{n} p_i^2 u_i^2(x_i)}$
$h_{a,in}$	Value							0.01 % $h_{a,in}$	$\frac{1}{\sqrt{3}}$	$\frac{\partial Q_a}{\partial h_{a,in}}$	$\sqrt{\sum_{i=1}^{n} p_i^2 u_i^2(x_i)}$
$h_{a,out}$	Value							0.01 % $h_{a,out}$	$\frac{1}{\sqrt{3}}$	$\frac{\partial Q_a}{\partial h_{a,out}}$	$\sqrt{\sum_{i=1}^{n} p_i^2 u_i^2(x_i)}$
Combined Uncertainty											$u_c(y) = \sqrt{\sum_{i=1}^{n} c_i{}^2 u^2(x_i)}$
Expanded Uncertainty											$U = k \cdot u_c(y)$

E.2.3. Global heat transfer coefficient

The estimation of the uncertainty of the global heat transfer coefficient has been done by constructing the uncertainty budgets for each of the derived variables. The global heat transfer coefficient is a function of the heat duty, the logarithmic mean temperature difference and the correction factor.

$$U \cdot A = \frac{\dot{Q}_w}{F \cdot \Delta T_{LM,ccf}} \tag{E.7}$$

Both, the correction factor and the logarithmic mean temperature difference can be obtained from inlet and outlet water and solution temperatures.

Table E.3. Uncertainty budget for the global heat transfer coefficient of the small-scale air-solution contactors.

Variable X_i	Estimate x_i	Repeatability $u_1(x_i)$	Probability distribution p_1	Accuracy $u_2(x_i)$	Probability distribution p_2	Resolution $u_3(x_i)$	Probability distribution p_3	Reference data $u_4(x_i)$	Probability distribution p_4	Sensitivity coefficient ci	Uncertainty contribution $u_1(y_i)$
Q_w	Value							Table E.2	1	$\frac{\partial UA}{\partial Q_w}$	$\sqrt{\sum_{i=1}^{n} p_i^2 u_i^2(x_i)}$
$T_{w,out}$	Value	Std. Dev.	1	0.01	$\frac{1}{\sqrt{3}}$	0.01	$\frac{1}{2\sqrt{3}}$			$\frac{\partial UA}{\partial T_{w,out}}$	$\sqrt{\sum_{i=1}^{n} p_i^2 u_i^2(x_i)}$
$T_{w,in}$	Value	Std. Dev.	1	0.01	$\frac{1}{\sqrt{3}}$	0.01	$\frac{1}{2\sqrt{3}}$			$\frac{\partial UA}{\partial T_{w,in}}$	$\sqrt{\sum_{i=1}^{n} p_i^2 u_i^2(x_i)}$
$T_{s,out}$	Value	Std. Dev.	1	0.01	$\frac{1}{\sqrt{3}}$	0.01	$\frac{1}{2\sqrt{3}}$			$\frac{\partial UA}{\partial T_{s,out}}$	$\sqrt{\sum_{i=1}^{n} p_i^2 u_i^2(x_i)}$
$T_{s,in}$	Value	Std. Dev.	1	0.01	$\frac{1}{\sqrt{3}}$	0.01	$\frac{1}{2\sqrt{3}}$			$\frac{\partial UA}{\partial T_{s,in}}$	$\sqrt{\sum_{i=1}^{n} p_i^2 u_i^2(x_i)}$
Combined Uncertainty											$u_c(y) = \sqrt{\sum_{i=1}^{n} {c_i}^2 u^2(x_i)}$
Expanded Uncertainty											$U = k \cdot u_c(y)$

E.2.4. Dehumidified water ratio

The estimation of the uncertainty of dehumidified water ratio has been done by constructing the uncertainty budgets for each of the derived variables. The dehumidified water ratio is a function of the volumetric air flow rate, the air density the air humidity ratio and the contact surface:

$$\Delta\Omega = \frac{v_{a,}}{A} \cdot (\rho_{a,in} \cdot W_{a,in} - \rho_{a,out} \cdot W_{a,out}) \quad \text{(E.8)}$$

Both, moist air density and humidity ratio depend on its temperature and relative humidity. Volumetric flow rate is a function of the air velocity and the diameter of the air duct. Contact surface depends on the tube diameter and length, and number of tubes.

Table E.4. Uncertainty budget for the dehumidified water ratio of the small-scale air-solution contactors.

Variable X_i	Estimate x_i	Repeatability $u_1(x_i)$	Probability distribution p_1	Accuracy $u_2(x_i)$	Probability distribution p_2	Resolution $u_3(x_i)$	Probability distribution p_3	Reference data $u_4(x_i)$	Probability distribution p_4	Sensitivity coefficient ci	Uncertainty contribution $u_1(y_i)$
V_a	Value	Std. Dev.	1	3 % v_a	$\frac{1}{\sqrt{3}}$	0.01	$\frac{1}{2\sqrt{3}}$			$\frac{\partial \Delta\Omega}{\partial V_a}$	$\sqrt{\sum_{i=1}^{n} p_i^2 u_i^2(x_i)}$
d_{ad}	Value	Std. Dev.	1	0.001	$\frac{1}{\sqrt{3}}$	0.001	$\frac{1}{2\sqrt{3}}$			$\frac{\partial \Delta\Omega}{\partial d_{ad}}$	$\sqrt{\sum_{i=1}^{n} p_i^2 u_i^2(x_i)}$
$T_{a,in}$	Value	Std. Dev.	1	0.2	$\frac{1}{2}$	0.01	$\frac{1}{2\sqrt{3}}$			$\frac{\partial \Delta\Omega}{\partial T_{a,in}}$	$\sqrt{\sum_{i=1}^{n} p_i^2 u_i^2(x_i)}$
$T_{a,out}$	Value	Std. Dev.	1	0.2	$\frac{1}{2}$	0.01	$\frac{1}{2\sqrt{3}}$			$\frac{\partial \Delta\Omega}{\partial T_{a,out}}$	$\sqrt{\sum_{i=1}^{n} p_i^2 u_i^2(x_i)}$
$H_{a,in}$	Value	Std. Dev.	1	2 % $H_{a,in}$	$\frac{1}{2}$	0.01	$\frac{1}{2\sqrt{3}}$			$\frac{\partial \Delta\Omega}{\partial H_{a,in}}$	$\sqrt{\sum_{i=1}^{n} p_i^2 u_i^2(x_i)}$
$H_{a,out}$	Value	Std. Dev.	1	2 % $H_{a,out}$	$\frac{1}{2}$	0.01	$\frac{1}{2\sqrt{3}}$			$\frac{\partial \Delta\Omega}{\partial H_{a,out}}$	$\sqrt{\sum_{i=1}^{n} p_i^2 u_i^2(x_i)}$
d_0	Value	Std. Dev.	1	0.001	$\frac{1}{\sqrt{3}}$	0.001	$\frac{1}{2\sqrt{3}}$			$\frac{\partial \Delta\Omega}{\partial d_o}$	$\sqrt{\sum_{i=1}^{n} p_i^2 u_i^2(x_i)}$
L_t	Value	Std. Dev.	1	0.001	$\frac{1}{\sqrt{3}}$	0.001	$\frac{1}{2\sqrt{3}}$			$\frac{\partial \Delta\Omega}{\partial L_t}$	$\sqrt{\sum_{i=1}^{n} p_i^2 u_i^2(x_i)}$
$\rho_{a,in}$	Value							0.001 % $\rho_{a,in}$	$\frac{1}{\sqrt{3}}$	$\frac{\partial \Delta\Omega}{\partial \rho_{a,in}}$	$\sqrt{\sum_{i=1}^{n} p_i^2 u_i^2(x_i)}$
$\rho_{a,out}$	Value							0.001 % $\rho_{a,out}$	$\frac{1}{\sqrt{3}}$	$\frac{\partial \Delta\Omega}{\partial \rho_{a,out}}$	$\sqrt{\sum_{i=1}^{n} p_i^2 u_i^2(x_i)}$
$W_{a,in}$	Value							0.001 % $h_{a,in}$	$\frac{1}{\sqrt{3}}$	$\frac{\partial \Delta\Omega}{\partial h_{a,in}}$	$\sqrt{\sum_{i=1}^{n} p_i^2 u_i^2(x_i)}$
$W_{a,out}$	Value							0.001 % $h_{a,out}$	$\frac{1}{\sqrt{3}}$	$\frac{\partial \Delta\Omega}{\partial h_{a,out}}$	$\sqrt{\sum_{i=1}^{n} p_i^2 u_i^2(x_i)}$
Combined Uncertainty											$u_c(y) = \sqrt{\sum_{i=1}^{n} c_i{}^2 u^2(x_i)}$
Expanded Uncertainty											$U = k \cdot u_c(y)$

E.3. Uncertainty calculation for the performance parameters of the absorber

E.3.1. Heat duty

The estimation of the uncertainty of the heat duty has been done by constructing the uncertainty budgets for each of the derived variables. The heat duty is a function of the chilled water inlet and outlet temperatures, as well as the water volumetric flow rate, water density and water specific heat. This means:

$$Q_{w,abs} = v_{w,abs} \cdot (\rho_{w,out,abs} \cdot c_{p,w,out,abs} \cdot T_{w,out,abs} - \rho_{w,in,abs} \cdot c_{p,w,in,abs} \cdot T_{w,in,abs}) \quad \text{(E.9)}$$

Thermodynamic properties of water depend on temperature.

Table E.5. Uncertainty budget for the heat duty of the absorber.

Variable X_i	Estimate x_i	Repeatability $u_1(x_i)$	Probability distribution p_1	Accuracy $u_2(x_i)$	Probability distribution p_2	Resolution $u_3(x_i)$	Probability distribution p_3	Reference data $u_4(x_i)$	Probability distribution p_4	Sensitivity coefficient ci	Uncertainty contribution $u_1(y_i)$
$v_{w,abs}$	Value	Std. Dev.	1	0.2 % v_w	$\frac{1}{2\sqrt{3}}$	0.01	$\frac{1}{2\sqrt{3}}$			$\frac{\partial Q_{w,abs}}{\partial v_{w,abs}}$	$\sqrt{\sum_{i=1}^{n} p_i^2 u_i^2(x_i)}$
$T_{w,out,abs}$	Value	Std. Dev.	1	0.01	$\frac{1}{\sqrt{3}}$	0.01	$\frac{1}{2\sqrt{3}}$			$\frac{\partial Q_{w,abs}}{\partial T_{w,out,abs}}$	$\sqrt{\sum_{i=1}^{n} p_i^2 u_i^2(x_i)}$
$T_{w,in,abs}$	Value	Std. Dev.	1	0.01	$\frac{1}{\sqrt{3}}$	0.01	$\frac{1}{2\sqrt{3}}$			$\frac{\partial Q_{w,abs}}{\partial T_{w,in,abs}}$	$\sqrt{\sum_{i=1}^{n} p_i^2 u_i^2(x_i)}$
$c_{p,w,out,abs}$	Value							0.1 % $c_{p,w,out,abs}$	$\frac{1}{\sqrt{3}}$	$\frac{\partial Q_{w,abs}}{\partial c_{p,w,out,abs}}$	$\sqrt{\sum_{i=1}^{n} p_i^2 u_i^2(x_i)}$
$c_{p,w,in,abs}$	Value							0.1 % $c_{p,w,in,abs}$	$\frac{1}{\sqrt{3}}$	$\frac{\partial Q_{w,abs}}{\partial c_{p,w,in,abs}}$	$\sqrt{\sum_{i=1}^{n} p_i^2 u_i^2(x_i)}$
$\rho_{w,out,abs}$	Value							0.001 % $\rho_{w,out,abs}$	$\frac{1}{\sqrt{3}}$	$\frac{\partial Q_{w,abs}}{\partial \rho_{w,out,abs}}$	$\sqrt{\sum_{i=1}^{n} p_i^2 u_i^2(x_i)}$
$\rho_{w,in,abs}$	Value							0.001 % $\rho_{w,in,abs}$	$\frac{1}{\sqrt{3}}$	$\frac{\partial Q_{w,abs}}{\partial \rho_{w,in,abs}}$	$\sqrt{\sum_{i=1}^{n} p_i^2 u_i^2(x_i)}$
Combined Uncertainty											$u_c(y) = \sqrt{\sum_{i=1}^{n} c_i^2 u^2(x_i)}$
Expanded Uncertainty											$U = k \cdot u_c(y)$

E.3.2. Air cooling

The estimation of the uncertainty of the air cooling has been done by constructing the uncertainty budgets for each of the derived variables. The air cooling is a function of the air volumetric flow rate, air density and air enthalpy. This means:

$$Q_{a,abs} = v_{a,abs} \cdot \rho_{a,out,abs} \cdot (h_{a,in,abs} - h_{a,out,abs}) \quad \text{(E.10)}$$

Both, moist air density and enthalpy depend on its temperature and relative humidity. Volumetric air flow rate is a function of the differential pressure air measurement, whose equation is given by the air handling unit manufacturer.

Therefore (E.10) equation can be written as:

$$Q_{a,abs} = 95\frac{\sqrt{\Delta p_{a,abs}}}{3600} \cdot \rho_{a,out,abs} \cdot (h_{a,in,abs} - h_{a,out,abs}) \quad \text{(E.11)}$$

Table E.6. Uncertainty budget for the air cooling of the absorber.

Variable X_i	Estimate x_i	Repeatability $u_1(x_i)$	Probability distribution p_1	Accuracy $u_2(x_i)$	Probability distribution p_2	Resolution $u_3(x_i)$	Probability distribution p_3	Reference data $u_4(x_i)$	Probability distribution p_4	Sensitivity coefficient ci	Uncertainty contribution $u_1(y_i)$
$\Delta p_{a,abs}$	Value	Std. Dev.	1	0.7	$\frac{1}{2}$	0.1	$\frac{1}{2\sqrt{3}}$			$\frac{\partial Q_{a,abs}}{\partial \Delta p_{a,abs}}$	$\sqrt{\sum_{i=1}^{n} p_i^2 u_i^2(x_i)}$
$T_{a,in,abs}$	Value	Std. Dev.	1	0.2	$\frac{1}{2}$	0.01	$\frac{1}{2\sqrt{3}}$			$\frac{\partial Q_{a,abs}}{\partial T_{a,in,abs}}$	$\sqrt{\sum_{i=1}^{n} p_i^2 u_i^2(x_i)}$
$T_{a,out,abs}$	Value	Std. Dev.	1	0.2	$\frac{1}{2}$	0.01	$\frac{1}{2\sqrt{3}}$			$\frac{\partial Q_{a,abs}}{\partial T_{a,out,abs}}$	$\sqrt{\sum_{i=1}^{n} p_i^2 u_i^2(x_i)}$
$H_{a,in,abs}$	Value	Std. Dev.	1	2 % $H_{a,in,abs}$	$\frac{1}{2}$	0.01	$\frac{1}{2\sqrt{3}}$			$\frac{\partial Q_{a,abs}}{\partial H_{a,in,abs}}$	$\sqrt{\sum_{i=1}^{n} p_i^2 u_i^2(x_i)}$
$H_{a,out,abs}$	Value	Std. Dev.	1	2 % $H_{a,out,abs}$	$\frac{1}{2}$	0.01	$\frac{1}{2\sqrt{3}}$			$\frac{\partial Q_{a,abs}}{\partial H_{a,out,abs}}$	$\sqrt{\sum_{i=1}^{n} p_i^2 u_i^2(x_i)}$
$\rho_{a,out,abs}$	Value							0.001 % $\rho_{a,out}$	$\frac{1}{\sqrt{3}}$	$\frac{\partial Q_{a,abs}}{\partial \rho_{a,out,abs}}$	$\sqrt{\sum_{i=1}^{n} p_i^2 u_i^2(x_i)}$
$h_{a,in,abs}$	Value							0.01 % $h_{a,in,abs}$	$\frac{1}{\sqrt{3}}$	$\frac{\partial Q_{a,abs}}{\partial h_{a,in,abs}}$	$\sqrt{\sum_{i=1}^{n} p_i^2 u_i^2(x_i)}$
$h_{a,out,abs}$	Value							0.01 % $h_{a,out,abs}$	$\frac{1}{\sqrt{3}}$	$\frac{\partial Q_{a,abs}}{\partial h_{a,out,abs}}$	$\sqrt{\sum_{i=1}^{n} p_i^2 u_i^2(x_i)}$
Combined Uncertainty											$u_c(y) = \sqrt{\sum_{i=1}^{n} c_i{}^2 u^2(x_i)}$
Expanded Uncertainty											$U = k \cdot u_c(y)$

E.3.3. Global heat transfer coefficient

The estimation of the uncertainty of the global heat transfer coefficient has been done by constructing the uncertainty budgets for each of the derived variables. The global heat transfer coefficient is a function of the heat duty, the logarithmic mean temperature difference and the correction factor.

$$U \cdot A_{abs} = \frac{\dot{Q}_{w,abs}}{\Delta T_{LM}} \quad \text{(E.12)}$$

The logarithmic mean temperature difference can be obtained from inlet and outlet water and solution temperatures.

Table E.7. Uncertainty budget for the global heat transfer coefficient of the absorber.

Variable X_i	Estimate x_i	Repeatability $u_1(x_i)$	Probability distribution p_1	Accuracy $u_2(x_i)$	Probability distribution p_2	Resolution $u_3(x_i)$	Probability distribution p_3	Reference data $u_4(x_i)$	Probability distribution p_4	Sensitivity coefficient ci	Uncertainty contribution $u_1(y_i)$
$Q_{w,abs}$	Value							Table E.5	1	$\frac{\partial UA_{abs}}{\partial Q_{w,abs}}$	$\sqrt{\sum_{i=1}^{n} p_i^2 u_i^2(x_i)}$
$T_{w,out,abs}$	Value	Std. Dev.	1	0.01	$\frac{1}{\sqrt{3}}$	0.01	$\frac{1}{2\sqrt{3}}$			$\frac{\partial UA_{abs}}{\partial T_{w,out,abs}}$	$\sqrt{\sum_{i=1}^{n} p_i^2 u_i^2(x_i)}$
$T_{w,in,abs}$	Value	Std. Dev.	1	0.01	$\frac{1}{\sqrt{3}}$	0.01	$\frac{1}{2\sqrt{3}}$			$\frac{\partial UA_{abs}}{\partial T_{w,in,abs}}$	$\sqrt{\sum_{i=1}^{n} p_i^2 u_i^2(x_i)}$
$T_{s,out,abs}$	Value	Std. Dev.	1	0.03	$\frac{1}{\sqrt{3}}$	0.01	$\frac{1}{2\sqrt{3}}$			$\frac{\partial UA_{abs}}{\partial T_{s,out,abs}}$	$\sqrt{\sum_{i=1}^{n} p_i^2 u_i^2(x_i)}$
$T_{s,in,abs}$	Value	Std. Dev.	1	0.01	$\frac{1}{\sqrt{3}}$	0.01	$\frac{1}{2\sqrt{3}}$			$\frac{\partial UA_{abs}}{\partial T_{s,in,abs}}$	$\sqrt{\sum_{i=1}^{n} p_i^2 u_i^2(x_i)}$
Combined Uncertainty											$u_c(y) = \sqrt{\sum_{i=1}^{n} {c_i}^2 u^2(x_i)}$
Expanded Uncertainty											$U = k \cdot u_c(y)$

E.3.4. Mass transfer coefficient in the air side

The estimation of the uncertainty of the mass transfer coefficient in the air side has been done by constructing the uncertainty budgets for each of the derived variables. According to the mathematical model described in Section 5.2, the mass transfer coefficient is calculated from an equation system with 12 unknown variables. In any case, the measurements required for its calculation are the solution inlet temperature, density and flow rate, the moist air inlet and outlet temperature and relative humidity, the air flow, the inlet and outlet water temperature and the water flow rate. Due to the complexity of this calculation, the uncertainty propagation is calculated with the Uncertainty propagation tool of the EES.

Table E.8. Uncertainty budget for the mass transfer coefficient in the air side of the absorber..

Variable X_i	Estimate x_i	Repeatability $u_1(x_i)$	Probability distribution p_1	Accuracy $u_2(x_i)$	Probability distribution p_2	Resolution $u_3(x_i)$	Probability distribution p_3	Reference data $u_4(x_i)$	Probability distribution p_4	Sensitivity coefficient ci	Uncertainty contribution $u_i(y_i)$
$\Delta p_{a,abs}$	Value	Std. Dev.	1	0.7	$\frac{1}{2}$	0.1	$\frac{1}{2\sqrt{3}}$			$\frac{\partial \sigma_{a,abs}}{\partial \Delta p_{a,abs}}$	$\sqrt{\sum_{i=1}^{n} p_i^2 u_i^2(x_i)}$
$m_{s,in,abs}$	Value	Std. Dev.	1	0.001	$\frac{1}{2\sqrt{3}}$	0.001	$\frac{1}{2\sqrt{3}}$			$\frac{\partial \sigma_{a,abs}}{\partial m_{s,in,abs}}$	$\sqrt{\sum_{i=1}^{n} p_i^2 u_i^2(x_i)}$
$\rho_{s,in,abs}$	Value	Std. Dev.	1	0.1	$\frac{1}{2}$	0.1	$\frac{1}{2\sqrt{3}}$			$\frac{\partial \sigma_{a,abs}}{\partial \rho_{s,in,abs}}$	$\sqrt{\sum_{i=1}^{n} p_i^2 u_i^2(x_i)}$
$T_{s,in,abs}$	Value	Std. Dev.	1	0.01	$\frac{1}{\sqrt{3}}$	0.01	$\frac{1}{2\sqrt{3}}$			$\frac{\partial \sigma_{a,abs}}{\partial T_{s,in,abs}}$	$\sqrt{\sum_{i=1}^{n} p_i^2 u_i^2(x_i)}$
$T_{a,in,abs}$	Value	Std. Dev.	1	0.2	$\frac{1}{2}$	0.01	$\frac{1}{2\sqrt{3}}$			$\frac{\partial \sigma_{a,abs}}{\partial T_{a,in,abs}}$	$\sqrt{\sum_{i=1}^{n} p_i^2 u_i^2(x_i)}$
$T_{a,out,abs}$	Value	Std. Dev.	1	0.2	$\frac{1}{2}$	0.01	$\frac{1}{2\sqrt{3}}$			$\frac{\partial \sigma_{a,abs}}{\partial T_{a,out,abs}}$	$\sqrt{\sum_{i=1}^{n} p_i^2 u_i^2(x_i)}$
$H_{a,in,abs}$	Value	Std. Dev.	1	2 % $H_{a,in,abs}$	$\frac{1}{2}$	0.01	$\frac{1}{2\sqrt{3}}$			$\frac{\partial \sigma_{a,abs}}{\partial H_{a,in,abs}}$	$\sqrt{\sum_{i=1}^{n} p_i^2 u_i^2(x_i)}$
$H_{a,out,abs}$	Value	Std. Dev.	1	2 % $H_{a,out,abs}$	$\frac{1}{2}$	0.01	$\frac{1}{2\sqrt{3}}$			$\frac{\partial \sigma_{a,abs}}{\partial H_{a,out,abs}}$	$\sqrt{\sum_{i=1}^{n} p_i^2 u_i^2(x_i)}$
$T_{w,out,abs}$	Value	Std. Dev.	1	0.01	$\frac{1}{\sqrt{3}}$	0.01	$\frac{1}{2\sqrt{3}}$			$\frac{\partial \sigma_{a,abs}}{\partial T_{w,out,abs}}$	$\sqrt{\sum_{i=1}^{n} p_i^2 u_i^2(x_i)}$
$T_{w,in,abs}$	Value	Std. Dev.	1	0.01	$\frac{1}{\sqrt{3}}$	0.01	$\frac{1}{2\sqrt{3}}$			$\frac{\partial \sigma_{a,abs}}{\partial T_{w,in,abs}}$	$\sqrt{\sum_{i=1}^{n} p_i^2 u_i^2(x_i)}$
v_w	Value	Std. Dev.	1	0.2 % v_w	$\frac{1}{2\sqrt{3}}$	0.01	$\frac{1}{2\sqrt{3}}$			$\frac{\partial \sigma_{a,abs}}{\partial v_w}$	$\sqrt{\sum_{i=1}^{n} p_i^2 u_i^2(x_i)}$
Combined Uncertainty											$u_c(y) = \sqrt{\sum_{i=1}^{n} {c_i}^2 u^2(x_i)}$
Expanded Uncertainty											$U = k \cdot u_c(y)$

E.4. Uncertainty calculation for the performance parameters of the regenerator

E.4.1. Heating rate in the regenerator

The estimation of the uncertainty of the heating rate in the regenerator has been done by constructing the uncertainty budgets for each of the derived variables. The heating rate in the regenerator is a function of the hot water inlet and outlet temperatures, as well as the water volumetric flow rate, water density and water specific heat. This means:

$$Q_{w,reg} = v_{w,reg} \cdot (\rho_{w,in,reg} \cdot c_{p,w,in,reg} \cdot T_{w,in,reg} - \rho_{w,out,reg} \cdot c_{p,w,out,reg} \cdot T_{w,out,reg}) \quad \text{(E.13)}$$

Thermodynamic properties of water depend on temperature.

Table E.9. Uncertainty budget for the heating rate in the regenerator.

Variable X_i	Estimate x_i	Repeatability $u_1(x_i)$	Probability distribution p_1	Accuracy $u_2(x_i)$	Probability distribution p_2	Resolution $u_3(x_i)$	Probability distribution p_3	Reference data $u_4(x_i)$	Probability distribution p_4	Sensitivity coefficient ci	Uncertainty contribution $u_i(y_i)$
$v_{w,reg}$	Value	Std. Dev.	1	0.2 % $v_{w,reg}$	$\frac{1}{2\sqrt{3}}$	0.01	$\frac{1}{2\sqrt{3}}$			$\frac{\partial Q_{w,reg}}{\partial v_{w,reg}}$	$\sqrt{\sum_{i=1}^{n} p_i^2 u_i^2(x_i)}$
$T_{w,out,reg}$	Value	Std. Dev.	1	0.01	$\frac{1}{\sqrt{3}}$	0.01	$\frac{1}{2\sqrt{3}}$			$\frac{\partial Q_{w,reg}}{\partial T_{w,out,reg}}$	$\sqrt{\sum_{i=1}^{n} p_i^2 u_i^2(x_i)}$
$T_{w,in,reg}$	Value	Std. Dev.	1	0.01	$\frac{1}{\sqrt{3}}$	0.01	$\frac{1}{2\sqrt{3}}$			$\frac{\partial Q_{w,reg}}{\partial T_{w,in,reg}}$	$\sqrt{\sum_{i=1}^{n} p_i^2 u_i^2(x_i)}$
$c_{p,w,out,reg}$	Value							0.1 % $c_{p,w,out,reg}$	$\frac{1}{\sqrt{3}}$	$\frac{\partial Q_{w,reg}}{\partial c_{p,w,out,reg}}$	$\sqrt{\sum_{i=1}^{n} p_i^2 u_i^2(x_i)}$
$c_{p,w,in,reg}$	Value							0.1 % $c_{p,w,in,reg}$	$\frac{1}{\sqrt{3}}$	$\frac{\partial Q_{w,reg}}{\partial c_{p,w,in,reg}}$	$\sqrt{\sum_{i=1}^{n} p_i^2 u_i^2(x_i)}$
$\rho_{w,out,reg}$	Value							0.001 % $\rho_{w,out,reg}$	$\frac{1}{\sqrt{3}}$	$\frac{\partial Q_{w,reg}}{\partial \rho_{w,out,reg}}$	$\sqrt{\sum_{i=1}^{n} p_i^2 u_i^2(x_i)}$
$\rho_{w,in,reg}$	Value							0.001 % $\rho_{w,in,reg}$	$\frac{1}{\sqrt{3}}$	$\frac{\partial Q_{w,reg}}{\partial \rho_{w,in,reg}}$	$\sqrt{\sum_{i=1}^{n} p_i^2 u_i^2(x_i)}$
Combined Uncertainty											$u_c(y) = \sqrt{\sum_{i=1}^{n} {c_i}^2 u^2(x_i)}$
Expanded Uncertainty											$U = k \cdot u_c(y)$

E.4.2. Global heat transfer coefficient

The estimation of the uncertainty of the global heat transfer coefficient has been done by constructing the uncertainty budgets for each of the derived variables. The global heat transfer coefficient is a function of the heat duty, the logarithmic mean temperature difference and the correction factor.

$$U \cdot A_{reg} = \frac{\dot{Q}_{w,reg}}{\Delta T_{LM}} \quad \text{(E.14)}$$

The logarithmic mean temperature difference can be obtained from inlet and outlet water and solution temperatures.

Table E.10. Uncertainty budget for the global heat transfer coefficient of the regenerator.

Variable X_i	Estimate x_i	Repeatability $u_1(x_i)$	Probability distribution p_1	Accuracy $u_2(x_i)$	Probability distribution p_2	Resolution $u_3(x_i)$	Probability distribution p_3	Reference data $u_4(x_i)$	Probability distribution p_4	Sensitivity coefficient ci	Uncertainty contribution $u_1(y_i)$
$Q_{w,reg}$	Value							Table E.9	1	$\frac{\partial UA_{reg}}{\partial Q_{w,reg}}$	$\sqrt{\sum_{i=1}^{n} p_i^2 u_i^2(x_i)}$
$T_{w,out,reg}$	Value	Std. Dev.	1	0.01	$\frac{1}{\sqrt{3}}$	0.01	$\frac{1}{2\sqrt{3}}$			$\frac{\partial UA_{reg}}{\partial T_{w,out,reg}}$	$\sqrt{\sum_{i=1}^{n} p_i^2 u_i^2(x_i)}$
$T_{w,in,reg}$	Value	Std. Dev.	1	0.01	$\frac{1}{\sqrt{3}}$	0.01	$\frac{1}{2\sqrt{3}}$			$\frac{\partial UA_{reg}}{\partial T_{w,in,reg}}$	$\sqrt{\sum_{i=1}^{n} p_i^2 u_i^2(x_i)}$
$T_{s,out,reg}$	Value	Std. Dev.	1	0.03	$\frac{1}{\sqrt{3}}$	0.01	$\frac{1}{2\sqrt{3}}$			$\frac{\partial UA_{reg}}{\partial T_{s,out,reg}}$	$\sqrt{\sum_{i=1}^{n} p_i^2 u_i^2(x_i)}$
$T_{s,in,reg}$	Value	Std. Dev.	1	0.03	$\frac{1}{\sqrt{3}}$	0.01	$\frac{1}{2\sqrt{3}}$			$\frac{\partial UA_{reg}}{\partial T_{s,in,reg}}$	$\sqrt{\sum_{i=1}^{n} p_i^2 u_i^2(x_i)}$
Combined Uncertainty											$u_c(y) = \sqrt{\sum_{i=1}^{n} {c_i}^2 u^2(x_i)}$
Expanded Uncertainty											$U = k \cdot u_c(y)$

E.4.3. Mass transfer coefficient in the air side

The estimation of the uncertainty of the mass transfer coefficient in the air side has been done by constructing the uncertainty budgets for each of the derived variables. According to the mathematical model described in Section 5.2, the mass transfer coefficient is calculated from an equation system with 12 unknown variables. In any case, the measurements required for its calculation are the solution inlet temperature and flow rate, the moist air inlet and outlet temperature and relative humidity, the air flow, the inlet and outlet water temperature and the water flow rate. Due to the complexity of this calculation, the uncertainty propagation is calculated with the Uncertainty propagation tool of the EES.

Table E.11. Uncertainty budget for the mass transfer coefficient in the air side of the regenerator.

Variable X_i	Estimate x_i	Repeatability $u_1(x_i)$	Probability distribution p_1	Accuracy $u_2(x_i)$	Probability distribution p_2	Resolution $u_3(x_i)$	Probability distribution p_3	Reference data $u_4(x_i)$	Probability distribution p_4	Sensitivity coefficient ci	Uncertainty contribution $u_i(y)$
$\Delta p_{a,reg}$	Value	Std. Dev.	1	0.7	$\frac{1}{2}$	0.1	$\frac{1}{2\sqrt{3}}$			$\frac{\partial \sigma_{a,reg}}{\partial \Delta p_{a,reg}}$	$\sqrt{\sum_{i=1}^{n} p_i^2 u_i^2(x_i)}$
$v_{s,reg}$	Value	Std. Dev.	1	1 % $v_{s,reg}$	$\frac{1}{2\sqrt{3}}$	0.001	$\frac{1}{2\sqrt{3}}$			$\frac{\partial \sigma_{a,reg}}{\partial m_{s,reg}}$	$\sqrt{\sum_{i=1}^{n} p_i^2 u_i^2(x_i)}$
$T_{s,in,reg}$	Value	Std. Dev.	1	0.03	$\frac{1}{\sqrt{3}}$	0.01	$\frac{1}{2\sqrt{3}}$			$\frac{\partial \sigma_{a,reg}}{\partial T_{s,in,reg}}$	$\sqrt{\sum_{i=1}^{n} p_i^2 u_i^2(x_i)}$
$T_{a,in,reg}$	Value	Std. Dev.	1	0.2	$\frac{1}{2}$	0.01	$\frac{1}{2\sqrt{3}}$			$\frac{\partial \sigma_{a,reg}}{\partial T_{a,in,reg}}$	$\sqrt{\sum_{i=1}^{n} p_i^2 u_i^2(x_i)}$
$T_{a,out,reg}$	Value	Std. Dev.	1	0.2	$\frac{1}{2}$	0.01	$\frac{1}{2\sqrt{3}}$			$\frac{\partial \sigma_{a,reg}}{\partial T_{a,out,reg}}$	$\sqrt{\sum_{i=1}^{n} p_i^2 u_i^2(x_i)}$
$H_{a,in,reg}$	Value	Std. Dev.	1	2 % $H_{a,in,reg}$	$\frac{1}{2}$	0.01	$\frac{1}{2\sqrt{3}}$			$\frac{\partial \sigma_{a,reg}}{\partial H_{a,in,reg}}$	$\sqrt{\sum_{i=1}^{n} p_i^2 u_i^2(x_i)}$
$H_{a,out,reg}$	Value	Std. Dev.	1	2 % $H_{a,out,reg}$	$\frac{1}{2}$	0.01	$\frac{1}{2\sqrt{3}}$			$\frac{\partial \sigma_{a,reg}}{\partial H_{a,out,reg}}$	$\sqrt{\sum_{i=1}^{n} p_i^2 u_i^2(x_i)}$
$T_{w,out,reg}$	Value	Std. Dev.	1	0.01	$\frac{1}{\sqrt{3}}$	0.01	$\frac{1}{2\sqrt{3}}$			$\frac{\partial \sigma_{a,reg}}{\partial T_{w,out,reg}}$	$\sqrt{\sum_{i=1}^{n} p_i^2 u_i^2(x_i)}$
$T_{w,in,reg}$	Value	Std. Dev.	1	0.01	$\frac{1}{\sqrt{3}}$	0.01	$\frac{1}{2\sqrt{3}}$			$\frac{\partial \sigma_{a,reg}}{\partial T_{w,in,reg}}$	$\sqrt{\sum_{i=1}^{n} p_i^2 u_i^2(x_i)}$
$v_{w,reg}$	Value	Std. Dev.	1	0.2 % $v_{w,reg}$	$\frac{1}{2\sqrt{3}}$	0.01	$\frac{1}{2\sqrt{3}}$			$\frac{\partial \sigma_{a,reg}}{\partial v_{w,reg}}$	$\sqrt{\sum_{i=1}^{n} p_i^2 u_i^2(x_i)}$
Combined Uncertainty											$u_c(y) = \sqrt{\sum_{i=1}^{n} c_i{}^2 u^2(x_i)}$
Expanded Uncertainty											$U = k \cdot u_c(y)$